

University of Southampton Research Repository

Copyright © and Moral Rights for this thesis and, where applicable, any accompanying data are retained by the author and/or other copyright owners. A copy can be downloaded for personal non-commercial research or study, without prior permission or charge. This thesis and the accompanying data cannot be reproduced or quoted extensively from without first obtaining permission in writing from the copyright holder/s. The content of the thesis and accompanying research data (where applicable) must not be changed in any way or sold commercially in any format or medium without the formal permission of the copyright holder/s.

When referring to this thesis and any accompanying data, full bibliographic details must be given, e.g.

Thesis: Author (Year of Submission) "Full thesis title", University of Southampton, name of the University Faculty or School or Department, PhD Thesis, pagination.

Data: Author (Year) Title. URI [dataset]

University of Southampton

Faculty of Environmental and Life Sciences

School of Geography and Environmental Science

**Assessing Eco-Geomorphic Interactions Across Scales Using Novel UAV Based
Remote Sensing Techniques and Modelling**

by

Christopher Tomsett

ORCID ID 0000-0002-6916-6063

<https://orcid.org/0000-0002-6916-6063>

Thesis for the degree of Doctor of Philosophy

November 2021

University of Southampton

Abstract

Faculty of Environmental and Life Sciences

School of Geography and Environmental Science

Doctor of Philosophy

Assessing Eco-Geomorphic Interactions Across Scales Using Novel UAV Based Remote Sensing Techniques and Modelling

by

Christopher Tomsett

The importance of vegetation within the fluvial domain is well established, influencing both flow and morphology, and has long been recognised as a key component of the river corridor. Despite this, adequately capturing the spatial and structural variability of vegetation for us to understand the eco-geomorphic feedbacks occurring at a range of scales remains a challenge. Currently, the focus of this research takes place at either the individual plant scale, looking into vegetation-flow interactions, or at larger scales, attempting to spatially discretise vegetation for bulk roughness metrics. Subsequently, hydrodynamic models are typically based around these bulk roughness values which exclude vegetation structure. The aim of this research is to attempt to bridge this gap and link the different scales of analysis to improve our understanding of eco-geomorphic interactions. This is achieved by: (1) Examining current remote sensing methods that may be used for fluvial research, (2) Developing a novel UAV based remote sensing system to collect plant scale data for reach scale analysis, (3) Extracting trait-based metrics for individual plants and upscaling these to reach scale extents, (4) Implementing these traits-based parameters in to a 2D hydrodynamic model. At present, the main trade offs in remote sensing centre around scale and resolution, whereby capturing larger areas reduces the detail of the phenomena being studied. Structure from Motion (SfM) photogrammetry has helped to bridge this gap yet fails to reconstruct topography in vegetated reaches and cannot resolve vegetation structure. These drawbacks have herein been overcome with the introduction of UAV based laser scanning techniques, capable of accurately capturing topography in vegetated reaches as well as resolving vegetation structure. This data can be used to extract traits-based vegetation metrics, identify individual guilds within a river corridor, and be scaled to spatially discretise vegetation structure at reach scales. Guilds are then evaluated against monitored morphological change to investigate eco-geomorphic feedbacks. These vegetation metrics and classifications are subsequently used to parameterise a 2D hydrodynamic model, showing the impact that vegetation discretisation methods have on model outputs. This research has developed methods for obtaining reach scale data on vegetation structure to better inform our understanding of eco-geomorphic feedbacks. The robustness and scalability of these methods presents future avenues of research, both within the fluvial domain and for other environmental research applications, where eco-geomorphic feedbacks have a major influence in shaping the Earth's surface.

Table of Contents

Table of Contents	i
Table of Tables.....	vii
Table of Figures	ix
Research Thesis: Declaration of Authorship	xiii
Acknowledgements	xv
Definitions and Abbreviations	xvi
Chapter 1 Introduction	1
1.1 Relevant Scales of Eco-Geomorphology	2
1.2 Characterising Vegetation Complexity	5
1.3 Thesis Aims and Research Questions.....	6
1.4 Thesis Outline	7
Chapter 2 Remote sensing of river corridors: A review of current trends and future directions.....	9
2.1 Abstract	9
2.2 Introduction.....	9
2.2.1 Review Structure.....	11
2.3 River Corridor Remote Sensing.....	11
2.3.1 A Brief History of Remote Sensing of River Corridors.....	11
2.3.2 Current Monitoring Methods	14
2.3.2.1 Roughness and Grain size.....	14
2.3.2.2 Flow Characteristics.....	16
2.3.2.3 Water Quality.....	17
2.3.2.4 Morphology.....	18
2.3.2.5 Vegetation.....	21
2.3.2.6 Flooding.....	24
2.3.3 Real-World Cross-Scale Applications.....	25
2.4 The State of the Art.....	25
2.5 Future Directions.....	28
2.5.1 UAVs – Uncrewed Aerial Vehicles	28
2.5.2 AUVs – Autonomous Underwater Vehicles	29
2.5.3 USVs – Uncrewed Surface Vehicles	29

Table of Contents

2.5.4	Real Time Monitoring Using Internet of Things (IoT)	30
2.5.5	Satellite Remote Sensing.....	30
2.6	Key Challenges.....	31
2.7	Concluding Remarks	32
Chapter 3 Development and testing of a UAV laser scanner and multi-spectral camera system for eco-geomorphic applications.....		35
3.1	Abstract.....	35
3.2	Introduction	35
3.3	Development of a UAV Laser Scanner and Multispectral Camera Sensor System.....	38
3.3.1	Components of the System.....	38
3.3.1.1	Applanix APX-15 Inertial Navigation System (INS).....	39
3.3.1.2	Velodyne VLP-16 Laser Scanner.....	40
3.3.1.3	MicaSense RedEdge-MX Multispectral Camera.....	40
3.3.1.4	Associated Hardware.....	41
3.3.2	Assembly of the System.....	42
3.4	Field Deployment of the System.....	43
3.5	Data Processing Workflow	44
3.5.1	UAV Laser Scanner and Multispectral Camera Processing	44
3.5.1.1	Inertial Navigation System Processing.....	44
3.5.1.2	UAV Laser Scanner Raw Data Processing.....	46
3.5.1.3	Combining Laser Scanner and Positional Data	47
3.5.1.4	Offset and Boresight Angles	47
3.5.1.5	MicaSense Multispectral Imagery SfM Workflow.....	49
3.5.2	Data Processing for Comparison and Error Analysis.....	49
3.5.2.1	Absolute Accuracy Assessment	50
3.5.2.2	Relative Accuracy Assessment—Repeatability	50
3.6	Results	51
3.6.1	Absolute Accuracy of UAV-LS and UAV-MS (SfM)	51
3.6.2	Relative Accuracy of Surveys: Repeatability	52
3.6.2.1	Comparison of UAV-LS and UAV-MS Derived SfM for the Same Dates	52
3.6.2.2	Repeatability of Survey Methods: Comparisons Across Dates	52

3.7	Discussion.....	54
3.7.1	UAV Laser Scanner and Multispectral System.....	54
3.7.2	Eco-Geomorphic Applications	55
3.8	Conclusions and Future Work.....	58
Chapter 4 Exploring the 4D scales of eco-geomorphic interactions along a river corridor using repeat UAV Laser Scanning (UAV-LS), multispectral imagery, and a functional traits framework..... 61		
4.1	Abstract	61
4.2	Introduction.....	61
4.2.1	The Importance of Vegetation	63
4.2.2	Plant Functional Traits.....	63
4.2.3	Hydrologically Relevant Functional Traits.....	66
4.2.4	Remote Sensing of River Corridor Vegetation	67
4.2.5	Aims.....	68
4.3	Study Site.....	69
4.4	Methods.....	70
4.4.1	Long Term (Decadal) Analysis	70
4.4.2	Field Collection of High Resolution 4D data.....	71
4.4.3	Vegetation Functional Trait Extraction	73
4.4.3.1	Point Cloud Segmentation	73
4.4.3.2	Trait Metric Extraction.....	74
4.4.3.3	Guild Identification.....	76
4.4.3.4	Linking Traits to Reach Scale Metrics	77
4.4.3.5	Reach Scale Guild Classification	78
4.4.4	Morphological Change.....	80
4.5	Results.....	80
4.5.1	Decadal Scale Change	80
4.5.2	Hydrologically Relevant Trait Analysis.....	83
4.5.2.1	Extraction and Analysis of Traits.....	83
4.5.2.2	Linking PCA Clusters to Reach Scale UAV-LS Data	84
4.5.2.3	Creation of Seasonal Reach Scale Guilds Maps.....	86
4.5.3	Morphological Change.....	88

Table of Contents

4.6	DISCUSSION.....	89
4.6.1	Multi-Decadal Evolution.....	89
4.6.2	Trait Extraction and Guild Formation.....	90
4.6.3	Reach Scale Guild mapping.....	92
4.6.4	Eco-Geomorphic Change.....	93
4.7	Remote Sensing of Plant Functional Traits: What Next?.....	95
4.8	Conclusion.....	97
Chapter 5 Accurate representation of seasonal vegetation structure in a hydrodynamic model.		99
5.1	Abstract.....	99
5.2	Introduction.....	99
5.3	Aims.....	101
5.4	Methods.....	102
5.4.1	Delft3D.....	102
5.4.1.1	Modelling Scenarios.....	102
5.4.1.2	Model Grid.....	102
5.4.1.3	Model Timescales.....	104
5.4.1.4	Boundary Conditions.....	105
5.4.1.5	Sediments.....	105
5.4.1.6	Channel Morphological Adjustment.....	110
5.4.1.7	Roughness and Vegetation.....	112
5.4.2	Data Analysis.....	117
5.5	Results.....	117
5.5.1	Morphological Change.....	117
5.5.2	Peak Flows.....	121
5.5.3	Bar vs Vegetation Bank Changes.....	123
5.6	Discussion.....	125
5.7	Conclusion and Future Work.....	130
Chapter 6 Synthesis and conclusion.....		133
6.1	Research Synthesis.....	133
6.2	Future Work.....	140
6.3	Conclusion.....	142

List of References.....145

Table of Tables

Table 3-1	The band characteristics of the MicaSense RedEdge-MX multispectral sensor.	41
Table 3-2	Absolute errors of each survey method when compared to measured GNSS check points, separated by levels of vegetation obstruction.	51
Table 4-1	Summaries of the data collection methods used on each survey date.	72
Table 4-2	Description of guilds used for training the random forest classifier, showing the number of training objects from the image segmentation and the training size area.	78
Table 4-3	Transect statistics showing the difference between large vegetation present and absent sections, for when avulsions are included and excluded.	80
Table 4-4	Standard deviations in trait values as a percentage of the mean values for herbaceous and tree guilds.	83
Table 5-1	Model run scenarios used in this study, explaining the vegetation representation and whether these vary through time.	102
Table 5-2	Grainsize distributions established via mechanical and manual sieve shaking for all three sampled locations as well for the combined values.	110
Table 5-3	Values of critical shear stress (τ_{crit}) for erosion to take place which are spatially varied according to the below vegetation classifications.	112
Table 5-4	Manning's N roughness values used for the seasonal and non-seasonal modelling approaches.	115
Table 5-5	The characteristics used to model drag forces based on plant structure within the vegetation module.	116

Table of Figures

Figure 1-1	A comparison of a simplified Earth as an abiotic (A) and biotic (B) system as outlined in (Corenblit and Steiger, 2009).	1
Figure 2-1	Key features and scales of the floodplain.....	12
Figure 2-2	A comparison of the spatial resolution and extent of various common survey methods along with temporal resolution, end user cost, and ease of data analysis in the subsequent bar graphs.	13
Figure 2-3	An example of roughness calculations performed across a restored channel. SfM methods were used to obtain a DEM before using detrended standard deviation values to obtain surface roughness.	15
Figure 2-4	The relationships between survey imagery resolution from UAV aircraft and the geospatial precision (based off of RMSE and standard deviation values) for both topographic and bathymetric surveys.....	19
Figure 2-5	The effects of including spatially variable roughness across two discharge magnitudes on bed shear stress.	23
Figure 3-1	The key components of the developed UAV laser scanner and multispectral camera system for mounting on a UAV platform such as a DJI M600.	39
Figure 3-2	The components of the sensor package assembled within a lightweight plastic box for testing, here mounted on a DJI M600 multirotor platform.....	42
Figure 3-3	Study site of the River Teme, showing the flight lines used for all surveys from which laser scanning and imagery were captured.	43
Figure 3-4	Post-processing results of the Applanix APX-15 data showing how forwards and backwards Kalman filtering reduces errors.....	45
Figure 3-5	Impact of the distance from scanner on accuracy and flight overlap clipping.	46
Figure 3-6	Calculation of offset and boresight angles using an iterative process between multiple passes (from different directions) over an identifiable feature, in this case an electricity pylon.....	48
Figure 3-7	Locations of different accuracy assessment methods.	50

Table of Figures

Figure 3-8	Differences between UAV-LS- and UAV-MS-derived SfM point clouds for the each of the 5 survey dates across the stable patches.	52
Figure 3-9	Distributions of errors and mean +/- standard deviation of errors (in m) between surveys for the stable ground patches on different dates for: (A) UAV-LS method; and (B) UAV-MS-derived SfM methods.....	53
Figure 3-10	Comparisons of UAV-LS- and UAV-MS-derived SfM methods between April and June 2021 for each of the six stable ground patches, highlighting the spatial variability in accuracy for SfM-derived models compared to UAV-LS methods.	54
Figure 3-11	Extracted cross section (see Figure 3-7 for locations) comparisons of UAV-MS derived SfM point clouds (red) and UAV-LS point clouds (blue)	56
Figure 3-12	Difference in NDVI values across the study reach between September 2020 and February 2020 surveys.....	58
Figure 4-1	Study Site of the River Teme and the long term water level at the Knighton gauge station 3km downstream.	69
Figure 4-2	Vegetation trait extraction, from an individual raw point cloud to a cylindrical model and frontal area.	75
Figure 4-3	Random forest classifier out of bag accuracy and variations in band importance for guild classification.	79
Figure 4-4	Results from the decadal DSAS analysis.....	81
Figure 4-5	Historical analysis of avulsion development across the floodplain.....	82
Figure 4-6	PCA analysis of both herbaceous and tree guilds to investigate differences in trait characteristics.	84
Figure 4-7	Results of seasonal analysis (X-axis within subplots) of different reach scale metrics (Y-axis) from UAV-LS and UAV-MS data for each identified guild (X-axis).....	85
Figure 4-8	Resulting classification from reach scale analysis for the areas covered by both UAV-LS and UAV-MS data. Note the over classification of shrubs and bushes, especially at the edge of larger wooded guilds.....	87

Figure 4-9	Individual band importance in the final classification and confusion matrix from the accuracy assessment.....	88
Figure 4-10	Morphological change throughout the monitoring period, showing the spatial variation in erosion and deposition as well as the net change in sediment.	89
Figure 4-11	Bivariate classification of eco-geomorphic process form interactions, with examples highlighting the stabilising effect of vegetation.	94
Figure 4-12	The impact of undercutting within a heavily wooded reach, highlighting how the influence of vegetation on and interaction with flow changes through a plant's life cycle.	96
Figure 5-1	Model domain grid, monitoring locations, and water level inputs.....	103
Figure 5-2	How both erosion and deposition are accounted for in the various sublayers of the model domain.....	106
Figure 5-3	The sublayers used within the model setup to represent the likely composition across the floodplain, channel, and bars. Note that the relative depths of each layer are not to scale.	107
Figure 5-4	Image classification of riverbanks to obtain coarse sediment fraction percentage.....	108
Figure 5-5	Grainsize distribution plots for each of the three sample location sites and the combined final distributions.	109
Figure 5-6	Random forest classifier out of bag accuracy and variations in band importance for Manning's roughness land cover classes.....	113
Figure 5-7	Elevation changes across the study area for the entire modelling period for the different representation of vegetation with the model.....	118
Figure 5-8	Erosion and deposition that occurred during throughout the modelling run (in lighter shades) and those that occurred during the high flow event (in darker shades).....	120
Figure 5-9	Comparison of two new channel developments at separate locations (A and B) between the different Manning's based vegetation roughness approaches.	121

Table of Figures

Figure 5-10	Comparisons of depth averaged flow velocities (ms-1) across the study site, including channel and floodplain, for the peak flow event on the 21st January.	122
Figure 5-11	Comparison of erosion and deposition rates at two locations (A and C) based on the shear stress being exerted on a cell.....	124
Figure 5-12	Observed morphological change at the field site between September 2020 and June 2021, a time period comparable to the model run time.....	126
Figure 5-13	Image of the study site (model domain boundary approximated in red) during a flood event in February 2020.....	128
Figure 6-1	Comparison of vegetated cross sections for UAV-MS SfM derived point clouds (red) and from UAV-LS point clouds (blue).	135
Figure 6-2	Vegetation metric extraction technique introduced in Chapter 4, showing the processing routine taking a raw vegetation point cloud and producing cylindrical models and 2D frontal areas.	137

Research Thesis: Declaration of Authorship

Print name: Christopher Tomsett

Title of thesis: Assessing Eco-Geomorphic Interactions Across Scales Using Novel UAV Based Remote Sensing Techniques and Modelling

I declare that this thesis and the work presented in it are my own and has been generated by me as the result of my own original research.

I confirm that:

1. This work was done wholly or mainly while in candidature for a research degree at this University;
2. Where any part of this thesis has previously been submitted for a degree or any other qualification at this University or any other institution, this has been clearly stated;
3. Where I have consulted the published work of others, this is always clearly attributed;
4. Where I have quoted from the work of others, the source is always given. With the exception of such quotations, this thesis is entirely my own work;
5. I have acknowledged all main sources of help;
6. Where the thesis is based on work done by myself jointly with others, I have made clear exactly what was done by others and what I have contributed myself;
7. Parts of this work have been published as:
 - Tomsett, C. and J. Leyland (2019). "Remote sensing of river corridors: A review of current trends and future directions." River Research and Applications **35**(7): 779-803. <https://doi.org/10.1002/rra.3479>
 - Tomsett, C. and J. Leyland (2021). "Development and Testing of a UAV Laser Scanner and Multispectral Camera System for Eco-Geomorphic Applications." Sensors **21**(22): 7719. <https://doi.org/10.3390/s21227719>

Conceptualisation was undertaken by C.T. and J.L. Review of and data extraction from current literature was undertaken by C.T. Sensor development was done by C.T., with guidance provided by J.L. Field data was collected by C.T. and J.L. Error analysis, processing workflow, and code development was done by C.T. Modelling design by C.T. with guidance from J.L. Data processing, modelling and analysis of results was performed by C.T. Figure creation and editing was done by C.T. Original draft was prepared by C.T., subsequent reviews and edits by C.T. and J.L. J.L. has agreed to this declaration of authorship.

Signature:Date:.....

Acknowledgements

The completion of this thesis would not have been possible without the extensive support I have received throughout the past four years and beyond, for which I will be eternally grateful.

Firstly, I would like to thank my supervisor, Dr Julian Leyland. He has always been available to discuss ideas, keep me on track, improve me as a researcher, and has invested a significant proportion of his time into my research. From being taught and inspired as an undergraduate, through to my time as a PhD student, I have thoroughly enjoyed working with him and look forward to future projects together. More importantly, he has become a great friend who has supported me through difficult periods, offered words of wisdom, and never fails to find humour in any situation., all of which I am very thankful for.

I would also like to acknowledge the wider group of people in the Geography and Environmental Science department who have supported me, with countless members of staff offering words of advice, guidance on methods, and a friendly chat whenever needed. Thanks also to the technicians within the department who have helped with my project from day one, providing me with training and help in the field.

I have been incredibly lucky to undertake my PhD in a supporting environment filled with great people, many of whom have become great friends. Their countless support, motivation, and most importantly, being an outlet for my lunch time rants, has not gone unnoticed or unappreciated. I would like to thank all those who helped me on my fieldwork, especially to Andrea for his endless enthusiasm and commitment to joining me on expeditions to the River Teme. Thanks to Nathaniel, Luke, and Martin, for providing me with much amusement, technical advice, and for getting Leroy Lita to wish me luck. Thanks also to Rhys and Bhavik, both of whom have encouraged me to pursue and got me through my PhD. Through endless coffees, care packages, and catch ups, you have provided the support and guidance I needed.

None of this would be possible without my family, who have consistently supported me through all of life's endeavours and encouraged me throughout. Thank you for always being there when I need it the most, being a source of inspiration, and for getting me to this point.

Finally, a special mention goes to my best friend and wife, Jess, who has only ever supported me and ensured that this thesis could be completed. You have always been my biggest supporter, and throughout the past two years when things were at their hardest, you have kept me positive, happy, and smiling, bringing out the best in me and my work. Thank you for everything you have done for me, it has helped me more than you will ever know or believe.

Definitions and Abbreviations

ADCP	Acoustic Doppler Current Profiler
ADV	Acoustic Doppler Velocimeter
ALS.....	Airborne Laser Scanning
CHM	Canopy Height Model
DBH.....	Diameter at Breast Height
DEM	Digital Elevation Model
DTM	Digital Terrain Model
DLS	Downwelling Light Sensor
DSAS	Digital Shoreline Analysis System
GCP	Ground Control Point
GNSS	Global Navigation Satellite System
GPS	Global Positioning System
GSD	Ground Sampling Distance
IGS	International GNSS Service
IMU	Inertial Motion Unit
INS	Inertial Navigation System
MBES.....	Multi Beam Echo Sounder
MBO	Maximum Branching Order
MLS.....	Mobile Laser Scanner
MVS	Multi View Stereo
NDVI.....	Normalised Difference Vegetation Index
NDWI.....	Normalised Difference Water Index
PIV	Particle Image Velocimetry
PPK.....	Post-Processed Kinematic
PPS	Pulse Per Second

PCA.....	Principal Components Analysis
QSM.....	Quantitative Structural Modelling
RGB	Red Green Blue
RINEX	Receiver Independent Exchange Format
SAR	Synthetic Aperture Radar
SCE.....	Shoreline Change Envelope
SfM	Structure from Motion
SIFT	Scale Invariant Feature Transform
SSC	Suspended Sediment Concentration
TLS.....	Terrestrial Laser Scanning
UAV	Uncrewed Aerial Vehicle
UAV-LS.....	UAV Laser Scanning
UAV-MS.....	UAV Multi Spectral
USV.....	Uncrewed Surface Vehicle
UTC.....	Coordinated Universal Time

Chapter 1 Introduction

Despite the known influence of vegetation on flow and morphology, attempts to fully capture the structural variability of plants beyond patch scale have yet to be realised. This is necessary to enhance our understanding of eco-geomorphic feedbacks across a range of scales. The importance of vegetation in modulating geomorphic processes has been recognised across space and time and in nearly all Earth surface process domains (Istanbulluoglu and Bras, 2005; Corenblit and Steiger, 2009; Davies and Gibling, 2010; Corenblit *et al.*, 2011; Gurnell, 2014). The role of vegetation is broad, interacting with the climate and atmosphere, modifying soils and substrates, and directly influencing flows of matter and energy (Fig 1-1; Corenblit and Steiger (2009)).

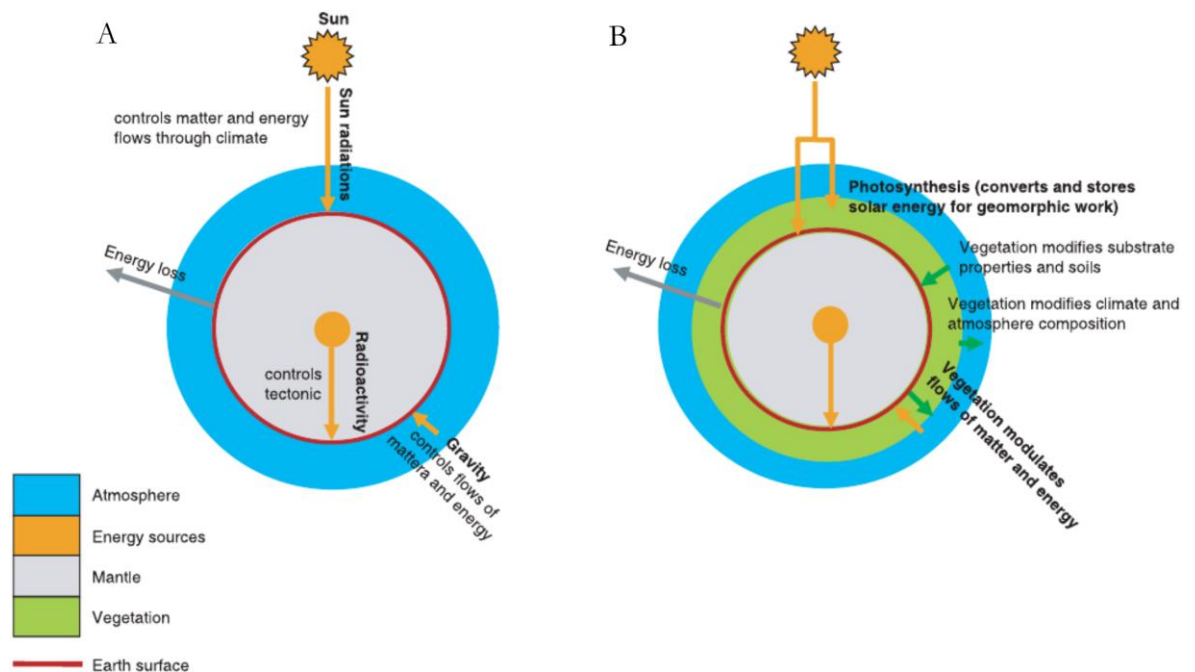


Figure 1-1 A comparison of a simplified Earth as an abiotic (A) and biotic (B) system as outlined in (Corenblit and Steiger, 2009). This highlights the importance of vegetation when considering geomorphological change and the various roles vegetation plays in shaping our landforms.

The focus of this research is on the latter of these, the role of vegetation in modulating fluid flows, herein specifically in the context of fluvial eco-geomorphic interactions. In relation to landscape modification by sediment mobilising flows of water, vegetation distribution and structure has been shown to dominate the resultant control that is exerted on landform production (Manners *et al.*, 2015; Diehl *et al.*, 2018; Butterfield *et al.*, 2020). Despite this, to date, little attention has been focused on trying to better characterise the complex structure of

vegetation through time and across the larger (10^0 - 10^1 km) spatial scales that are relevant to river catchment development.

1.1 Relevant Scales of Eco-Geomorphology

The four dimensional river system approach outlined by Ward (1989) discretised interactions along pathways in the upstream and downstream (longitudinal) dimension, channel to floodplain (lateral) dimension, channel to groundwater (vertical) dimension, and along the temporal (time) dimension. The first three dimensions can all change throughout the fourth dimension of time, based on interactions between each other. Many sub-disciplines are involved in the management and research of these dimensions through time, be it hydrologists, geomorphologists, ecologists, chemists, or engineers. Success in multidisciplinary approaches can be assessed based on how well these sub-disciplines combine to answer a specific lack of understanding (Pickett *et al.*, 1995). A significant component of the lateral dimension is the interaction between channel, banks, and the wider floodplain; which in turn is influenced by factors such as hydraulic conditions, underlying geology, and vegetation. These interactions themselves are nested across both temporal and spatial scales, with channel units ranging from the fine sub-feature scales through to landform scale basin systems, and vegetation ranging from individual vegetation components to complete community ecosystems (Thoms and Parsons, 2002). It is only through recognising that different components and sub-disciplines interact across a range of spatial and temporal scales that advances in understanding can be made. This is what makes eco-geomorphological research important, by accepting that hydrology influences ecology and morphology and vice versa, and through attempting to conduct research in a manner that seeks to include these feedbacks where possible in a holistic manner.

Vegetation can be analysed at a range of scales, from the effects of separate plant parts, individual plants, assemblages of plants, through to plant communities and entire ecosystems. The scales at which they are monitored are typically related to the processes and landforms which they influence. For example, the impacts of individual stems effect the magnitude of trailing turbidity, whereas plant assemblages aggregate this in to changes in flow conditions, and scaling to community and ecosystem scales effects floodplain connectivity and morphological response. However, creating links between these scales of analysis and the subsequent hydraulic influences is challenging, especially given the range of vegetation and hydraulic conditions that are present globally before the influences of local topography and soil properties are accounted for.

However, as vegetation is a key component of the river corridor, adequately accounting for its influence is necessary. Current research clearly demonstrates the variability in impact that different vegetation forms have on river corridors, and how differences in plant types have considerable impact on properties such as drag and soil cohesion. Although the measurement of single stems is relatively straight forward, branching structures and those with foliage are far harder to measure (James *et al.*, 2008), making it challenging to successfully discretise the effects of riparian vegetation. At the individual scale, plant height and vertical distribution play a key role in flow modulation, especially with the variable flow depths altering the fraction of plant biomass interacting with water (Nepf and Vivoni, 2000; Lightbody and Nepf, 2006). This is an important component not always accounted for, whereby the changing flow levels lead to changes in flow resistance, with different flow responses depending on the plants vertical structure. Depending on flow depths, plant frontal area and foliage may be altered, with foliated plants having larger surface areas that can exert a greater force for re-profiling during submergent flow (Järvelä, 2002b; Whittaker *et al.*, 2013). This reconfiguration can be accounted for by measuring the re-profiled frontal area (e.g. Vasilopoulos, 2017) or by reducing the coefficient of drag (Armanini, Righetti and Grisenti, 2005).

Below the surface, root strength and distribution can be used to infer binding strength and stability, and help to create more stabilised channels (Gran and Paola, 2001; Tal and Paola, 2007). The distribution of roots may be more influential than the root strength itself, leading to an overall increase in soil cohesion (Abernethy and Rutherford, 2001; Yu *et al.*, 2020). Matching above and below ground biomass is therefore necessary when examining individual plant impacts on flow and subsequent morphological change, as has been modelled by Caponi, Vetsch and Siviglia (2020). The importance of different plant structural features and foliage above and below ground is consistently noted by various authors, however their interactions at larger scales are just as important. The drag coefficients typically identified for a single plant are not comparable to those in patches of similar vegetation (James *et al.*, 2008), for example increases in drag coefficients are identified when increasing plant density (Kim and Stoesser, 2011) but clumping the same biomass in to areas of low and high density compared to an even distribution also effects flow (Sand-Jensen, 2008). Therefore, the spatial distribution of vegetation is just as important as the characteristics and density of vegetation patches themselves. Despite individual stems and their arrangements causing local variations in scour and trailing deposits (Follett and Nepf, 2012), it is at larger scales where the effect of vegetation on morphology becomes more apparent. This may manifest in changes in topography depending on the vegetation cover, with deposition increasing with a greater proportion of vegetation cover due to in increases in floodplain roughness (Gran and Paola, 2001; Bertoldi, Gurnell and Drake, 2011b). Heavily

vegetated channels also have an increased presence of large woody debris, having an influence on both in and out of channel morphology leading to increases in depositional landforms relative to non-blockaded channels (Jeffries, Darby and Sear, 2003; Sear *et al.*, 2010). The aggraded nature of root properties will also help to stabilise channels and switch reaches from braided to singular channels (Tal and Paola, 2007), therefore the depositional features caused by above ground roughness are matched with below ground stability to help create stabilised channels.

The complexities introduced by deciding what scales to analyse vegetation at for the purpose of a study are compounded by the temporally varying nature of vegetation. Seasonality is of great importance, especially considering flooding happens both during winter and summer months, with future projections of heavy rainfall events increasing for much of Europe suggesting a strong likelihood in increased flooding events (Douville *et al.*, 2021). Although seasonality of individual plants has somewhat been addressed by the comparison of foliated and defoliated stems (e.g. Wilson *et al.*, 2003; Vasilopoulos, 2017), seasonality has rarely been an explicit aim. Yet as these studies have shown, the inclusion of foliage not only affects flow, but also plant re-profiling, and as such the characteristics of the plant will change drastically between different seasons. Moreover, many of the plants studied are perennial herbaceous species that are not present year-round. Areas with seasonal vegetation are therefore likely to be experiencing different bulk roughness for different time periods, something that is not commonly accounted for. In channel monitoring showed peaks in determined Manning's n roughness values within early summer seasons associated with the channel coverage of macrophytes (Champion and Tanner, 2000), supported by Cotton *et al.* (2006) who found peaks in coverage from June and July led to increases in hydraulic roughness. Accounting for temporal variations in roughness led to a distinct improvement in correlation between observed and modelled water surface elevations (Song *et al.*, 2017), yet the use of temporal roughness elements are not standard. This may be due to difficulties in accurately discretising the floodplain vegetation, or from obtaining good quality seasonal data to assess the impacts seasonality has on vegetation presence, although efforts to improve parametrisation that include seasonality have been presented (Västilä and Järvelä, 2018). Yet, finding methods to transition from small scale, highly localised dynamics, to large scale seasonal vegetation coverage is a key research question. This will ensure that the modelling performed is both hydraulically relevant, computationally efficient, and applicable to real world scenarios, so that decisions made as a result are effective and supported by the science.

1.2 Characterising Vegetation Complexity

Discretising vegetation in models typically necessitates the use of a roughness parameter which can account for the effect of vegetation on the flow field. The use of Manning's n is a common approach to account for the effects of vegetation, having been assessed in numerous studies (Chow, 1959; Petryk and Bosmajian, 1975; Noarayanan, Murali and Sundar, 2012). Yet, this lumped approach groups many forms of resistance together into a singular value, eliminating the nuance and variability in vegetative drag. Manning's n is typically used in modelling to determine the variation in resistance across the domain (Cobby *et al.*, 2003b) with some models including a depth element to vary Manning's n based on flow depths (Anderson, Rutherford and Western, 2006) or a seasonal component (Kourgialas and Karatzas, 2013). However, these methods make assumptions on the characteristics of vegetation based on user interpretation of images or field inspection in conjunction with previously used values. This in essence ignores the actual function of vegetation, its complexity, and properties under various flow conditions, whereas characterisation of vegetation should be physically based (Jalonen *et al.*, 2014). Flume and field experiments have shown the variation in roughness at different flow depths and speeds, as well as from the resolution and methods of foliage frontal area discretisation (Järvelä, 2002b;2004; Västilä and Järvelä, 2014; Vasilopoulos, 2017). Therefore, it can be assumed that to fully account for the vegetation within a study site, a deeper perspective beyond broad classification of types and associated roughness values is likely required.

How researchers spatially discretise and map vegetation is therefore of considerable importance, and depending on the level of detail required, the purpose of the mapping, and the scale of the study, may ultimately influence research findings. Muller (1997) recognised an increased likelihood in the use of remote sensing for riparian vegetation and highlighted the need for increasing spatial resolution and spatially orientated classification algorithms. It was rightly pointed out that a single layer cannot represent all aspects of vegetation, and this is a problem that has persisted as to what scale should vegetation be measured. However, it was also noted that if the classification is based on sound scientific methods, then this may pave the way for broader uses. This has certainly been the case, with both high-resolution terrestrial and satellite-based methods allowing for ever increasing resolution of individual plants, as well as improved spatially complex and accurate reach scale mapping. Vegetation of multiple scales can now be classified from TLS (Terrestrial Laser Scanning) surveys in topographically complex environments (Brodu and Lague, 2012) and be subsequently analysed to reveal internal structures as well as vertical profiles which can be used for flow modelling and roughness estimates (e.g. Manners, Schmidt and Wheaton, 2013; Jalonen *et al.*, 2015; Vasilopoulos, 2017). However, Lague (2020) noted that given the fundamental role vegetation plays in eco-

geomorphic feedbacks that the use of such data had not been fully realised for the potential to resolve complex interactions between vegetation and flow. Likewise, the increasing spatial resolution of satellite imagery and extent of ALS (Airborne Laser Scanning) surveying has led to an increase in analysis of riparian vegetation for both classification problems (Yang, 2007; Antonarakis, Richards and Brasington, 2008b) as well more detailed analysis such as log jam monitoring (Bertoldi, Gurnell and Welber, 2013b; Abalharth *et al.*, 2015).

The above summarises how there have been great advances in our understanding of plant scale influences of flow and large-scale classifications of vegetation from remote sensing, yet there seems to be few attempts to cross these scales to apply local vegetation modelling to large scale datasets. Manners, Schmidt and Wheaton (2013) used their local scale TLS data to inform a larger scale model of vegetation frontal areas from ALS, and in forestry linking TLS to ALS has been used to verify large scale modelling methods (Lindberg *et al.*, 2012; Brede *et al.*, 2019), but fluvial applications are still less common. Advances in remote sensing technology and new approaches to classifying vegetation by looking beyond traditional hydrology methods may enable the improved understanding of our eco-geomorphic interactions. There is an area of research which is a missing link between our fine scale understanding, and the large-scale applications of this knowledge due to an inability to transfer this knowledge from one scenario to another. These eco-geomorphic feedbacks are variable and will depend on underlying factors such as climate, sediment, and morphology (Wiel and Darby, 2007), but better characterisation of vegetation via traits-based analysis may help to minimise this variability and improve applicability between similar reaches. This may also allow for improved calculation of roughness values or for the introduction of more explicit structural models in hydrodynamic modelling.

1.3 Thesis Aims and Research Questions

The aim of this research is to establish a new way of characterising vegetation to assess the role that it plays in modulating eco-geomorphic feedbacks across time and space. Specifically, the following Research Questions (RQ) will be tackled:

RQ1: What is the current state-of-the-art in river corridor remote sensing and how can it potentially be used to measure eco-geomorphic feedbacks?

RQ2: What properties of vegetation are important in relation to modulation of fluvial geomorphic change? Can these be readily measured and quantified using remote sensing, so that variations in vegetation and morphology can be readily assessed through space and time?

RQ3: Does how we represent vegetation in relation to complexity and temporal evolution in fluvial model domains matter? What can novel representations of vegetation tell us about the eco-geomorphic feedbacks of a river system?

1.4 Thesis Outline

The physical development and construction of a novel environmental sensing system was a key component of the NEXUSS DTP training programme. This DTP was specifically designed to utilise smart and autonomous observing systems to improve sustained and high-resolution observations to tackle environmental science challenges. This multi-disciplinary approach that crosses both environmental and engineering research is jointly funded by NERC and EPSRC and consequently this thesis exhibits elements from both of these approaches.

The thesis structure is centred around four papers that together tackle the central aim and Research Questions outlined above.

Chapter 2 (Paper 1, <https://doi.org/10.1002/rra.3479>) Tackles RQ1 in presenting an overview of the current river corridor surveying techniques and seeking to outline some of the challenges and opportunities that the research community face when using remote sensing to monitor the fluvial corridor.

Chapter 3 (Paper 2, <https://doi.org/10.3390/s21227719>) Tackles parts of both RQ1 and RQ2 in developing and testing the state-of-the-art Uncrewed Aerial Vehicle mounted sensing package that is used in papers 3 and 4. The accuracy of the developed system and consistency between surveys is assessed using ground control points and sections of stable ground. The benefits of the system are outlined with examples from the field site and potential applications introduced.

Chapter 4 (Paper 3, Submitted to Earth Surface Dynamics) Tackles RQ2 by establishing methods for extracting hydrologically relevant functional traits of vegetation using the developed UAV sensing package and linking these to geomorphic change to assess eco-geomorphic interactions over larger scales without the need for intensive ground-based fieldwork. The paper establishes the historical context and current patterns of morphological change within a study site by monitoring vegetation traits at high resolution over a year and a half field campaign. The spatial distribution of guilds is established for the study site using upscaling approaches from individual vegetation models. The connection between vegetation and morphology is then discussed, with the potential for the wider application of these methods highlighted.

Chapter 1

Chapter 5 (Paper 4, Intention to submit to Geomorphology/ESPL) Tackles RQ3 by using the novel traits-based vegetation classification to underpin the modelling approach of the study site. The spatial distributions of guilds identified in Paper 3 are used to parameterise the vegetation component of a 2D hydrodynamic model through space and time, with results compared to traditional bulk metrics that relate vegetation to a roughness parameter.

Chapter 6 concludes the work by revisiting the RQs and the challenges identified in Paper 1, outlining how future work might evolve, and considering the wider applications for eco-geomorphic research.

Chapter 2 Remote sensing of river corridors: A review of current trends and future directions

2.1 Abstract

River corridors play a crucial environmental, economic and societal role, yet also represent one of the world's most dangerous natural hazards, making monitoring imperative to improve our understanding and to protect people. Remote sensing offers a rapidly growing suite of methods by which river corridor monitoring can be performed efficiently, at a range of scales, and in difficult environmental conditions. This paper aims to evaluate the current state and assess the potential future of river corridor monitoring, whilst highlighting areas which require further investigation. We initially review established methods which are used to undertake river corridor monitoring, framed by the context and scales upon which they are applied. Subsequently we review cutting edge technologies which are being developed, focussed around UAV and multi-sensor system advances. We also 'horizon scan' for future methods which may become increasingly prominent in research and management, citing examples from within and outside of the fluvial domain. Through review of the literature it has become apparent that the main gap in fluvial remote sensing lies in the trade-off between resolution and scales. However, prioritising process measurements and simultaneous multi-sensor data collection is likely to offer a bigger advance in understanding than purely from better surveying methods. Challenges regarding the legal deployment of more complex systems, as well as effectively disseminating data into the science community are amongst those that we propose need addressing. However, the plethora of methods currently available means researchers and monitoring agencies will be able to identify suitable techniques for their needs.

2.2 Introduction

Rivers play a crucial environmental and societal role, providing food, water, nutrients, flood and drought mitigation, transport and potential energy, as well as providing habitats and supporting biodiversity that encourage recreational use (Postel and Richter, 2012). These ecosystem services are incredibly valuable, with freshwater resources contributing a significant component of the global natural capital (Costanza *et al.*, 1997). This explains why 82% of the world's population live on previously flooded land (Dilley *et al.*, 2005), whilst 87% have a river as their closest water body (Kummu *et al.*, 2011). Conversely, rivers can present a considerable hazard to those in their vicinity, primarily through flooding (Hirabayashi *et al.*, 2013). Flooding is identified as the most

dangerous natural hazard, accounting for 43% of all disasters between 1995-2015, with flood events likely to become more severe as a result of climate change (UNISDR and CRED, 2015). Alongside flooding, bank erosion represents a hazard to those communities who reside near river banks (Thakur, Laha and Aggarwal, 2012; Islam and Guchhait, 2017). However, world rivers are degrading in terms of water quality, sediment loads, and overall ecological diversity (Vörösmarty *et al.*, 2010). Simultaneously, increasing rates of change in land cover across floodplains are affecting the hydrological regime; impacting on ecology, erosion, and flooding (Gregory, 2006; Wasson *et al.*, 2010; Remondi, Burlando and Vollmer, 2016). It is therefore imperative to monitor river corridors to i) understand associated processes, ii) evaluate the nature of evolving hazards, iii) maintain ecological sustainability, and iv) to preserve their integrity as a resource for future generations.

For the purposes of this review, 'river corridors' can be defined broadly to include river channels, riparian zones, floodplains, and associated fluvial deposits, forming an overall classification framework which can be used to aid research and management (Harvey and Gooseff, 2015). The dynamic interactions across the river corridor are especially important in the context of applied river management, whereby a holistic approach is necessary. River corridor units feed into management strategies and applied research, covering areas including hydrological exchange (Malard *et al.*, 2002; Smith *et al.*, 2008; Harvey and Gooseff, 2015), ecosystem functionality (Stanford and Ward, 1993; Brunke and Gonser, 1997; Poole, 2002), monitoring of restored reaches (Bernhardt *et al.*, 2007; Kail *et al.*, 2007; Schneider *et al.*, 2011), and geomorphic evolution (Richards, Brasington and Hughes, 2002; Ollero, 2010; Magdaleno and Fernandez-Yuste, 2011).

Ultimately, we cannot view rivers as points or lines, but as spatially continuous mosaics of information (Fausch *et al.*, 2002). Remote sensing techniques provide the ideal solution for river corridor monitoring due to their non-intrusive nature, wide ranging spatial coverage, and repeatability. In order to fully understand the river corridor we need data that is continuous over various scales, with remote sensing being the ideal solution to achieve this, allowing us to test the theory that has been presented, and provide a basis for our understanding of the fluvial form. Over time, river corridor research has been transformed through technological advances making surveys more accurate, efficient, and resolute both spatially and temporally (Marcus and Fonstad, 2010; Entwistle, Heritage and Milan, 2018). Each advance in remote sensing allows subsequent progression in understanding. This enables novel research into the processes that are shaping river corridors, across scales ranging from grain dynamics to landform hydrological analysis. Herein, we define remote sensing in the broadest sense; as any relevant non-invasive form of data collection.

2.2.1 Review Structure

This review aims to outline both current and future methods which are employed to aid our understanding of the river corridor. Remote sensing offers multiple techniques for monitoring various components of the river corridor (Figure 2-1a). There are two key distinguishing factors that determine appropriate data collection techniques; i) the domain to which they are applied and ii) the spatial scale and resolution over which they are applicable. Herein we have structured the review around these key considerations, firstly revisiting the developments in river corridor remote sensing since the mid-20th century, before reviewing techniques across various domains, focussing within these on the scales over which methods are deployed. For the purposes of this review, we define the scales of monitoring based around the morphological units outlined in Figure 2-1b to provide a structure for the review and context for the following discussion. We also seek to highlight studies that combine multiple remote sensing techniques, such that they are developing new insight into river corridors before ‘horizon scanning’ to try and suggest a future agenda for the remote sensing of river corridors. Finally, we outline the key challenges that will need to be addressed in order for the techniques and methods identified to progress to a point where they can be broadly applied.

2.3 River Corridor Remote Sensing

2.3.1 A Brief History of Remote Sensing of River Corridors

In order to provide context for where we are, and where we may be heading, it is useful to know where we started in terms of remote sensing in the fluvial domain. During the 20th Century, researchers began using early forms of remote sensing by studying aerial photos to investigate fluvial morphology and the driving processes involved (Leopold and Langbein, 1966; Fairbairn, 1967; Kinoshita, 1967; Coleman, 1969). The launch of the Landsat program in 1972 led to a rapid uptake in remote sensing for fluvial research (Mertes, 2002), for example to identify former river channels (Ghose, Kar and Husain, 1979), investigate water quality and suspended sediment (Aranuvachapun and Walling, 1988), map flood hazards (Rango and Anderson, 1974), and understand the interactions between rivers and vegetation (Salo *et al.*, 1986). By the turn of the century, it was considered that data with a resolution of 1 m was classed as high resolution (Mertes, 2002), however this is no longer the case. Developments in ALS (Airborne Laser Scanning) facilitated high resolution collection of topographic data over large areas, allowing an improvement in the accuracy of data collected for applications such as flood modelling (Cobby, Mason and Davenport, 2001; Bowen and Waltermire, 2002; Ruiz *et al.*, 2002). The decision to stop degrading GPS data in 2000 facilitated more widespread use of remote sensing. Sub-surface

techniques more traditionally reserved for oceanic studies began to be used on fluvial systems for research in the early 2000's, with the deployment of Acoustic Doppler Current Profiling (ADCP) and Multi Beam Echo Sounding (MBES) methods (Shields *et al.*, 2003; Muste, Yu and Spasojevic, 2004; Parsons *et al.*, 2005). Further improvements in resolution, but with limiting spatial extent, came through the use of Terrestrial Laser Scanning (TLS) in the late 2000's (Heritage and Hetherington, 2007; Milan, Heritage and Hetherington, 2007), breaking through the previous limits of spatial resolution offered by ALS and that were alluded to by Mertes (2002). Finally, a proliferation in the use of Uncrewed Aerial Vehicles (UAVs) in recent years has allowed the collection of high resolution imagery from which dense models of the earth's surface are created over areas greater than achieved by TLS (Lejot *et al.*, 2007; Westoby *et al.*, 2012; Fonstad *et al.*, 2013).

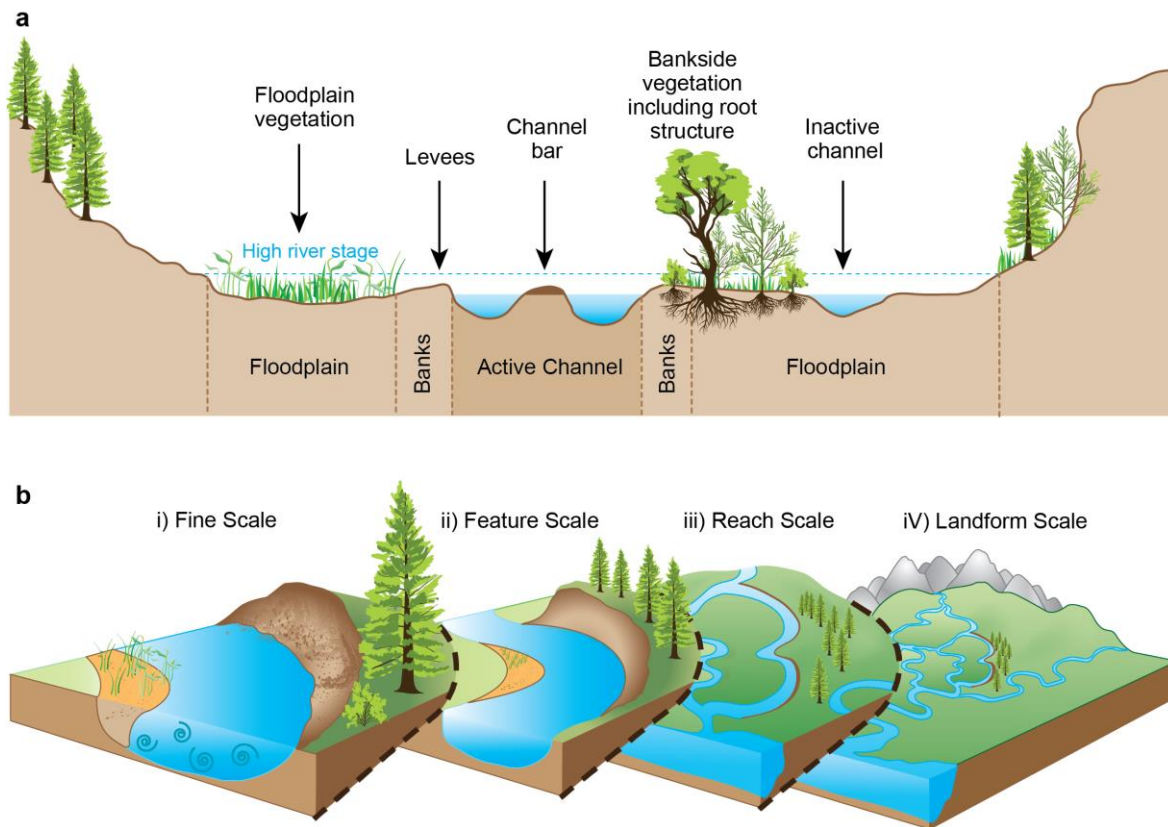


Figure 2-1 Key features and scales of the floodplain. a) The key natural features of a river corridor, including an active channel, floodplains, sediment deposits, relic channels, and vegetation components. b) A conceptual framework of river corridor scales across which we review research and applications herein, ranging from the (i) fine scale, (ii) feature scale, (iii) reach scale to the (iv) landform scale.

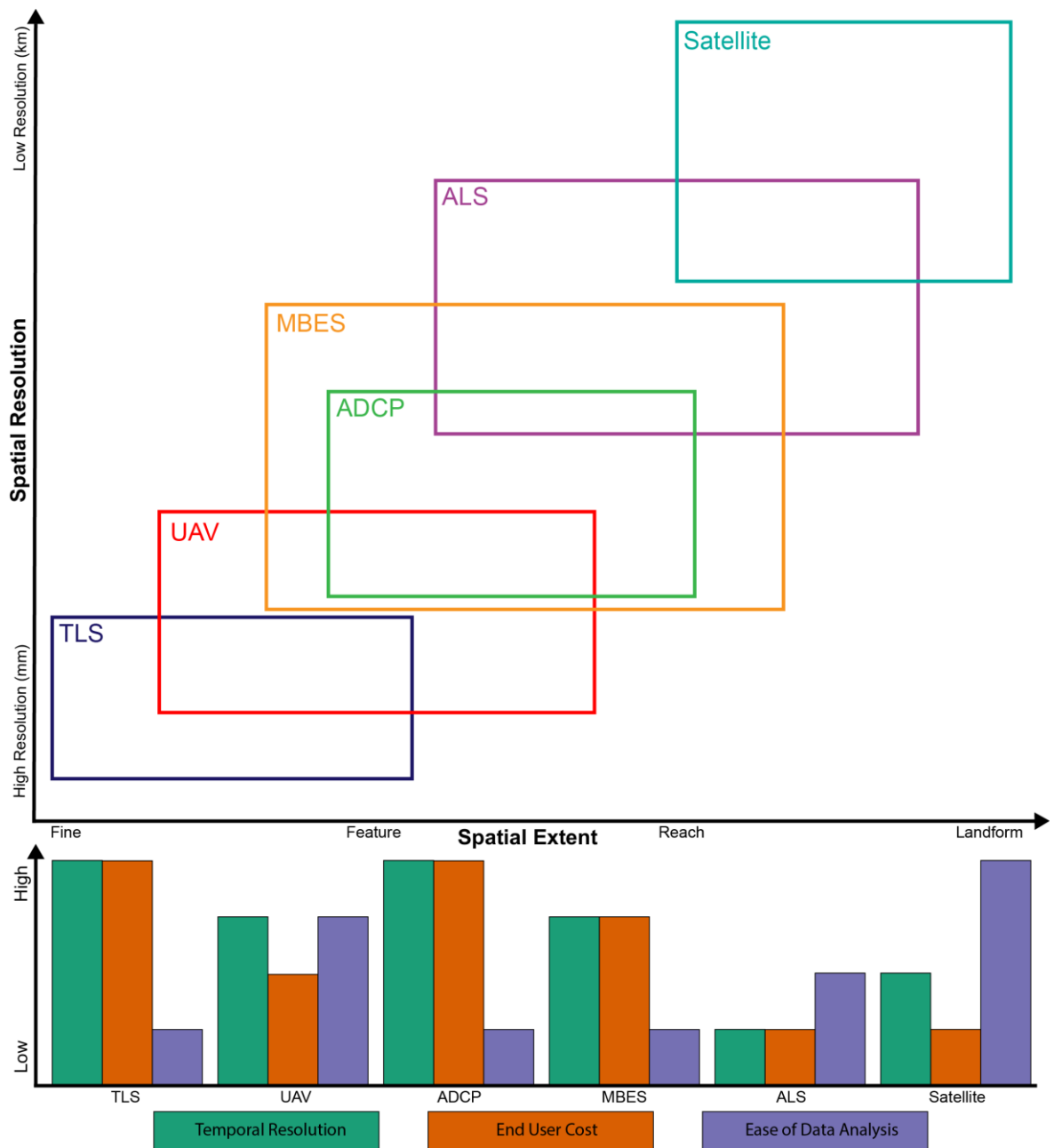


Figure 2-2 A comparison of the spatial resolution and extent of various common survey methods along with temporal resolution, end user cost, and ease of data analysis in the subsequent bar graphs. It should be noted that end user cost is based on typical examples, for example purchasing TLS equipment is expensive, whereas despite satellite data being expensive to produce, they are freely available in most circumstances. Despite ALS data being free in many circumstances to end users, it is limited in terms of temporal resolution and coverage, with further data collection being very expensive. The top panel was inspired by a similar concept developed in Figure 12 of Bangen, Wheaton, Bouwes, Bouwes, and Jordan (2014).

Whether or not there has been the genuine emergence of a sub discipline in river sciences devoted to remote sensing, as proposed by Marcus and Fonstad (2010), is perhaps open for debate. We would argue that the remote sensing tools reviewed herein and the associated technical developments that we highlight are used across many disciplines of river science, driven by a desire to better understand the physical processes at work and effectively manage these systems.

2.3.2 Current Monitoring Methods

One of the strengths of remote sensing lies in the broad range of temporal and spatial extents over which methods can be applied (Figure 2-2). However, there is no ‘perfect technique’, with factors such as cost, scale, and repeatability all playing an important role in determining the most appropriate method for a user (Figure 2-2). Many of the methods used have been thoroughly reviewed and can be used to inform researchers for deployment and processing, e.g. UAV imagery (Westoby *et al.*, 2012), TLS (Telling *et al.*, 2017), ALS (Hofle and Rutzinger, 2011), ADCP (Muste, Yu and Spasojevic, 2004), MBES (Jha, Mariethoz and Kelly, 2013), as well as comparing between methods for bathymetric modelling (Kasvi *et al.*, 2019). However, the aim of this review is not to provide a methodological overview, but rather to evaluate the range of applications and how each approach can enhance our understanding of the river corridor.

2.3.2.1 Roughness and Grain size

Bed and bank studies have predominantly utilised statistical analysis of dense point clouds to extract roughness metrics. TLS has primarily been used to examine fine scale roughness due to the high point density, for example in exploring gravel bars (Heritage and Milan, 2009), variations in roughness pre- and post-flood (Picco *et al.*, 2013), roughness across differing climatic drivers (Storz-Peretz *et al.*, 2016), and bank skin drag coefficients (Leyland *et al.*, 2015). Importantly, research into how scan locations and grid cell size impacts roughness calculations has been undertaken to improve deployment (Baewert *et al.*, 2014) and examining the potential for bed roughness extraction with through water laser scanning has expanded the versatility of TLS (Smith, Vericat and Gibbins, 2011).

Over larger spatial domains, roughness tends to be derived from overhead imagery. Structure from Motion (SfM) techniques have been used for roughness calculations in flume experiments (Morgan, Brogan and Nelson, 2017; Pearson *et al.*, 2017) as well as field studies (Smith and Vericat, 2015; Woodget and Austrums, 2017; Piton *et al.*, 2018) and river restoration analysis (see Figure 2-3, (Marteau *et al.*, 2017)). UAV SfM therefore provides the ability to upscale the spatially limited static terrestrial based methods to feature and reach scales. Currently, calculating

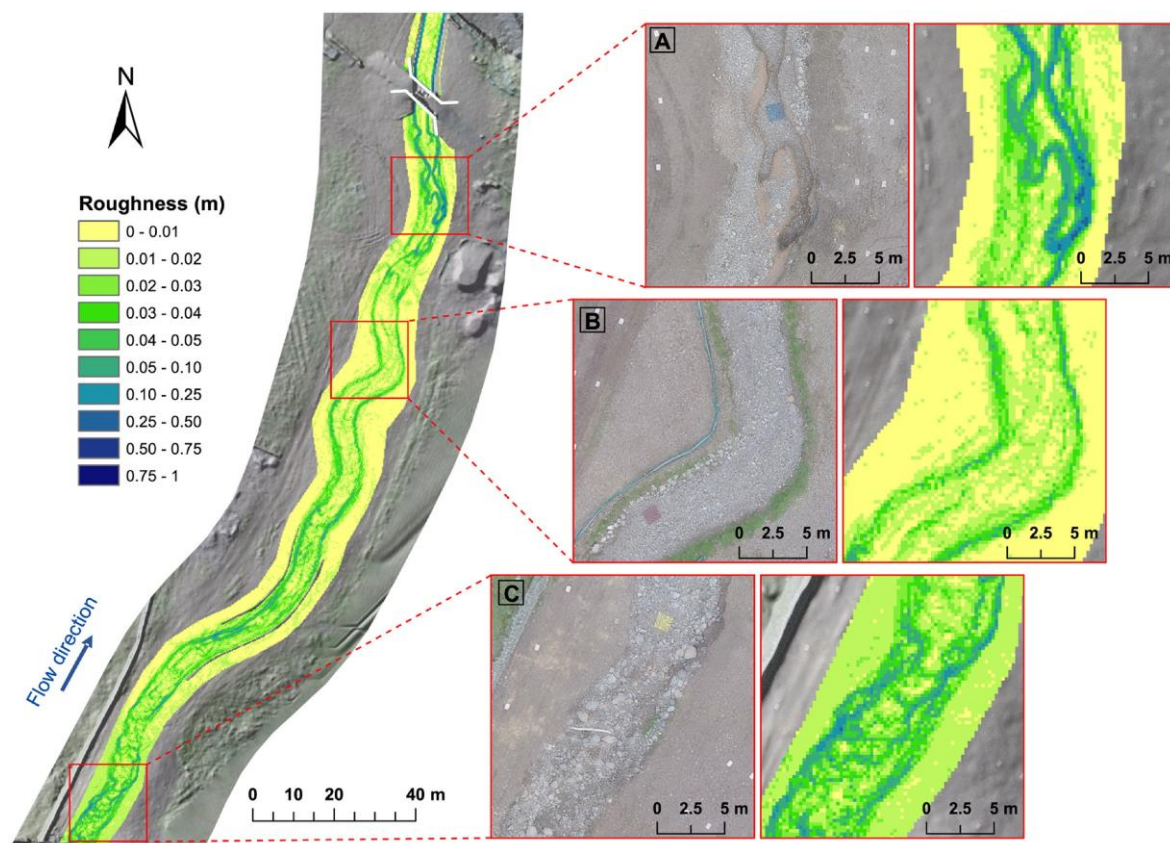


Figure 2-3 An example of roughness calculations performed across a restored channel. SfM methods were used to obtain a DEM before using detrended standard deviation values to obtain surface roughness. Repeat surveys allow the change in roughness to be monitored through time as the channel adjusts. Such results can be used to highlight processes such as channel margin sorting, as well as be fed back into hydrodynamic modelling. This presents an example of how high-resolution roughness can be scaled up to analyse reach scale process and form interaction. Reprinted from ‘Application of Structure-from-Motion photogrammetry to river restoration’, by Marteau et al. (2017).

roughness over large areas is time consuming and further compounded by SfM data suffering from smoothing effects (Smith and Vericat, 2015; Cook, 2017). Yet, ever increasing computer power may help extensive, high resolution, roughness models become more feasible.

Below water, MBES techniques are predominantly used for bathymetric topography, although research by both Guerrero and Lamberti (2011) and Konsoer *et al.* (2017) utilised MBES data to investigate bed roughness across a range of study sites. Despite the methods not being fully explored, MBES data may provide insight into bed and bank roughness across reach scales and greater.

Grain size is somewhat harder to extract. Traditional image-based methods relate image texture to grain size (Carbonneau, Bergeron and Lane, 2005; Graham, Rice and Reid, 2005). More recent methods exploit SfM topography with high resolution imagery (0.0015 m pixel size) from low flight heights (Langhammer *et al.*, 2017) and through relationships between roughness and in field grain size measurements (Woodget and Austrums, 2017; Carbonneau, Bizzi and Marchetti, 2018). Work by Woodget, Fyffe and Carbonneau (2018) demonstrated how image texture on a series of individual images outperformed orthomosaics and SfM roughness measures. However, derived relationships may struggle in poorly sorted reaches (Pearson *et al.*, 2017) and where sediment placement is irregular, causing the axis of measurement to be inconsistent.

TLS produces data volumes similar to those from SfM and thus is hampered by similar processing constraints. The technique has been successfully used to investigate grain size packing distribution (Hodge, Brasington and Richards, 2009), variations between systems (Storz-Peretz *et al.*, 2016), submerged grain size (Smith, Vericat and Gibbins, 2011), and grain size on large, complex gravel systems using Mobile Laser Scanning (MLS) (Wang *et al.*, 2011a). Through-water TLS is ineffective for deeper channels, where instead, MBES data has been used to infer grain size using statistical inference techniques (Snellen *et al.*, 2013; Eleftherakis *et al.*, 2014). However, the extensive calibration involved and limited spatial applicability restricts the scale of application over which the methods can be used.

2.3.2.2 Flow Characteristics

Both Acoustic Doppler Velocimeters (ADV) and ADCPs are used to investigate flow dynamics. The former is used to primarily investigate flow characteristics such as velocity and turbulence in both flume (Lawless and Robert, 2001; Schindler and Robert, 2005; Buffin-Belanger *et al.*, 2006; Abad and Garcia, 2009) and field setups (Lane *et al.*, 1998; Buffin-Belanger and Roy, 2005; Strom and Papanicolaou, 2007; Wilcox and Wohl, 2007). Likewise, ADVs have also been used to investigate applied management problems such as weir construction (Bhuiyan, Hey and Wormleaton, 2007) and the effects of ship wakes on near bank flow (Fleit *et al.*, 2016). However, the requirement for a static deployment somewhat limits their application beyond fine scales.

Across feature and reach scales, ADCP sensors can be used to better understand flow dynamics; such as investigating the influence of surface ice on vertical separation and helical flow structures (Lotsari *et al.*, 2015), the complex flow properties in the Mekong (Hackney *et al.*, 2015), better calibration of a Delft3D flow model (Parsapour-Moghaddam and Rennie, 2018), as well as river confluence mixing processes (Gualtieri *et al.*, 2018). At the reach scale, ADCPs have been used

to investigate flow variation through dynamic morphological systems (Guerrero and Lamberti, 2011), flow interaction with dune bed morphology (Parsons *et al.*, 2005), and flow patterns through a variety of meandering, straight, and abandoned channels (Shields *et al.*, 2003). With increasing portability and potential platform autonomy (Flener *et al.*, 2015), the deployment versatility of such sensors is likely to improve further beyond their already extensive range of deployment opportunities.

Field based Particle Image Velocimetry (PIV) operates over smaller spatial extents, tracking tracer particles in a fluid over interrogation windows using pattern recognition (Adrian, 1991; Detert and Weitbrecht, 2015). Most systems are static for continual monitoring (Creutin *et al.*, 2003; Jodeau *et al.*, 2008; Gunawan *et al.*, 2012), yet advances in positional and attitudinal data has allowed helicopters (Fujita and Hino, 2003; Fujita and Kunita, 2011) and more recently UAVs (Detert and Weitbrecht, 2015; Tauro *et al.*, 2015; Bolognesi *et al.*, 2017; Thumser *et al.*, 2017) to improve spatial coverage. The method shows promise, producing velocity measurements within 5-8% of those measured from total station tracking (Bolognesi *et al.*, 2017). Future work is looking to eliminate the need for artificial tracers and create a more versatile methodology (Charogiannis, Zadrazil and Markides, 2016; Legleiter, Kinzel and Nelson, 2017; Thumser *et al.*, 2017), which would likely result in more widespread use of PIV as a field based method.

Over larger spatial scales, calibrating against river width has allowed satellite sensors to provide discharge to within 10% of observed values (Bjerklie *et al.*, 2005). To overcome issues with box channels, whereby river width does not increase with discharge, it is possible to use river island size for calibration (Feng *et al.*, 2012). However, the sensitivity of the method is limited by the pixel resolution of the satellite image.

2.3.2.3 Water Quality

Static ADV and ADCP deployments are able to be used to estimate Suspended Sediment Concentrations (SSC) in the water column through use of acoustic backscatter under laboratory (Schindler and Robert, 2004; Ha *et al.*, 2009) and field conditions (Elci, Aydin and Work, 2009; Chanson *et al.*, 2011; Leyland *et al.*, 2017). Likewise, the acoustic backscatter from MBES sensors can be used to infer SSC, having been tested in controlled and field conditions (Simmons *et al.*, 2010; Simmons *et al.*, 2017), providing the opportunity to collect SSC data across feature and reach scales, yet their use is not currently widespread.

At the reach scale and beyond, estimates of SSC require the use of satellite imagery. Medium resolution imagery (20-30 m) has been used to investigate SSC at the confluence of the

Mississippi and Missouri Rivers, both of which have differing sediment regimes (Umar, Rhoads and Greenberg, 2018), as well as along the Yangtze (Wang *et al.*, 2009). However, the majority of studies tend to use coarser (250 m) MODIS data focussing on large, well gauged, rivers such as the Yangtze (Wang and Lu, 2010), the Amazon (Mangiarotti *et al.*, 2013; Santos *et al.*, 2018), the Changjiang (Lu *et al.*, 2006) and the Solimoes (Espinoza-Villar *et al.*, 2018), utilising statistical relationships between observed SSC values with red and infra-red spectral bands. However this method is limited to those rivers with continual monitoring of discharge and suspended sediment and large enough to be observed from satellites, therefore alternative methods are required across smaller extents.

Despite water quality estimates derived from remote sensing being well established in estuarine and coastal zones (Brando and Dekker, 2003; Hellweger *et al.*, 2004; Chen, Hu and Muller-Karger, 2007), it is less well developed in the fluvial domain. However, efforts have been made to obtain fluvial water quality data from UAV imagery, such as pollution detection (Lega and Napoli, 2010; Lega *et al.*, 2012). Attempts to replicate satellite data procedures relating spectral data to chlorophyll-a, Secchi disc depth, and turbidity with UAV imagery have been limited in success (Su, 2017; Larson *et al.*, 2018). Regardless, the increasing use of UAVs in river corridor monitoring will likely improve methods for water quality monitoring.

2.3.2.4 Morphology

By far the largest volume of research in river corridor monitoring relates to the measurement and monitoring of morphology through the production of Digital Elevation Models (DEMs). Applications of modern data collection techniques such as TLS and SfM now outweigh traditional point based survey techniques in the literature. These new techniques are particularly well suited for surveying of small features which typically demand high accuracy, high resolution data, to detect small changes between surveys.

TLS enables users to overcome the spatial limitations of cross-sectional surveys, especially in the downstream direction, through increased point density (Resop and Hession, 2010; O'Neal and Pizzuto, 2011). Analysis such as creating DEMs of difference (DoDs), comparing voxel models, and point cloud analysis have all utilised TLS data for investigating morphological evolution (Milan, Heritage and Hetherington, 2007; Heritage and Milan, 2009; Resop and Hession, 2010; O'Neal and Pizzuto, 2011; Starek *et al.*, 2013; Leyland *et al.*, 2015). The advent of MLS has enabled these studies to expand beyond the typical spatial constraints of TLS, producing high resolution datasets across reach scales (Alho *et al.*, 2009; Lotsari *et al.*, 2015; Leyland *et al.*, 2017).

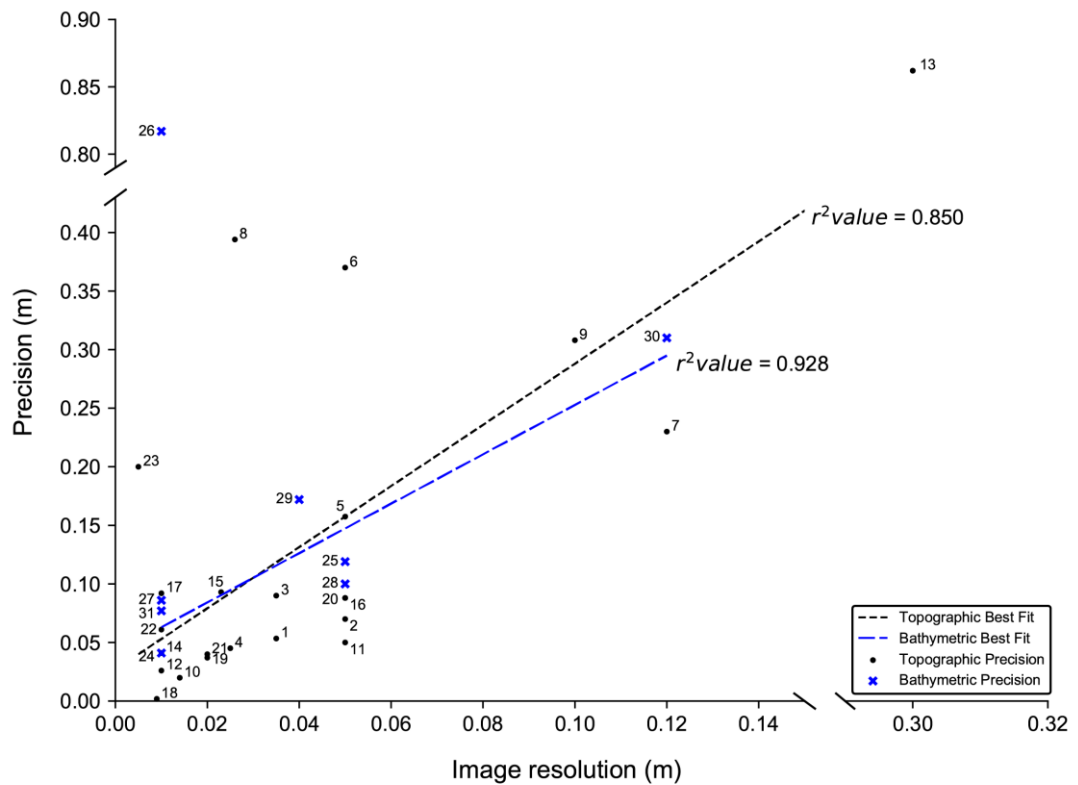


Figure 2-4 The relationships between survey imagery resolution from UAV aircraft and the geospatial precision (based off of RMSE and standard deviation values) for both topographic and bathymetric surveys. Note the higher r^2 value for bathymetric data is due to the exclusion of outlier point number 26 and the relatively fewer number of studies in this area. The X and Y axis are broken in order to focus on where the data points are clustered. The numbers alongside data points refer to the publications from which data was extracted for the plot, with some papers citing both topographic and bathymetric precisions as well as multiple test sites and are therefore included twice: 1. Brunier et al. (2016) 2. Vericat, Brasington, Wheaton, and Cowie (2009) 3. Coveney and Roberts (2017) 4. Casado et al. (2016) 5. Lejot et al. (2007) 6. Dietrich (2016) 7. Javernick et al. (2014) 8. Cook (2017) 9. Smith and Vericat (2015) 10. Watanabe and Kawahara (2016) 11. Van Iersel et al. (2016) 12. Tournadre, Pierrot-Deseilligny, and Faure (2014) 13. Young et al. (2017) 14. Bagheri et al. (2015) 15. (Mirijovsky, Michalkova, Petyniak, Macka, & Trizna, 2015) 16. A. D. Tamminga et al. (2015) 17. Woodget et al. (2017) 18. Woodget et al. (2015) 19. Miřijovský and Langhammer (2015) 20. A. Tamminga et al. (2015) 21. Jaud et al. (2016) 22. Dietrich (2017) 23. Clapuyt, Vanacker, and Van Oost (2016) 24. Bagheri et al. (2015) 25. A. Tamminga et al. (2015) 26. Woodget et al. (2017) 27. Woodget et al. (2015) 28. A. D. Tamminga et al. (2015) 29. Shintani and Fonstad (2017) 30. Javernick et al. (2014) 31. Dietrich (2017).

UAV imagery produces data at similar resolutions to TLS, usually with lower accuracy (see Figure 2-4) but covering larger areas. The ease of setup and data collection makes it an ideal tool for repeat surveying, which allows work to be carried out over specific time intervals such as on seasonal or annual cycles (Mirijovsky and Vavra, 2012; Flener *et al.*, 2013; Miřijovský and Langhammer, 2015; Smith and Vericat, 2015; Brunier *et al.*, 2016; Cook, 2017; Marteau *et al.*, 2017) as well as targeting specific high discharge events (Tamminga, Eaton and Hugenholtz, 2015; Watanabe and Kawahara, 2016). It is also possible to use UAV derived topographic models to classify geomorphic features such as new versus old gravel accumulations (Langhammer and Vackova, 2018), showing some potential beyond morphological change detection which future work might pursue.

To capture larger reach and landform scale morphology currently requires the use of ALS or satellite imagery. At the reach scale, ALS has been combined with historical topographic data (De Rose and Basher, 2011; James *et al.*, 2012), used to monitor planform shift (Lallias-Tacon, Liebault and Piegay, 2014), and assessed the potential for gully erosion (Perroy *et al.*, 2010). Likewise, this data can also be used to classify channel characteristics such as riffle, pool, and step sequences (Marchamalo *et al.*, 2007; Cavalli *et al.*, 2008), identify features such as alluvial fans and river terraces (Jones *et al.*, 2007), as well as automate channel network and geometry extraction (Passalacqua *et al.*, 2010). Landform scale studies do exist, with studies on the Mississippi River (Kessler *et al.*, 2012), the Lockyer Creek (Croke *et al.*, 2013), and the Blue Earth River (Thoma *et al.*, 2005), all utilising readily available LiDAR data to analyse morphological evolution, but they are often limited to regions with the financial capabilities to collect ALS data.

Satellite data analysis and application has typically been limited to large rivers such as the Ganges and Brahmaputra (Baki and Gan, 2012; Hossain, Gan and Baki, 2013), the Mekong (Kummu *et al.*, 2008), the Jamuna (Baki and Gan, 2012), the Yellow River (Chu *et al.*, 2006), and the Selawik and Yukon (Rowland *et al.*, 2016) due to limited pixel resolution. Uses of satellite imagery include automatic calculation of river widths based on classified centrelines (Pavelsky and Smith, 2008; Yamazaki *et al.*, 2014) as well as analysing the relationship between river width and multiple variables across a range of rivers wider than 90 m with discharge values between 100 to 50,000 m³s⁻¹ using Landsat imagery (Frasson *et al.*, 2019). Satellite data can also be used to identify channel networks much like ALS (Isikdogan, Bovik and Passalacqua, 2015) and also monitor channel reactivation through the use of Synthetic Aperture Radar (SAR) (Jung *et al.*, 2010; Oyen *et al.*, 2012). However, recent and future improvements in satellite image resolution will expand the potential of this method to smaller systems (Khorram *et al.*, 2016).

The methods above focus on subaerial analysis, as despite the subsurface being equally important, it is considerably more challenging to measure. At fine scales, through-water laser scanning shows potential in acquiring bed morphological data, requiring careful calibration for optimal results (Deruyter *et al.*, 2015). However there is evidence to suggest that increasing depths reduce accuracy due to laser attenuation (Smith, Vericat and Gibbins, 2011). Similarly, surface instability and sediment concentration have been shown to have an even greater impact on accuracy (Smith and Vericat, 2014).

Similarly, both spectral depth techniques (Lejot *et al.*, 2007; Legleiter, 2012; Javernick, Brasington and Caruso, 2014; Tamminga *et al.*, 2015; Tamminga, Eaton and Hugenholtz, 2015; Shintani and Fonstad, 2017) and through water SfM (Javernick, Brasington and Caruso, 2014; Bagheri, Ghodsian and Saadatseresht, 2015; Woodget *et al.*, 2015; Dietrich, 2017; Shintani and Fonstad, 2017) from UAV imagery can be used to collate high-resolution bathymetric datasets. The latter relies on clear water for optimal results whilst the former relies on higher SSC to produce variations in spectral reflectance. Whilst no method clearly outperforms the other, it is apparent that choosing an appropriate technique is site and condition dependent.

Currently, reach and larger scale bathymetric surveying relies heavily on boat based MBES systems which can operate in a wide range of water conditions, being used extensively for research into the morphology of river beds and their interactions with flow dynamics (Carling *et al.*, 2000; Parsons *et al.*, 2005; Best *et al.*, 2010; Guerrero and Lamberti, 2011; Hackney *et al.*, 2015; de Almeida *et al.*, 2016; Leyland *et al.*, 2017).

Alternatively, green wavelength ALS can collect bathymetry over lengths from one to tens of kilometres (Kinzel *et al.*, 2007; Hildale and Raff, 2008; Kinzel, Legleiter and Nelson, 2013), yet footprint size which reduce accuracy and point density are limiting factors (Tonina *et al.*, 2019). Despite these methods being available, the extra challenge in obtaining them makes bathymetric analysis less prominent in the literature. There has also been promise in using light aircraft to fly imaging sensors such as the Compact Airborne Spectrographic Imager (CASI) which are capable of collecting bathymetric data up to depths of 10 m in clear waters with errors in the region of 0.2 m (Legleiter *et al.*, 2016; Legleiter and Fosness, 2019)

2.3.2.5 Vegetation

Vegetation is present across all river corridor domains, whether interacting with flow, influencing bank stability, or contributing to floodplain roughness. At fine scales, resolving the spatial extent of vegetation and discretising vegetation structure are crucial for establishing hydraulic roughness. The reasonable canopy penetration and high spatial resolution makes TLS

methods favourable. TLS based voxel models in combination with flume tests are used to analyse plant drag and motion, highlighting differential flows in the canopy and sub-canopy layers (Boothroyd *et al.*, 2017; Vasilopoulos, 2017). TLS has also been used to identify leafless Manning's *n* values for different species across various flow scenarios (Antonarakis *et al.*, 2009), investigate spatially variable flow dynamics at differing depths due to submerged riparian vegetation (see Figure 2-5, (Manners, Schmidt and Wheaton, 2013)), and provide a link between vegetation roughness and subsequent trailing bar morphology (Bywater-Reyes, Wilcox and Diehl, 2017). Identifying and quantifying areas of vegetation at the fine scale is important for applying drag coefficients, with Brodu and Lague (2012) successfully classifying TLS scans whilst Jalonen *et al.* (2015) identified and calculated woody area from voxel models. For larger areas, boat based MLS may provide opportunities for improved bank vegetation models (Alho *et al.*, 2009; Saarinen *et al.*, 2013).

UAV imagery has been used to monitor changes in vegetation pre- and post-flood (Watanabe and Kawahara, 2016), for investigating floodplain grassland phenology (Van Iersel *et al.*, 2016) and to improve habitat classification (Casado *et al.*, 2016; Rapple *et al.*, 2017; Woodget *et al.*, 2017). However, it is less useful for characterising individual vegetation structure, requiring multiple surveys in leaf on and off conditions (Dandois *et al.*, 2017).

ALS shows the greatest utility in river corridor vegetation monitoring. At reach scales, ALS has been used for riparian zone classification (Gilvear, Tyler and Davids, 2004; Antonarakis, Richards and Brasington, 2008a; Michez *et al.*, 2013), assessment of wood and debris retention (Bertoldi, Gurnell and Welber, 2013a; Abalharth *et al.*, 2015), upscaling from TLS models (Manners, Schmidt and Wheaton, 2013), creating rainfall interception models (Berezowski *et al.*, 2015), as well as for linking vegetation to morphological and anthropogenic contexts and needs (Bertoldi, Gurnell and Drake, 2011a; Cartisano *et al.*, 2013; Picco *et al.*, 2017). At landform scales, ALS has been used to identify sources and volumes of woody debris (Kasprak *et al.*, 2012), the health of riparian ecosystems (Michez *et al.*, 2013), the influence of vegetation on groundwater connectivity (Emanuel *et al.*, 2014), bank stability (McMahon *et al.*, 2017), and water temperature through shading (Greenberg *et al.*, 2012; Wawrzyniak *et al.*, 2017; Loicq *et al.*, 2018). ALS therefore contributes heavily to our understanding of riparian vegetation, and despite potential drawbacks such as cost and mobilisation, is a key method to consider for monitoring activities.

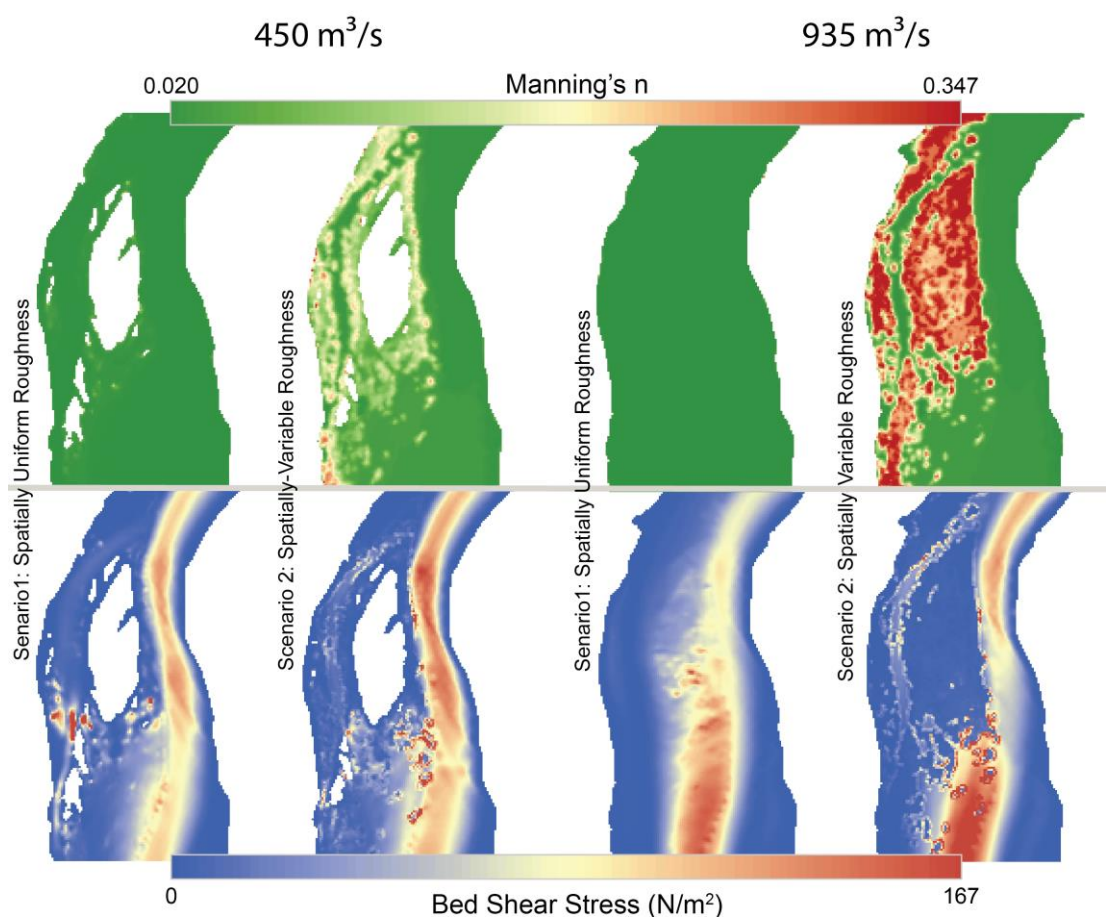


Figure 2-5 The effects of including spatially variable roughness across two discharge magnitudes on bed shear stress. Roughness variation was derived from using plant scale TLS scans that were upscaled to LiDAR datasets to provide better informed roughness parameterisation when compared to spatially uniform measures. The differences in bed shear stress as a result of using spatially variable roughness highlights the importance of accounting for individual vegetation form and the subsequent impacts this can have on river morphology. Reprinted from ‘Multiscalar model for the determination of spatially explicit riparian vegetation roughness’, by Manners et al. (2013).

Most studies utilising satellite data create classifications (e.g. Yang (2007)) before investigating the temporal dynamics of vegetation, studying agricultural pressures (Apan, Raine and Paterson, 2002; Jupiter and Marion, 2008), differing seasons (Makkeasorn, Chang and Li, 2009; Wang *et al.*, 2011b) and deforestation (Macedo *et al.*, 2013) for example. Moreover, vegetation indices can be used to construct relationships between plant traits and spectral imagery. The Enhanced Vegetation Index (EVI) has been used to quantify evapotranspiration for mixed structure riparian forests (Nagler *et al.*, 2005), the Normalised Difference Vegetation Index (NDVI) can be related to surface and groundwater (Fu and Burgher, 2015) or floodplain vegetation health

and heterogeneity (Wen, Yang and Saintilan, 2012), and the Vegetation Disturbance Index (VDI) can identify areas prone to gully rejuvenation after wildfires (Hyde *et al.*, 2016).

By combining datasets, ALS and airborne imagery aided understanding of the ecological health of riparian vegetation over 12,000 km², identifying key areas that required ecosystem health management (Michez *et al.*, 2017). Likewise, high resolution (2.4 m) Quickbird imagery and ALS data has contributed towards the production of hydrodynamic roughness models which are comparable with those obtained through traditional methods (Forzieri *et al.*, 2010; Forzieri *et al.*, 2011), as well as to improving riparian vegetation classification across landform scales (Arroyo *et al.*, 2010a). The structural and intensity data provided by ALS provides a good trade-off between requisite detail and spatial coverage (Johansen, Phinn and Witte, 2010), despite the low temporal resolution which limits such studies to specific time intervals (Figure 2-2).

2.3.2.6 Flooding

Flooding is an important physical process that facilitates channel-floodplain connectivity as well as posing an environmental hazard. Remote sensing provides data through which we can better understand, predict, and monitor flood events, across a range of scales.

Perhaps the most common flood relevant dataset that is produced is the DEM. Despite DEMs commonly being created for reach scale (and larger) flood models, high resolution DEMs have helped to improve local flood modelling in Glasgow compared to historical datasets (Coveney and Roberts, 2017) and local flood models produced for a rural village in the Apuseni Mountains, Transylvania, using a low cost setup to assess risk to a local school (Şerban *et al.*, 2016). Despite no model validation in the latter case, it demonstrates the potential to improve understanding in typically low priority locations.

Despite small scale studies existing (e.g. Cavièdes-Voullième *et al.* (2013)), it is more common for flood models to use ALS data over large areas to provide topographic information (Fang *et al.*, 2010; Castellarin, Di Baldassarre and Brath, 2011; Karim *et al.*, 2012; Heritage *et al.*, 2019), providing the optimum trade-off between detail and coverage. Improvements in satellite derived elevation models such as those from TanDEM-X (12 m resolution) also opens the possibility for larger scale DEMs for flood modelling (Krieger *et al.*, 2007). ALS can be utilised to parameterise floodplain roughness in conjunction with satellite imagery (Straatsma and Baptist, 2008) and importantly allow for better mesh discretisation to account for local variations in roughness (Cobby *et al.*, 2003a). Satellite imagery is also typically used as a calibration and validation method (Di Baldassarre, Schumann and Bates, 2009) as well as for flood boundary delineation which often utilises SAR interferometry to overcome cloud cover (Horritt, Mason

and Luckman, 2001; Townsend, 2001; Frappart *et al.*, 2005; Martinez and Le Toan, 2007; Kuenzer *et al.*, 2013; Martinis, Kersten and Twele, 2015), although there are examples using spectral imagery (Proud *et al.*, 2011; Amarnath, 2014; Kuenzer *et al.*, 2015). Due to the scales commonly used in modelling applications and associated calibration and validation, this is likely to remain the most common technique for reach and landform scale studies.

2.3.3 Real-World Cross-Scale Applications

It is clear from the review above that remote sensing techniques are widely used across a range of domains in the river corridor, but that most of the examples cited relate to research applications. However, there are numerous examples of these techniques being transferred to applied contexts. For example, many nations now routinely collect ALS data to create national datasets of topography that can be easily accessed by the public (e.g. United Kingdom (Environment Agency, 2017), Australia (Geoscience Australia, 2018), United States (USGS, 2018)). The use of ARC-Boats, a remotely piloted Uncrewed Surface Vehicle (USV) developed by HR Wallingford and the UK Environment Agency, has enabled new practices to be developed for collecting flow, depth, and SSC data. This is designed with end users in mind and being operated in various countries around the world such as Canada and New Zealand (HR Wallingford, 2014). TLS has been employed by the National Trust on the River Ouse to produce 3D models (National Trust, 2018) used for research and science communication. Recently, there has been a demonstrable uptake in the use of UAV equipment in industry, most likely due to their versatility and relatively low cost. They have been used for monitoring programmes on the River Dee in Wales (Cranfield University, 2018) and the Forth River Trust conservation, protection, and enhancement schemes (Forth Rivers Trust, 2018). As well as monitoring, they are also used to detect leaks from water networks (Thames Water, 2018) and have the potential to be used to monitor poor farming practices (WWF, 2018) which increases runoff and sediment delivery in to the fluvial domain. Likewise, the use of Sentinel 2 satellite imagery has helped to inform DEFRA (Department for Environment Food and Rural Affairs) about areas that may be hotspots for sediment pollution from excessive runoff (Richman and Hambidge, 2017). It is clear that remote sensing methods are primed to expand beyond research applications, with a likelihood that their use will become increasingly common practice in the future.

2.4 The State of the Art

A plethora of studies that are undertaking remote sensing of river corridors across a range of domains and scales have been highlighted. Here, we present the state of the art in river corridor remote sensing, primarily relating to the use of UAVs and multi-instrument sensing.

Despite widespread use of UAV imagery in the literature, there is an inherent reliance on Ground Control Points (GCPs) for georeferencing. Eliminating this requirement reduces field time and allows surveys to take place in inaccessible locations. By recording high accuracy positional and attitudinal information of a sensor, the need for GCPs is largely eliminated (Gabrlik, 2015), enabling greater levels of autonomy. Global Navigation Satellite Systems (GNSS) and Inertial Motion Unit (IMU) sensors, in conjunction with post-processing techniques, known as Post Processing Kinematic positioning, allow the user to locate a sensor and the resulting location of each pixel on the Earth's surface (Mostafa and Hutton, 2001; Mian *et al.*, 2015). However, precise knowledge of camera parameters such as focal length and distortion are still required for accurate model location (James and Robson, 2014). This also enables the use of small form factor laser scanners (such as the Velodyne LiDAR Puck, <https://velodynelidar.com/vlp-16.html>) to acquire UAV based Laser Scanning (UAV-LS). Originally, the majority of these systems relied on large UAVs (Nagai *et al.*, 2009; Lin, Hyypä and Jaakkola, 2011; Gally *et al.*, 2016; Deng *et al.*, 2017), however lightweight systems have been developed which can be mounted onto smaller platforms (Mader *et al.*, 2015; Roca *et al.*, 2016; Tommaselli and Torres, 2016; Jaakkola *et al.*, 2017; Nakano *et al.*, 2018). Currently the high accuracy GNSS and IMU systems required for UAV-LS and direct georeferencing are expensive (upwards of £20K for UAV-LS and ~£5K for direct georeferencing at the time of writing). A continued reduction in equipment costs will likely lead to an increased uptake in these methods, opening up avenues of research in previously inaccessible or dangerous locations or under hazardous conditions.

Combining multiple platforms and sensors is an exciting area of research that is yielding insights regarding river corridor function. The use of multi-platform configurations is not new, with multiple studies having combined ALS and satellite imagery datasets (Gilvear, Tyler and Davids, 2004; Arroyo *et al.*, 2010a; Forzieri *et al.*, 2010). However, there is evidence that interest in combining multiple high resolution datasets obtained from both terrestrial, airborne, and surface systems is growing. Examples include combining aerial imagery from UAV platforms with ALS (Legleiter, 2012) and MLS (Flener *et al.*, 2013), bathymetric ALS and UAV-LS (Mandlburger *et al.*, 2015), airborne imagery and ALS (Rapple *et al.*, 2017), as well as multiple UAV flights with imagery and laser configurations (Mader *et al.*, 2015). This has enabled researchers to improve their modelling of combined sub-aerial and sub-surface morphology, better understand riparian vegetation encroachment, and enhance current data integration approaches, all of which would be more challenging through single dataset analysis.

Alongside solely airborne techniques, the combination of USVs and UAVs has become more prominent. Although there are examples of UAVs being used to 'tether' USVs (Alvarez *et al.*,

2018; Bandini *et al.*, 2018), the majority of studies operate the platforms separately. By combining the two techniques it is possible to collate information on either the topographic and bathymetric or the above and below canopy nature of a river corridor. Young *et al.* (2017) utilised a low cost system to survey storage tanks in Bangalore with sub metre accuracy. A more advanced setup by Alvarez *et al.* (2018) obtained correlation results to ground truth data of $R > 0.98$ by combining echo sounder and SfM techniques. Alternatively, UAV and USV platforms can both collect imagery in addition to acoustics to improve estuarine mapping when compared to UAV imagery alone (Mancini *et al.*, 2015), although both methods are limited by vegetation shadowing. Powers, Hanlon and Schmale (2018) performed USV tracking of a tracer dye 'pollutant' from UAV imagery, demonstrating the power of real time combined datasets which may improve sampling and data acquisition, especially in unknown or difficult to observe environments.

Numerous vessels allow for simultaneous fluvial data collection. Both ADCP and MBES data were collected by Guerrero and Lamberti (2011), Hackney *et al.* (2015), and Leyland *et al.* (2017) for concurrent process and form measurements that are spatially and temporally homogenous, an imperative for inferring flow-bed interactions. Manufacturers are increasingly providing solutions for simultaneous bathymetric and topographic data collection from small vessels for coastal research which could easily be deployed in the fluvial domain (Kongsberg, 2013; Unique Group, 2018).

UAV surveys that utilise multiple sensor payloads have focussed on combining laser scanners and imagery for disaster recovery and river monitoring (Nagai *et al.*, 2009), high temporal, spatial, and spectral resolution landscape dynamics research (Gallay *et al.*, 2016), and forestry mapping (Jaakkola *et al.*, 2010). However, most studies currently focus on the use of one sensor on UAV deployments due to weight implications relating to flight time endurance.

Currently, state of the art remote sensing tools are in their infancy. The majority of future development will revolve around two key themes, i) producing highly accurate data in a timely and cost effective manner, and ii) processing this data to gain maximum insight. The former will rely on technological enhancement of sufficient progress to reduce the costs of high grade IMU units that are small enough to be mounted on autonomous platforms. The latter requires advances in Big Data handling and point cloud/spatial data analysis techniques to handle the significant quantities of data produced and leverage the understanding from these sensors. Much like the proliferation of TLS and SfM techniques which have progressed through proof of concept phases and are now routinely used, multi sensor integration and high accuracy altitudinal information will likely follow a similar path.

2.5 Future Directions

The following section seeks to ‘horizon scan’ for the technological advances which may contribute to enhanced river corridor monitoring in the near future.

2.5.1 UAVs – Uncrewed Aerial Vehicles

UAV swarm technology may enable fluvial research and monitoring to be performed more efficiently. Swarm technology presents an architecture which is scalable, efficient, robust, and helps to mitigate certain aspects of risk associated with UAV deployment (Howden, 2009; Zhao *et al.*, 2017). UAV swarms can either be controlled using group decision making or individual agent response (Howden, 2009); with coverage either being ‘distributed’ into defined zones of operation or ‘free’ for optimum coverage through parallel decision making (San Juan, Santos and Andujar, 2018). Applications for swarm mapping have included surveillance missions, search and rescue operations, weed mapping, and oil spill mapping (Howden, 2009; Nigam *et al.*, 2012; Pitre, Li and Delbalzo, 2012; Albani, Nardi and Trianni, 2017; Odonkor *et al.*, 2017; San Juan, Santos and Andujar, 2018). However, studies remain focussed on using simulations to either test algorithms (Almeida, Hildmann and Solmaz, 2017; Chen, Ye and Li, 2017; Yang *et al.*, 2017; Zhao *et al.*, 2017) or data processing techniques (Casbeer *et al.*, 2006; Ruiz, Caballero and Merino, 2018). Despite the lack of real world testing due to physical and legal constraints, swarm technology may enable rapid acquisition of data for river corridor applications on unprecedented scales.

UAV object tracking provides the opportunity for smarter surveying deployments. Current work has utilised machine learning to recognise a defined object and subsequently track it (Trilaksono *et al.*, 2011; Rodriguez-Canosa *et al.*, 2012; Bian *et al.*, 2016). There has been a recognised need for such methods to be implemented in environmental research practices (Pereira *et al.*, 2009), with detection and tracking already being applied to features such as rivers, canals, and roads (Rathinam *et al.*, 2007; Rathinam, Kim and Sengupta, 2008; Lee and Hsiao, 2012; Lin and Saripalli, 2012; Zhou *et al.*, 2015). Despite the potential, there seems to be little uptake in applied river corridor research, whereby pre-determined or non-autonomous flights are the norm. The heavy lift requirements, difficulty in isolating features in spectrally homogenous environments, and the potential for false feature identification currently hinders use (Rathinam *et al.*, 2007; Lee and Hsiao, 2012). If these issues can be overcome, the potential for platforms to routinely monitor with little human input is attractive when considering highly dynamic fluvial environments.

2.5.2 AUVs – Autonomous Underwater Vehicles

Traditionally utilised in the marine environment, AUVs use active sensing to guide them through missions such as maintaining survey depth for consistent resolution sea bed mapping (Maier *et al.*, 2013; Covault *et al.*, 2014; Brothers *et al.*, 2015; Tubau *et al.*, 2015), coral reef mapping (Armstrong and Singh, 2012), submarine lava identification (McClinton and White, 2015), and sea bed classification (Lucieer *et al.*, 2013). Terrestrial water applications are less common and require careful consideration due to the complex motion of water alongside the need for improved object detection and avoidance (Zhao, Lu and Anvar, 2010; Li *et al.*, 2012). However fluvial research has employed AUVs to collect variables such as temperature, salinity, conductivity, and nitrate flows in both autonomous and semi-autonomous systems (Tester *et al.*, 2006; Singh *et al.*, 2007). Likewise, flow patterns and sediment loading have been studied in estuarine conditions (Kruger *et al.*, 2007; Rogowski, Terrill and Chen, 2014) as well as reservoir surveying (Socuvka and Veliskova, 2015), showing the range of conditions AUVs can operate within. AUVs are also capable of tracking features such as pipelines and elevation contours in real world and simulated environments (Bennett and Leonard, 2000; Ortiz, Simo and Oliver, 2002; Fiorelli *et al.*, 2006; Fallon *et al.*, 2013; Xiang *et al.*, 2016; Sfahani, Vali and Behnamgol, 2017). This may allow smarter sub-surface fluvial surveying techniques whereby AUVs can navigate river channels effectively, collating datasets over large areas with minimal human input or risk.

2.5.3 USVs – Uncrewed Surface Vehicles

Like UAV surveys, USVs use GNSS equipment and IMUs to provide accurate sensor locations for data collection. USV deployment in fluvial environments range from topographic to biophysical data collection (Casper *et al.*, 2009; Mancini *et al.*, 2015; Wei and Zhang, 2016; Suhari and Gunawan, 2017; Young *et al.*, 2017). The majority of these systems focus on bathymetric data collection from echo sounders, yet there are examples of both camera and water quality sensors being used (Casper *et al.*, 2009; Mancini *et al.*, 2015), as well as sensors for tracking and analysing simulated pollutants in freshwater environments (Powers, Hanlon and Schmale, 2018). Not only do USVs provide the potential for collating bathymetry and water properties, but also the surrounding terrestrial environment such as bank morphology and vegetation. USV surveying is likely to follow a similar pattern to UAVs in their increasing use for environmental research, whereby the technology becomes advanced enough for users to deploy a vessel with minimum human input, even in more challenging flow conditions.

2.5.4 Real Time Monitoring Using Internet of Things (IoT)

The IoT in environmental monitoring is becoming increasingly prominent, with the technology available for a suite of uses. IoT is the extension of the internet in to physical devices that perform a role (Miorandi *et al.*, 2012). Sensors communicate between devices through networks, frameworks, and control centres, to share information and analyse data (Gubbi *et al.*, 2013; Mitra *et al.*, 2016). IoT has been used for environmental applications in remote and inaccessible locations for hazard response networks and monitoring research (Miorandi *et al.*, 2012; Martinez *et al.*, 2017).

IoT in the hydrological domain has focussed on engineering and infrastructure monitoring. For example, the South to North River Project in China uses over 100,000 sensors with 130 differing purposes to monitor water quality, infrastructure, and security (Staedter, 2018), all of which is fed in to a cloud infrastructure updated as frequently as every 5 minutes. Similar installations on smaller scales include active river and wetland management for water treatment (Wang *et al.*, 2013), real time sewage monitoring in the UK to mitigate flooding scenarios (Edmondson *et al.*, 2018), as well as conceptual designs of flood embankment monitoring systems (Michta *et al.*, 2017). Uses for research include groundwater and river monitoring to better inform hydrological traits related to climatic variables, infiltration, and surface run off (Shi, Zhang and Wei, 2014; Malek *et al.*, 2017). Being able to effectively utilise the data captured over an IoT infrastructure may see the greatest development. Effectively using various machine learning techniques on big datasets can aid in the prediction of flood events in real time as demonstrated by Bande and Shete (2017) and Furquim *et al.* (2018). IoT monitoring networks not only benefit research applications, but will have a large impact on applied monitoring techniques, providing near real time information for better decision making, improving overall monitoring efficiency and performance.

2.5.5 Satellite Remote Sensing

Given the role of satellites in revolutionising our view of fluvial systems, it would be remiss not to point out future developments in this technology, which are centred around the launch of a greater number of platforms with payloads delivering data for increasingly focused applications. The NASA based Surface Water and Ocean Topography (SWOT) mission (NASA, 2019a) will be used to study the volumes of freshwater available in medium to large lakes and rivers, helping to understand water availability and any such related hazards. Similarly, the NASA-ISRO SAR mission (NASA, 2019b) will be used to map flood extents for hazard monitoring, but also improve monitoring of groundwater, benefiting those seeking to address questions linking

groundwater to surface water supply. Alongside specific sensors, the increasing availability of higher resolution imagery below 1 m such as provided by WorldView3 (Longbotham *et al.*, 2014) will provide a large repository of data that may be of use to river corridor monitoring. As river corridors are affected by wider hydrological and environmental conditions, missions such as the Water Cycle Observation Mission (WCOM) which is observing the water cycle under global change (Shi *et al.*, 2016), alongside ESA Biomass and Fluorescence Explorer (FLEX) missions which will help in understanding root zone soil moisture and transpiration rates respectively (McCabe *et al.*, 2017), will all help to improve our holistic understanding of river corridors.

Alongside advances in sensors, the way in which data is processed and automated will also impact river corridor monitoring. With satellites producing such vast quantities of data, there is a need for big data infrastructure, as previously alluded to, in regard to satellite systems. These systems would likely capture, process, analyse, and create outputs to inform decision in an automated process (Rathore *et al.*, 2015; Raspini *et al.*, 2018). Methods that would benefit from such a structure are beginning to be employed within the river corridor which would provide the potential for continual monitoring (Durand *et al.*, 2016; Gleason, Garambois and Durand, 2017; Frasson *et al.*, 2019). Yet there will still be the need for improved algorithms to cope with the inherent environmental variability that is present across the globe.

2.6 Key Challenges

The proliferation of monitoring techniques and their application to river corridors means that we are in a ‘golden age’ of remote sensing in this domain. Research applications are broad and proof of concept work has delivered many innovations in platforms, sensors and data processing techniques. Nonetheless, before innovative autonomous remote sensing solutions are routinely adopted for applied river corridor management, we believe that there are five key challenges that the community, and others, must address:

1. *Platform innovation*: Whilst sensors are now well developed, platforms currently rely on human interaction for direct or assisted control in defining survey routines. Adequate object detection and avoidance alongside improved autonomy will allow for true smart systems operating beyond line of sight and in challenging conditions, performing adaptive sampling for optimal data collection over larger areas.
2. *Processing innovation*: Current systems have accepted methods of best practice for the production of repeatable and comparable datasets. Increasing platform autonomy needs to be accompanied by the development of computationally efficient and robust methods for data processing. Given the volumes of data being produced by mobile laser scanning and SfM techniques for example, big data and machine learning processing techniques

need to be embraced and such methods should be embedded as routine tools within appropriate community repositories (see 5. below).

3. *Efforts to improve process monitoring:* Current techniques focus heavily on remotely sensing morphology. Process data (i.e. river flow characteristics) are challenging to acquire at the desired temporal and spatial scales and we urge the community to push the boundaries in this domain. Utilisation of multi-platform and/or multi-sensor integration to collect simultaneous process and form measurements may lead to the biggest gains in environmental understanding across the river corridor.
4. *Legislation for autonomous systems:* A significant barrier that is to be overcome before the routine use of autonomous and multi-platform systems is the legislation around operational safety, with restrictions on the operational range (e.g. within line of sight) a current limitation. Those regularly involved in river monitoring and research using these platforms need to be involved in the development of appropriate regulations by advocating safe use and practice within the domain. This should involve discussion with those implementing and developing the relevant laws, and the creation of best operating practice guidelines for other researchers and practitioners to follow.
5. *A river corridor data repository:* The routine availability of remotely sensed river corridor data is patchy at best. Open data repositories such as the DEFRA Data Services Platform (<https://environment.data.gov.uk/>) and the Channel Coastal Observatory (Southwest Regional Coastal Monitoring Programme, 2009) are demonstrating the benefits of well organised, open source data. A shift towards the community making their collected data available to a wider audience through an equivalent repository will enable others to benefit from information the original owners may have viewed as redundant, benefiting the community as a whole.

2.7 Concluding Remarks

This review reveals the sheer volume of remote sensing methods that are currently used to monitor various domains of the river corridor across a range of scales. This may include finer scale studies which utilise TLS, through to larger scale studies that use ALS and satellite data to support research and applied monitoring, with UAV imagery allowing for reach scale topographic analysis alongside sub-surface data from MBES and ADCP sensors. The majority of the work in the river corridor focusses on morphological evolution, with the processes that drive such topographic change being more difficult to observe. We advocate a shift towards improved process measurement techniques to better understand the interactions between flow, morphology, and associated ecological response. This will be facilitated by improved capabilities

to collect simultaneous process and form measurements on multi sensor platforms, as well as by the ever improving processing power required to deal with the resultant large datasets.

The remote sensing tools now at our disposal, make it possible to obtain extensive and accurate datasets that were previously unattainable, for use in a variety of applications in river corridor research and management. Remote sensing techniques are enabling new insights into complex interacting areas, for example riparian vegetation and flow interactions and the resultant evolution of channel morphology. The evolution of techniques and decreasing equipment costs have helped progress research, management, and industrial applications, allowing users to select the most suitable from a plethora of techniques. The monitoring needs of river corridor researchers and managers can likely be met through remote sensing techniques, meaning that careful identification of the desired spatial and temporal resolution, alongside the required outcomes are likely the most important factors in deciding which methods to use.

Chapter 3 Development and testing of a UAV laser scanner and multi-spectral camera system for eco-geomorphic applications.

3.1 Abstract

While Uncrewed Aerial Vehicle (UAV) systems and camera sensors are routinely deployed in conjunction with Structure from Motion (SfM) techniques to derive 3D models of fluvial systems, in the presence of vegetation these techniques are subject to large errors. This is because of the high structural complexity of vegetation and inability of processing techniques to identify bare earth points in vegetated areas. Furthermore, for eco-geomorphic applications where characterization of the vegetation is an important aim when collecting fluvial survey data, the issues are compounded, and an alternative survey method is required. Laser Scanning techniques have been shown to be a suitable technique for discretizing both bare earth and vegetation, owing to the high spatial density of collected data and the ability of some systems to deliver dual (e.g., first and last) returns. Herein we detail the development and testing of a UAV mounted LiDAR and Multispectral camera system and processing workflow, with application to a specific river field location and reference to eco-hydraulic research generally. We show that the system and data processing workflow has the ability to detect bare earth, vegetation structure and NDVI type outputs which are superior to SfM outputs alone, and which are shown to be more accurate and repeatable, with a level of detection of under 0.1 m. These characteristics of the developed sensor package and workflows offer great potential for future eco-geomorphic research.

3.2 Introduction

The use of Uncrewed Aerial Vehicles (UAVs) with camera sensors and associated Structure from Motion (SfM) techniques has proliferated in recent years with the development of small, high-endurance aircraft, high-quality lightweight camera sensors, processing software, and increased computer processing power (Colomina and Molina, 2014). SfM techniques enable the rapid acquisition of topographic data from a variety of platforms. The versatility of platforms and applications has led to a proliferation of studies within the Earth sciences (see Westoby *et al.*, 2012) and beyond (e.g. Haala *et al.*, 2011; Stek, 2016), becoming one of the most widely used high-resolution topographic data collection techniques for characterizing small to medium (10^0 - 10^1 km²) areas. In hydrology and fluvial geomorphology, the use of UAVs and SfM has been

extensively reviewed (e.g. Carrivick and Smith, 2019; Fawcett, Blanco-Sacristán and Benaud, 2019); however, eco-geomorphic and eco-hydraulic applications have been limited to land cover and vegetation classification mapping exercises based on high-resolution ortho-imagery, rather than derivation of 3D scene characteristics relating to terrain and vegetation structure. The primary reason for this is that SfM alone is limited in its ability to resolve such complex scenes as outlined by Iglhaut *et al.* (2019). Below, we provide some background to SfM, identify the related issues with the technique, and list the aims of this research, which seeks to provide a sensor solution capable of overcoming these issues.

SfM relies on the principle that a 3D scene can be constructed from a series of randomly orientated but overlapping photos. SfM uses simultaneous calculations of scene geometry and camera resection in a bundled adjustment technique (Snavely, 2009; Westoby *et al.*, 2012), iteratively adding photos to refine the bundle adjustment calculations (James and Robson, 2012). These refinements typically apply a least squares minimization method, as there are multiple potential solutions for each set of images (Snavely, 2009). This bundle adjustment process requires the identification of features that can be distinctively tracked between photos, regardless of lighting conditions and camera orientation using variants of Scale Invariant Feature Transform (SIFT) algorithms (Lowe, 1999; Westoby *et al.*, 2012). Despite the attractiveness of SfM as a survey technique, several limitations remain, relating to (i) image quality and overlap and (ii) transformation of a processed cloud into a real-world co-ordinate system. SIFT algorithms use colour gradients, as opposed to absolute pixel values, to determine features in multiple images (James and Robson, 2012; Fonstad *et al.*, 2013). The number of detectable features identified is directly associated with the output model quality; consequently, poor-quality images may have fewer detectable points and reduce final model quality. Likewise, high image overlap levels are necessary for improving the number of detectable features in multiple images (Micheletti, 2015). As a result, good-quality images do not necessarily produce good-quality models, as outlined in Tomsett and Leyland (2019).

Prominent features are used to create a sparse point cloud, defined in ‘image space’, which can then be transformed into a chosen coordinate system using Ground Control Points (GCPs) (Fonstad *et al.*, 2013). Dense Multiview Stereo matching (MVS) is then undertaken to produce a highly detailed three-dimensional (3D) model by searching for optimum matches (Furukawa and Ponce, 2010). This process also allows for the removal of areas with higher errors due to the limited matching of features (Micheletti, 2015). Transformation of these points relies on good-quality GCPs spread across the study area, capturing changes in elevation in order for a globally optimum solution to be produced (Kraus, 2007). Incorrect GCP placement or reduced GCP accuracy may affect the solving of collinearity equations which can subsequently propagate

through the model (Fonstad *et al.*, 2013; Wolf P, 2014). Assigned GCP locations are then used to perform a seven-parameter transformation, shifting, and rotating the image across three planes, as well as scaling the model (Fonstad *et al.*, 2013; Eltner *et al.*, 2016). The importance of GCPs is self-evident. However recent advances in the miniaturization of high-resolution positioning and orientation sensors, as well as reducing costs, has led to the rise of a new technique which uses ‘direct georeferencing’. The main purpose of direct georeferencing is to enable the collection of 3D data without the need for GCPs. This allows both streamlined in-field data collection and post processing whereby the need for many GCPs is removed (Nagai *et al.*, 2004; Turner, Lucieer and Wallace, 2014). However, the technique does not negate the need to include quality controls and checks to ensure data quality.

In addition to the methodological issues outlined above, the suitability and accuracy of SfM can vary substantially, especially in relation to terrain complexity and vegetation cover. While, in principle, low flight heights and high-resolution cameras enable spatial resolutions of up to 0.005 m (Clapuyt, Vanacker and Van Oost, 2016), in practice, model resolutions for bare river reaches are typically between 0.02 and 0.05 m; see (see Tomsett and Leyland, 2019). Steep and overhanging terrain reduces the number of detectable points in an image resulting in poor reconstruction in these locations (Cook, 2017). Vegetation not only reduces the ability to see (i.e., detect and resolve) the study area terrain, it is also not easily or accurately reconstructed by SfM. Both Cook (2017) and Dietrich (2016) noted that vegetation was sometimes fully captured, but was also often excluded altogether, depending on size and density. UAV SfM is simply not able to resolve the internal structure of vegetation. In relation to an exemplar SfM resolved tree crown, Fawcett, Blanco-Sacristán and Benaud (2019) noted that “...the internal structure of this tree could only ever be captured by active laser scanning methods...”. A compounding factor of taller vegetation is shaded areas, particularly in leaf-on conditions. Shaded regions appear homogenous and lack the required features to be detected and matched between image pairs, creating areas of low quality within the final models (Brunier *et al.*, 2016). Vegetation therefore inhibits the SfM processing workflow, leading to a reduction in quality of the final outputs.

Laser scanning offers a solution to the problems identified above; it is not subject to transformation errors or image quality and overlap related processing errors and it is capable of penetrating complex porous structures such as vegetation, thereby resolving some internal structure and some bare earth terrain points. Terrestrial Laser Scanners have been deployed with great success to elucidate eco-geomorphic processes (see the review by Lague, 2020), but they are limited in the scale of application by the need for multiple static setups to capture scenes. UAV-based Laser Scanning (UAV-LS), which combines miniaturized motion sensors and Global Navigation Satellite Systems (GNSS) with lightweight and low-powered laser scanners,

has the potential to allow the collection of high-resolution data across relatively large areas. To date, exploration of such systems has been primarily focused on forestry applications (e.g. Wallace *et al.*, 2016; Jaakkola *et al.*, 2017; Brede *et al.*, 2019), with a few notable exceptions (e.g. Lin *et al.*, 2019; Resop, Lehmann and Hession, 2019; Jacobs *et al.*, 2021). However, the off-the-shelf UAV-LS systems used are typically expensive (~GBP 60k—150k for YellowScan or Riegl RiCopter) and often require ongoing subscriptions to bespoke post-processing software, making them prohibitive in terms of purchase and maintenance costs for many practitioners. Yet the potential for improved data capture, especially in vegetated reaches, set them apart from current survey methods especially in relation to eco-geomorphology.

The potential for improved data capture in vegetated reaches also lends itself to improving spectral data collection. The use of multispectral cameras which obtain imagery at wavelengths beyond the visible spectrum allow a greater understanding of vegetation properties. These have subsequently been used to improve understanding in fields of ecology, coastal monitoring, wildfires, and for above and below water surface analysis (Doughty and Cavanaugh, 2019; Samiappan *et al.*, 2019; Gomez Selvaraj *et al.*, 2020; Taddia *et al.*, 2020). Despite their deployment in several scenarios and increasing efforts to standardise methods between surveys (Assmann *et al.*, 2019; Stow *et al.*, 2019), there is still more to be done to obtain consistency between surveys.

The aims of this research are to (i) develop a relatively lower cost sensor package using off-the-shelf laser scanning and multi-spectral camera components which are capable of characterizing terrain and vegetation structure; (ii) establish a post-processing technique that is capable of resolving the collected data in real world co-ordinate systems; and (iii) assess the accuracy and repeatability of both UAV-LS and UAV-MS data products against each other and ground check points in the real world, with reference to eco-geomorphic applications.

3.3 Development of a UAV Laser Scanner and Multispectral Camera Sensor System

For the purposes of this paper, references to UAV-LS (UAV Laser Scanning) and UAV-MS (UAV Multispectral) refer to the results of data collection from each sensor, not the entire system.

3.3.1 Components of the System

The sensor setup is made up of four main constituent parts. The sensor package (a laser scanner and a multispectral camera), an Inertial Navigation System (INS), GNSS input, and a mini-PC for data collection and storage. The complete setup allows for fully georeferenced imagery and

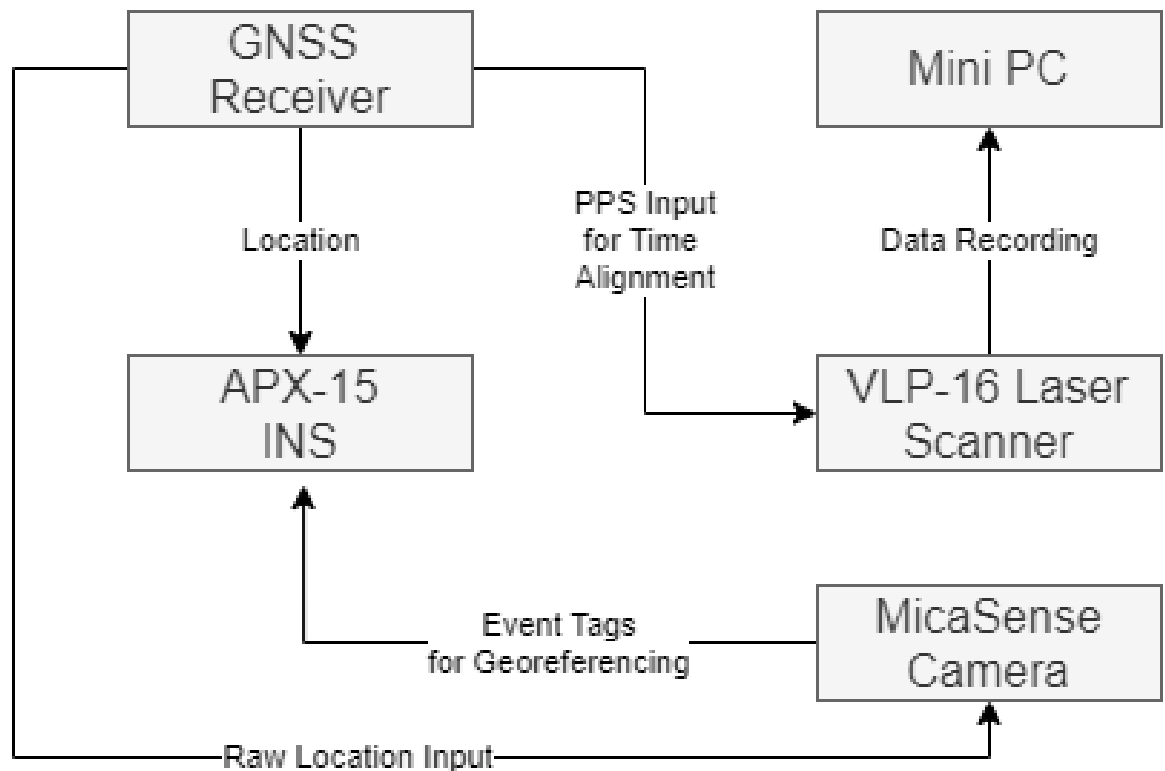


Figure 3-1 The key components of the developed UAV laser scanner and multispectral camera system for mounting on a UAV platform such as a DJI M600.

point clouds without the need for collecting GCPs. Figure 3-1 demonstrates how these components are broadly interlinked to provide the datasets required.

The sections below provide detail of each of the sensors and the role they play in the data collection process, commenting on the accuracy of each component of the system.

3.3.1.1 Applanix APX-15 Inertial Navigation System (INS)

The Applanix APX-15 is a MEMS (micro-electromechanical systems)-based inertial navigation system with a GNSS receiver providing lightweight georeferencing for UAV platforms (Applanix, 2017), costing ~GBP 13k in 2017. The MEMS unit uses accelerometers and gyroscopes to resolve both linear movement as well as orientation, collected at a rate of 200 Hz. The unit is light at 60 g and has dimensions of 67×60 mm for easy UAV integration. It can interpret 336 GNSS channels over several constellations for high accuracy surveying. After processing, the outputted position and orientation is produced at a rate of 200 Hz for improved georeferencing accuracy. Manufacturer stated positioning is accurate from 0.02–0.05 m with roll and pitch accuracies of 0.025 degrees and heading accuracy of 0.080 degrees after post-processing, values corroborated by Stöcker *et al.* (2017) when assessing the unit for direct georeferencing.

The unit is capable of outputting a PPS signal (Pulse Per Second) for precise time integration with external devices. This is essential for accurate georeferencing and is an input to the laser scanner to avoid clock drift. In our setup this is set to provide the time on the rising edge of the pulse, in line with the laser scanner specifications (see Section 3.3.1.2). It also receives event signals to store the exact timings when a multispectral image (see Section 3.3.1.3) was captured to allow accurate post-processing of images with positional data.

3.3.1.2 Velodyne VLP-16 Laser Scanner

The Velodyne VLP-16 (puck lite) is a compact form, low-power laser scanner that is optimal for use on UAVs due to its low weight of 590 g (Velodyne Lidar, 2018), costing ~GBP 5k in 2018. The VLP-16 uses 16 laser emitter-detector pairs (903 nm wavelength) which have dual return capability to collect points 360 degrees around the sensor with a viewing angle of 30 degrees. The sensor uses a time-of-flight method to determine distance to an object. It can collect up to 300,000 points per second up to a range of 100 m from the sensor. The scanner has a claimed accuracy of ± 0.03 m (Velodyne Lidar, 2018), with consistent calibration between units which are stable across a range of temperatures and for long term deployments (Glennie, Kusari and Facchin, 2016).

The VLP-16 requires a Pulse Per Second (PPS) input to prevent clock drift from start-up totalling around 5 s per day (Velodyne Lidar, 2016). This equates to roughly 0.07 s by the end of a 20-min flight, and subsequently while flying at 5 ms^{-1} would incur an error of up to 0.35 m. As a result, the APX-15 PPS output is used for accurate synchronisation of clocks between the two sensors.

The VLP-16 outputs data packets for each rotation of the scanner over Ethernet UDP (User Datagram Protocol), which can then be processed in real time or saved (Velodyne Lidar, 2016). In the current setup, this data is monitored using the free network monitoring software Wireshark and saves a packet capture (.pcap) file to the on-board mini-PC for post fieldwork download and further analysis.

3.3.1.3 MicaSense RedEdge-MX Multispectral Camera

The MicaSense RedEdge-MX is a five-band multispectral camera, with wavelengths ranging from blue to infra-red (see Table 3-1), including a red edge band designed to enhance separation between different vegetation characteristics. The camera is compact and lightweight at 230 g and includes a global shutter to decrease distortion and eliminate the need for a gimbal (MicaSense, 2021). It cost ~GBP 5k in 2018. Imagery has a ground sampling distance of 8 cm at 120 m and less at the flight heights used in the surveys performed herein (<50 m).

Table 3-1 The band characteristics of the MicaSense RedEdge-MX multispectral sensor.

Band	Wavelength (nm)	Band Width (nm)
Blue	475	32
Green	560	27
Red	668	14
Red-Edge	717	12
Near Infra-Red	842	57

The camera can be triggered in multiple ways. Our setup uses a timer method to capture photos every 1.5 s to maximise forward overlap. This overcomes the shortfall in sidelap due to the relatively narrow field of view of under 50 degrees meaning at flight heights of 50 m, flight path separation of ~ 23 m is required for attaining 50% sidelap in images. The camera also produces a top of frame output which outputs a signal at the start of image exposure accurate to a few tens of nanoseconds (MicaSense, 2018), this is then communicated to the APX-15 and recorded as an image event in the flight logs. This provides accurate timestamps from which to extract post-processed position and orientation data for multispectral image processing.

Two methods for obtaining consistent lighting procedures between surveys are used in data capture. First, a manufacturer supplied calibration panel is deployed to adjust for the reflectance values to those that would be expected when imaging the panel. In addition, a Downwelling Light Sensor (DLS) collects data on ambient lighting conditions before writing these to the metadata of each image produced. The DLS is connected directly to the camera and sits on top of the UAV for optimum unimpeded data collection. It is placed away from the other antennae to reduce any interference which may affect the true ambient conditions being recorded. This information is then applied in post-processing to adjust the reflectance values of the images to maintain consistency within the survey and between successive surveys.

3.3.1.4 Associated Hardware

A Tallysman antenna with L1/L2 capabilities is used to collect GNSS signals across several bands from multiple constellations. The mini-PC is a compact and lightweight Fitlet-i10 (from Fit-PC) which has a low power consumption and runs a basic Windows 10 operating system. This is controlled via an external laptop using a proxy Wi-Fi host and the free TightVNC remote desktop application viewer on the host laptop (<https://www.tightvnc.com/>, version 2.8.63, last accessed: 17/11/2021). The status of the APX-15 can be checked during flight to monitor the alignment of the INS based on the initialization procedures (see Section 3.4). The MicaSense camera and recording of the raw VLP-16 data are started before take-off. This also acts as a method to check data in the field and extract data from the sensor setup post field deployment.

3.3.2 Assembly of the System

Each sensor has specific voltage requirements, but we found that 11.1 V satisfied the APX-15, VLP-16, and mini-PC, with an in-line transformer altering the voltage from 11.1 V to 5 V for the MicaSense camera. The setup is powered by a 2650 mAh LiPo battery, which is enough to power the unit for spin up, calibration, survey, cool down, and data download (up to 45 min per charged battery).

Each component is mounted within or on a lightweight survey box (Figure 3-2). The VLP-16 is mounted externally with a single screw aligned with two mounting lugs either side for consistent offset calculations, and at a 90-degree pitch angle (forward) scanning across track perpendicular to the flight lines for maximum coverage. The MicaSense camera is mounted with 4 locating screws to keep consistent positioning, as is the APX-15 board so that the X, Y, Z and roll, pitch, and yaw offsets are consistent between flights. The total weight of this survey setup comes in just under 2.5 kg, allowing for flight times of around 20 min using a DJI M600 multirotor aircraft with standard batteries. The unit is then attached on to a DJI mounting plate which sits below the UAV. The mounting plate has dampeners attached between the plate and the UAV to reduce vibrations being passed to the INS, laser scanner, and camera as these are known to have a negative impact on accuracy (Lin, Hyyppa and Jaakkola, 2011).



Figure 3-2 The components of the sensor package assembled within a lightweight plastic box for testing, here mounted on a DJI M600 multirotor platform.

Offsets between each of the sensors were measured in the lab before being input into the APX-15 internal memory for processing of each flight. However, as the accuracy of the lab offsets

could not be quantified, a calibration procedure has been performed to tighten the offsets before roll, pitch, and yaw adjustments are checked for each survey, as detailed in Section 3.5.1.4.

3.4 Field Deployment of the System

We used a DJI M600 multirotor aircraft for deployment, although in principle the sensor package could be mounted on any airframe that can carry a ~ 2.5 kg payload and perform the required initialization procedure (see below). For the purposes of this study, data from five separate deployments on a ~ 1 km reach of the River Teme (Figure 3-3) made in February, July and September 2020 and April and June 2021 were used. The River Teme is a gravel bed river with alluvial banks that showcases active erosion and deposition processes and exhibits several vegetation types, from grasses to large deciduous trees. A survey-grade Leica GS10 GNSS base station was deployed for each survey, recording raw RINEX observation data for post-processing routines.

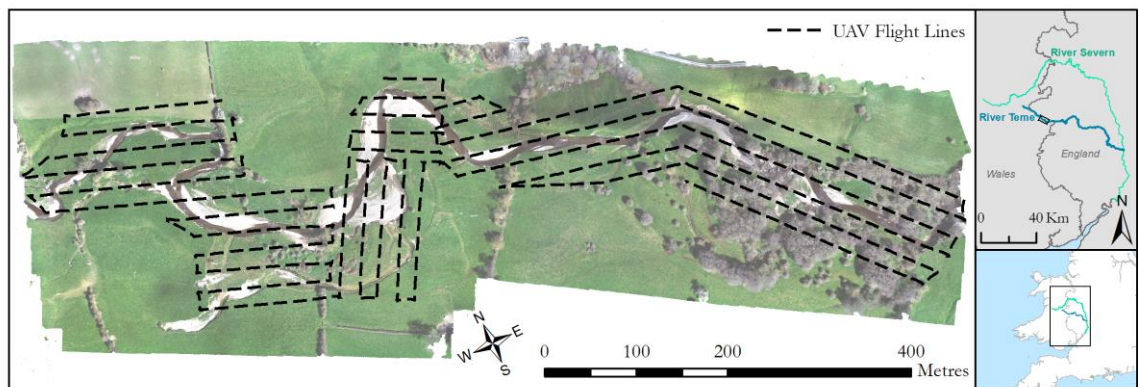


Figure 3-3 Study site of the River Teme, showing the flight lines used for all surveys from which laser scanning and imagery were captured. Imagery taken from April 2021. Inset shows the location of the study site within the UK and the location of the River Teme, a tributary of the River Severn.

The laser scanner and MicaSense camera package collect data in tandem and so flight lines (shown on Figure 3-3) and speeds (4 m/s) were optimised to provide scan lines for the entire river corridor which delivered at least 50% sidelap and 75% forward overlap for the multispectral imagery. Once powered on, the data from the laser scanner is set to record on the mini-PC via a remote desktop connection and the MicaSense is set to run through its setup, including capture of calibration panel images, via a web browser. The APX-15 requires 5–10 min of static data logging both before and after flights to aid forward and backward motion post processing, so is left to stand for this time.

Once ready to fly, the UAV is flown to an elevation of 10 m to perform an initialisation sequence for the INS, consisting of flying at speed forwards, backwards, left, and right to excite and initialise the accelerometers, resulting in a fully aligned heading (confirmed via the INS status). After initialisation, the aircraft is set to auto mode to follow the predetermined flight path (Figure 3-3). Prior to landing, the initialisation movements of flying forward, backwards, left, and right are performed again to aid in the backwards processing.

3.5 Data Processing Workflow

The following sections outline the workflows developed to process raw field data into spatially referenced products for further analysis. Both the laser scanner and MicaSense multispectral imagery use the same positional raw data, and therefore follow similar initial processing routines.

3.5.1 UAV Laser Scanner and Multispectral Camera Processing

Processing requires three main strands: positional data processing, Velodyne data configuration, and the georeferencing of each data product. The same initial processes to determine position are loosely followed for camera locations when processing multispectral data, with differences to the output data generated.

3.5.1.1 Inertial Navigation System Processing

Initially, all raw base station data in RINEX format is uploaded to a web service such as AusPos (<https://gnss.ga.gov.au/auspos>, last accessed: 17/11/2021), whereby the nearest IGS (International GNSS Service) stations are used to correct the position of the base to levels of accuracy as high as 0.02 m (assuming minimum 4 h of raw observations). The reports generated by these services are used to improve the position quality of the original RINEX file by updating the coordinates of the base station or through the download of a new RINEX file with the updated headings depending on the servers being used. This can then be used in the processing of rover data collected by the UAV GNSS receiver.

The positional information from the Applanix APX-15 system is processed using Applanix processing software. This is best done once precise ephemeris data for the satellite is known, to ensure the highest level of precision. Ephemeris accuracy is one of the many factors that can affect the quality of GNSS data being collected. Broadcast ephemeris data initially approximates satellite position, but can be up to 2 h old, whereas precise ephemeris data is based on a monitoring network of ground stations and available at 15 min intervals (Ma, Wang and Li,

2019). Broadcast errors can subsequently be in the range of 1–6 m (Ma, Wang and Li, 2019), with precise ephemeris data recommended for cm-level ground-based positioning (Karaim, Elsheikh and Noureldin, 2018). The post-processed base station is used in conjunction with Applanix IN-Fusion technology (Scherzinger and Hutton, 2021) to deliver better positioning information when a reduced number of satellites are visible. This routine uses both forward and backward Kalman filtering, designed to estimate unknown variables over time, and uses this to improve positional accuracy (Kim and Bang, 2018). The resultant reported positional accuracy of the sensor package is typically in the range 0.01–0.02 m horizontally and 0.02–0.03 m vertically (Figure 3-4A). This is assumed to represent the horizontal accuracy of the system in the absence of any field data collected to assess horizontal accuracy. Roll and pitch reported accuracies are within the 0.05–0.10-degree range, with increased standard deviation values during turning; while heading accuracies predominantly vary between 0.2–0.3 degrees, with accuracy decreasing during straight line flight (Figure 3-4B). This is likely due to slower flying speeds reducing the certainty of the trajectory being calculated. However, the impact of post processing on both the positional and attitudinal data is significant. Improvements in positional location are an order of magnitude improved post processing (Figure 3-4A), with similar levels of

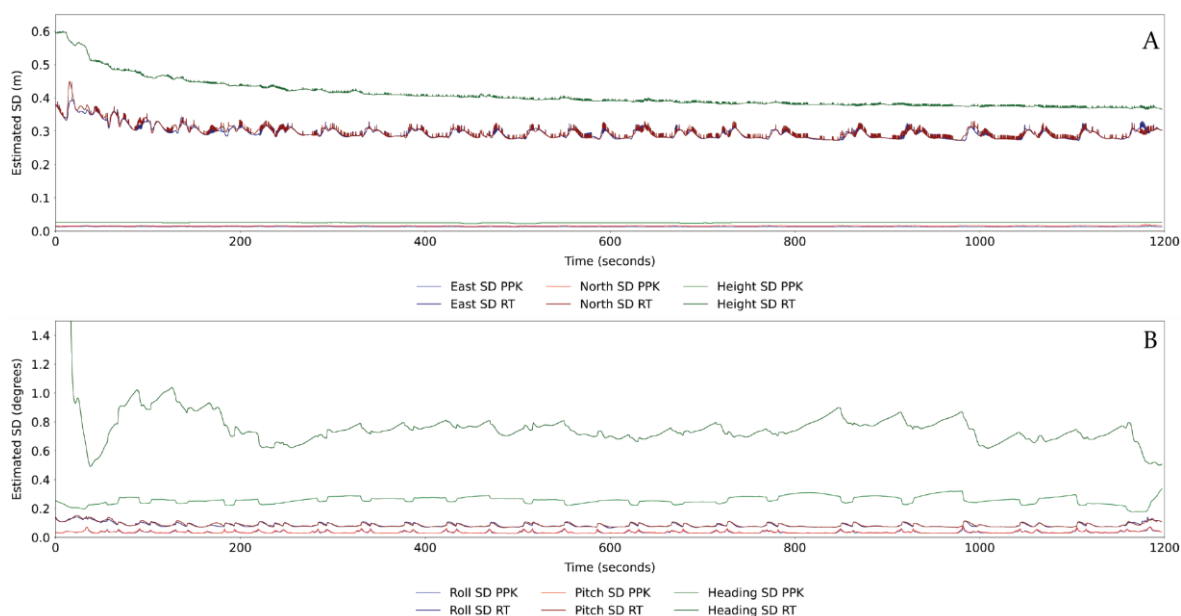


Figure 3-4 Post-processing results of the Applanix APX-15 data showing how forwards and backwards Kalman filtering reduces errors in the (A) X, Y, and Z position of the sensor by an order of magnitude while having a similarly distinct impact on (B) roll and pitch values. Despite relatively larger errors in heading, the post processing helps to minimise the drift in values throughout transects. PPK = Post Processed Kinematic positioning, RT = Real Time positioning, SD = standard deviation.

improvement seen in the attitudinal data (Figure 3-4B). The processed positional data is then exported at a rate 200 Hz (position every 0.005 s) and in the projected coordinate system of choice for combination with the laser scanner and MicaSense camera.

3.5.1.2 UAV Laser Scanner Raw Data Processing

The freeware Veloview (<https://www.paraview.org/veloview/>, version 3.5, last accessed: 17/11/2021) is used to read, display, and output the raw VLP-16 data. Extraneous data from when the platform is initialising on the ground is clipped using the first and last flight line times. Although positional error does not propagate with distance from the sensor, errors in roll, pitch, and heading will (see Figure 3-5A). Therefore, to limit the effects of this, but to maintain a high ground point density, a filter with maximum distance from the sensor of 50 m in the X and Y planes was applied. Overlapping flight lines in the field were 25 m at maximum, with most flight lines 20–22 m apart, resulting in a minimum of 50% overlap whereby the points from the scan line would be overlapped by at least one other scan (see Figure 3-5B), but in most cases this would be higher. This overlap maximises point density and accuracy and allows for large extents of the study area to be covered in a single flight. The clipped and filtered data is exported to a series of individual time-stamped ‘scans’ containing a location relative to the sensor centre and intensity. These scans are then ready to be combined with the positional and attitudinal data from the Applanix APX-15.

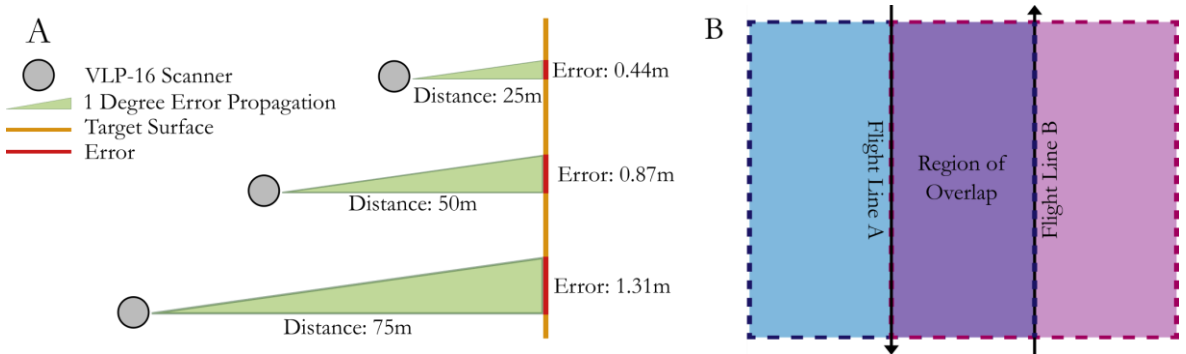


Figure 3-5 Impact of the distance from scanner on accuracy and flight overlap clipping. (A) Visualisation of how increasing distance from the target surface leads to increasing error associated with any incorrect calculations of roll, pitch, and yaw. The errors calculated are based on a 1-degree miscalculation from a nadir facing laser beam in one direction (i.e., just roll error). (B) The region of overlap that is maintained during cropping to maintain at least two viewing angles of each ground point within the survey, especially important for vegetated reaches.

3.5.1.3 Combining Laser Scanner and Positional Data

The VLP-16 and Applanix APX-15 positional data are combined using custom python scripts (available at https://github.com/christomsett/Direct_Georeferencing.git, last accessed: 17/11/2021) designed to join the two datasets together and produce a final georeferenced point cloud. The workflow accounts for two timing discrepancies that are presented: (i) the VLP-16 references time from the start of the last hour in microseconds, whereas the positional data refers to decimal seconds of the current GPS week; and (ii) there is a discrepancy between UTC time and GPS time, currently 18 leap seconds. Once timestamp discrepancy has been accounted for, a simple join is made based on the nearest time between the two datasets' time fields. Mismatches in the output rates of both sensors results in a non-perfect synchronization of position and scan data, with a maximum offset in time of 0.0025 s. Surveys are conducted at a maximum speed of 4 ms^{-1} , resulting in a maximum error introduced by the time stamp discrepancy of 0.01 m. Based on our data, 80% of all errors due to the timestamp inconsistency are below 0.008 m and 40% are below 0.004 m. Consequently, the relative impact of the timing error is less than the positional accuracy of the system. Next, the scan points are adjusted for the roll pitch and heading of the sensor at the relevant timestamp. A rotation matrix for each point is defined and is then applied to create points relative to the sensor adjusted for roll, pitch, and heading. Finally, points can be transformed using the sensor location into real world coordinates, producing a fully georeferenced point cloud.

3.5.1.4 Offset and Boresight Angles

To accurately combine the INS and VLP-16 data, it is imperative that accurate offsets and boresight angles are calculated to reduce inconsistencies between surveys (Hauser, Glennie and Brooks, 2016). If these are not accurately measured and adjusted, errors will be introduced into the final model (Mostafa, 2002; Rau *et al.*, 2011). As discussed in Section 3.5.1.2, the relative positional errors of the offsets do not propagate with distance from the sensor. These are initially calculated through the measurements of offsets in the X, Y, and Z planes from a fixed point for each of the INS, VLP-16, and GNSS antenna. These were defined in the lab through handheld measurement and information on sensor dimensions as specified by the manufacturer. This allows the relative positions between each component to be calculated and inputted in to the Applanix software so that the exported positional data accounts for these offsets. The software used also refines these offsets on the fly based on data from the INS, providing an optimal solution. The GNSS antenna is fixed to the UAV via a singular mounting screw, and so is fixed in position each flight. However, while the position of the mounting of the UAV laser

scanner sensor system box (Figure 3-2) is fixed relative to the UAV, the box is subject to small variations in mounting angles between flights.

An iterative process to establish optimum roll and pitch offsets on an identifiable feature (e.g., an electricity pylon) is undertaken for each flight. The initial steps include angles from -1 to 1 in steps of 0.5 , before narrowing these down based on visual inspection (Figure 3-6). As can be seen from Figure 3-6, this approach allows the identification of trends of change, in this instance moving towards a roll offset of $+1$ and keeping the pitch offset at 0 degrees resulted in the closest alignment of the pylon and the electricity wires. This is then refined to check for a smaller range of values between the two best combinations of roll, pitch, and heading. In this instance, this evolved testing values of roll between 0.8 and 1.2 , and pitch of -0.2 and 0.2 . Once an optimum solution has been found, an adjustment is made to alter all roll, pitch, and yaw values before applying the rotation matrix noted in 4.1.3, above. Future work may refine this process to automatically detect the best fit through an ordinary least squares approach.

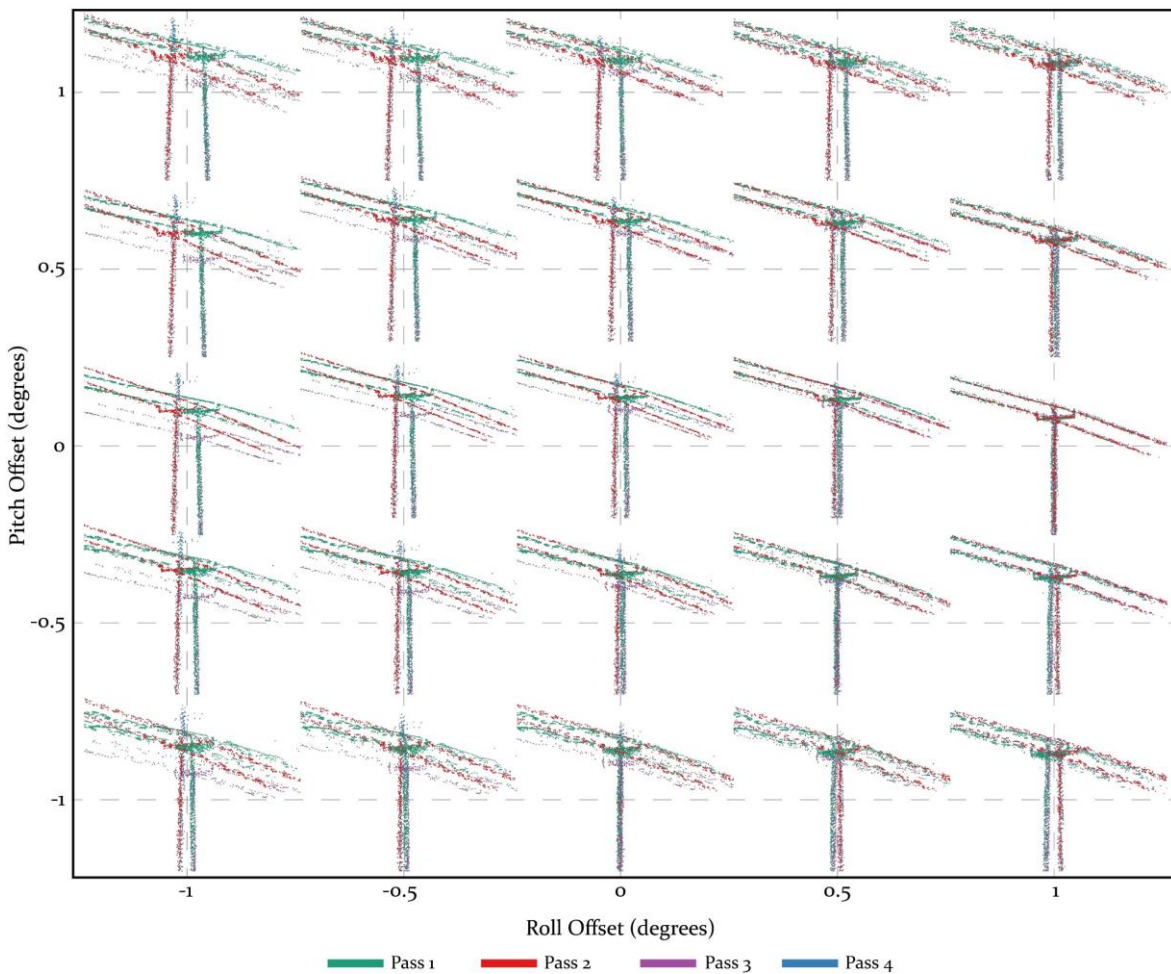


Figure 3-6 Calculation of offset and boresight angles using an iterative process between multiple passes (from different directions) over an identifiable feature, in this case an electricity pylon.

3.5.1.5 MicaSense Multispectral Imagery SfM Workflow

To create a position file related to each set of images, custom python scripts (available at https://github.com/christomsett/Direct_Georeferencing.git, last accessed: 17/11/2021) are used to combine the positional tags output from processing the Applanix APX-15 data with each photo taken, accounting for GPS and UTC timing discrepancies between the data. In addition, as each waveband of imagery is suffixed with a 1–5, multiple images have to be given the same positional information, which is written to a database in a format that is readable as reference data for Agisoft Metashape for SfM processing.

Images are loaded in to Agisoft Metashape as a multi camera system, whereby the separate suffixed images are treated as one in the processing workflow, as opposed to attempting to align them separately. Reference data are loaded and assigned to each photo, with accuracy of these coordinates specified as 0.05 m in all three directions and 0.5 degrees in roll, pitch, and heading. This allows for error in position and orientation to be accounted for, as well as any offset or boresight errors introduced to be overcome by the processing workflow. This is in line with the findings noted by Stöcker *et al.* (2017), who noted a reduced weighting on the accuracy of external camera orientation led to higher accuracy results in post processing. The photos are then aligned to the highest possible quality to get updated location and orientation of the camera. At this point, the GCPs are used to refine this alignment further; however, the image resolution (~0.035 m) of the multispectral camera introduces some error by impeding precise placement of target centres. Next, a dense point cloud is built alongside mesh and texture surfaces, using high-quality processing settings. These are used to create a tiled model of the study site along with orthomosaics and DEMs at 0.04 m resolution. These models and the dense point cloud are subsequently exported as fully georeferenced datasets.

3.5.2 Data Processing for Comparison and Error Analysis

The processing workflows outlined above result in a UAV-LS-derived point cloud and a MicaSense SfM-generated orthomosaic and point cloud, for each of the five survey dates. Herein, we aim to compare the datasets in two ways: (i) assess the absolute error of the laser scan and SfM data compared to surveyed ground checkpoints; and (ii) assess relative between-survey accuracy, by comparing areas that experience no morphological change. The latter allows the quantification of a level of detection of change by analysing the repeatability of the surveys between techniques and across survey dates.

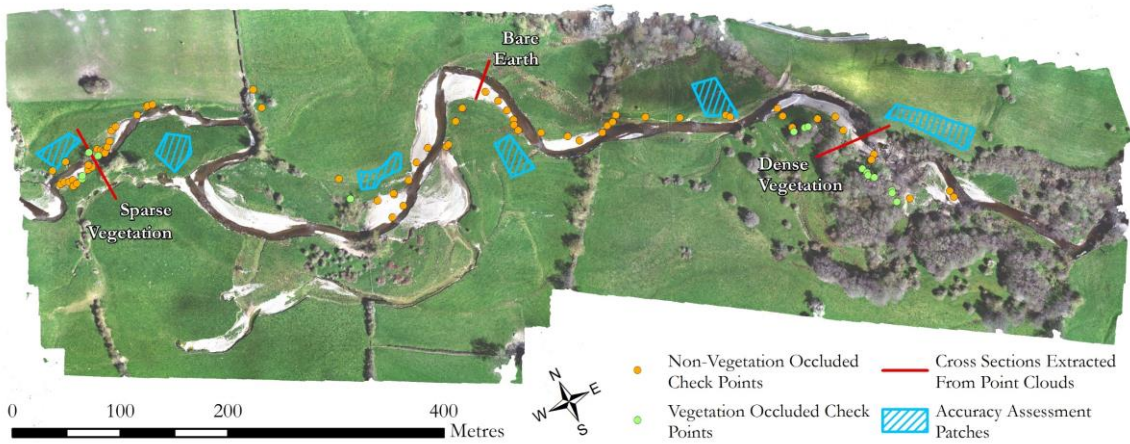


Figure 3-7 Locations of different accuracy assessment methods. GPS points along the river corridor used for absolute accuracy assessment, including a selection of points which were occluded by vegetation. Highlighted patches are the 6 stable areas used for relative accuracy assessment (see 4.2.2). The cross sections relate to those used in the discussion (6.2) to compare UAV-MS SfM and UAV-LS point clouds.

3.5.2.1 Absolute Accuracy Assessment

A total of 82 points were collected on 14/04/2021 using a Leica GS10/GS15 base and real-time kinematic rover, including 15 points in locations occluded from overhead view by vegetation (Figure 3-7). Survey accuracy was assessed by performing cloud to cloud distances (using the open-source CloudCompare software <https://www.danielgm.net/cc/>, version 2.11.3, last accessed: 17/11/2021) between these point locations and recording the absolute deviation from the measured point in the X, Y, and Z components. Cloud-to-cloud distances were used over point to DEM methods to remove the influence of DEM creation on results and make sure a comparison was made to the most local, observable point.

3.5.2.2 Relative Accuracy Assessment—Repeatability

Six stable patches (defined as no bare earth change through the survey period) of ground were identified, these being located on areas of land away from the active channel margin. Each patch measured in the range of 690–1350 m² and contained between 680,000 and 1,200,000 points in each of the surveys (approximately 890–950 points per square metre). For each point cloud, the patches were extracted and compared between one another in the following way: (i) between UAV laser scanner and multispectral SfM-derived clouds for the same date; and (ii) between each of the methods individually across all dates. The former helps to compare two methods to derive the same surface, the latter assesses the repeatability of each method. For the purposes of analysis, the patches are combined together and not analysed individually.

3.6 Results

3.6.1 Absolute Accuracy of UAV-LS and UAV-MS (SfM)

For the 82 ground check points, the mean error from the UAV-LS was -0.182 m, with a standard deviation of 0.140 m (Table 3-2). This implied that the UAV-LS underestimated the distance from the scanner to the surface, with most of the points being above their true ground locations. The average point offset in the combined X and Y plane was 0.012 m, with only 14 (16.5%) points over 0.05 m from the check points. For the same 82 locations, the mean UAV-MS error was -0.469 m and the standard deviation was 0.381 m, suggesting the same direction of error as the UAV-LS. This implies some degree of this error may be due to vertical offset errors during the sensor set up relative to the GNSS receiver on top of the UAV.

For vegetated points, the UAV-LS had a mean error of -0.110 m with a standard deviation of 0.180 m. Although the mean error for vegetated points was lower, the variation in this error was slightly higher. There were higher deviations in the X and Y plane, with an average distance apart of 0.055 m, which is to be expected with a lower below canopy point density, but this appeared to have little effect on the mean error. The UAV-MS appears to perform equally well based on mean error, with a value of -0.181 m; however, the spread of error within vegetated sections is greater, with a standard deviation of 0.572 m and a range of errors over 2 m. This is likely the result of the dense cloud failing to identify the correct depths of points through the canopy, or the ground being obscured completely. This highlights the performance of the UAV-LS method whereby the quality of the resultant point cloud is less diminished by vegetation especially in comparison to the performance of the UAV-MS SfM in heavily vegetated areas.

Table 3-2 Absolute errors of each survey method when compared to measured GNSS check points, separated by levels of vegetation obstruction.

Sensor	Category	Summary Statistics (m)				
		Mean Error (Z)	Standard Deviation (Z)	Min	Max	Range
UAV-LS	Unvegetated	-0.182	0.140	-0.366	0.424	0.790
	Vegetated	-0.116	0.181	-0.285	0.299	0.584
UAV-MS	Unvegetated	-0.469	0.381	-1.023	1.085	2.108
	Vegetated	-0.181	0.572	-0.915	1.085	2.000

3.6.2 Relative Accuracy of Surveys: Repeatability

3.6.2.1 Comparison of UAV-LS and UAV-MS Derived SfM for the Same Dates

Three of the surveys (February and July 2020 and June 2021) show very good agreement in the data, with mean errors of between 0.03 and 0.06 m, with standard deviations of under 0.05 m (Figure 3-8). This implies that both the direct georeferencing of the UAV laser scanner and the SfM-derived point cloud are of high quality, with two separate methods obtaining similar results for the same pieces of Earth.

Conversely, there seems to be greater discrepancy in elevations between the methods for surveys in October 2020 and April 2021, showing a greater level of skew in the histograms and multiple peaks. The mean errors are an approximate order of magnitude larger at 0.10 m but more importantly the variation in error increases just as much (Figure 3-8). Therefore, the confidence in these surveys is lower than others, but are still suitable when investigating morphological change at scales which are typically one and two magnitudes of change larger than this.

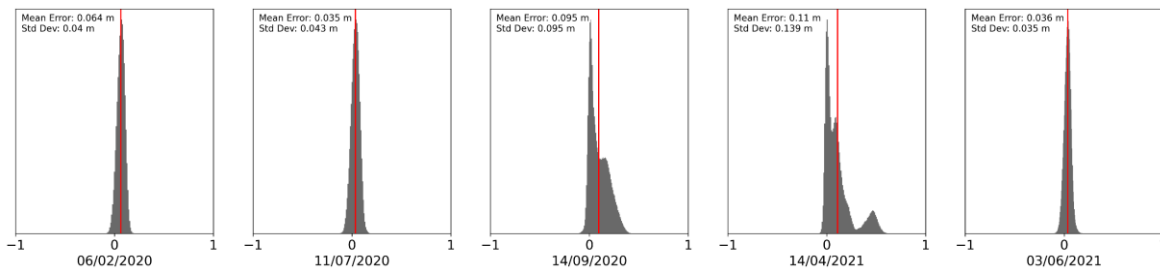


Figure 3-8 Differences between UAV-LS- and UAV-MS-derived SfM point clouds for the each of the 5 survey dates across the stable patches. Vertical red lines show the position of the mean error in m. This highlights the similarity between both methods for obtaining clouds with some discrepancies on two of the survey dates.

3.6.2.2 Repeatability of Survey Methods: Comparisons Across Dates

When comparing between the same method on different dates, the first date chronologically is used as the reference cloud, with the latter date the cloud to be compared. As such, a positive difference shows that the latter date points have higher elevation values than the reference (earlier) cloud. Figure 3-9A shows the comparison of stable ground points between different UAV-LS clouds. The agreement between each pair of surveys is very high, with all mean errors being under 0.1 m and 7 of the 10 combinations having mean errors under 0.05 m. Only comparisons with surveys in February 2020 show any evidence in the histograms of multiple peaks in errors, with all other surveys having a consistent singular peak. These peaks are narrow, with all standard deviations being under 0.1 m, and with most having standard deviations under

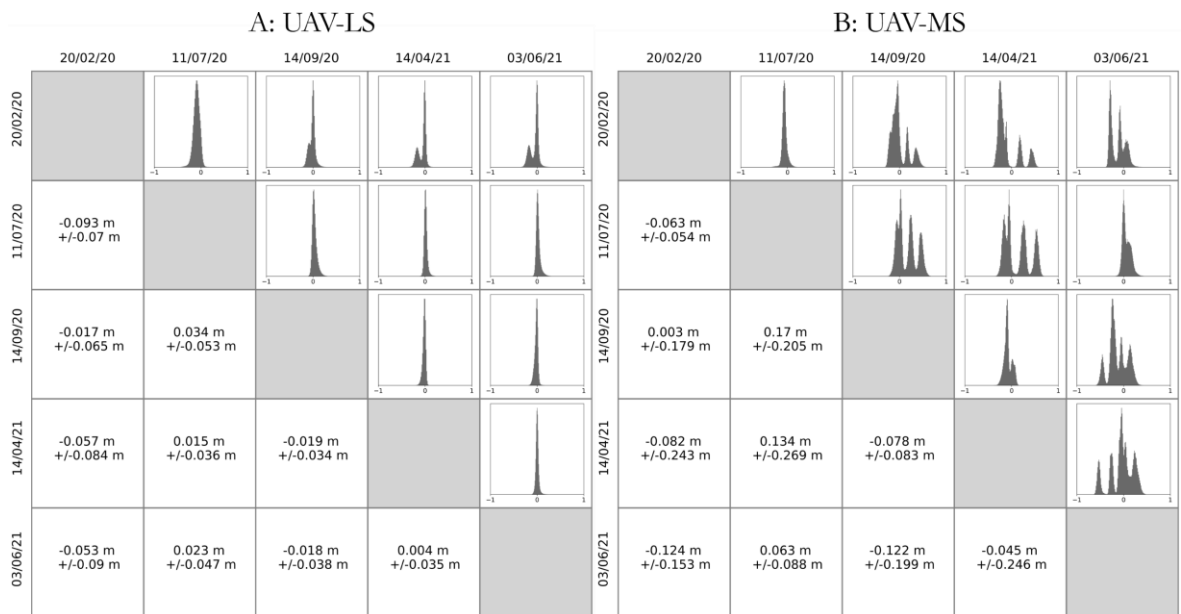


Figure 3-9 Distributions of errors and mean \pm standard deviation of errors (in m) between surveys for the stable ground patches on different dates for: (A) UAV-LS method; and (B) UAV-MS-derived SfM methods.

0.05 m, suggesting a minimum level of detection of 0.1 m for the UAV laser scanner method when comparing change between two surveys.

In contrast, the error assessment from the UAV-MS derived SfM processing (Figure 3-9B) suggests that the quality of reconstruction does not present consistent results. The mean errors between pairs of surveys is good, with six of the 10 surveys having values of under 0.1 m; however, the standard deviation of errors is far greater, with seven survey pairs having standard deviations over 0.1 m. This comparison suggests that the errors described in Section 3.6.2.1 and Figure 3-8 are likely a result of SfM reconstruction.

The histograms in Figure 3-9B show multiple error peaks, suggesting a spatial variation in error across the stable patches. Figure 3-10 shows a comparison of the Z errors between point clouds from April 2021 and June 2021 for the UAV-LS and UAV-MS datasets in each of the patches. While the UAV-LS data shows a spatially consistent magnitude of error, the UAV-MS appears to show a non-consistent pattern of change, exhibiting both under- and overestimation. It is likely that these patterns are caused not by incorrect location information (i.e., the direct-georeferencing) of the cameras themselves based on the success of the UAV-LS, but rather in the reconstruction and transformation of the image data into the chosen coordinate system. Patches that are close to each other having similar error supports this. This would explain why there is no consistent pattern in the error across survey combinations as seen in Figure 3-9, as each set of images is processed and fitted optimally, the error produced will be different. This

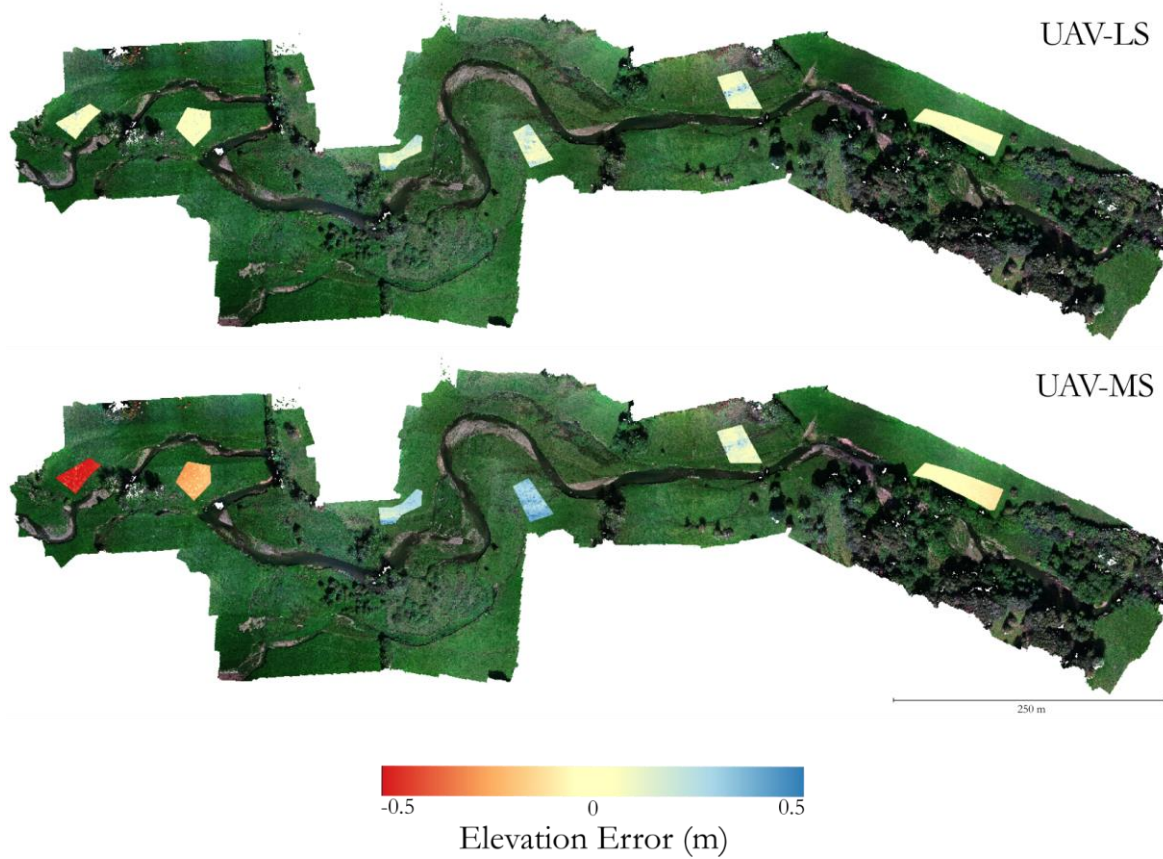


Figure 3-10 Comparisons of UAV-LS- and UAV-MS-derived SfM methods between April and June 2021 for each of the six stable ground patches, highlighting the spatial variability in accuracy for SfM-derived models compared to UAV-LS methods.

causes the different peaks in errors and for some models to over and under predict elevation in relation to each other.

3.7 Discussion

3.7.1 UAV Laser Scanner and Multispectral System

We assembled a small, <2.5 kg sensor package at a total cost of around GBP 24k (2018 prices), representing a significant saving over commercially available systems, which can cost as much as GBP 150k. UAV-LS absolute accuracy ranged from 0.1 to 0.2 m, but minimum levels of detection based on repeatability comparisons revealed were less than 0.1 m, with most surveys being <0.05 m. These values compare to similar ones reported, for example, by Lin *et al.* (2019) in their coastal application of UAV laser scanning and Jacobs *et al.* (2021) for snow depth mapping. By comparison, SfM-derived terrain products showed large errors between surveys, most likely based on variable reconstruction and transformation. Nonetheless, the direct georeferencing and navigation techniques used herein show great promise for future

applications and remove the need for many GCPs, instead using just a few as check points with the errors between surveys still less than the magnitudes of change associated with mobile river reaches.

3.7.2 Eco-Geomorphic Applications

This paper has focused mainly on the development and application of a UAV-based laser scanning system, but the purpose for developing such a sensor package is for research into eco-geomorphic processes along river corridors. The key innovation in using UAV-based laser scanning instead of (or along with) SfM-derived models is that laser scanning techniques are capable of capturing complex surface features and some measure of vegetation structure (Resop, Lehmann and Hession, 2019; Lague, 2020). It is not within the scope of this study to assess the ability of UAV-LS to collect vegetation structure, nor to derive metrics associated with this. However, Figure 3-11 provides a visual comparison between UAV-LS and UAV-MS SfM point clouds from three cross sections along the study reach, covering bare earth (A), sparse vegetation (B), and a dense wooded section (C). Despite a drop in point density, the laser scanner better captures the vertical face of the deeply incised river bank in the bare earth cross section, morphology that is smoothed by the SfM reconstruction. SfM is known to struggle at capturing steep banks and overhanging topography due to the reconstruction techniques upon which it relies (Smith, Asal and Priestnall, 2004; Cook, 2017), and this can be seen here for the relatively small vertical bank faces of around 1 m shown in Figure 3-11A.

In addition, the water surface can be identified in both sets of data. Despite the wavelength of the laser scanner (903 nm) being prone to absorption in water, some returns clearly mark out the surface across the bare earth cross section. The SfM-derived results show much higher levels of noise, likely due to surface features and reflection from the moving water increasing the number of erroneous key tie points in the processing steps (Woodget *et al.*, 2015; Dietrich, 2017; Shintani and Fonstad, 2017). Studies have used the surface reflections of laser scanning to assume a water surface elevation (Legleiter, 2012), which is more difficult to obtain from SfM techniques (Woodget *et al.*, 2015). This water surface can then be used to obtain bathymetry by applying refractive corrections to SfM depths in shallow water where the riverbed is visible. A combination of these methods may allow for improved bathymetry from SfM methods by obtaining both subsurface and surface measurements. However, the noise present in this shallow river section highlights the practical difficulties of obtaining bathymetry from imagery.

In the vegetated cross sections, two key observations are made: (i) the vegetation structure is well captured by the UAV-LS; and (ii) the bare earth morphologies of the river and floodplain

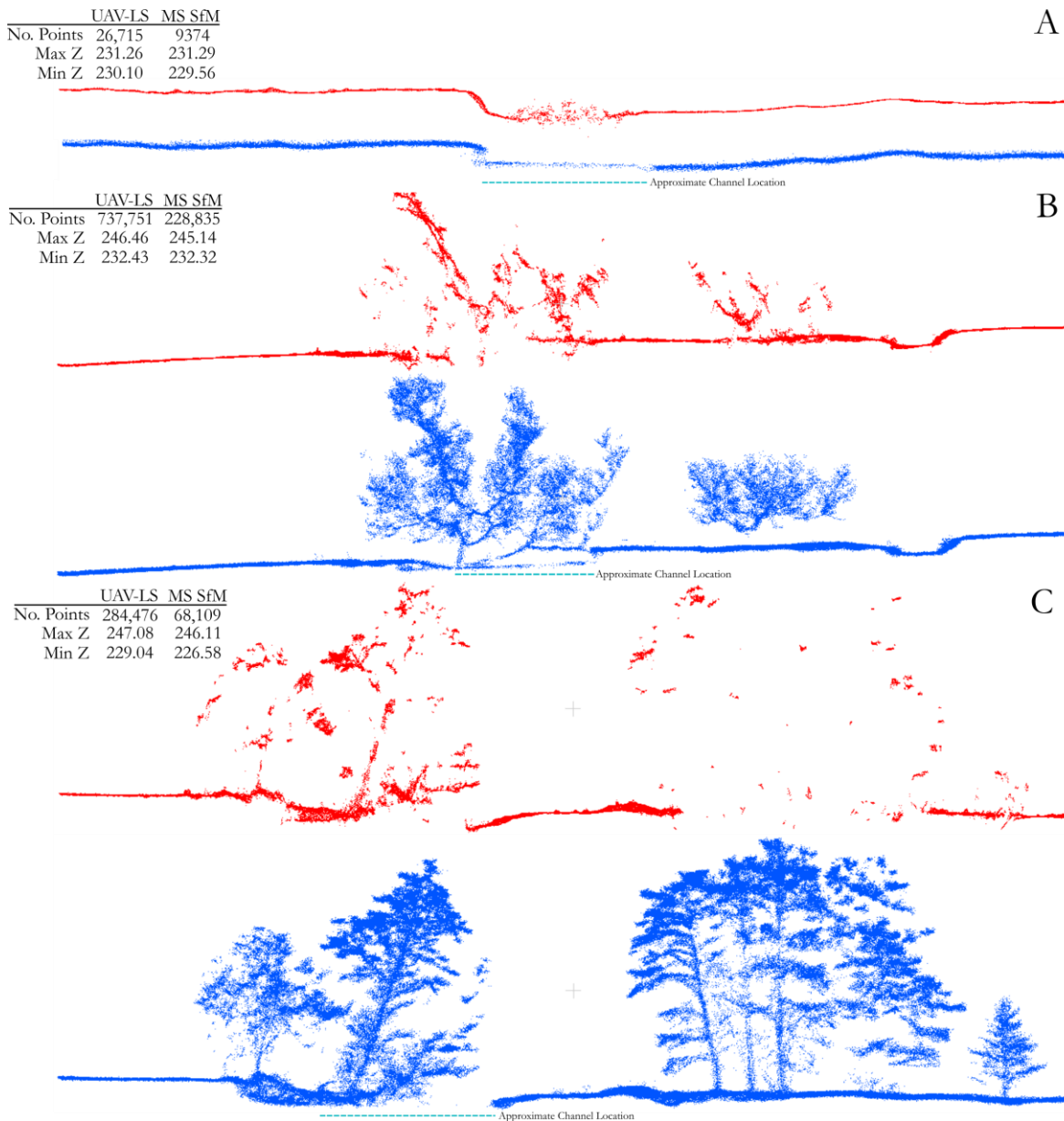


Figure 3-11 Extracted cross section (see Figure 3-7 for locations) comparisons of UAV-MS derived SfM point clouds (red) and UAV-LS point clouds (blue) for (A) bare earth; (B) sparse vegetation; and (C) dense wooded vegetation. Statistics show the number of points within each cloud, and the minimum and maximum elevation values.

are equally captured. Despite the variable point density within the canopy from the UAV-LS data, the locations of features such as trunks and low hanging branches are clearly identifiable. This is relevant when considering the impact of vegetation on high flow events where interaction between these features modulates flow patterns. In comparison, the resultant point cloud from the UAV-MS fails to identify many structural elements in the sparse woodland cross section, and even fewer in the dense patches with only a few tree crown points. For studies that aim to observe and quantify vegetation and flow interactions, SfM-based reconstructions have been shown to be unsuitable. In addition, when considering geomorphic change, few bare earth

points beneath dense canopies are detected, severely limiting the ability to construct a DEM, with high error potential as outlined in Section 3.6.1. In the bare earth cross sections (Figure 3-11A), the cut bank location and angle is fully resolved from the UAV laser scanning data where the SfM reconstruction smooths the feature. There are also several erroneous points in the SfM reconstruction of dense woodland far below the true ground layer (Figure 3-11C), which would propagate through into increased errors in derived digital terrain models produced from the data. This is likely due to the reduced relative number of points per scan for the SfM-derived clouds as identified on Figure 3-11. Moreover, any possibility of obtaining water surface or bathymetry data in these vegetated reaches from SfM is removed, yet there is evidence of water surface detection in panel B for the UAV-LS data despite being directly below the canopy. Overall, it would therefore appear that for reaches where there is a large presence of tall, complex vegetation, SfM methods alone are not best suited to eco-geomorphic research.

The multispectral data offer some exciting opportunities, for example, making use of the additional near-Infrared wavelength to derive NDVI (Normalised Difference Vegetation Index)-type products linked with the vegetation cover (e.g. Marchetti *et al.*, 2020). Such datasets have been shown to improve classifications of vegetation, for example over desert areas (Al-Ali *et al.*, 2020), and have great potential to be combined with structural data to improve estimation of biomass and vegetation functional type. Measurements of NDVI throughout the year and identification of the magnitude, direction, and temporal rates of change may help in the classification of vegetation. For example, larger changes in NDVI values from winter to summer may indicate the presence of seasonally dependent vegetation. Long-term trends in NDVI can be linked to the underlying fluvial conditions (e.g. Nallaperuma and Asaeda, 2020), as well as used for monitoring changes in vegetation extent across periods of varying flow conditions (e.g. Bertoldi, Drake and Gurnell, 2011). Such research traditionally uses satellite imagery over larger areas, but the advent of compact multispectral systems allows for these interactions to be investigated at the finer spatial resolutions demonstrated herein. For example, Figure 3-12 highlights the change in NDVI from winter to summer across a bar in our study site, a ~100 m feature over which traditional satellite imagery such as Landsat would capture 1–4 pixels of data. Resolving this level of detail will enable identification of vegetation-flow interactions providing eco-geomorphic insights in addition to those offered from traditional satellite or visible wavelength UAV imagery. While the use of UAV-based multispectral sensing in fluvial research has focussed predominantly on vegetation quality or hydraulic properties such as suspended sediment (Rossi, Mammi and Pelliccia, 2020; Ren *et al.*, 2021), the opportunities to apply methods developed for satellite data at a finer resolution makes combining multispectral rather than traditional RGB imagery with UAV-LS data an exciting prospect for future research.

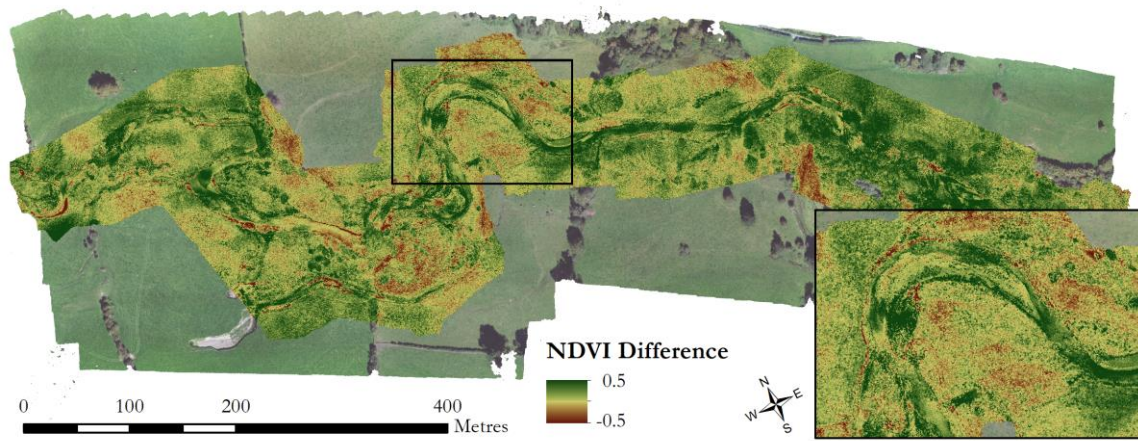


Figure 3-12 Difference in NDVI values across the study reach between September 2020 and February 2020 surveys. Brown values indicate a decrease in NDVI values and green an increase. Inset shows an enlarged version of a meander and point bar feature, with the large increases in NDVI likely indicating regions of perennial colonisation of sediment deposits by herbaceous pioneer species.

3.8 Conclusions and Future Work

Having provided a proof-of-concept for the sensor package, and quantified the minimum level of detection at 0.1 m, we have shown that UAV-LS and UAV-MS sensors are capable of delivering high-resolution 3D point clouds and imagery which are able to discretise vegetation structure and spectral response. These methods demonstrate that riparian vegetation can be quantified and analysed at a level of detail that is hitherto unprecedented, capturing additional detail that will allow new insight to be gained in relation to eco-geomorphic interactions. The benefits of obtaining enhanced structural data that cannot be captured by SfM methods alone are evident, and combining the two methods together opens up new avenues of research. For densely vegetated river corridors (and other domains), the benefits of using UAV-LS have been highlighted, with the addition of a multispectral rather than traditional RGB camera allowing additional useful vegetation metrics to be measured.

Future work should seek to use the data to establish metrics which are able to better characterise vegetation function in relation to river corridor evolution. The sensor package developed here, along with comparable commercial units, shows great promise for being able to quantify co-evolving vegetation and geomorphic change through time, allowing researchers to begin to explore the roles of seasonality, plant maturity and die-back in relation to fluvial dynamics. Furthermore, the potential increase in descriptive functional metrics would be advantageous to

machine learning techniques which might seek to link vegetation, geomorphic change, and river flow dynamics through time.

Chapter 4 Exploring the 4D scales of eco-geomorphic interactions along a river corridor using repeat UAV Laser Scanning (UAV-LS), multispectral imagery, and a functional traits framework.

4.1 Abstract

Vegetation plays a critical role in the modulation of fluvial process and morphological evolution. However, adequately capturing the spatial variability and complexity of vegetation characteristics remains a challenge. Currently, most of the research seeking to address these issues takes place at either the individual plant scale or via larger scale bulk classifications, with the former seeking to characterise vegetation-flow interactions and the latter identifying spatial variation in vegetation types. Herein, we devise a method which extracts functional vegetation traits using UAV laser scanning and multispectral imagery, and upscale these to reach scale guild classifications. Simultaneous monitoring of morphological change is undertaken to identify eco-geomorphic links between different guilds and the geomorphic response of the system in the context of long-term decadal changes. Identification of four guilds from quantitative structural modelling based on analysis of terrestrial and UAV based laser scanning and two further guilds from image analysis was achieved. These were upscaled to reach-scale guild classifications with an overall accuracy of 80% and links to magnitudes of geomorphic activity explored. We show that different vegetation guilds have a role in influencing morphological change through the stabilisation of banks, but that limits on this influence are evident in the prior long-term analysis. This research reveals that remote sensing offers a solution to the difficulty of scaling traits-based approaches for eco-geomorphic research, and that these methods may be applied to larger areas using airborne laser scanning and satellite imagery datasets.

4.2 Introduction

Fluvial eco-geomorphic interactions are co-dependent, complex, and variable across space and time, representing a continued area of interest within river research (Thoms and Parsons, 2002). The diversity of eco-geomorphology in river corridors can be attributed to surrounding land use, existing morphology, and flood regimes (Naiman, Decamps and Pollock, 1993), whilst this same diversity simultaneously influences the flow of water and sediment, ultimately affecting morphology (Diehl *et al.*, 2017) and floodplain conveyance (Nepf and Vivoni, 2000). The role

of vegetation within the river corridor is well established, benefiting the local ecology (Sweeney *et al.*, 2004; Harvey and Gooseff, 2015) alongside playing a role in natural flood management schemes and reconnecting channels and floodplains (Lane, 2017; Wilkinson *et al.*, 2019), especially for small catchments where land cover is more influential for flooding (Blöschl *et al.*, 2007). This is important when considered against a backdrop of a rapidly changing climate where flow extremes are more varied, flooding more likely (UNISDR and CRED, 2015), and riparian vegetation is likely to undergo shifts in composition (Palmer *et al.*, 2009; Rivaes *et al.*, 2014). Consequently, adequately measuring and monitoring vegetation within the fluvial domain is critical to understanding how these systems will respond to varying climatic and hydrological conditions.

The characterisation of riparian vegetation distribution over larger (>1 km) scales has typically relied upon the use of coarse classifications such as those identified in the Water Framework Directive (e.g. Gilvear, Tyler and Davids, 2004), using techniques such as aerial imagery and satellite remote sensing (see Tomsett and Leyland, 2019). Any characterisation must be scalable and geographically transferable to cover the vast range of different fluvial landscapes whilst still accounting for the complexity presented within river corridors. Over-simplified, coarse classifications may altogether miss the vegetation complexity that exists, whilst conversely, highly detailed models tend to be necessarily localised and less transferable to alternate systems and scenarios. Traits-based classifications, developed and used within ecology, offer a scalable and transferable approach which can be applicable to the fluvial domain (Diehl *et al.*, 2017). They have been shown to be useful for modelling topographic response to changing vegetation, sediment, and flow conditions (Diehl *et al.*, 2018; Butterfield *et al.*, 2020). However, challenges remain in broad application of this approach, with the characterisation of vegetation in the highly detailed manner required to extract traits metrics being challenging over larger (e.g. >1 km) scales.

To address these gaps, herein we examine the scales over which different traits can be collected from remote sensing methods and assess how well these traits can be used to establish eco-geomorphic relationships. We use a UK based temperate river as an exemplar site to demonstrate the effectiveness of novel remote sensing techniques for characterising vegetation. We investigate the limits of trait detection and the scales at which they are most appropriately used to enhance eco-geomorphic understanding, enabling us to establish the applicability of these methods to a variety of river corridor environments. Below we introduce the concepts of plant functional traits and hydraulically relevant traits before establishing the aims of this research.

4.2.1 The Importance of Vegetation

It is well understood that vegetation plays a key role within the river corridor and that how vegetation is modelled can affect the outcomes of hydrodynamic simulations. Channels with in-stream vegetation may experience roughness values an order of magnitude higher than non-vegetated channels (De Doncker *et al.*, 2009), capable of reducing velocities by up to 90% (Sand-Jensen and Pedersen, 1999). However, foliage type and how vegetation is modelled affect the influence that the vegetation has on flow (James *et al.*, 2008). The challenges posed by quantifying in-stream vegetation means that it is often difficult to make estimations of in-stream roughness (O'hare *et al.*, 2011). Conversely, above water vegetation is easier to measure and monitor depending on the scales of analysis. Banks are typically eroded via mechanisms of mass failures or entrainment (Hughes, 2016) and so any stabilising effects of vegetation must influence these processes. Vegetation can reduce stream power, increase soil cohesion, and influence soil moisture levels, all of which can help to reduce erosion (Simon *et al.*, 2000; Fox *et al.*, 2007; Kang, 2012). Bank collapse is influenced by three dominant factors, the extra mass of the vegetation, the shear strength provided by root reinforcement, and changes to bank pore water pressure (Wiel and Darby, 2007), with above ground biomass therefore directly influencing the mechanical and hydraulic properties of the substrate (Gurnell, 2014). The above ground biomass also has a direct influence on river flow and sediment transport when submerged (Gurnell, 2014), although this is stage dependent and depends on plant volume and structure.

4.2.2 Plant Functional Traits

Functional traits originate from ecological research, whereby criticism of using functional types led to a need for a more robust system of classification for ecological studies. Functional types represent vegetation based on its morphology and physiology, amongst other factors (Box, 1981; Box, 1996), but these attributes can exhibit greater variation within functional types as opposed to between them (Wright *et al.*, 2005; Reich, Wright and Lusk, 2007), as well as not varying between different types at all (Van Bodegom *et al.*, 2012). Assessment of plants based on their functional traits has been seen as a method to overcome the shortcomings of the classic typological approach (Quétier *et al.*, 2007).

Much like the attributes of a plant type, plant functional traits are morphological, physiological, or phenological attributes that are measurable at the individual plant level (Savage, Webb and Norberg, 2007; Violle *et al.*, 2007; Kattge *et al.*, 2011). These measures can either be direct measures of a function such as photosynthesis or be a surrogate measure for a function such as

leaf area. To be classed as ‘functional’ for ecology, traits must affect either plant growth, reproduction, or survival (Violle *et al.*, 2007). Traits can either be effect or response based, depending on whether they have an influence on or are influenced by their wider environment (Violle *et al.*, 2007). The benefit of traits-based methods is the applicability between different sites without needing species specific data (McGill *et al.*, 2006). Therefore, the findings of community response to factors such as land use or climatic gradients (e.g. De Bello, Lepš and Sebastià, 2006; Garnier *et al.*, 2006) can be applied to a different location with similar trait composition. This is possible through the creation of guilds. Guilds can be used to group plants with similar traits together (Lytle *et al.*, 2017), providing a scalable framework for eco-geomorphic research.

Traits-based approaches are well suited for eco-geomorphic research due to the strong environmental gradients within fluvial systems (Naiman *et al.*, 2005). Vegetation responds to hydrological variables, such as water availability and disturbance events (Hupp and Osterkamp, 1996) whilst also influencing flow, sediment transport, and morphological stability (Gurnell, 2014), meaning that the bi-directional nature of this relationship maps well onto a traits-based framework. O'Hare *et al.* (2016) have assessed the traits of nearly 500 species that influence river processes, revealing evidence of a broad link between plant form, distribution, and stream power within the UK (O'hare *et al.*, 2011). Moreover, traits-based approaches allow for a more comprehensive view on eco-geomorphic interactions than a purely taxonomic approach due to the environmental conditions having a larger influence on trait compositions than species compositions (Corenblit *et al.*, 2015; Göthe *et al.*, 2017).

To date, the majority of traits-based research has focussed on ecological responses to hydrological conditions. For example, inundation likelihood has been shown to increase the presence of plants with longer and younger leaves (Stromberg and Merritt, 2016; McCoy-Sulentic *et al.*, 2017) whilst also being less woody (Kyle and Leishman, 2009; Stromberg and Merritt, 2016), with frequent inundation and higher stress environment necessitating greater flexibility. Conversely, plants in lower stress environments tend to be taller with longer life cycles (Kyle and Leishman, 2009; Stromberg and Merritt, 2016; McCoy-Sulentic *et al.*, 2017). Factors such as nutrient loading (Baattrup-Pedersen *et al.*, 2016; Lukacs *et al.*, 2019), light conditions (Baattrup-Pedersen *et al.*, 2015), carbon availability (Lukacs *et al.*, 2019), and anthropogenic interference (Baattrup-Pedersen, Larsen and Riis, 2002; O'Briain, Shephard and Coghlan, 2017) are all key controllers of trait composition, with the environmental conditions better related to trait, rather than species, composition (Göthe *et al.*, 2017). Furthermore, individual species have been shown to demonstrate differing traits depending on external stresses. *Populus nigra* trees were found to be smaller, have greater flexibility, and had a higher number of structural roots

at a bar head when compared to a bar tail (Hortobágyi *et al.*, 2017). Further work demonstrated that the smaller species at the bar head were incapable of trapping sediment when compared to those at the bar tail (Hortobágyi *et al.*, 2018), highlighting the importance of traits rather than taxonomic approaches.

Hydrological variability can also influence trait assemblages. For example, mean flood frequency across 15 sites was found not to be related to trait diversity, whereas the magnitude of a 20-year flood and the variability in flood frequency (when they occurred during the year) were both related to trait diversity (Lawson *et al.*, 2015). Species richness was decreased in field experiments of artificial flooding and drought, although trait diversity was more tolerant to drought conditions overall (Baattrup-Pedersen *et al.*, 2018). Rivers with more variable flows tend to encourage pioneer species, whilst those with prolonged periods of drought see an increased abundance of water tolerant species (Aguiar *et al.*, 2018). As a result, these responses mean successful river restoration projects should focus on the type of restoration more than the extent (Göthe *et al.*, 2016). Taxonomic approaches can still perform equally well for fluvial studies, but traits-based approaches tend to account for local and regional conditions better (Tabacchi *et al.*, 2019), which is necessary for scalability.

Research into effect traits and their geomorphic influence has received less attention as traits concepts have only recently started to be explored in hydrological research. However, as noted by Corenblit *et al.* (2015), the interactions between plant traits and fluvial systems are linked, with hydrological conditions affecting plant establishment and survival and plant morphological traits affecting morphology and subsequent establishment. There is evidence that changing traits can alter the morphological evolution of channels, with invasive species that have higher branching densities and less flexibility increasing aggradation through reductions in near bed velocities (Manners *et al.*, 2015). Guild location impacts the morphological response, with analysis of bars showing different responses downstream and also laterally based on the traits of the dominant species in these directions (Hortobágyi *et al.*, 2018). This is supported by Butterfield *et al.* (2020) who when examining changes in multi-annual elevation found that guilds at different locations, experiencing different hydraulic conditions, had differing impacts, but also that guilds could not explain all the variation in morphological response. It was found that differing canopy architectures that interacted with flow were likely to be the prominent driver of topographic response, supporting the research of Manners *et al.* (2015). However, trait diversity can impact morphological response as much as the individual traits, with combinations of guilds interacting to alter responses (Hortobágyi *et al.*, 2018), from which spatially averaging to areas of dominant guilds may oversimplify the complexity of interactions.

4.2.3 Hydrologically Relevant Functional Traits

Not all vegetation functional traits are relevant when considering direct relationships between vegetation, hydrology, and morphology. Moreover, not all traits can be obtained from remote sensing techniques, a necessary requirement when upscaling to larger domains. Below we identify the vegetation traits that are directly relevant to river systems and which can potentially be captured via remote sensing techniques, thereby allowing the upscaling of any developed methods of characterisation.

Existing studies that have considered vegetation-flow interactions have focused on plant height and frontal area as key metrics which explain momentum exchanges in river flows. The height of the plant affects the amount of interaction (Nepf and Vivoni, 2000), with varying flow depth determining the proportion of the plant frontal area which is submerged. Frontal area is an often used proxy for the scale of obstruction and is a component of the drag formulation which can have a larger impact on flow conditions than the selection of a drag coefficient (Järvelä, 2004; Wilson *et al.*, 2006). However, the limitations of 2D metrics to describe the complex nature of plants has been highlighted, with the use of 3D data and plant volume offered as improved methods (Whittaker *et al.*, 2013; Vasilopoulos, 2017).

Under various flow conditions, the frontal area of a plant may change due to flexing and reshaping, with studies showing that not accounting for this can limit the results of drag models (Sand-Jensen, 2008; Whittaker *et al.*, 2013). A higher leaf area increases the momentum absorbing area of plants with de-leafed vegetation not bending until a higher threshold velocity is reached (Järvelä, 2002a; Wilson *et al.*, 2003). Drag has been calculated using leaf area, although not a 1:1 relationship it was shown to be suitable for estimating vegetative resistance (Jalonen, Järvelä and Aberle, 2012). The contribution of foliage to resistance decreases with flow speed, Whittaker *et al.* (2013) noting a drop in the drag contribution of foliage from 75% to 20-50% at speeds under and over 0.5 ms^{-1} respectively. This is due to the reshaping of plant structure during higher flows leading to reductions in drag (Armanini, Righetti and Grisenti, 2005), with the rate at which this reduction happens being plant dependent (Järvelä, 2002b; James *et al.*, 2008; Boothroyd *et al.*, 2017). The vertical distribution of plants also has a significant impact on flow, with different vertical distributions such as step changes or continuous variations, impacting flow differently and being more important than multi-plant arrangement (Lightbody and Nepf, 2006; Jalonen, Järvelä and Aberle, 2012).

The arrangement of plants is still important in determining bulk drag, with drag coefficient values for a single foliated stem not representative of stems occurring in bulk vegetation (James *et al.*, 2008). Higher plant densities within a channel lead to an increase in drag coefficients,

however the arrangement of vegetation within the channel has a negligible impact (Järvelä, 2002b; Kim and Stoesser, 2011). Sand-Jensen (2008) identified that there was a difference in downstream flow between evenly distributed plants and the same biomass distributed into high density clumps, with the former providing the larger increase in drag and impeding flow the most. Therefore, spatial variation in plant distribution may be more important than the density of the patches themselves. A higher stem density does result in more scour around stems and deposition to be further from the scour sites, however overall deposition does not increase with increased stem density (Follett and Nepf, 2012).

Whilst both vegetation structure and distribution of individual plants directly impact flow, many other vegetation traits can impact sediment transport processes, for example through playing a role in altering the erodibility of periodically submerged banks or bar surfaces, or through increased resistance from root structures. Although vegetation height, frontal area, and leaf area are all key effect traits which can be measured directly, accounting for secondary impacts of vegetation related to below ground biomass for example, and how all traits vary spatially and temporally remains the challenge for advancing our understanding of eco-geomorphic interactions.

4.2.4 Remote Sensing of River Corridor Vegetation

Although many of these traits are inherently measurable in the field, many of them are not obtainable from current remote sensing methods. Direct trait extraction for riparian vegetation from airborne (i.e. large scale) remote sensing has not yet been utilised to enhance eco-geomorphic studies. Currently, collection of trait data relies on direct ground based field surveys and lab analysis, or species are identified in the field and traits taken from databases (e.g. TRY database (Kattge *et al.*, 2020)). Methods are often dependent on site access, species richness, and variation within the study area (Palmquist, Sterner and Ralston, 2019), utilising methods such as quadrat surveying or transect sampling. This technique is effective for establishing traits but is limited by the spatial extent of ground coverage. Some variables inevitably require databases to avoid substantial disturbance, such as root characteristics (e.g. Stromberg and Merritt, 2016; Aguiar *et al.*, 2018; Baattrup-Pedersen *et al.*, 2018), although databases should be used with caution; for example, maximum plant height is not related to the plant submergence height at the time of a particular flow event, and great variation can be seen in both effect and response traits for a singular species (Hortobágyi *et al.*, 2017; Hortobágyi *et al.*, 2018). Therefore, accounting for temporal and spatial variation in traits is important and highlights the need for temporally and spatially relevant data collection.

For fluvial research, multispectral imagery can be used to determine species using supervised and unsupervised classifications with good accuracy (Butterfield *et al.*, 2020). Outside of fluvial research there is an increasing awareness of the potential of remote sensing methods to help drive the scalability of functional traits, especially in relation to physical traits such as plant height, leaf area index, phenology, and biomass (Abelleira Martínez *et al.*, 2016; Aguirre-Gutiérrez *et al.*, 2021), yet considerable limitations remain due to the uncertainty in relating spectral and physical properties to functional traits (Houborg, Fisher and Skidmore, 2015). Upscaling localised high resolution data is possible however, for example from TLS (Terrestrial Laser Scanning) to large scale ALS (Airborne Laser Scanning) data (Manners, Schmidt and Wheaton (2013).

Advances in UAV (Uncrewed Aerial Vehicle) remote sensing can create an important link between these two scales of data collection. UAV data collection allows high resolution imagery and active remote sensing methods such as laser scanning to be conducted on large reaches relatively easily (Tomsett and Leyland, 2019), increasing coverage and providing a middle ground for relating local to large scale data. Multispectral cameras have already helped to improve the classification of vegetation from UAVs (Al-Ali *et al.*, 2020), and active UAV-LS (UAV Laser Scanning) has also been shown to be comparable in estimating tree structures to TLS methods (Brede *et al.*, 2019). Such methods therefore present an opportunity to not only classify vegetation by types and assign them to guilds, but to define guilds based on characteristics acquired from remote sensing directly, before upscaling this to reach scale classifications.

4.2.5 Aims

The aim of this research is to develop a set of scalable traits-based 3D vegetation metrics which can be used to assess spatial and temporal (i.e. 4D) variation and importance of eco-geomorphic interactions on an exemplar UK river system. This is achieved using the following specific objectives:

1. Undertake an assessment of the longer term (multi-decadal) eco-geomorphic evolution of the channel using satellite remote sensing, to compare planform evolution within vegetated and non-vegetated channel sections.
2. Identify and select hydrologically relevant traits which can be extracted from high resolution remote sensing data.
3. Establish the presence of vegetation guilds (those with similar traits) for the river reach, based on exploratory analysis and object orientated random forest classifications.

4. Compare the spatial extent of these guilds to morphological change over the study period to establish eco-geomorphic feedbacks.

4.3 Study Site

The exemplar site is located on the upper course of the River Teme on the English-Welsh border in the UK (Figure 4-1A). The study area consists of two broader regions; the upstream section consisting of open grassland with patches of heterogeneous vegetation, and the downstream section which flows through denser vegetation. The River Teme is a highly mobile, gravel bed river within an alluvial floodplain which exhibits numerous avulsions. There is active lateral erosion of the channel, depositional gravel bar features, and woody debris dams across the study site (Figure 4-1A). The reach has typically low flows (Figure 4-1B), with an average depth of 0.69 m (+/- 0.15 m) throughout the year with slightly higher average flow depths in the winter months (November – February, 0.79 m +/- 0.15 m). 95% of river depth has been below 0.99 m and 99.9% of the flow depth has been below 1.48 m. The largest recorded river



Figure 4-1 Study Site of the River Teme and the long term water level at the Knighton gauge station 3km downstream. A) Study Site Location on the River Teme, UK. Inset images show active bank erosion and a large debris dam caused by falling trees. B) River Gauge Level at the Knighton monitoring station ~1 km downstream from study reach, data available from 2002 – present.

depth was 2.85 m on the 16th February 2020 during Strom Dennis. Figures are obtained from a gauge station 3 km downstream of the study site, starting from the earliest gauge record.

4.4 Methods

4.4.1 Long Term (Decadal) Analysis

To assess the longer-term context of eco-geomorphic interactions within the study reach, historical satellite imagery was analysed to identify channel mobility in relation to riparian vegetation. Channel mobility was assessed by digitising bank edges across multiple years. This method is well established and has been used previously to study the evolution of a large river confluence (Dixon *et al.*, 2018) and for multi-decadal analysis of a single river (Gupta, Atkinson and Carling, 2013; Yao *et al.*, 2013), to identify the drivers of morphological change. These have typically been restricted to coarse (e.g. 30 m ground resolution) satellite datasets, with planform change only detectable if it is greater in magnitude than the image resolution. This can result in mixed pixels; where multiple land cover and vegetation types are misidentified into one category (Henshaw *et al.*, 2013). Here we make use of high spatial resolution imagery from Google Earth (0.5 - 2 m, source dependent) and Pleiades (0.5 m) to identify historical changes in channel location and vegetation cover. Google Earth historical imagery for the years 2000, 2006, 2008, and 2009 and Pleiades data from 2013, 2015, 2016, 2018, and 2020 were used from which bank lines were digitised, resulting in 20 years of channel evolution. Banks under tree cover were identified where possible using a mix of spectral bands (Pleiades data only) to highlight channel position. To account for the images being taken at various time periods throughout the years and subsequently having different flow regimes, bank tops were digitised as opposed to water edges to reduce uncertainty resulting from variable flow stage. The exception to this was where no clear bank top was present, for example on the large bars, where evidence of usual high flows from colour changes and trash lines in the imagery were used to guide digitisation of bankfull channel width.

All analysis of bank movement was performed in ArcGIS using the Digital Shoreline Analysis System (DSAS, (Himmelstoss *et al.*, 2018)) with a 1.5 km long baseline created for both left and right banks based on the dominant river planform trend. Transects were cast every 5 m and manually edited where necessary in order to intersect the outermost bank, especially on tight meander bends. The Shoreline Change Envelope (SCE), the distance between the nearest and furthest bank from the baseline, is used to infer total channel mobility throughout the reach.

To assess the impact of vegetation, the channel was classified into two classes: those containing structurally large vegetation and those that did not. Areas classed as containing structurally large vegetation could either include a small number of trees clumped around the channel, a linear section of vegetation on one bank, or larger areas of vegetation such as woodland. These regions were user defined based on all of the image sets available and were used to group transects within regions containing large vegetation and those that did not, for comparison of the SCE statistics. As vegetation may have an influence on both the local scale and broader reach scale morphology, the analysis was repeated for changes excluding the reoccupation of new or former channels (classed as avulsions). To achieve this, DSAS transects that spanned across two separate channels from different years were removed. Each individual channel was then reanalysed using separate baselines, consequently the impact on the results from channel switching can be isolated and removed.

Statistical comparison was undertaken of the SCE values for sections containing large vegetation and sections that did not. These could be used to identify any differences in the SCE values and therefore inferred mobility of these sections, and the influence vegetation may have on planform evolution. To investigate the morphological process of avulsions, the development of new channels between satellite images was also tracked. New and developing channels which were visible in satellite imagery were digitised for each set of images. These were compared to UAV flood extent imagery from February 2020 alongside historical LiDAR data from 2007 of the river corridor and qualitatively assessed in relation to how topography and flood events influence planform, and the processes by which channel switching occurs.

4.4.2 Field Collection of High Resolution 4D data

High resolution UAV-LS (UAV Laser Scanning) and UAV-MS (UAV Multispectral Imagery) were collected over the entire reach through February 2020 until June 2021, capturing all seasonality. To complement these flights, Terrestrial Laser Scanning (TLS) surveys of vegetated and bar sections were undertaken to gain a benchmark ultra-high-resolution dataset for comparison to the UAV-LS and for characterising small herbaceous vegetation. A UAV-RGB (Red Green Blue) survey was also undertaken during overbank flow on the falling limb of Storm Dennis in February 2020, to identify the flood extent. Table 4-1 summarises the survey dates, extents, and data collection methods.

Table 4-1 Summaries of the data collection methods used on each survey date. Overviews of survey extent are given for each date, as well as the sensors deployed and the survey statistics for each method. TLS point density is based on the resultant point cloud after registration. Ground Sampling Distance (GSD) is the resolution of the resultant orthomosaics. UAV-LS point density is taken once cleaning of the raw clouds has taken place.

Date	Survey	Sensor	Point Density/GSD
06/02/2020 (Winter)	Whole Reach	UAV-LS	778 m ²
		UAV-MS	0.04 m GSD
18/02/2020 (Winter)	Whole Reach	UAV-RGB	0.02 m GSD
16/07/2020 (Summer)	Subsection	UAV-LS	810 m ²
		UAV-MS	0.04 m GSD
		TLS	16,000 m ²
14/09/2020 (Autumn)	Whole Reach	UAV-LS	762 m ²
		UAV-MS	0.04 m GSD
14/04/2021 (Spring)	Whole Reach	UAV-LS	791 m ²
		UAV-MS	0.04 m GSD
03/06/2021 (Summer)	Whole Reach	UAV-LS	804 m ²
		UAV-MS	0.04 m GSD

A detailed outline of the UAV based sensor set up, processing routine and accuracy assessment can be found in Tomsett and Leyland (2021), with a short overview of the system provided below. UAV-LS and UAV-MS were collected using a DJI Matrice 600 Pro multirotor aircraft, capable of flying for 20 minutes per flight. Two sets of batteries allow for the spatially complex 1 km reach of the River Teme to be captured with some redundancy. Multispectral imagery was obtained from a MicaSense RedEdge MX camera, collecting imagery with a ground resolution of ~ 0.035 m across five spectral bands, consisting of blue (475 nm), green (560 nm), red (668 nm), red-edge (717 nm), and near infra-red (842 nm) wavelengths (MicaSense, 2021). The laser scanner is a Velodyne VLP-16 Puck Lite, firing 16 laser-detector pairs at approximately 300,000 points per second, with a 360° horizontal and 30° vertical field of view. The sensor has a range of up to 100 m and a typical ranging accuracy of ± 0.03 m (Velodyne Lidar, 2016). Both sensors use direct georeferencing from an Applanix APX-15, which utilises multi-frequency GNSS and MEMS (Micro Electro-Mechanical System) inertial motion unit to provide post processed positional and orientation accuracies up to 0.02 m and 0.025° respectively (Applanix, 2016). This removes the need for extensive GCP placement throughout the reach. Georeferenced point clouds from the laser scanner and Structure from Motion based point

clouds and orthomosaics from the multispectral imagery were produced, both with vertical accuracy under 0.1 m. UAV-RGB imagery was collected from a DJI Inspire 2 with a Zenmuse X4S camera, resulting in a ground resolution of 0.017 m from a flight height of 60 m. An on-board EMLID REACH M2 provides positioning accuracy of up to 0.015 m when post-processed (EMLID, 2021), with a connection to the on board camera to allow image captures to be timestamped to assist with the SfM processing. TLS data was captured in July 2020 using a Leica P20 Scanstation, collecting high resolution (0.0031 m point spacing at 10 m distance from scanner, resulting in a mean point density of 16,000 points per m² within the area of interest) scans of two locations. The first, an area of channel containing large vegetation at the inlet of the study site (two convergent TLS scans), and the second, part of a large meander bend in the centre of the study area (four convergent TLS scans) where large vegetation was absent. Targets were used to register scans together, acquired using a Leica TS06 total station, with a resultant scan registration accuracy of +/- 0.007 m.

4.4.3 Vegetation Functional Trait Extraction

The workflow developed to extract plant functional traits consisted of five steps: (1) Separation of individual plant point clouds that could be used for analysis, (2) Analysis of these individual clouds to extract metrics related to their traits, (3) Separation of plants into herbaceous and woody guilds by adapting the classification from Diehl *et al.* (2017) based on similar traits, (4) Identification of guild properties extractable from temporal UAV-LS and UAV-MS datasets for reach scale classification inputs, and (5) Use of an object-based random forest classifier to determine the spatial discretisation of guilds.

4.4.3.1 Point Cloud Segmentation

A number of automatic methods exist to classify very dense point cloud scenes into different groups (e.g. Brodu and Lague, 2012; Zhong *et al.*, 2016). However, the majority of these are designed for very high-resolution TLS datasets and so here a semi-automated approach was employed. Smaller vegetation whose structural composition cannot be fully resolved from UAV-LS data were analysed from the summer TLS survey. Automatic classification of ground/non-ground points was performed using the progressive morphological filter in the LidR package (Roussel *et al.*, 2020) before manually segmenting in CloudCompare (<https://www.danielgm.net/cc/>) to create individual plant models (Figure 4-2, *Raw Point Cloud*).

For the herbaceous plants, leaves and flowering parts were removed from the clouds so as not to interfere with the quantitative structural modelling (QSM). Although foliage is important, for the methods used herein they could not be accounted for due to point densities. Any statistical

outliers were detected, removing points 2.5 standard deviations and above the mean distance between points, resulting in a dataset consisting of 37 herbaceous plants.

Tree segmentation also used a combination of manual and automatic classification based on surveys in leaf-off conditions exposing the full internal tree structure. 24 trees were selected from across the reach representing a range of structures and sizes from which complete models could be created. As above, initial separation of ground and vegetation points was performed using a progressive morphological filter. Whilst automatic classification methods such as CANUPO exist (Brodu and Lague, 2012), the UAV-LS point densities necessitated the manual extraction of individual trees, prior to interactive filtering using a number of statistical measures. Local volume density helped to separate points distinct from the main tree woody structure, whilst linearity metric filters (how aligned points are within a set radius) remove points that are highly complex or not part of the main tree structure. The statistical outlier removal tool and a final manual check can then be used to remove any remaining erroneous points. This resulted in a point cloud of predominantly large branches, with a clearer structural profile as can be seen in Figure 4-2 (*Filtered Point Cloud*). The thresholds for separating individual trees are size, structure, and point density dependent, hence the need for interactive selection.

This adds an element of user bias as to what is deemed a ‘main’ branch, but the lower density of UAV-LS scans makes this a necessary method before reconstructing vegetation models (Brede *et al.*, 2019). Shrubs and grasses whose structure could not be fully resolved from the UAV-LS or TLS data were not analysed for traits extraction. Aside from requiring many TLS scans to capture the extensive and complex branching networks of these plants, in eco-geomorphic terms a traits-based rather than bulk roughness approach is likely to be limited.

4.4.3.2 Trait Metric Extraction

For the reconstruction of vegetation stems into cylindrical models, the open source TreeQSM method was applied to the partitioned UAV-LS and TLS derived vegetation data (Brede *et al.*, 2019). TreeQSM utilises ‘patches’ to determine connected points in the vegetation cloud, before growing the tree structure by joining patches together to form a complete model (Raumonen *et al.*, 2013). These are created using user defined initial patch sizes to adjoin points, before refining the patch sizes using minimum and maximum sizes to create a complete model. This allows the coarse branch structure of the tree to be identified (Figure 4-2, *Segmented Point Cloud*). Sections are then generalised as cylinders for computational efficiency and as they provide a robust

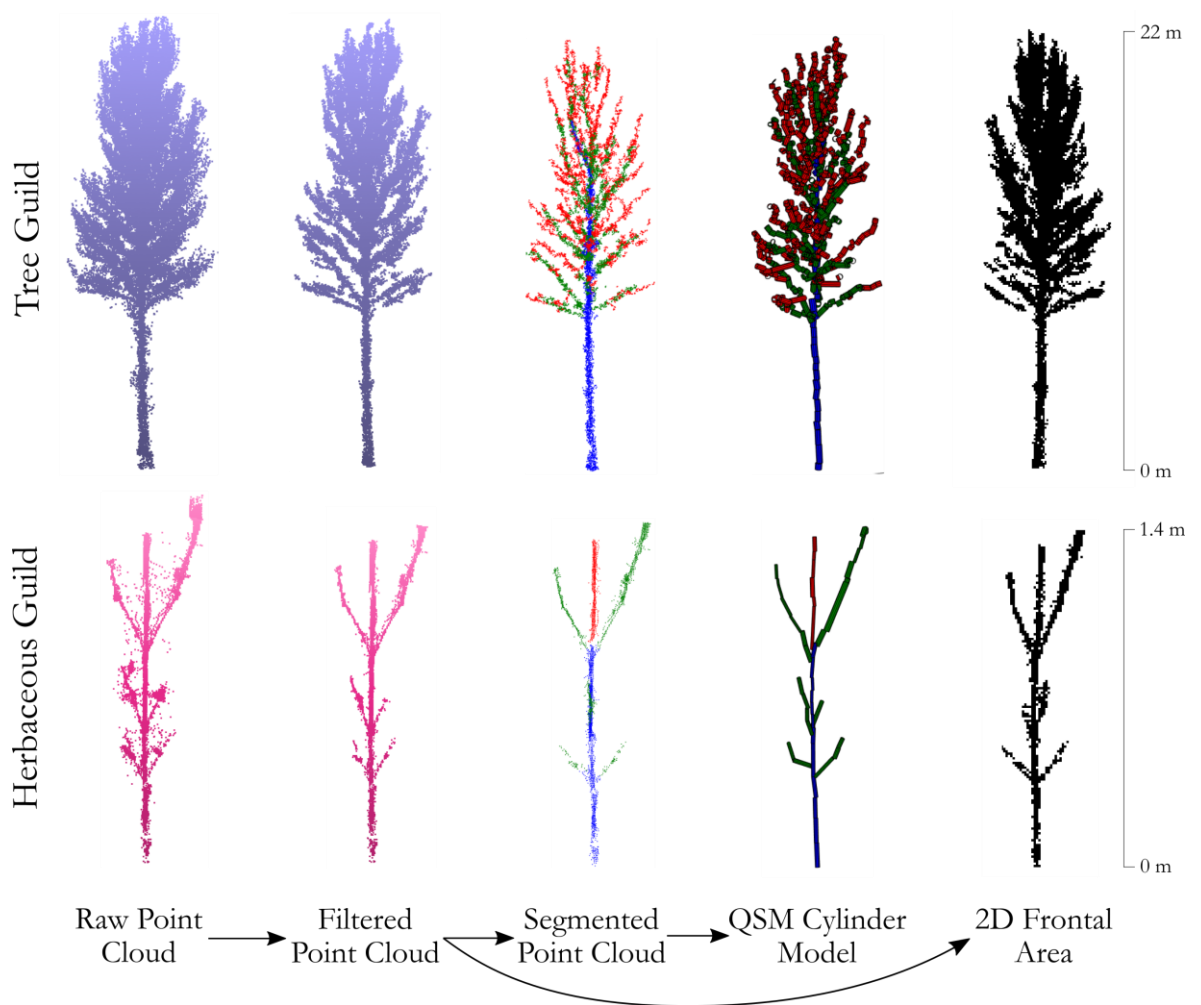


Figure 4-2 Vegetation trait extraction, from an individual raw point cloud to a cylindrical model and frontal area. The process is demonstrated for two extracted vegetation point clouds, a large tree within the study reach collected from UAV-LS data, and a small perennial on the central bar collected from TLS, note the difference in scales. The segmented point cloud is coloured by branching order from blue to red, with the cylinders coloured in the same manner.

representation of trees (Raumonen *et al.*, 2013). These cylinders can then be used to describe the overall structure and properties of the individual plant (Figure 4-2, *QSM Cylinder Model*). A full method description can be found in Raumonen *et al.* (2013). QSM methods have been noted to overstate the volume of smaller branches and are sensitive to noise in the data alongside variable point density (Hackenberg *et al.*, 2015; Fang and Strimbu, 2019). However, QSM reconstructs tree structures in a manner which resolve many of the hydraulically relevant vegetation traits.

Patch diameters (which are used to determine adjacent points within the same tree) were chosen following a parameter sensitivity exercise, with the range of values initially based around those of Raumonon *et al.* (2013) and Brede *et al.* (2019) for TLS and UAV-LS approaches respectively. A visual assessment was performed to identify parameters that created models similar to the point cloud structure due to the lack of reference data. After testing for the optimum patch sizes for reconstruction, the TLS scans of herbaceous vegetation initial patch diameter was set at a size of 0.005 m, with the second patch diameter minimum and maximum sizes of 0.002 and 0.01 m. The minimum cylinder radius was set to 0.005 m, prescribing the smallest detectable branch structure of the extracted herbaceous plants. For the UAV-LS derived tree data, the initial patch diameter was 0.2 m, with the second patch diameter minimum and maximum sizes of 0.1 and 0.5 m. The minimum cylinder radius was 0.1 m, based on manual measurements of tree branches within the point cloud that were detectable. For each plant model the cylinder reconstruction and variable extraction was repeated ten times. As the modelling begins at a random location each time the start point can affect the results, and so multiple averaged simulations provides a more accurate solution. The modelling produces a number of metrics, but for this study height, number of branches, diameter at breast height, volume, and maximum branching order, were collected. For each metric of interest, the average value and standard deviation of these values are taken from the ten runs.

The frontal areas of all segregated vegetation clouds were extracted alongside the construction of the cylinder models, based on the 2D methods described by Vasilopoulos (2017). For each discretised plant point cloud, the data was flattened from 3D to 2D by collapsing the data along a single horizontal dimension on a regular grid (Figure 4-2, *2D Frontal Area*). The grid resolution was set at half the width of the minimal detectable feature resolved by the QSM modelling; 0.005 m for the TLS derived herbaceous plants and UAV-LS 0.05 m for UAV-LS derived trees.

4.4.3.3 Guild Identification

Based on the separated points clouds, each were assigned to a guild based loosely on hydrologically relevant traits outlined in O'Hare *et al.* (2016) and Diehl *et al.* (2017). As outlined above, a decision was made to discretise grasses and shrubs using bulk roughness metrics due to their relative homogeneity and the need for ultra-high-resolution data. Short branching herbs and taller single stemmed herbs were identified, with discrepancies in flexibility, branching, and height, likely to influence hydrology differently. Woody vegetation was further split in to two guilds, those with high diameter at breast heights (DBH) that had low density of trunks and those with lower DBH that had a higher trunk density. The analysis was preformed separately for woody and herbaceous vegetation. As the aim was to identify characteristics that would

separate out the guilds from remotely sensed data, there was little need to compare woody and herbaceous species directly as height would be a dominant component.

In order to assess whether remotely sensed data could separate out plants into their guilds in a statistically robust way, a Principal Components Analysis (PCA) was undertaken to identify the variables which explained most variation within their derived metrics. The metrics used for the PCA analysis were those obtained from the QSM and frontal area calculations which were normalised to remove the influence of different scales (Alaibakhsh *et al.*, 2017). The principal components identified were used to inform the classification of reach scale guilds, identifying those variables that most explained the variation between guilds.

4.4.3.4 Linking Traits to Reach Scale Metrics

To scale the analysis from individual plants to the entire reach level, a method of linking plant scale traits to broader scale data is required. Convex hulls representing the spatial extent for each vegetation point cloud extracted and analysed above were used to define the regions from which UAV-LS and UAV-MS data were extracted. For small herbaceous vegetation, this was buffered by 0.25 m to account for any misalignment between TLS and UAV-LS clouds. For tree vegetation polygons this buffer was increased to 1 m to incorporate peripheral branches and leaves removed during point cloud filtering. Polygons for small branching trees and large shrubs were created based on field observations and UAV-MS imagery. A total of 11 polygons were created for this combined guild category, with 11 made for grasses, 8 for water classes, and 5 for gravel bars and bare earth. Within these polygons, multiple seasonal variables were extracted for scaling local guild identification to reach scale classification. The structural characteristics of the point cloud were extracted through TopCAT (Brasington, Vericat and Rychkov, 2012), obtaining the standard deviation, skewness, and kurtosis over a decimated grid at both 1 and 4 m resolutions, the latter to account for larger vegetation footprints. The 4 m resolution decimated grid only considered points classified as vegetation in the initial 'ground/other' point clouds to remove ground points from further analysis. To extract a Canopy Height Model (CHM), a bare earth digital terrain model (1 m resolution) was subtracted from a 0.25 m digital surface model incorporating the vegetation points. The Normalised Difference Vegetation Index (NDVI) across the reach was calculated using the red band along with both the red-edge and near infrared bands of the MicaSense orthomosaic images to produce two separate NDVI layers. As the red-edge can be used to separate out vegetation signatures, using a combination of both was expected to help differentiate plants with similar structural but different spectral properties. Analysis of structural and spectral data was performed for each of the four seasons to gain an insight in to how these properties vary

temporally. For each of the vegetation polygons, the attributes of each of these layers for each season were extracted using zonal statistics. The mean and standard deviation for each attribute for each season were then calculated across the different guilds for use in the classification model.

4.4.3.5 Reach Scale Guild Classification

To scale from guilds created from individual UAV-LS and TLS derived plants, to the entire reach, an object based random forest classification was undertaken. Object based approaches overcome some of the issues of variation and complexity in high resolution images (Myint *et al.*, 2011), improving continuity in the results (Duro, Franklin and Dube, 2012; Wang *et al.*, 2018). The RGB bands from the multispectral camera and the CHM were combined to create a 4-layer image from which to classify distinct objects. The Felzenszwalb Algorithm was applied which uses graph based image analysis to segment an image into its component parts based on the pixel properties (Felzenszwalb and Huttenlocher, 2004). This results in regions within the image being grouped based on them having similar properties according to the input layers, avoiding the salt and pepper effect found in traditional pixel by pixel classification approaches (Wang *et al.*, 2018).

In total, 644 training objects were identified using the previously discretised vegetation convex hull regions, with multiple objects present within each training sample (Table 4-2). A random forest classifier was then trained based on the layers that were deemed to distinguish between the different guilds, having proved an effective machine learning technique (Chan and Paelinckx, 2008; Adam and Mutanga, 2009; Adelabu and Dube, 2015), with a water mask included to reduce errors associated with varying flow stage. An analysis of model accuracy vs

Table 4-2 Description of guilds used for training the random forest classifier, showing the number of training objects from the image segmentation and the training size area.

Guild	No. of Training Objects	Training Area Size
Grasses	93	321 m ²
Branching Herbs	15	25 m ²
Single Stemmed Herbs	16	29 m ²
Branching Shrubs	135	388 m ²
Low DBH Trees	158	876 m ²
High DBH Trees	62	238 m ²
Bars	122	641 m ²
Water	41	157 m ²

number of forests showed a convergence of accuracy above 100 forests and a reduction in band importance variability above 300 forests (Figure 4-3). Higher variation in band importance suggested that the number of trees was influencing the likelihood of an optimal solution. This random forest classification was then applied to the remaining objects within the reach.

Due to the limited number of samples being used, there were not enough training samples to split into a training and test dataset. The multi-tree approach of random forests is constructed on a sample of the dataset and as such can be tested against itself to determine an out of bag accuracy score. It also successively adds and removes bands to determine the band importance in the classification (Adelabu and Dube, 2015). Alongside this self-assessment, for the final guilds classes a total of 80 random points were generated across the study site with an equal number in each outputted guild. These were manually classified using high resolution orthoimagery from a UAV-RGB (0.02 m resolution) survey and study site knowledge. The output classification was not visible when undertaking this assessment and the order of the points shuffled to remove user bias. The classified guilds map was then used to extract the predicted guilds of these points before a confusion matrix was utilised to assess the accuracy of the classification.

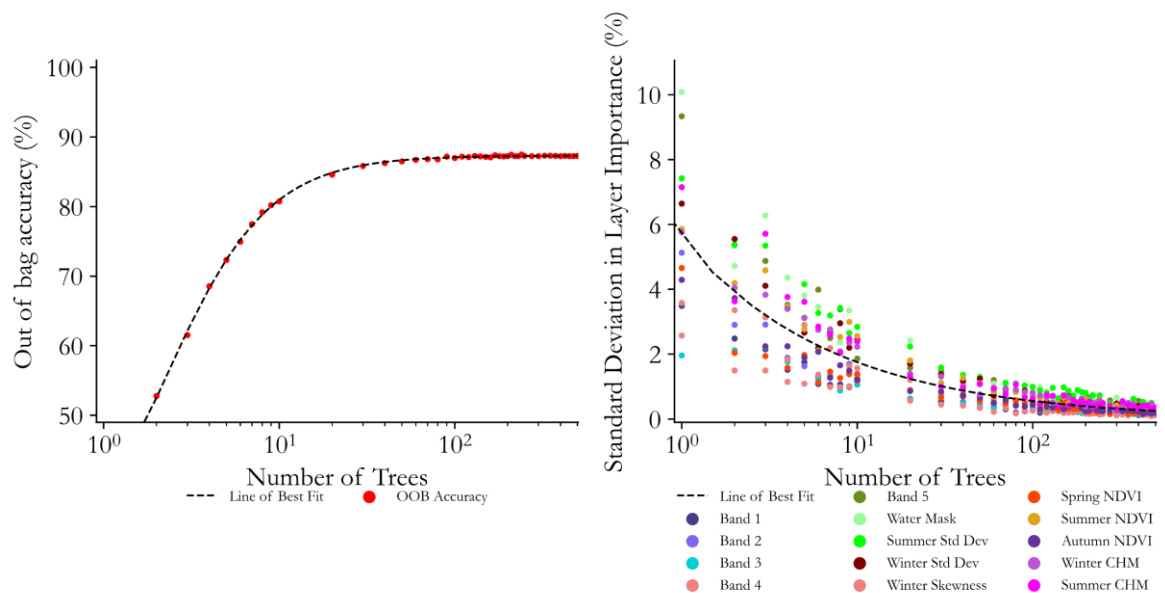


Figure 4-3 Random forest classifier out of bag accuracy and variations in band importance for guild classification. (Left) Out of bag accuracy scores for different numbers of trees used within the random forest classification, showing a distinct levelling off in accuracy after ~ 100 trees are used. (Right) The standard deviation in individual band importance across 10 sample runs to identify at what number of trees band importance becomes consistent across all runs, in this instance around 300 trees.

4.4.4 Morphological Change

The M3C2 algorithm (Lague, Brodu and Leroux, 2013) was employed to calculate morphological change, whereby the surface normals from a subsampled cloud of core points (here at 0.1 m resolution) are calculated, and change along the normal direction is identified with the calculation of a local confidence interval. This overcomes some of the limitations of traditional elevation model differencing which can't account for the direction of change. The benefits of using both SfM and UAV-LS data allows their respective drawbacks to be overcome through combining both datasets. SfM has been shown to perform poorly in vegetated reaches, whereas UAV-LS maintains good ground point densities, whereas SfM provides good continuity and high point densities in unobstructed areas. Therefore, in order to obtain good surface normals for assessing change the two clouds were merged (see Tomsett and Leyland (2021) for error analysis) and their vegetation removed through the use of the same progressive morphological filter used previously to produce resultant clouds which were then differenced using M3C2.

4.5 Results

4.5.1 Decadal Scale Change

Analysis of planform shift from the year 2000 through to 2020 has identified that the channel is highly mobile, experiencing rapid change in places as well as more gradual evolution in others. From the 586 bank transects cast, the average SCE (extent of bank movement) was 38 m whilst

Table 4-3 Transect statistics showing the difference between large vegetation present and absent sections, for when avulsions are included and excluded. N refers to the number of transects within each category.

	SCE statistics for each scenario				
	N	Mean	Median	Std. Deviation	Max
Large Vegetation Present (Inc. Channel Reoccupation)	220	48	24	41	121
Large Vegetation Absent (Inc. Channel Reoccupation)	348	35	27	27	101
Large Vegetation Present (Exc. Channel Reoccupation)	290	10	8	7	47
Large Vegetation Absent (Exc. Channel Reoccupation)	339	22	16	18	72

the median change was 25 m. The smallest change was 1 m whereas the largest was 120 m. Comparison of sections with large vegetation present and absent suggests there is a greater average mobility in vegetation present sections (Table 4-3). This goes against the assumption that vegetation helps to reduce channel mobility. However, Figure 4-4 suggests that the areas where the channel has remained predominantly stable through time have some vegetation influence. Of the four areas of significant change, only one appears to follow the traditional meander development model of lateral erosion leading to a cut off, with the three remaining sections showing likely avulsion or previous channel reoccupation. Analysis of channel mobility

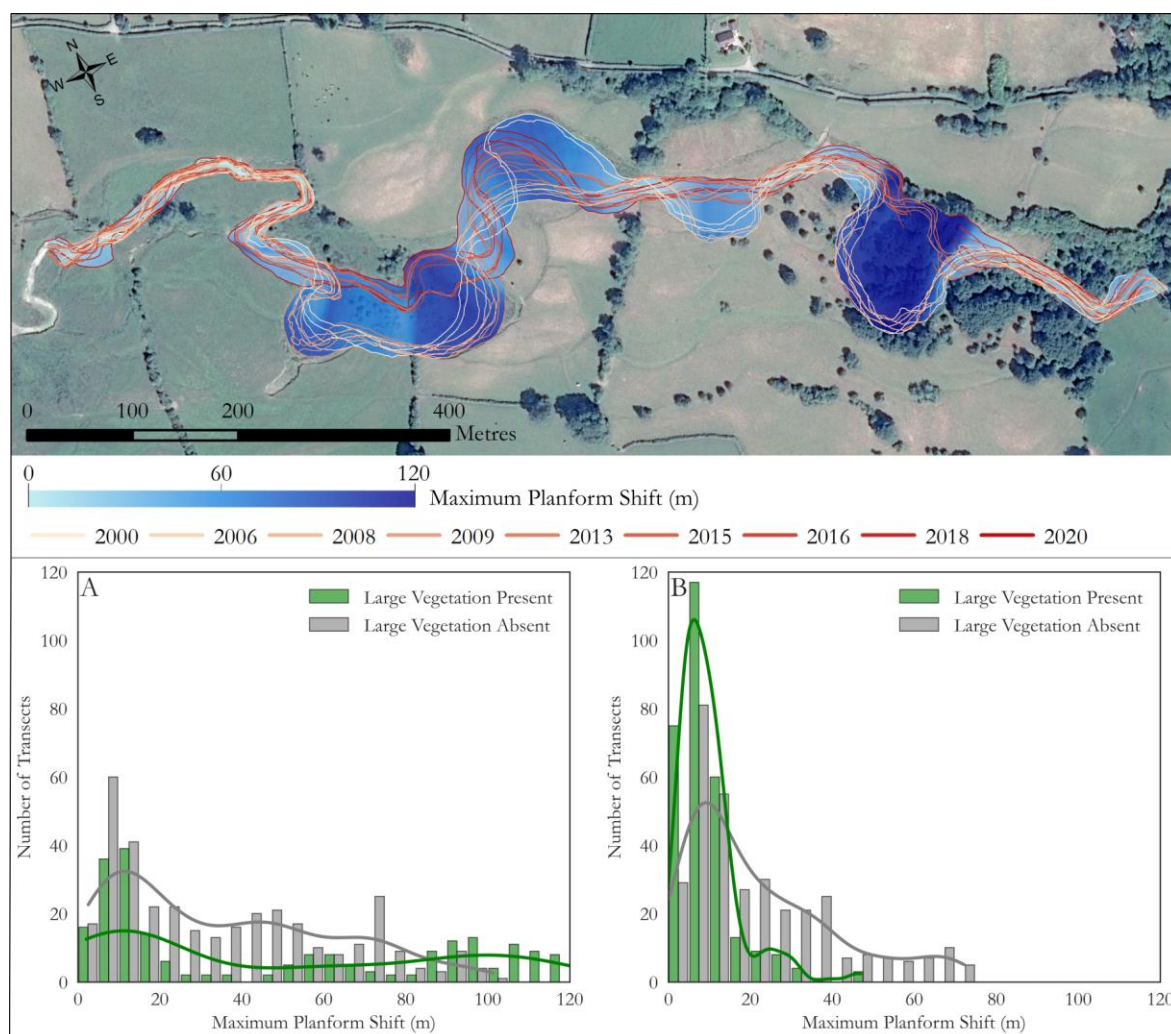


Figure 4-4 Results from the decadal DSAS analysis. Top Panel: DSAS results showing channel evolution from 2000 – 2020, with left- and right-hand banks digitised for each year. Spatial variability in maximum planform shift is shown in blue. Bottom Panel: A shows the range of SCE values from both the left- and right-hand banks combined, for sections classed as containing large vegetation and those that do not. B shows the SCE values when the effects of avulsion are removed from the data, for both large vegetation present and absent sections also.

excluding these avulsions indicates that reaches with large vegetation present have lower rates of lateral mobility, and that there is evidence of large vegetation reducing rates of planform shift.

Figure 4-4 (A) and (B) compares frequency of SCE values for sections with and without large vegetation being present, including and excluding avulsions. For reaches with large vegetation, removing the avulsions has a notable impact on the distribution, with many more transects falling within smaller SCE values. Although this shift is seen in the transects without large vegetation also, the change in distributions is less prominent and is supported by a smaller change in mean values, dropping from 35 m to 27 m for large vegetation absent reaches and from 48 m to 10 m for reaches with large vegetation present.

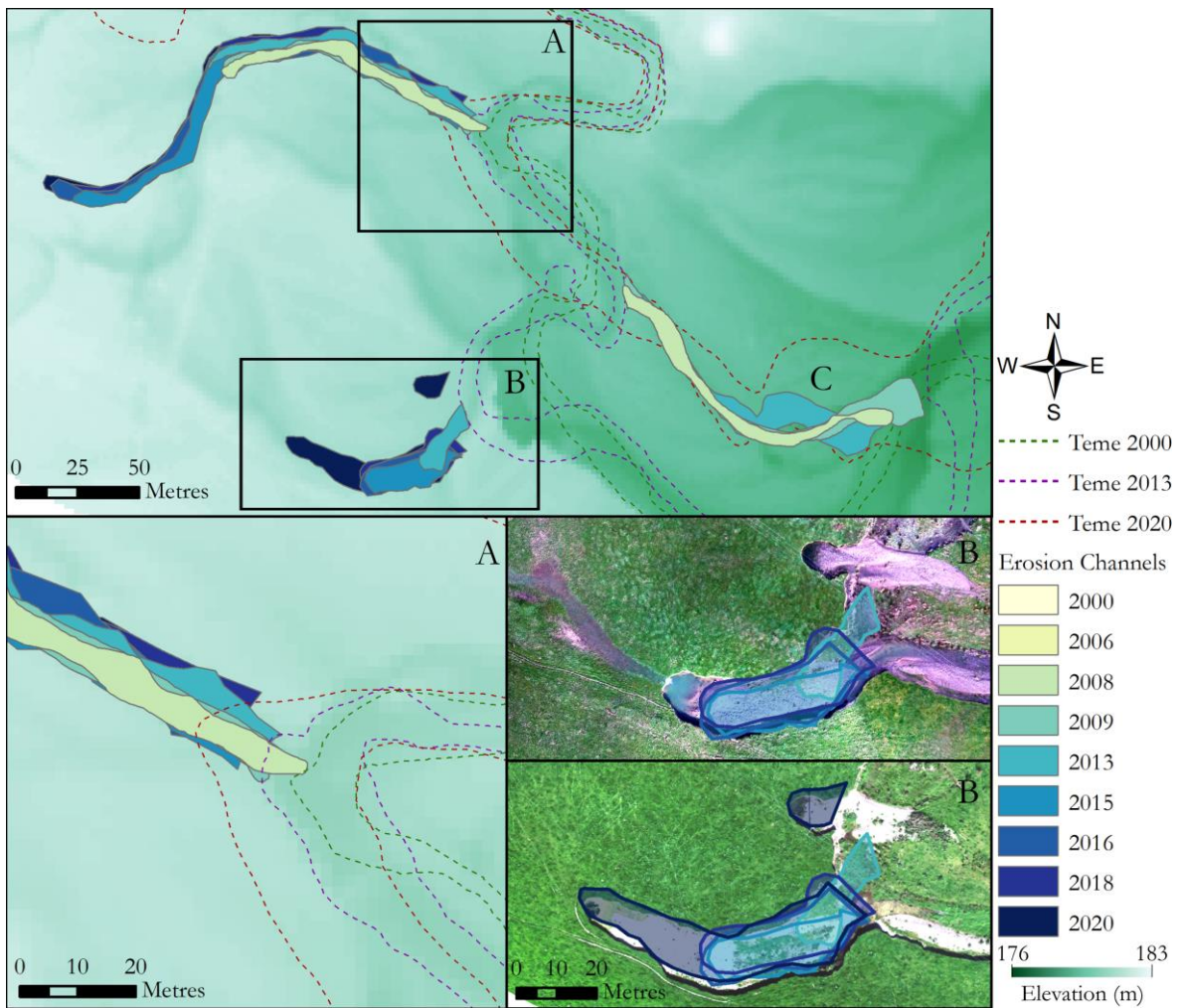


Figure 4-5 Historical analysis of avulsion development across the floodplain. The top panel shows two developing channels (A and B) across the floodplain and one channel neck cut off (C). The bottom left panel (Channel A) shows how this development is influencing successive planform shift, and the bottom right panels (Channel B) demonstrates how this is linked to overbank flow.

This channel switching appears to involve reoccupation of former channels that have lower floodplain elevations during overbank flow events. The three erosion channels in Figure 4-5 show the stages of progression. Feature C demonstrates a completed channel neck cut off for a double meander bend. Both features A and B appear to be developing during flood events, with the orthomosaic insets showing the overbank flow captured during a flood event and the resulting channel position post flood for feature B. This implies a consistent pattern in new channel development that occurs during successive overbank flow events.

4.5.2 Hydrologically Relevant Trait Analysis

4.5.2.1 Extraction and Analysis of Traits

The QSM analysis appears to output visually sensible results and produce models appropriate for the vegetation being modelled (see Figure 4-2). Table 4-4 shows the standard deviation of a selection of QSM metrics as a percentage of the mean value. The repeat modelling was more consistent for larger vegetation, with lower relative standard deviations. However, for some metrics such as number of branches, herbaceous plants with few branches may be adversely affecting the results. For example, plants with 5 stems having errors of +/- 1 branch is a 20% difference, whereas for 20 stems this is only 5%. Overall, model repeats appear to have good agreement with one another, and provide a basis for separating out vegetation with similar hydraulic functional traits.

Figure 4-6 shows the PCA plots of herbaceous vegetation metrics from the TLS scans (A) and woody vegetation metrics from the UAV-LS scans (B). It is clear that some separation of points through dominant metrics is possible, with both plots exhibiting two principal components capable of separating the defined guilds. Panel A shows the PCA plot for herbaceous vegetation. Height is a clear component between each guild, as well as volume. Although the number of branches was not a key component for separating guilds, branches per unit height explained some of the variability in the data. Taller plants may have a similar number of branches, and so

Table 4-4 Standard deviations in trait values as a percentage of the mean values for herbaceous and tree guilds. Guilds aggregated to include all herbaceous and tree data. Expressed as a percentage of mean due to the varying scales of data between the two guilds.

	Height	Number of Branches	DBH	Volume	MBO
Herbaceous Guilds	3.87	16.77	17.83	12.18	17.52
Tree Guilds	1.16	8.79	15.58	12.89	15.00

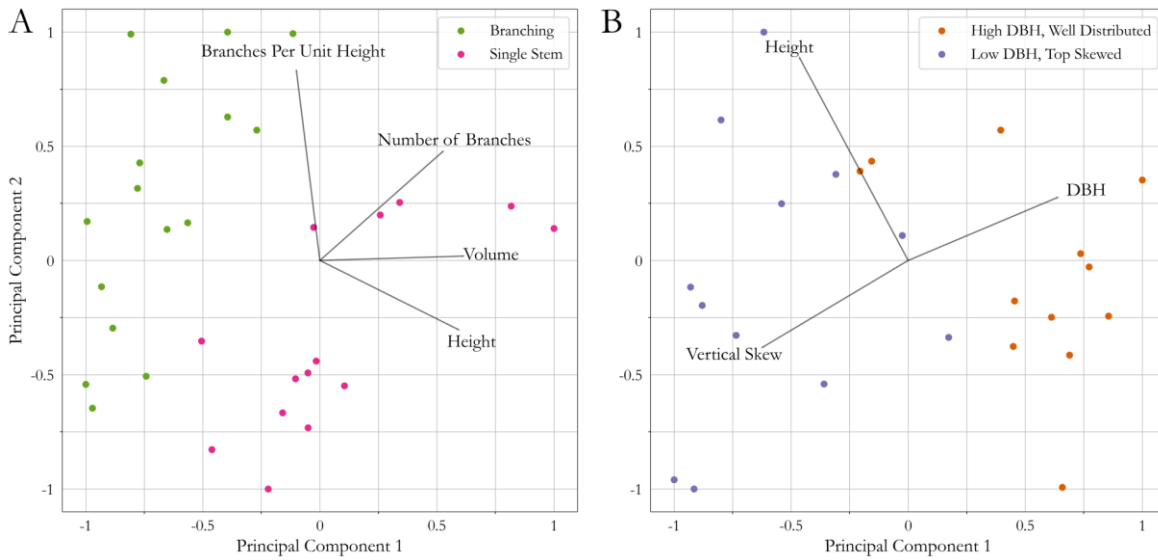


Figure 4-6 PCA analysis of both herbaceous and tree guilds to investigate differences in trait characteristics. Lines indicate direction of each variable that explains variation in the data.

accounting for plant height produces a density of branches independent of size to help explain plant structure. Of the four identified components, only the height is identifiable from the UAV-LS data for upscaling, however, point density and spectral properties may improve guild separation. Panel B shows the PCA plot for woody vegetation. Height is less important in distinguishing the two guilds than for herbaceous vegetation, yet trees under or over certain heights are likely to be one guild or the other suggesting minimum and maximum threshold values. For separating guilds, the most important components appear to be DBH and vertical skew which was expected as this was the basis for initial guild classes. DBH cannot always be easily extracted from UAV-LS data if it is incomplete, therefore as the vertical distribution acts in the same component direction, this can be used as a potential method for differentiating guilds. There is however considerable overlap in both of these PCA plots for woody and herbaceous vegetation. There are dominant trends such as the DBH and plant height for separation, but there is considerable variation within the guilds for their QSM based metrics which may impact the final classification.

4.5.2.2 Linking PCA Clusters to Reach Scale UAV-LS Data

Figure 4-7 shows the results of the seasonal analysis of different variables derived from UAV-LS and UAV-MS imagery for each of the guild classes. There are clear variables which can separate different guilds with ease, for example the height of the canopy is a key indicator between woody, herbaceous, shrub, and grass guilds. Separating out similar guilds does appear

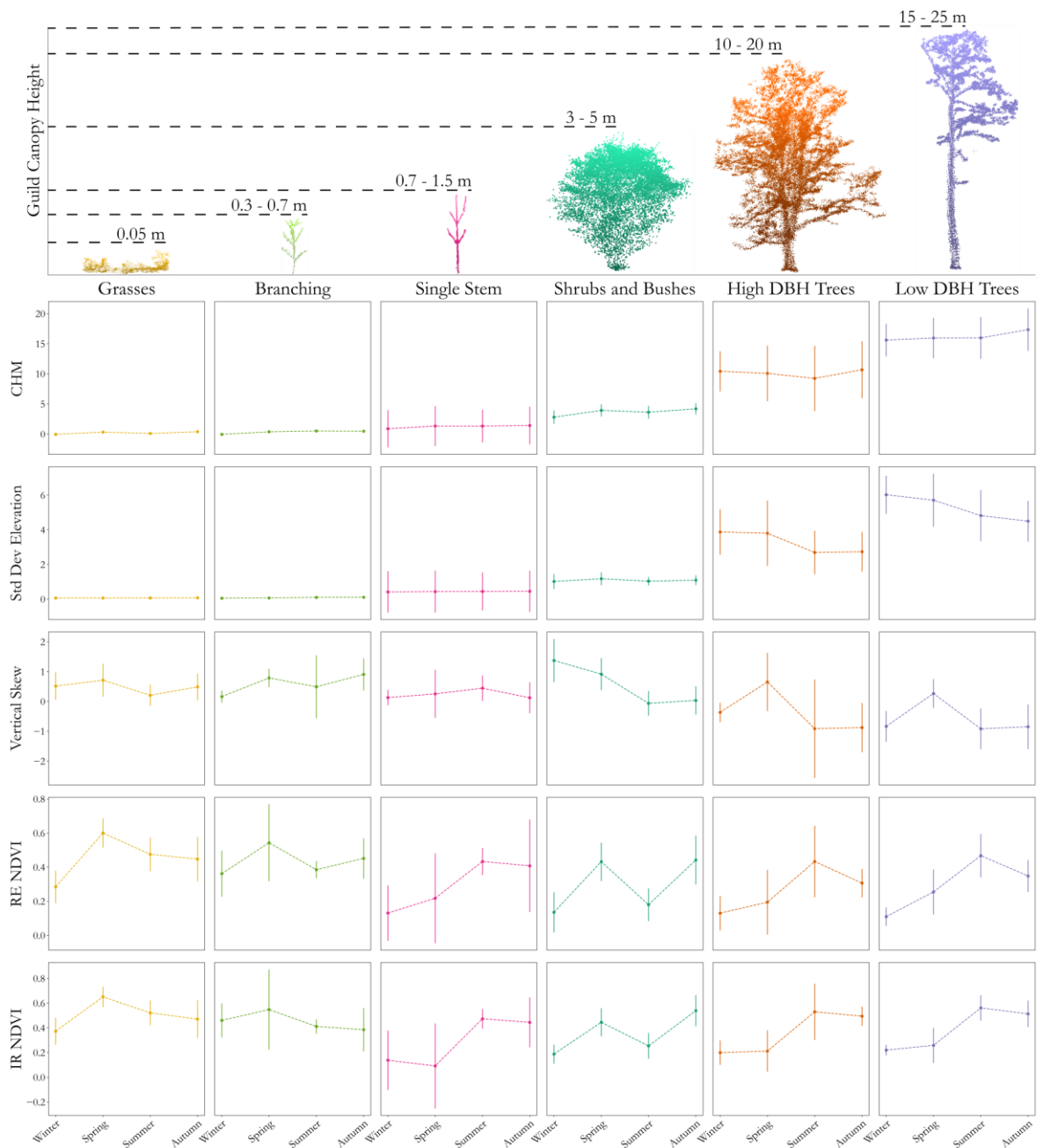


Figure 4-7 Results of seasonal analysis (X-axis within subplots) of different reach scale metrics (Y-axis) from UAV-LS and UAV-MS data for each identified guild (X-axis). The point clouds at the top provide an example point cloud of each guild class, with canopy height ranges acquired from trait extraction for the four analysed guilds and from the reach scale analysis for the remaining grass and shrub guilds. Error bars indicate one standard deviation around the mean, CHM (Canopy Height Model) is given in metres.

to be more nuanced. The High DBH and Low DBH woody guilds both have very similar values and seasonal patterns of changes in NDVI values as well as in their height. This is unsurprising as the PCA analysis showed, with height not a dominant factor in explaining variation with numerous samples showing crossover. Vertical skew did show guild separation, with the

samples used for QSM analysis collected in leaf off conditions. Figure 4-7 does suggest that changes in winter skew are visible between the two guilds, with a smaller amount of crossover as expected. Spring, summer, and autumn skewness is less informative, likely due to leaf on conditions effecting full tree reconstruction, with higher variability in results between the sample areas.

Separating out herbaceous guilds is also a challenge. Elevation values for single stemmed herbs are more variable and cross over in to grasses and multi-branching herbs. However, the mean elevation values are higher in line with the PCA analysis and may enable herbaceous guild separation. Likewise, the average skew values help to differentiate between classes, but again the variability in the data suggests it is harder to separate by structural content alone. Conversely, spectral data shows great promise in differentiating between guilds. Both the absolute values between herbaceous guilds show different as well as their seasonal patterns especially when utilising the red edge band for NDVI calculations.

4.5.2.3 Creation of Seasonal Reach Scale Guilds Maps

The resultant classification from guild classification can be shown in Figure 4-8 with many areas being classified as expected. There appears to be an over classification of the branching shrubs class based on initial comparisons with ortho-imagery, whereby the edges of larger vegetation and some predominantly grass regions appear to have been misclassified. This may be due to the large variation in structural and spectral characteristics of this guild which were less well accounted for. Herbaceous guilds were predicted in areas that were expected, in mobile areas of the channel where larger vegetation would find it more challenging to establish. The out-of-bag accuracy score when training the random forest classifier with 300 trees was 87.2%. Figure 4-9 A shows the importance of each band in the classifier, with structural elements proving key in separating guilds, especially using summer standard deviation of point elevations. The near infra-red band and winter standard deviation are the next most important elements, with the remaining individual spectral bands providing a smaller contribution to the classification. The higher importance of the two NDVI layers implies that providing the classifier with analysed image data is more useful than individual bands alone. Likewise, the canopy models alone are less informative than the variation in elevations when detecting guilds, supporting the use of manipulated rather than simple metrics to help improve classification.

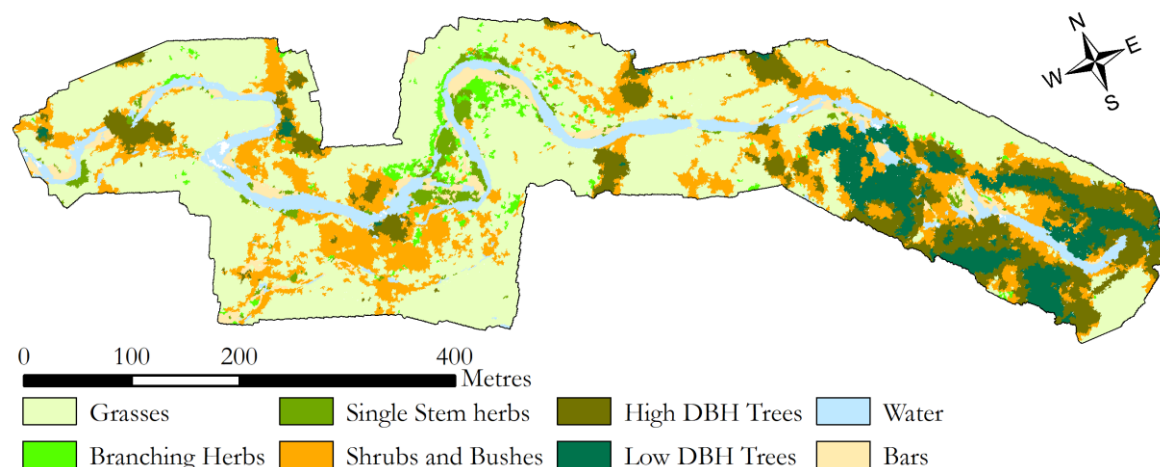


Figure 4-8 Resulting classification from reach scale analysis for the areas covered by both UAV-LS and UAV-MS data. Note the over classification of shrubs and bushes, especially at the edge of larger wooded guilds.

The confusion matrix can be seen in Figure 4-9 B comparing the number of check points that are correctly and incorrectly predicted. The overall model accuracy is 80%, lower than the out-of-bag prediction. However, this is not surprising as training areas were delineated based on complete structural profiles for the QSM analysis and the total number of samples used for training was small relative to the possible variation across the reach. There was a general over classification of points as grass guild, with only one grass control point incorrectly classed as branching herbs. Branching herbs which are more detectable from imagery and likely to return more laser scan points were classified reasonably well, only being misclassified as grass. Single branching herbs however were relatively poorly classified (50% accuracy), being misclassified as grass, branching herbs, and even water. However, their narrow structure and sparse spacing make them hard to identify from coarser imagery and they return fewer laser scan points. This class also exhibited the greatest variation in values when using reach scale metrics to evaluate guild samples. Shrubs were predominantly misclassified as branching herbs and grass, this may be due to the object segmentation not always isolating complete plants or including surrounding ground points which may have affected the classification. Low DBH trees with a top skew were classified well by the model, most likely due to their larger heights and winter skew, whereas higher DBH trees were misclassified as both low DBH trees and grass. The former likely due to the difficulty in separating out these two guilds which have subtle differences in certain classification layers such as winter skew, and the latter from surrounding data being included in an object likely from shadowing continuing an object outside its true bounds. However, of all 20 tree check points, only one was incorrectly classified as a guild with clearly different traits, a High DBH Tree as Grass (see Figure 4-9).

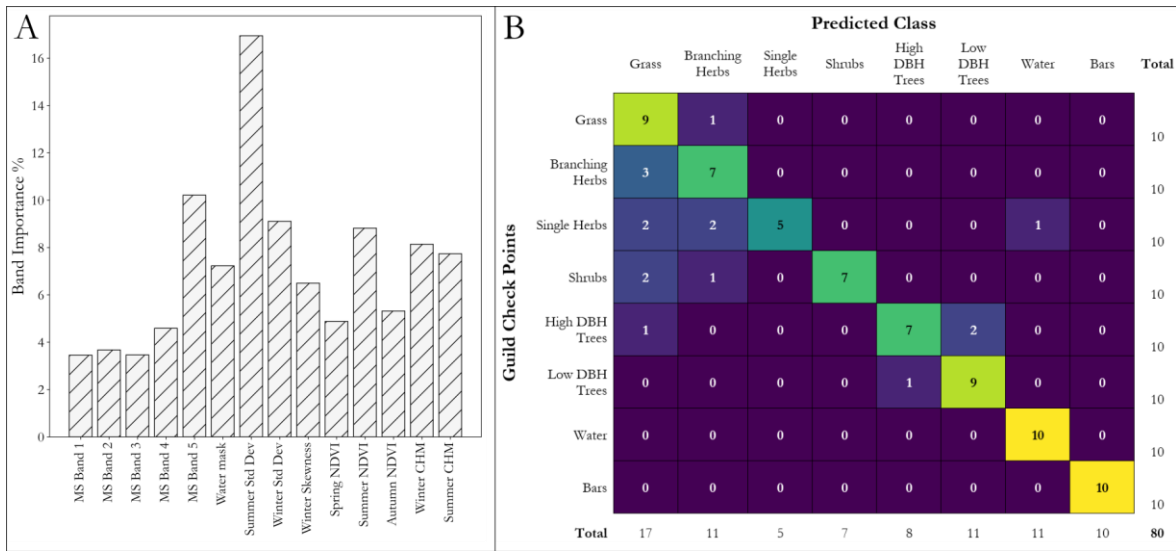


Figure 4-9 Individual band importance in the final classification and confusion matrix from the accuracy assessment. The band importance represents the contribution of an individual layer to the final classification. The confusion matrix demonstrates for which guilds the classification struggled, showing an over-classification of grasses and the poor detection of single stem herbs. The overall classification accuracy was 80%.

4.5.3 Morphological Change

As is expected, the majority of morphological change occurs over winter months when there are high flows (Figure 4-10). Conversely, over periods of lower flow during the summer both the extent and magnitude of change is reduced. Throughout the first winter period erosion occurs on the outer bank edges with fairly consistent planform evolution throughout the reach. Deposition is evident throughout the entire reach, however erosion is considerably more dominant than deposition, with almost 14,000 m³ of net erosion. The second winter appears to have more localised effects on morphology, with clear channel reshaping through the upper half of the study area. This has led to considerable deposition on both sides of the channel in areas of previously active erosion as well as localised erosional hot spots (~23,000 m³ net erosion). Both histograms within the winter seasons show a dominance in erosion overall. This is in line with previous long-term analysis which shows this as an area of high mobility with previous channel reshaping occurring. Over both winters, morphological change in the tree dominated downstream reach has undergone similar levels of change with areas of erosion and deposition influenced by the presence of large vegetation. Both summer periods have a greater degree of stability, with erosion and deposition taking place but in lower magnitudes. This is consistent throughout the reach with no hotspot areas of either deposition or erosion, with deposition showing to be more dominant overall.

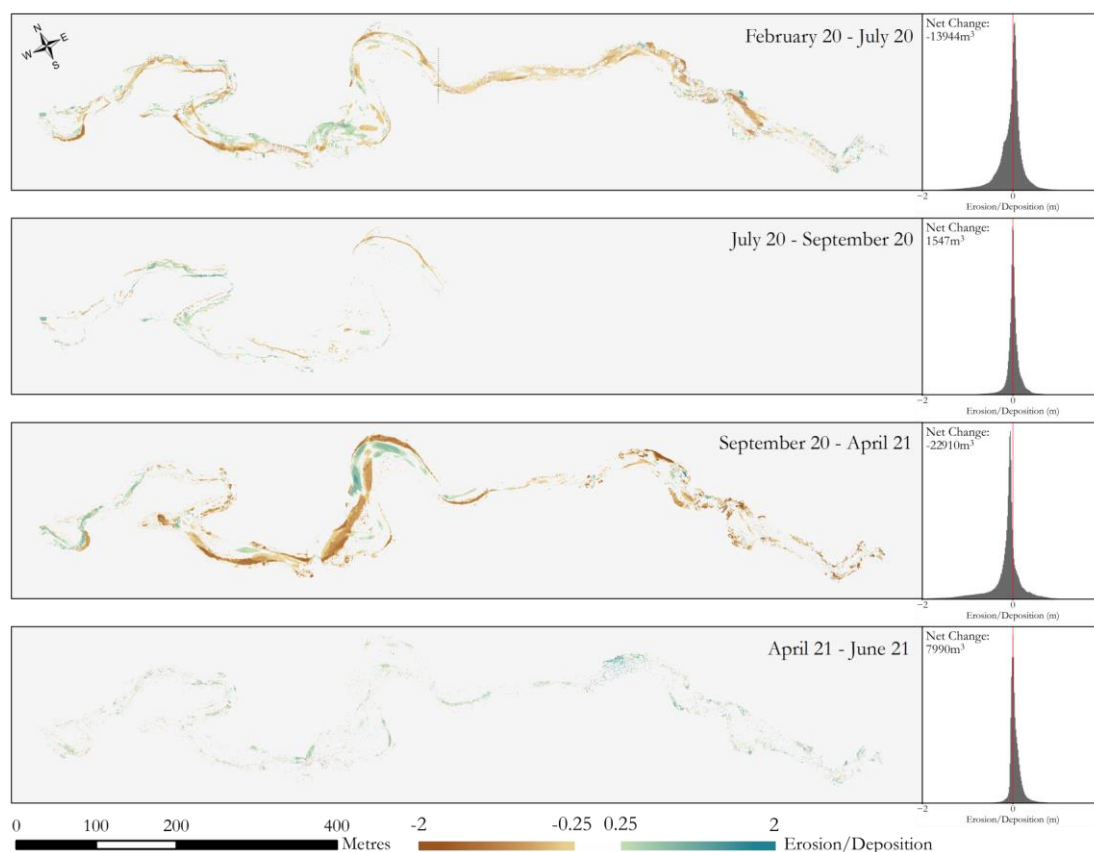


Figure 4-10 Morphological change throughout the monitoring period, showing the spatial variation in erosion and deposition as well as the net change in sediment. The dashed line for the time period of February – July 2020 indicates a separation in the analysis. Left of this line comparisons were made between February and July, whereas on the right they were made between February and September. In July, only half of the survey areas was captured. The stability of the reach over summer meant that it was inferred that any changes for this lower half of the reach between February and September were likely to have occurred during the February to July period where morphological activity was more prominent. The histograms adjacent to each time period show the distribution of magnitude of change, and whether this tends to be favouring net erosion or deposition.

4.6 DISCUSSION

4.6.1 Multi-Decadal Evolution

The multi-decadal evolution for this reach is complex and analysis of the formation of new channels implies that flood events might be a key control on the switching from one channel to another and the reoccupation of former channels. It is not possible to isolate a single variable that may cause such switches to take place, such as particular flow thresholds, baseline

conditions, vegetation, or soil characteristics. However, it does appear that areas influenced by large vegetation experience less localised bank evolution, with the vegetation constraining the channel to some degree. This does not appear to stop large switches in channel position into or away from vegetated sections. This implies that vegetation is playing a role in the stabilisation of channels up to some, as yet unidentifiable, threshold. The reoccupation of former channels implies that vegetation plays a lesser role than topography in these conditions, suggesting that whilst vegetation can have controls on channel evolution, these eco-geomorphic feedbacks are locale and flow condition dependent. This supports the concept of vegetation acting as river system engineers and providing an influence on channel morphology (Gurnell, 2014) and that varying vegetation densities may be impacting the resistance to morphological evolution (Bertoldi, Drake and Gurnell, 2011). Therefore, at a decadal scale, although vegetation may not be the sole control on planform evolution, it is shown to be an important factor in this reach of the River Teme.

4.6.2 Trait Extraction and Guild Formation

Current measurements of plant functional traits are still predominantly ground based and therefore limited by on site access (Palmquist, Sterner and Ralston, 2019), requiring extensive sampling to extract enough data to create guilds relevant to a particular study (e.g. Stromberg and Merritt, 2016; Diehl *et al.*, 2017; Hortobágyi *et al.*, 2017). Remote sensing of these traits is therefore a potentially novel way to collect data across large areas, depending on the vegetation size and methods of data collection. Although no ground truth data relating to traits was collected in the field, the assessment of variability in model construction suggests that the final cylindrical models were of good fit for the point clouds collected. This suggests that the use of remote sensing to collect structural trait data has an important role to play in eco-geomorphic research moving forward, especially once trade-offs in terms of time and spatial extent are accounted for.

The use of pre-determined rather than site specific guilds was a method employed by Butterfield *et al.* (2020) on the basis of guilds outlined in Diehl *et al.* (2017). The sites used in both of these studies were similar, and the application to a temperate UK based site is challenging. However, the comparatively smaller sample size used in this study, and the lack of a comprehensive guilds list for riparian vegetation, made using predetermined guilds described in Diehl *et al.* (2017) and O'Hare *et al.* (2016) justified. The lack of suitable ultra-high-resolution data reduced the number of herbaceous guilds to two, on which most distinction could be observed. The variation in woody vegetation created two guilds within this single previously outlined guild, as they were likely to have different hydraulic effect traits. This basis appears to have proved effective with

differences in structural characteristics which are likely to impact flow and subsequent morphology noted between the guilds during PCA analysis. Predominantly single stemmed herbs were taller, likely due to their improved structural standing, and although the number of branches was similar the number of branches per unit height was different. A taller, stronger, and less branching herb is going to have a distinctly different impact than a shorter more flexible one (Nepf and Vivoni, 2000; Järvelä, 2004; Sand-Jensen, 2008). Being able to differentiate successfully between these two highlights the success of the survey and trait extraction methods. Likewise, the difference in flow conditions between low DBH trees that are closely packed to less densely packed high DBH trees may show a resemblance to the influence found at smaller scales on plant density (Järvelä, 2002b; Kim and Stoesser, 2011). The relationship between DBH and vertical skew is not surprising; considering the higher plant spacing density the competition for space is likely higher, resulting in more mass higher up the tree profile. As plants cannot yet be easily differentiated by their DBH, using vertical skew gives promising results for upscaling to larger areas whereby ALS surveys may be able to differentiate between woody guilds for better informed hydrological analysis.

However, UAV-LS has been shown to overestimate canopy reconstruction volume (Brede *et al.*, 2019), which mirrors the over complexity demonstrated in Figure 4-2 (*QSM Cylinder Model*) with some awkwardly orientated cylinders. Extracting traits using remote sensing is novel and can outcompete ground-based methods for coverage but is not yet likely to match the accuracy and interpretive ability of in-field measurements. Moreover, use of TLS is highly localised with a limit to the survey extent that can be captured (Lague, 2020), meaning only a small number of samples can be analysed which may not reflect the full variation in vegetation morphology from differing hydrological and environmental conditions. The UAV-LS data, although covering more ground, does take significant levels of time to post-process and extract multiple individual vegetation models, although as the spatial extent of coverage increases, the time gains improve as the same vegetation models can be used to classify increasingly larger sites. Algorithms which can extract traits and classify large areas are likely to improve with the increasing availability of very high-grade commercial UAV-LS surveying equipment in much the same way that SfM methods developed, beginning to rival the resolution and accuracy of ground-based TLS.

Currently, UAV remote sensing methods can only obtain above ground structural traits, and although these make up a significant component of hydrologically relevant traits, they do eliminate the collection of traits such as root structure, strength, and plant flexibility. Both UAV-LS and TLS also struggle to capture the complex structures of shrubs, with TLS requiring too many scans to resolve the structure of enough samples and UAV-LS having too low point density and canopy penetration for such complex branching. However, methods pioneered by

Manners, Schmidt and Wheaton (2013) may help to overcome this by relating vertical profiles from TLS and ALS data to enable upscaling to larger extents.

4.6.3 Reach Scale Guild mapping

The benefits of remote sensing of plant traits does not come from individual plant analysis but from upscaling to larger extents. Using the same datasets provides continuity between both the individual analysis and reach wide guilds. Finding common features of defined guilds is more computationally effective than analysing individual plants throughout the reach at present. Using structural characteristics of the point cloud alongside spectral properties across time allows the absolute and temporal patterns of each layer to enhance guild classification. It is clear that distinctive separation between guild types can initially be made on canopy height, with this providing the clearest initial separation. The need for seasonal data is emphasised by the herbaceous guilds, whereby height is a useful separator but has large variability, whereas winter and spring NDVI values are more effective, supporting previous work emphasising the need for seasonal data to improve eco-geomorphic research (Bertoldi, Drake and Gurnell, 2011; Nallaperuma and Asaeda, 2020). Variations in NDVI were distinct between several guilds, both in absolute values and seasonal variation. Single stemmed herbs appear to be more seasonal, with lower winter values than multi stemmed herbs, whereas shrubs NDVI experience a dip in spring surveys as a consequence of flowering affecting spectral properties. When investigating differences in woody guilds, winter data collection is key, as in leaf off conditions the full tree structure is captured in more detail and so differences in skew which are related to DBH are better captured. Later in the year, these variables become more overlapped between guilds with greater variation. Therefore, the timing of data collection will likely impact classification results, with some guilds being better separated at different times of the year. For these methods to be applied elsewhere, it therefore follows that a seasonal monitoring approach is required.

The use of random forest classification for this study site has been successful and builds on the growing body of research for their application to high resolution classifications (Chan and Paelinckx, 2008; Adam and Mutanga, 2009; Adelabu and Dube, 2015). The misclassifications from the random forest classifier are in line with misclassifications experienced by Butterfield *et al.* (2020) when using multispectral imagery alone, with most misclassifications happening in guilds adjacent and most similar to the true class. Woody guilds appear to be buffered by shrub guilds, potentially resulting from the image segmentation not delineating the vegetation edge successfully. These locations are likely to have lower relative heights and so be misclassified as shrubs, whereas a better image segmentation may avoid these issues.

The resulting classification accuracy (Figure 4-8 and Figure 4-9 B) shows promise for linking local scale trait modelling to larger guilds, with good separation between broad guilds and promising initial results for separation between similar guilds. The presence of herbaceous species in the active meandering section is as expected, as these are more adaptable to changing and flood conditions whilst larger woody species are seen in more stable sections of the river when compared to the historical change, as these species require more stable hydraulic conditions (Kyle and Leishman, 2009; Stromberg and Merritt, 2016; Aguiar *et al.*, 2018). The classification herein advances work by (Butterfield *et al.*, 2020) who used imagery to classify species and subsequently assign guilds, whereas this method uses the structural and spectral characteristics to designate the spatial distribution of guilds, removing the species identification component. This is important as the same species may display varying traits-based on their proximity to the channel (Hortobágyi *et al.*, 2017) and as such, using the physical characteristics of plants can be seen as an advantage. The use of image segmentation to delineate similar areas also helps to reduce the salt and pepper effect of high-resolution data classifications and so provides an effective method when looking at high resolution structural and spectral features of a reach.

4.6.4 Eco-Geomorphologic Change

Given the hydrology of the river, the majority of morphological change occurs over the winter months as expected. The temporal resolution of the surveys is not capable of picking out whether this is the result of a single flow event or continuously high flows, however it is clear that significant geomorphological re-profiling can occur within a single winter. There appears to be more localised evolution in the second winter of surveying whereas the first winter appears to show more continual response throughout the reach. The singular lower peak in water levels for the second winter as opposed to several higher peaks in the first (see Figure 4-1) suggests that priming may be more important for large avulsions, whereby a singular flow event of lower magnitude can incite a greater resultant planform shift. The response in summer is much smaller both in terms of deposition and erosion, with little morphological change occurring unsurprisingly. What change does occur may be from reductions in bank support from high flows leaving banks exposed to collapse (Zhao *et al.*, 2020). The largest areas of change appear to be within the reaches absent of large vegetation, with the stable patches aligning well with those identified in the decadal analysis.

It is difficult to extract any definitive link between the types of morphological change occurring and the underlying vegetation. It is clear from the historical analysis that although vegetation plays a role in morphological evolution, it is not the sole driver of change. There are also a

number of unique features in the reach which are hard to categorise or group, morphologically speaking, with different vegetation patterns, hydraulic conditions, and pre-existing morphology adding complexity. However, by grouping guilds based on their potential ability to influence vegetation, and categorising erosion and deposition into bands of morphological change in either direction, it is possible to visualise the links between vegetation and morphological change.

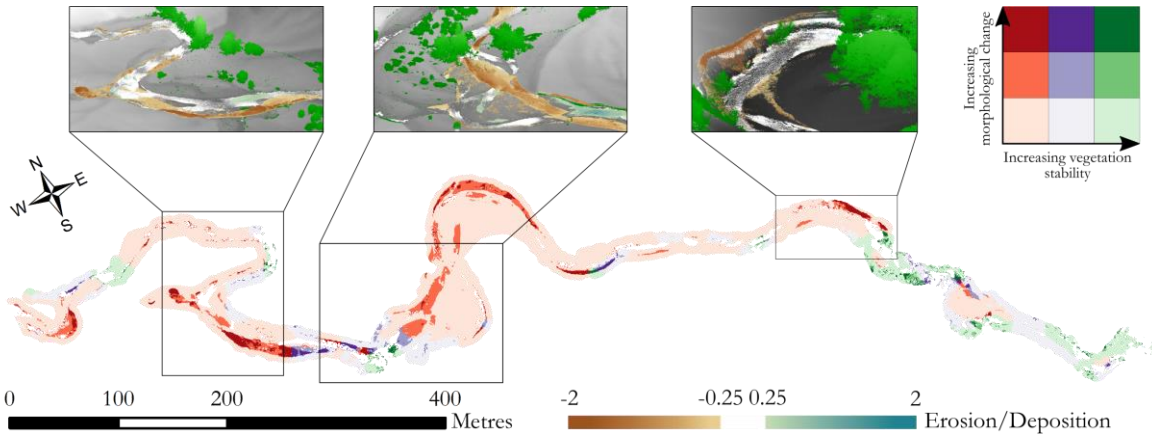


Figure 4-11 Bivariate classification of eco-geomorphic process form interactions, with examples highlighting the stabilising effect of vegetation. The bivariate colour scheme shows both the impact of the likely increase in stability from vegetation (red to green) and the increasing magnitudes of geomorphic change (light to dark shades). This allows both the presence and potential influence of vegetation to be mapped together. Vegetation stability was classed by grouping grasses and herbs, shrubs and bushes, and different woody tree guilds. Morphological change was split in to 0-1 m, 1-2 m, and greater than 2 m of change, regardless of whether this was erosion or deposition. Insets show patterns of erosion and deposition against the presence and absence of larger vegetation across various sections of the reach.

Figure 4-11 shows a bivariate classification of vegetation stability and morphological evolution. Grasses and herbaceous guilds are grouped along with bars as having the least morphological stability, followed by shrubs, and then woody guilds. Morphological evolution was split into 0 to 1 m of change, 1 to 2 m of change, and greater than 2m of change, which were chosen to represent the majority of change values. It is clear that most of the reach is shown in the lighter colour tones indicating low magnitudes of morphological change. However, areas with higher morphological change begin to become more apparent for areas of little vegetative stability, for example on the outer meander banks in several places. Darker oranges and purples are dominant in comparison to the areas of dark green. Although compared to the overall areas of each vegetation stability class you would expect fewer dark green regions, there is clear evidence of

light green patches where dark green patches may be expected had the vegetations stabilising effect not been present.

Some of these sections are highlighted in the panels of Figure 4-11 identifying regions where erosion may be expected but is not present. The left-hand panel shows a double meander bend, the first which has a heavily vegetated bank and the second which has little established vegetation. The total change in these two sections is dominated by erosion in the second meander bend which has a similar curvature to the first. The second bend does contain a knickpoint caused by overland flow which is not present in the first bend, yet the bend exit also shows far less erosion. Therefore, it is suggested that this dense patch of vegetation is having some stabilising effect, with soil cohesion increased, and flow velocities reduced. The central panel is just downstream and is constricted in planform by established vegetation, which despite substantial reworking across the survey period has remained relatively stable and exhibits deposition close to the vegetation on the left-hand bank. Subsequently, not only is the vegetation acting to stabilise banks, but likely slow the flow to encourage deposition in this area. Finally, the right-hand panel at the entrance to the region dominated by woody guilds is characterised by a large cut bank several metres in height that is progressively eroding, with the bulk of this erosion occurring just before entry into this woody guild dominated section. The vegetation on the outer bank is likely to play a stabilising role on the bank, until undercutting and removal of these trees occurs. There is evidence of such undercutting in action (Figure 4-12), suggesting that vegetation provides additional stability only as far as a given threshold, as was suggested in relation to the long-term decadal analysis.

4.7 Remote Sensing of Plant Functional Traits: What Next?

One of the key benefits of using remote sensing is the ability to quickly capture datasets over scales not possible with ground-based surveying. It is clear from the analysis herein that although the collection of data is fairly straightforward, the subsequent post processing time has to be taken into account. Yet once data has been processed, and the seasonality of the data acquired through spectral and structural characteristics, the success of the classification suggests that guilds can be classified for other sites that contain similar guilds, such as most temperate UK rivers which display these prominent guild types (O'Hare *et al.*, 2016), in much the same way as other research has used previous guild classes for similar environmental conditions (e.g. Butterfield *et al.*, 2020). It also allows guild analysis for regions that are more remote and less accessible to more traditional surveys. This improves the applicability and usability of traits methods when compared to more traditional taxonomic vegetation discretisation approaches.



Figure 4-12 The impact of undercutting within a heavily wooded reach, highlighting how the influence of vegetation on and interaction with flow changes through a plant's life cycle. The resulting creation of debris dams may lead to greater flow diversions, localised flooding, or scour points, changing the role of vegetation from offering stability to inducing erosion.

Combining vegetation structural and spectral data provides the opportunity to upscale to datasets collected via other platforms, with high resolution satellite imagery and ALS datasets offering the potential to improve the impact of such classification methods. This also allows the direct measurement of trait variability rather than investigating species variability and subsequently linking these to traits. The use of purely species data may remove some of the nuance in their traits, based on location, and so limit the applicability to fluvial research. Currently, the main difficulty with traits-based analysis is getting adequate data over large enough areas, this methodology provides a potential starting point from which a set of tools to classify different hydrologically relevant guilds across larger areas can be based. This may overcome some of the scale issues in linking guilds to geomorphic change which are currently known. Currently most large-scale studies link evolution to vegetation presence, and small studies are too localised to be applicable across wider areas. This research, although not large enough to be able to link guilds statistically to morphological evolution, demonstrates that by upscaling to combine enough hydraulic and morphological conditions may allow this to be possible.

It is important to understand how the role of guilds may change. Figure 4-12 shows a pre and post image of the channel in this section, suggesting large scale mobilisation of large wood. Being able to identify these changes is key, because the functional role large vegetation plays in the river corridor changes depending on its life stage. Our data suggests that large trees helps to stabilise the channel, likely through increases in soil cohesion and slowing flows during the flood stage. However, once a tree is undermined by erosion and collapses to form large woody debris,

it provides an increase in channel roughness and turbulence, diverts flow, and leads to knock on morphological impacts (Jeffries, Darby and Sear, 2003; Sear *et al.*, 2010). It is therefore important to consider that guilds and their influence are not stationary, but that they are dynamic through time both in terms of seasonality and life cycles. This must be considered when looking at the implications of guild dispersal and modelling, as the impact of changing from one state to another needs to be accounted for. Although the temporal evolution of guilds was not investigated, this presents itself as an area of future work, and the possibility to investigate traits-based methods to classify woody debris based on the surrounding vegetation structures.

The classification inputs predominantly focussed on structural and spectral characteristics of the vegetation; however it is widely shown that traits vary dependent on their underlying hydraulic and environmental conditions. It is therefore not inconceivable that such metrics may be used in future, such as to show inundation frequency or extent, to determine the likely composition of traits in these regions. This may take a more holistic approach and in cases where less structural data is present, allow for a more robust classification of guilds.

There are however several limitations to the methods. Variations in traits undetectable from TLS or UAV-LS methods will limit the ability to detect features for certain types of guild, such as those too small to resolve including different grasses or those with too complex structures, such as branching shrubs. Both of these are prominent features of UK river corridors and so their omission from the analysis is a limitation. However, they can still be mapped but would require in field trait collection or species identification for the use of trait databases (e.g. TRY (Kattge *et al.*, 2020)). The remote sensing equipment used for this research is not cheap (see Tomsett and Leyland, 2021, noting that our custom system is considerably more economical than commercial off-the-shelf packages) and requires a degree of expertise in processing and manipulating the data. However, commercial improvements are seeing more easy to deploy, cheaper, sensor systems being brought to the market, likely to have a positive impact on eco-geomorphic research in terms of allowing broad uptake of the methods developed herein for applied monitoring and river corridor management.

4.8 Conclusion

We have presented a novel method for collecting and extracting vegetation functional trait data that is relevant to eco-geomorphic research. Herein we used UAV-LS and UAV-MS datasets to advance our ability to collect high resolution 4D datasets, improving the spatial and temporal resolution of riparian vegetation monitoring and geomorphic change detection, allowing us to gain an insight into how riparian vegetation evolves and to better discretise the spatial variation

of vegetation in a manner that is applicable and scaleable over large river reaches. As such, we have been able to provide insight in to how traits-based frameworks for vegetation analysis can be linked to trends and patterns in morphological evolution at scales that were previously not attainable. We have also outlined the limits for current trait extraction from remote sensing techniques. UAV-LS can characterise larger vegetation structures and be used to upscale local TLS models, but even TLS is limited in its ability to characterise the spatial complexity of some vegetation traits at the resolution required to link with geomorphic change. This builds on current research which has analysed ecogeomorphic interactions on small river sections, or used species based imagery classification to determine large variations. The use of remote sensing allows data to be captured, analysed, related to broader dataset statistics, and upscaled to include larger reaches. Simultaneously, the same data allows for the collection of topographic responses to flow events which can be linked to the variation in vegetation. This analysis uses seasonality to improve the classification of guilds via changes in structural and spectral properties, advancing current methods available to the ecogeomorphology community. Despite some noted limitations, this research represents an important step towards better discretisation of traits across greater scales and the furthers the possibility of implementing widespread traits-based research.

Future research is needed to investigate the limits of various remote sensing methods in relation to their ability to be used for traits extraction and thereby improve understanding of a systems ecogeomorphic evolution. Of particular note is the currently untapped resource that exists in relation to coarse scale global coverage of land cover from which vegetation traits could be extracted using methods such as those presented herein to link the scales of analysis. These methods offer a bridge across scales, within which to consider the ways in which riparian vegetation within the river corridor is mapped, evaluated, and modelled through time, with implications for establishing new insights into the functioning of eco-geomorphic systems across scales ranging from river sections to intercontinental basins.

Chapter 5 Accurate representation of seasonal vegetation structure in a hydrodynamic model.

5.1 Abstract

The influence of vegetation on hydrological and morphological processes is well recognised, but research to adequately represent vegetation in hydrodynamic models is more limited in comparison. The use of bulk roughness parameters such as Manning's n have widely been used to account for spatial variations in vegetation, but the ways in which these bulk roughness values are assigned and estimated are subject to inaccuracies. Moreover, they will often take little account into the different structural roles of vegetation or their complexity through time, such as seasonality and colonisation. Within this paper we investigate the impact that different representations of vegetation and their seasonality have on model outcomes. We identify that switching between different methods of vegetation discretisation has a large impact on subsequent morphology and hydrodynamics. The timing of seasonal changes can lead to different evolution sequences and that the use of traits-based methods to represent vegetation can better represent channel stability in some locations but over stabilise the channel in others. The use of seasonal parameters led to planform evolution more akin to that identified through field observation, but that flood extent may have been better matched using traits-based approaches. The sensitivity of the model to changes in roughness values is discussed as well as the large impact a structurally based approach has. Moving forward, further investigation into the sensitivity of models to different vegetation parameters is required to fully understand how changes in vegetation composition may influence morphology. Any decisions made using hydrological monitoring which have a vegetative influence should acknowledge the importance of correct parametrisation, with such decisions being increasingly likely and important under an ever-changing global hydrological background.

Keywords: Vegetation, Hydrology, Modelling, Traits, Roughness, Geomorphology, Seasonality

5.2 Introduction

Vegetation plays a crucial role in river corridors, affecting flow velocities (Sand-Jensen and Pedersen, 1999; Whittaker *et al.*, 2013) and increasing cohesion in the substrate (Wiel and Darby, 2007; Gurnell, 2014). Vegetation can alter channel shape (Andrews, 1984), create variations in

water elevations and slope (Wang and Wang, 2007), impact deposition and erosional patterns (Gran and Paola, 2001; Bertoldi, Gurnell and Drake, 2011b), and provide root reinforcement (Zhu *et al.*, 2018). These influences happen at the local scale of individual plants through to patch and reach scale interactions between blocks of vegetation, with different plant structures, densities, and spacing all important factors in controlling the flow of water and channel morphology (Nepf and Vivoni, 2000; Sand-Jensen, 2008; Kim and Stoesser, 2011). As a result, vegetation is also seen as a potential solution to reducing flooding impact through the implementation of natural flood management techniques (Lane, 2017), with specific interventions for local catchments having potentially significant impacts (e.g. Jackson *et al.*, 2008).

Due to the difficulties associated with measurement and observation of natural river systems, fluvial geomorphologists often resort to the use of morphodynamic models to study the interactions between flow, sediment and morphology. More recently, in recognition of the first order control that vegetation can exert on a fluvial system, many studies have sought to try and incorporate vegetation controls into modelling frameworks (see the thorough reviews by Camporeale *et al.* (2013) and Solari *et al.* (2016)). For reach scale 2D modelling, variation in vegetation type and structure are typically accounted for by providing a roughness value assigned to each vegetation type, which can be varied spatially to account for vegetation composition. A typical approach would be to use the lookup table for flow in different channels from Chow (1959), with many modelling studies using such an approach. This can be used to determine variabilities in roughness values (Cobby *et al.*, 2003b; Casas *et al.*, 2010), with more complex implementations considering depth variations in roughness (Anderson, Rutherford and Western, 2006). However, errors introduced through the introduction of unsuitable classifications can lead to errors in water levels of decimetres (Straatsma and Huthoff, 2011), and matching field observations or classifications to reliable roughness parameters is subject to seasonal variations, survey resolution, and researcher experience (Song *et al.*, 2017).

The current state of the art in terms of vegetation structural representation in 2D models is to define X, Y and Z so that individual elements can be explicitly modelled (Crosato and Saleh, 2011; Vargas-Luna *et al.*, 2016). However, such discretisation across vegetated reaches has hitherto not been possible, relying on manual measurements of individual plants. Similarly, with one or two notable exceptions, more sophisticated representation of broad channel and floodplain vegetation in models has not been undertaken, despite advances in the high resolution characterisation of vegetation (Butterfield *et al.*, 2020; Tomsett and Leyland, In Review). Diehl *et al.* (2018) used a traits-based framework when constructing flow response curves to assess the effects of guilds (areas of vegetation with similar functional traits) on

morphological response and vice versa. Likewise, Caponi, Vetsch and Siviglia (2020) used different traits-based methods for allocating above and below ground biomass on dynamic bar systems during different flow events to assess mobility changes between different growth strategies. However, beyond this most functional trait-based research has focussed on in field observations in an attempt to link guilds to flow and geomorphic interactions (e.g. Hortobágyi *et al.*, 2018; Butterfield *et al.*, 2020).

In relation to temporal variation of vegetation (e.g. due to seasonality and growth), despite being well studied from an ecological point of view, it is still rarely accounted for in hydrodynamic modelling. Seasonal Manning's n values have been used to improve the calibration of modelling studies for water surface elevation and discharges to match observed field values (Song *et al.*, 2017). The amount of plant biomass, its cross-sectional area, and percentage cover have all been demonstrated to explain variation in Manning's n coefficients (De Doncker *et al.*, 2009; O'Hare *et al.*, 2010; De Doncker *et al.*, 2011), and as such it is clear that variations in biomass from seasonal cycles will influence channel roughness. This seasonal variation in biomass has been closely linked to seasonal variations in roughness through field analysis whereby variations in roughness follow the seasonal peaks when biomass is at its greatest (Gurnell and Midgley, 1994; Champion and Tanner, 2000; Cotton *et al.*, 2006; De Doncker *et al.*, 2009; De Doncker *et al.*, 2011). These principles have been accounted for in hydrodynamic modelling (e.g. Song, Schmalz and Fohrer, 2014; Song *et al.*, 2017), with Song *et al.* (2017) noting an increase in model fit from using seasonal values of Manning's n . Despite the majority of existing research being focused on the river channel alone, the same principles also apply to floodplain vegetation and its interactions with flow, flooding, and morphology.

5.3 Aims

The aim of this research is to establish a method for incorporating more accurate spatial and temporal vegetation characterisation into a 2D hydrodynamic model to assess how it impacts modelled outputs in terms of flow and morphology. This will be achieved through representation of a traits-based approach to characterising vegetation within a model domain simulating a small temperate UK river system, the River Teme. The different model outputs across the fluvial corridor will be compared to establish the differences that alternative methods of vegetation representation in a model can make, with results discussed within the context of other studies seeking to analyse eco-geomorphic feedbacks and future research requirements in this domain.

5.4 Methods

5.4.1 Delft3D

Herein, Delft3D (version 4.04.02), an open source depth averaged hydrodynamic model developed by Deltares, widely used for simulating flow, sediment transport, and morphological evolution (Lesser *et al.*, 2004; Deltares, 2021) is used. Delft3D has been widely used and proven to be an effective and validated model in a number of hydrodynamic studies (e.g. Gerritsen *et al.*, 2008; Williams *et al.*, 2013; Williams *et al.*, 2016; Parsapour, Rennie and Slaney, 2018). Delft3D simulates depth-averaged flows using Navier-Stokes equations with shallow water assumptions and the Boussinesq approximation for density. For the simulations undertaken here, the use of a 2D rather than 3D approach is deemed acceptable, as a trade off in allowing a larger domain to be modelled and because the downstream dominance of the flow will outweigh the importance of vertical momentum exchanges in the context of the scenarios explored.

5.4.1.1 Modelling Scenarios

A series of three scenarios were run to assess the impact of vegetation representation on hydraulic and geomorphic responses (Table 5-1). These three models used a combination of either Manning's n or traits-based cylindrical models for influencing flow, and these were either static throughout the year or seasonally varying. All other parameters were kept consistent throughout the modelling procedure to isolate the effects from vegetation alone.

Table 5-1 Model run scenarios used in this study, explaining the vegetation representation and whether these vary through time.

Run ID	Veg Rep	Time Varying	Details
1	Manning's n	No	Traditional Manning's n approach
2	Manning's n	Yes	Seasonally varying Manning's n approach
3	Traits	Yes	Seasonally varying traits-based approach

5.4.1.2 Model Grid

For this model, an equilateral grid comprising of 463 and 143 grid cells in the X and Y directions with a grid cell size of 2 m was created, covering a reach of the Teme ~0.9 x 0.3 km in size (Figure 5-1). This was surrounded by a closed boundary except at the entrance and exit of the study area where open boundary conditions were prescribed.

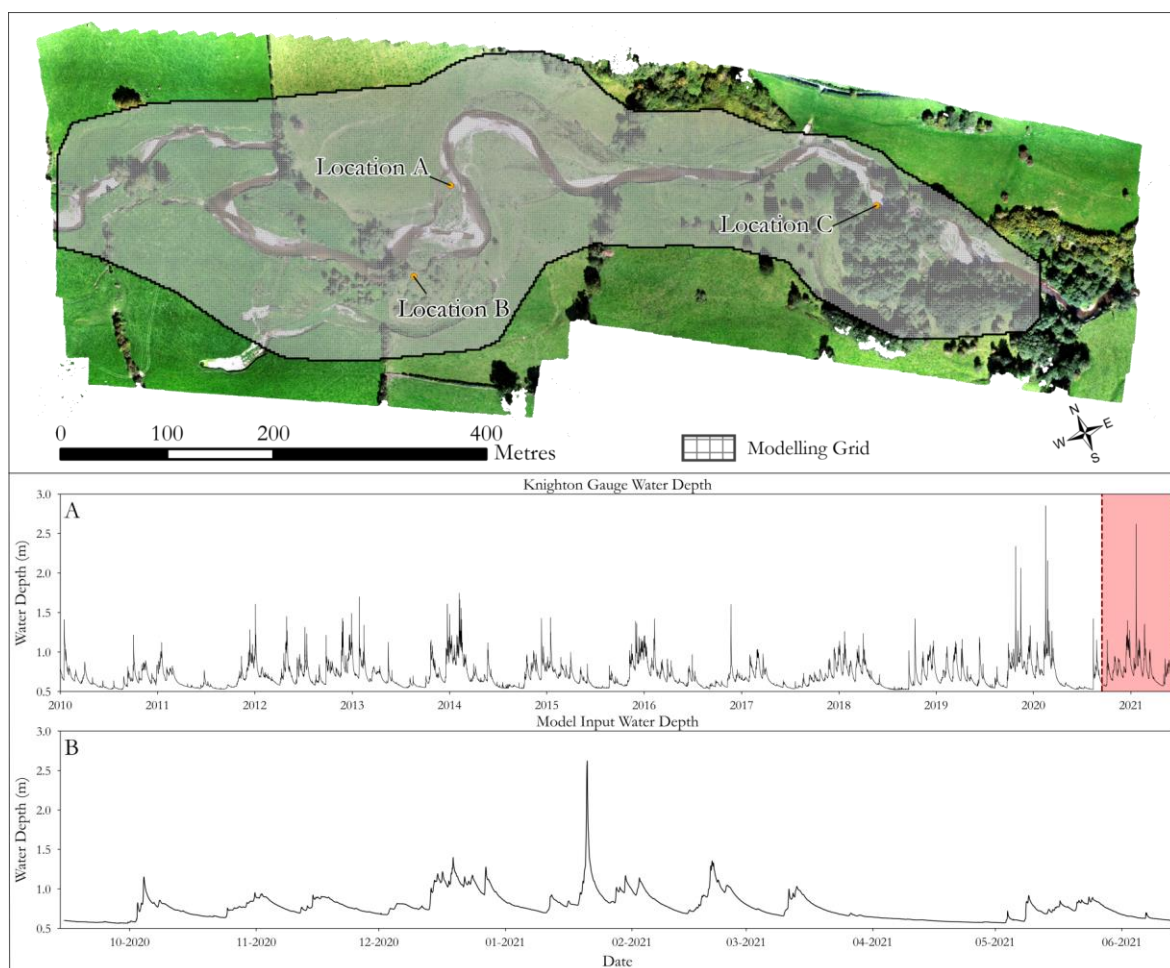


Figure 5-1 Model domain grid, monitoring locations, and water level inputs. Top Panel: Study site with the 2 x 2 m grid used within the modelling domain shown. Locations A, B, and C refer to locations used for analysing avulsion formation (A and B) and the impacts of different vegetation representation (A and C) as described in Section 5.5.2. Bottom Panel: (A) Long term hydrograph from water level stage downstream of study site from 1st January 2010 until 31st June 2021. Model time period highlighted in red. (B) shows the hydrograph used for the study obtained from a combination of in field data loggers, and inferred depth from the relationships between the in-field loggers and downstream gauge station.

The DTM (Digital Terrain Model) was created using a hybrid approach of both UAV-LS (UAV Laser Scanning) and UAV-MS (UAV Multispectral) data from surveys performed in February 2020. This survey was chosen as it had good ground coverage in vegetated areas and a high quality of Structure from Motion (SfM) output (see Tomsett and Leyland, In Review), creating accurate terrain models within the vegetated sections of the reach. Both datasets were cleaned of erroneous points and were classified into ground and non-ground points using a progressive morphological filter from the *lidR* package (Roussel *et al.*, 2020). The ground points of each point cloud were then combined in CloudCompare to gain the benefits of through canopy

surveying from UAV-LS and the through water survey capability of the UAV-MS SfM, giving a continuous terrain model for the study area exported as a 0.1 m raster.

The resultant DTM was then split to extract those pixels within the channel using a water mask derived from the SfM imagery, subsequently classified using a Random Forest Classifier and manually adjusted to overcome any misclassified or obscured points, such as under tree canopies. The water excluded raster was then interpolated between the dry points on the banks to create an estimate of water surface elevation (Moretto *et al.*, 2014). The difference between the water surface elevation and bed elevation was calculated to create a raster of water depth, from which a refraction index of 1.33 was applied to account for the effects of refraction in SfM reconstruction (Woodget *et al.*, 2015). The difference between the original and refracted depths was then computed before subtracting this from the original bed elevation to create a refraction adjusted bed elevation. Once adjusted, the new channel DTM and original separated non-channel DTM are combined to create a modified DTM. This DTM was then resampled to 2 m resolution for computational efficiency during the modelling process, using the average elevation for all cells within the resampled area. This was then smoothed using a two-step 3x3 low pass filter in order to minimise the effects of any bumps or sinks within the DTM which could hinder the modelling process.

5.4.1.3 Model Timescales

For each of the scenarios, the model run times totalled 10 months running from the 15th August 2020 to the 14th June 2021, capturing the dominant winter flows of the Teme. Tomsett and Leyland (In Review) previously showed that morphological change is driven by winter peak flows, with very low and stable flows occurring during the summer months (Figure 5-1). Moreover, the high resolution of the model and relatively large area being simulated required small time steps which subsequently impacts model run times. The model was set up to have a time step of 0.02 minutes (equivalent to just over 1 second) to avoid instabilities caused by using a relatively fine resolution 2 m grid, keeping the courant number value below the maximum suggested value (Deltares, 2021). This grid cell size is lower than those typically used within Delft (e.g. Rinaldi *et al.* (2008); Oorschot *et al.* (2016); Williams *et al.* (2016)) and as such this time step is also considerably smaller. Each model had a warmup time of 60 minutes in order to reach settled hydrological conditions, in which no morphological updates could take place to remove any artefacts from unstable water levels. The initial conditions for the runs were based off water elevations extracted from the water mask described above. When investigating seasonal changes, where the model was stopped and restarted, the restart files outputted by the

model were used to reinitialise the model so the conditions at the beginning of a run would exactly match those at the end of the preceding run.

5.4.1.4 Boundary Conditions

To obtain accurate model parametrisation, seven data level loggers were placed into the river throughout the study reach, collecting data from October 2020 until June 2021. These were designed to capture water levels at the model inflows and outflows, as well as to provide calibration data for assessing model performance. VanWalt LevelScout loggers were used in conjunction with an eighth logger collecting barometric air pressure. This is used to adjust the pressure values recorded by the in-channel loggers to obtain an estimate of water depth. Unfortunately, due to significant morphological change during deployment, only two loggers can be used to calibrate the model.

Data from these two loggers was used to prescribe boundary water level conditions. For fluvial modelling, Delft suggests the use of discharge boundaries at an inlet and water level at the outlet (Deltares, 2021). As a result, cross sections and flow velocity measurements were acquired from the field, but access during high flows, changing cross sectional areas, and limited survey repeats ultimately made relationships between water depth and discharge inadequate for prescribing boundary conditions. Consequently, it was decided that water levels were to be used to prescribe flow depths at the inlet boundary. The inlet conditions were related to those of the long-term downstream gauge to extend the diver data to also cover two months of preceding data to complete the run times. For the outlet boundary, a water level boundary prescribed by a discharge-depth relationship was determined using the model itself across a range of flow conditions, to minimise instabilities at the exit.

5.4.1.5 Sediments

Sediment boundary conditions were split into bedload and suspended inputs and assessed using sensitivity analysis whereby a small amount of sediment was input and conditions were set to transport rather than supply limited (as observed in the field). Two classes of sediment were specified in the model, first a non-cohesive sediment type used to represent bedload material, and second a cohesive sediment type which represented the alluvial sediments in the floodplain. When specifying sediments, Delft will typically mix the different sediment types into a homogenous layer with the relative volume of material based on the specified initial thickness. However, to model with stratified sediment, a separate input is required to get the correct layering in the bed material.

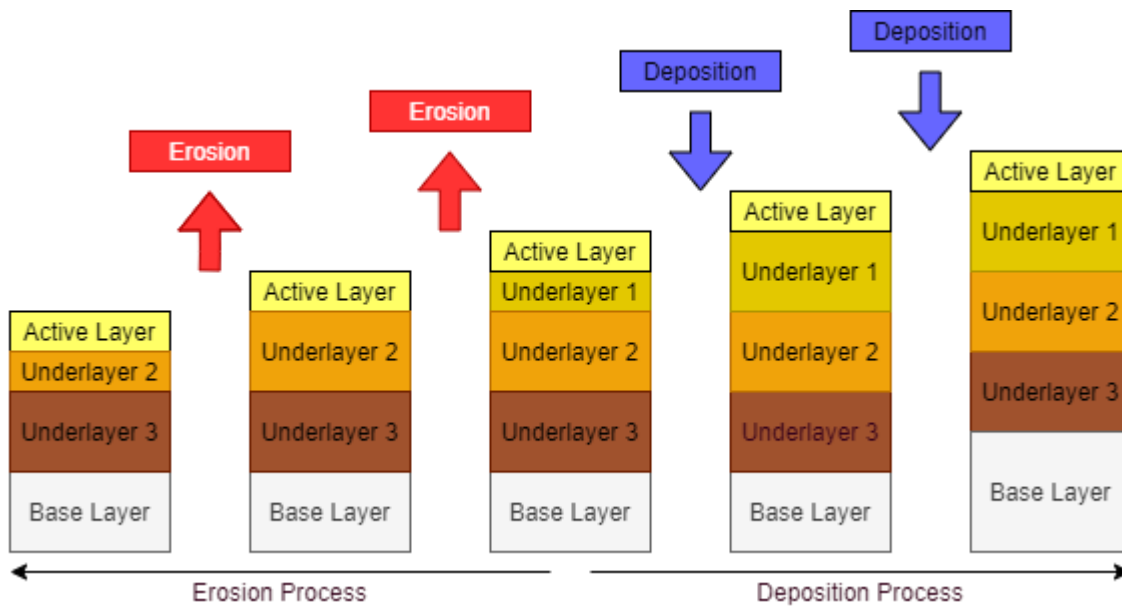


Figure 5-2 How both erosion and deposition are accounted for in the various sublayers of the model domain. Erosion moves sediment out of the active layer, sourced from the underlayer below, with deposition adding to the active layer which is then redistributed to the underlayers below.

Delft separates the layers in to three categories, a base layer, underlayers, and a transport layer. The top transport layer is of a specified thickness which remains constant throughout the simulation, determining the amount of sediment that is available for transport at any one-time step. Sediment is moved in and out of this layer depending on the flow conditions and subsequent transport calculations. The underlayers act as gatekeepers, transferring sediment of different sizes up or down the layers depending on what is required. The depth of these layers is set to a maximum and these are added to until the user defined max thickness of a layer. If all layers are at maximum thickness, then these are passed on to the base layer. During erosion, these underlayers are reduced until they are removed from the layering system, whereby erosion is then performed on the next layer down. Figure 5-2 demonstrates how this process works with a maximum of 3 underlayers of equal depth during erosion and sedimentation (adapted from Moerman (2010)).

In essence, erosion in the active layer, leads to a removal of sediment which is then replaced by the first holding layer beneath it, reducing the depth of this holding layer. During deposition, sediment is added to the layer that sits below the active layer. If the layer below is of different sediment type, e.g. cohesive being deposited on non-cohesive, then the composition of that layer is adjusted accordingly.

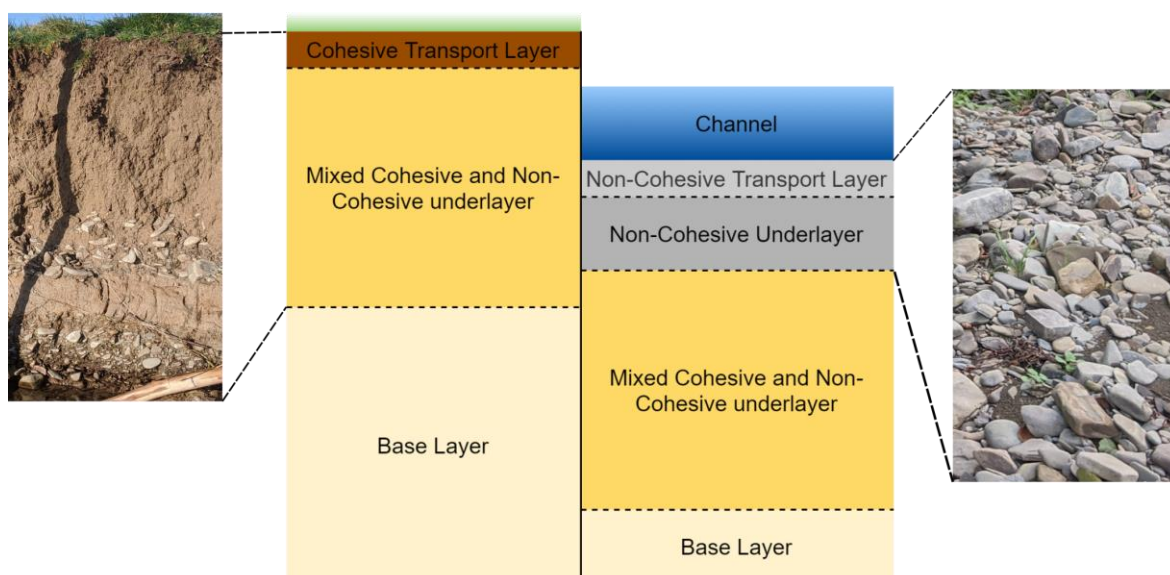


Figure 5-3 The sublayers used within the model setup to represent the likely composition across the floodplain, channel, and bars. Note that the relative depths of each layer are not to scale.

For this model, a base layer of a 50-50 mix of cohesive and non-cohesive sediment was used. This was overlaid by a 5 m thick layer of cohesive sediment across the entire reach that has a 15% volume mix of coarse fractions incorporated in. Throughout the channel and bars there was a 1 m layer of non-cohesive bedload sediment added to this cohesive layer. Finally, a 0.2 m active layer was specified, with spatially varying volumes of sediment where 100% of the active layer was non-cohesive across the channel and bars, and 100% of the active layer was cohesive across areas outside the channel and bar regions (Figure 5-3). The depth of these layers was estimated as no in field observations of stratigraphy were collected. Observation of exposed river bank suggest a fine cohesive dominated sediment with some larger fractions present. This was the primary basis for assigning the relative fractions of sediment in each layer. The 15% volume of non-cohesive sediment in the first underlayer is based off image classification of exposed banks. Figure 5-4 shows images taken from the field showing exposed banks containing a mixture of cohesive fines and coarse fractions. These were automatically classified using k-mean unsupervised classification to extract these coarse fractions, for which the number of these pixels were compared to the overall. For 4 images that had a reasonable quality of classification based on visual assessment, it was established that a 15% volumetric approach of coarse sediments should be used, as the classification in general missed out some smaller coarse fractions not clear in the original image. Figures 5-4 shows the classified image and the segregated image from which coarse volume fraction was assumed. Although an assumption is made that this mixing is present throughout the reach, in the absence of any intensive sampling

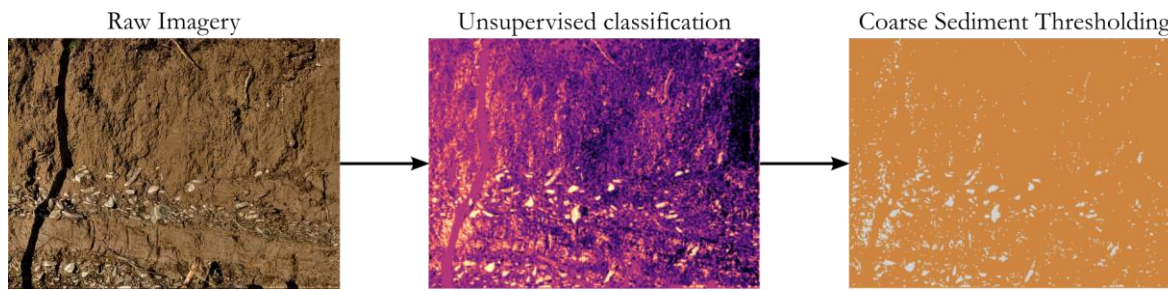


Figure 5-4 Image classification of riverbanks to obtain coarse sediment fraction percentage.

Basic steps taken were: (1) Raw imagery taken in the field, (2) Classification of image through unsupervised k-means clustering, (3) Segmentation to identify individual coarse sediment fractions.

of sediment this provides an estimate of the amount of coarse material that will be released into the system during lateral erosion. This is important to consider during morphological evolution and avoids only cohesive sediment entering the system during lateral erosion.

The overall stratigraphy was based off a number of images, such as in Figure 5-3 which suggested the layering approach taken in the model is correct. Figure 5-3 shows that on the bank edges there is often an active layer that consists predominantly of cohesive materials, which then becomes a greater mix of coarse material further down. This is the reasoning for a purely cohesive active layer of 0.2 m across the floodplain before coarse fractions become present. Although there is distinctive layering in the substructure, not enough information is present to create a fully representative depth model of this. Figure 5-3 also shows an image of the surface of a bar, highlighting the dominance of coarse fractions which justify the use of a coarse fractions only active layer in the channel and on the bars.

The grainsize of the non-cohesive bedload sediment was established from the collection of field samples. Samples were collected from three locations: at the centre of the channel, the channel's edge, and on an adjacent bar, incorporating a mixture of surface and subsurface material. In total, 11.05 kg (dry weight) of sediment was collected. The samples were kept separate from one another and dried in an oven at 50 degrees Celsius for 96 hours to remove any moisture present. Once dried, each sample was weighed before being placed into a mechanical sieve shaker to separate sediment at diameters 64, 32, 16, 8, 4, 2, and 1 micron. Sediments under 1 micron were then sieved by hand to separate out grainsizes of 0.75, 0.50, 0.25, 0.125, 0.063 microns. The material captured by each sieve was then removed and weighed separately to identify the mass at each diameter interval. This data was then analysed using GRADISTAT (Blott and Pye, 2001) for each location to extract the grainsize distribution for input in to the model. The grainsize distributions for each of the three sites can be seen in Figure 5-5 alongside a combined distribution across all sites.

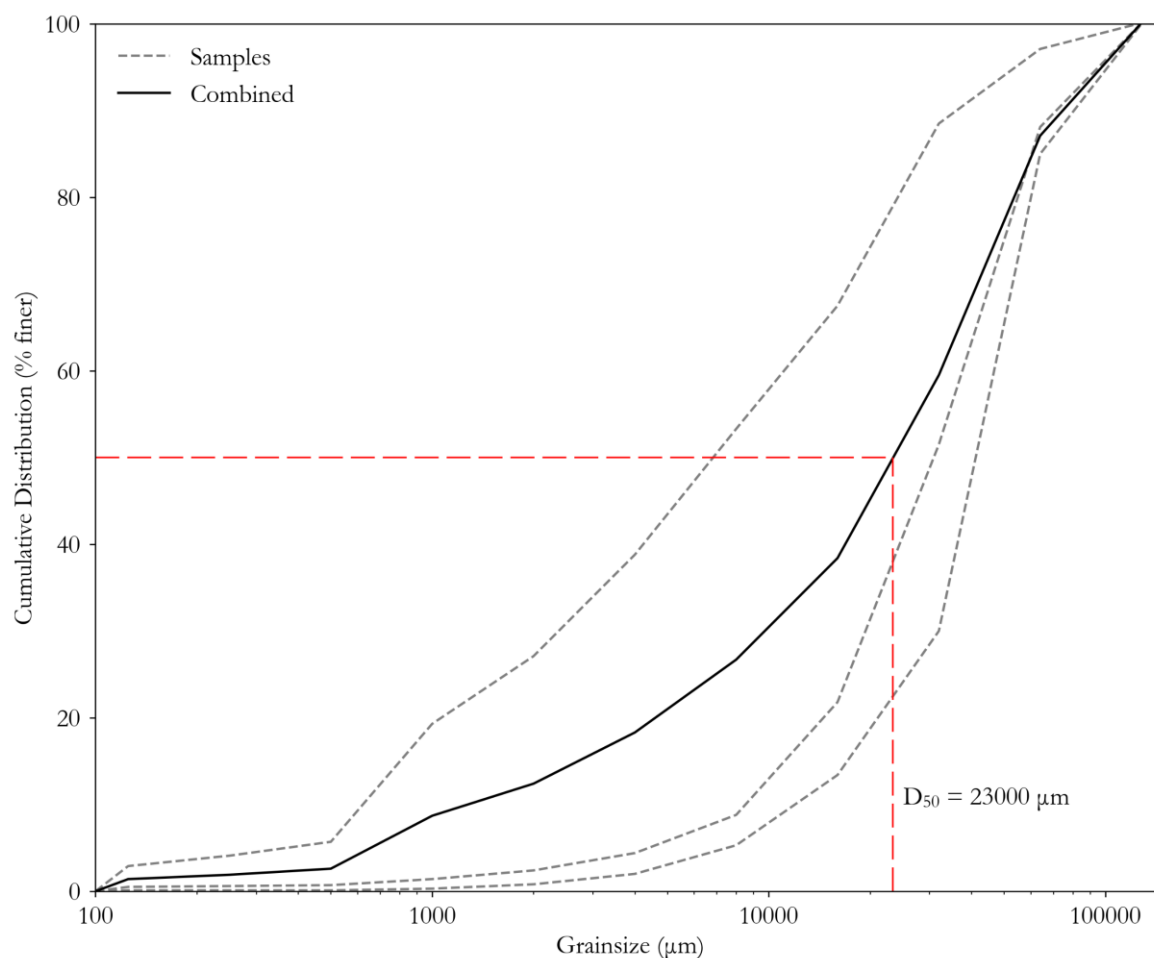


Figure 5-5 Grainsize distribution plots for each of the three sample location sites and the combined final distributions. The red line shows the D_{50} of the final combined distribution.

The resulting values for each sample and combined are shown in Table 5-2, with only samples from the channel centre consisting of a large proportion (10%) of material under 4 mm in diameter. Samples from the edge of the channel and bar were classed as medium gravels (8-16 mm) whereas sediment in the channel was classed as fine gravels (4-8 mm) based on classifications by Udden (1914) and Wentworth (1922). Sediment in the channel centre was deemed to be poorly sorted whereas sediment at the channel edges were deemed to be very well sorted as expected. The D_{10} , D_{50} , and D_{90} of the combined samples were subsequently used to assign the grainsize distribution properties into the model.

Table 5-2 Grainsize distributions established via mechanical and manual sieve shaking for all three sampled locations as well for the combined values.

Sediment Characteristics	Sample Sites			
	Channel Centre	Channel Edge	Bar	Combined
D ₁₀ (µm)	688	12015	8546	1256
D ₅₀ (µm)	6851	40924	30785	23353
D ₉₀ (µm)	39389	254769	125509	175391

5.4.1.6 Channel Morphological Adjustment

For the modelling of rivers, Delft uses a secondary flow calculation to account for perpendicular flow experienced through a river bend as described by (Van Rijn, 1993), overcoming the lack of vertical grid within 2D models. By accounting for secondary flow, adjustments in the direction of bed shear stress away from the direction of depth averaged flow are accounted for, which in turn affects bed load transport (Deltares, 2021). This directly impacts morphological simulations and subsequently allows for meander development and lateral shift within the domain. In order for lateral erosion to be modelled, Delft requires some parameters to be tuned in order to determine the rate of change. This includes the erosion of adjacent dry cells by reallocating shear stress (ThetSD) and a coefficient value to account for the effects of secondary flow on bedload transport (Espir). ThetSD allocates a percentage of erosion on a wet cell to an adjacent dry cell to implement bank erosion in a simplistic manner (Lesser *et al.*, 2004). ThetSD allows river sinuosity to develop and avoids over deepening at outer banks, but does not always represent realistic change compared to observed data (Williams *et al.*, 2016; Banda and Meon, 2018). Espir influences the magnitude of effect spiral flow has on bedload transport, with higher values proportioning a greater component of subsequent direction to that prescribed by spiral flow.

In order to test the sensitivity to these values, a cross computation was undertaken for a high flow period, with bed load transport and subsequent erosion assessed. The extent of deviation from a baseline (middle value) scenario was assessed, and erosion used as a proxy in order to determine suitable values qualitatively, as no reference values could be obtained. Despite quantitative analysis against monitored erosion showing little variation in erosion and deposition volumes across various ThetSD values, the model experienced variations in bedload transport across values ranging from 0.5 – 1, with 1 having much higher levels of erosion and bedload transport directions different to expected. This led to the selection value of ThetSD as 0.75, in

line with other studies using Delft to monitor planform change (Javernick, 2013; Williams *et al.*, 2016; Banda and Meon, 2018). Values for Espir were varied from the base line advised by Delft of 1 for inclusion to 0.5, with the value of 1 creating higher rates of lateral erosion without introducing spurious bed load transport rates and directions. This affect is similar to that noted by Frölke (2017) and uses values in line with Meer *et al.* (2011).

Bedload transport was calculated using the Meyer-Peter-Muller formula with a calibration factor of 0.047 as outlined by Delft (Deltares, 2021). Changes in morphology were updated within the simulation and fed back into the hydrodynamics so that channel evolution would affect future hydrodynamic processes. The morphological scale factor was set to 1, whereby no multiplication of geomorphic change was applied to the erosion and or deposition processes. Critical shear stress (τ_{crit}) was determined using a sediment composition approach with secondary data available from the Teme and also from studies that have collected information on shear stress globally. Data collected by Pears *et al.* (2020) at Broadwas on the Teme identified sand % content of between 15-35% from core samples, giving an indication of the type of soil within the floodplain. As such, studies using jet tests, cohesive strength meters, and velocity profiles were used to suggest a range of values that should be tested. The average value for τ_{crit} was 1.3 Pa for banks described as silty or sandy or having cohesive properties (Julian and Torres, 2006; Darby, Rinaldi and Dapporto, 2007; Rinaldi *et al.*, 2008; Darby *et al.*, 2010), whereas for clay banks this was seen to be higher with average calculations from turbulent flows suggesting a τ_{crit} of around 8.5 Pa (Gaskin *et al.*, 2003). Although the composition of cohesive sediment was not established for the study site, the sand contents identified by Pears *et al.* (2020) downstream and visual assessment would suggest a sandy silty mix is more likely.

Given the role of vegetation root structures in decreasing the erodibility of beds and banks and increasing the critical shear stress required for erosion to take place (Millar and Quick, 1998; Wiel and Darby, 2007), a spatially varying shear stress for erosion was implemented whereby values obtained from the wider literature were used to assess the impacts of above ground vegetation on below ground erodibility. Research by Julian and Torres (2006) identified that grass increased the erodibility of cohesive sediments by a factor of 1.97, and as such this is used as a first guide to suggest a base level of τ_{crit} for cohesive sediments. Furthermore, research in to critical stress variation by Millar and Quick (1998) and Huang and Nanson (1998), comparing the impact of trees compared to grass for similar sediment types, indicated a further increase in τ_{crit} by a factor of 1.74. Here we make use of the detailed traits-based vegetation characterisation of Tomsett and Leyland (In Review) to allow variation in τ_{crit} between different vegetation guilds. As the effects of root cohesion should be added to erosion models, and that increases in soil cohesion are related with increasing root area (Waldron, 1977; Yu *et al.*, 2020), it is clear that

different guilds will likely have different root properties and thus effect erodibility. Root distribution may be more influential than the root strength itself (Abernethy and Rutherford, 2001), and as poplar roots (Low DBH) tend to take up less soil than willow roots (High DBH), and although they have longer roots overall, they are not necessarily as deep, poplar trees were considered to have a smaller increase in τ_{crit} (Ceulemans, McDonald and Pereira, 1996; Phillips, Marden and Suzanne, 2014). Shrub roots τ_{crit} values were kept the same as previous vegetation values. These Low DBH and High DBH guilds increased values of τ_{crit} were based on one and two standard deviations above the mean values based on data by Millar and Quick (1998) and Huang and Nanson (1998) respectively, so that the increases were still within measured ranges of increased soil cohesion values. Final values for all vegetation types within the runs are provided in Table 5-3.

Table 5-3 Values of critical shear stress (τ_{crit}) for erosion to take place which are spatially varied according to the below vegetation classifications. For traits-based approaches, grass is split in to grasses and herbaceous vegetation, and established vegetation split into shrubs and the two guilds of woody trees.

Class and Guilds	τ_{crit} (Pa/Nm⁻²)
Grass	2.56
Established Vegetation	4.46
Single Stem and Multi-Stem Herbs	3.75
Shrubs	4.46
Low DBH Trees	6.52
High DBH Trees	8.60

5.4.1.7 Roughness and Vegetation

For a simple Manning's roughness-based approach, four land cover classes were defined; large vegetation, grasses, bars, and water. A combination of both multispectral imagery and laser scan data were used to define these. The use of the Infrared band of the multispectral imagery was used in combination with the red and green bands to create NDVI (Normalised Difference Vegetation Index) and NDWI (Normalised Difference Water Index) layers to enable maximal spectral differentiation between classes. This is especially useful in areas of varying brightness, where the relative amount of light reflected across bands is similar, but the absolute values differ compared to unshaded areas. Two structural datasets were used to improve classification results. Surface variation in a 0.5 m search radius was calculated within the CloudCompare software (<https://www.danielgm.net/cc/>), and a Canopy Height Model (CHM) produced to identify the height of vegetation. The CHM was produced by identifying ground points and non-ground

points using a progressive morphological filter within the LidR package (Roussel *et al.*, 2020), before creating both elevation models for the vegetation and bare-Earth points and computing the difference between the two. The use of structural data can help separate out different vegetation elements with similar spectral properties and those that have been hampered by shading also.

Training samples were manually digitised within ArcGIS based on the high resolution orthoimagery. For training, the number of samples for grass and small herbaceous vegetation was 16883 (4221 m²), for large shrubs and tall vegetation 3952 (988 m²), for bars 2040 (510 m²), and for water 4626 (1,1567 m²). A random forest classification was used to classify in to the four initial classes. The original 0.04 m orthomosaics were resampled to 0.5 m with the surface variation and CHM rasters snapped to the same size and extent before being stacked into a multi-layer raster dataset. This created a nine-layer dataset (5 image bands, 2 indices, and 2 structural) from which to train the random forest model.

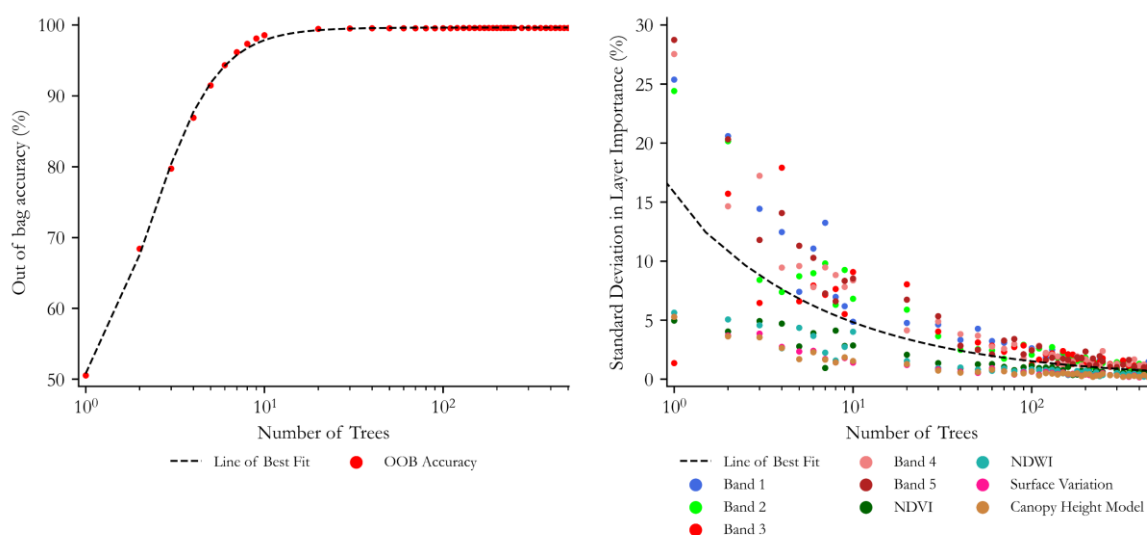


Figure 5-6 Random forest classifier out of bag accuracy and variations in band importance for Manning’s roughness land cover classes. (Left) Out of bag accuracy scores for different numbers of trees used within the random forest classification, showing a distinct levelling off in accuracy after 7 trees are used. (Right) The standard deviation in individual band importance across 10 sample runs to identify at what number of trees bands importance became consistent across all runs, in this instance around 300 trees.

The number of trees used was based on an analysis of Out-Of-Bag (OOB) accuracy and the Standard Deviations (SD) of band importance based on data from the September survey. Models were fitted with n trees of 1 – 500 in varying incremental steps with each model fitted

10 times; resultant means of OOB accuracy and SD of individual layer importance were assessed until both measures stabilised. Both of these elements are deemed important due to consistency in tree architecture and removing bias (Chan and Paelinckx, 2008; Adelabu and Dube, 2015). The OOB accuracy quickly increased at low number of trees before stabilising after the inclusion of 7 trees (Figure 5-6 A). The layer importance S.D. quickly decreased with additional trees from upwards of +/- 25% to below +/- 5% once 40 trees were used, and below +/- 2% when 300 trees were used (Figure 5-6 B). Consequently, 300 trees were chosen for initial classifications of all surveys.

This methodology was applied to both summer and winter datasets so that the spatial variation in both summer and winter Manning's roughness could be utilised. The OOB accuracies for these classifications were predicted at 99.7% for both winter and summer vegetation discretisations. These models were then applied to the remaining dataset to create a reach scale classification. In order for the classification not to appear patchy, the outputted values were grouped into contiguous zones of the same class, and any zones whose surface area was less than 4 m² were removed on the basis that any area this size would be less than one whole grid cell in the model and so the other, majority class should be the dominant type. This filling was determined by spatial proximity to the nearest class adjoining each vacated cell.

Each of these zones was then re-classed to represent their roughness values based on comparisons with descriptions and roughness values provided by Chow (1959). For large vegetation, there is also assumed to be some level of understory based on field observations, increasing roughness compared to some other forested descriptors. For the seasonally variable roughness values, the upper and lower limits provided by Chow (1959) were used to define roughness, and the spatial variation in vegetation at each stage used (i.e. the removal of some herbaceous vegetation zones on the bars that are not present in the winter). The values used for the continual roughness values are based on the central value of the seasonal upper and lower limits, these can be seen in Table 5-4.

Table 5-4 Manning's N roughness values used for the seasonal and non-seasonal modelling approaches. Non-seasonal values are the average of the summer and winter, each of which was selected based on the reference table provided by Chow (1959).

Land Cover Class	Manning's N Value		
	Non-Seasonal	Summer	Winter
Channel	0.043	0.045	0.040
Bar	0.040	0.040	0.040
Grass	0.033	0.035	0.030
Established Vegetation	0.110	0.120	0.100

In order to successfully assess the use of traits-based vegetation characterisation for hydrodynamic modelling, a method of representing guilds beyond the typical conversion to bulk roughness is required. Delft is capable of implementing a rigid 3D vegetation model which is based on vegetation structure and is depth dependent and can be applied to 2D hydrodynamic modelling (Deltares, 2021). This is represented as a friction force created by multiple cylindrical elements in flow where the friction force is calculated as:

$$F(z) = \frac{1}{2} \rho_0 C_D \phi(z) n(z) u(z)^2 \quad [N/m^3] \quad [1]$$

Whereby ρ_0 equates to the reference density of water (kg/m^3), C_D is the coefficient of drag for a cylinder, $\phi(z)$ is the number of stems per unit area (m^{-2}), $n(z)$ is the stem width (m), and $u(z)$ the horizontal flow velocity (m/s), with the latter three elements all a function of plant height. Therefore, the reference data required for vegetation input are the diameter and number of stems, their drag coefficients, all relative to the plant height. This allows for the interactions with flow and vegetation to change depending on the flow depth and plant height, a current limitation in a number of vegetation models.

This is implemented into the model using a plant description file. Each file provides the plant stem diameter, the number of stems, its coefficient of drag, and the plant density for the different vegetation classes. Four guilds were identified from remote sensing data collected by Tomsett and Leyland (In Review) and a further two classified from subsequent orthoimagery. For these four guilds, the number of stems at various heights was determined and the stems widths at these heights. As the model assumes cylindrical structures, the coefficients of drag were determined based on literature into the effects of foliage when added to cylindrical and natural structures and the impact of vegetation re-profiling. The plant density was calculated

from the raw TLS and UAV-LS data captured during the field campaigns. To identify individual trunks, an area of each guild was selected, and the vegetation point cloud (no ground points) inverted. From this, local maxima were identified to locate the base of individual plants, the number of maxima summed and divided by the area from which the search took place, resulting in the number of plants per m². For the two classes discretised without structural information, grasses continued to be represented using Manning's roughness due to the lack of plant height and the fact that most of the interactions are happening near the bed, as is assumed when using

Table 5-5 The characteristics used to model drag forces based on plant structure within the vegetation module. These characteristics vary with height, and so values are adjusted up to a maximum vertical level from which no further influence is exerted. Values of drag coefficients are specified to incorporate leaf-on and leaf-off conditions based on the wider literature.

		Characteristics					
		Height	Diameter of Stem (m)	No of Stems	Drag Coefficient		Density (plants/m ²)
					Winter	Summer	
Vegetation Class	Single Stemmed herb	0	0.012	1	1	1.5	1.63
		0.5	0.012	3	0.8	1.3	
		1.5	0.012	3	0.8	1.3	
	Branching Herb	0	0.011	1	1	1.3	1.16
		0.1	0.011	4	0.8	1.1	
		1	0.011	4	0.8	1.1	
	Shrubs	0	0.08	2	1.2	1.2	2
		0.1	0.08	5	1.2	1.5	
		5	0.08	5	1.2	1.5	
	Low DBH Trees	0	0.47	1	1	1	0.11
		1.5	0.38	1	1	1	
		7	0.19	3	1	1.5	
		20	0.095	3	1	1.5	
	High DBH Trees	0	0.81	1	1	1	0.01
		1.5	0.78	2	1	1	
		4	0.39	4	1	1.5	
		15	0.195	8	1	1.5	

Manning's n . For shrubs, values were obtained from the literature to obtain above ground plant features. Field based identification observed a dominant species of hawthorn at various life stages, and values for stem thickness and density were obtained. Stem diameters of 0.08 m were used in line with diameters identified from previous field based research (Hodgkin, 1984; Williams and Buxton, 1986; Good, Bryant and Carlill, 1990; Herbst *et al.*, 2007) and the number of stems set to 5 for all heights above 0.1 m (Herbst *et al.*, 2007; Tanentzap *et al.*, 2012). The vertical distribution of number of branches was varied between each species to explain their vertical structure, and was assigned either based on the modelling from Tomsett and Leyland (In Review) or from the wider literature. The values used and vertical structure can be found in Table 5-5. These values were used in the model scenario which used guild classification outputs from Tomsett and Leyland (In Review). Each guild area was converted to Delft polygon format and named in accordance with the guild plants files, creating a spatially discretised guild map for the domain.

5.4.2 Data Analysis

Data analysis was performed in two strands. The first looks at spatially varying indicators of hydrodynamic output, such as elevation change, across the entire domain. These are compared between different vegetation discretisation methods employed within the study site, assessed either by investigating over the entire model run or by selecting the specific time of peak flow. Alongside the spatial variation, 3 cell locations (A, B, and C, see Figure 5-1) are used to investigate the different morphological responses throughout the model. Locations A and B are used to compare how avulsions are formed in the model between the two Manning's based representations of roughness. These sites both contain either herbaceous or grass vegetation. Likewise, locations A and C are used to compare the impact of all three representations on bed shear stress and morphological response. Location A still maintains a herbaceous vegetation type, whereas location C is found within the wooded section towards the end of the study area.

5.5 Results

5.5.1 Morphological Change

The results from the modelling outputs show large variations in morphological response to different vegetation discretisation methods (Figure 5-7). Most notable are the extremes in erosional and depositional response from the seasonal traits-based and Manning's approaches, whereby the former presents a much more stable channel overall and the latter a more mobile and actively eroding channel. When using a consistent Manning's n approach, there is limited

Mannings N

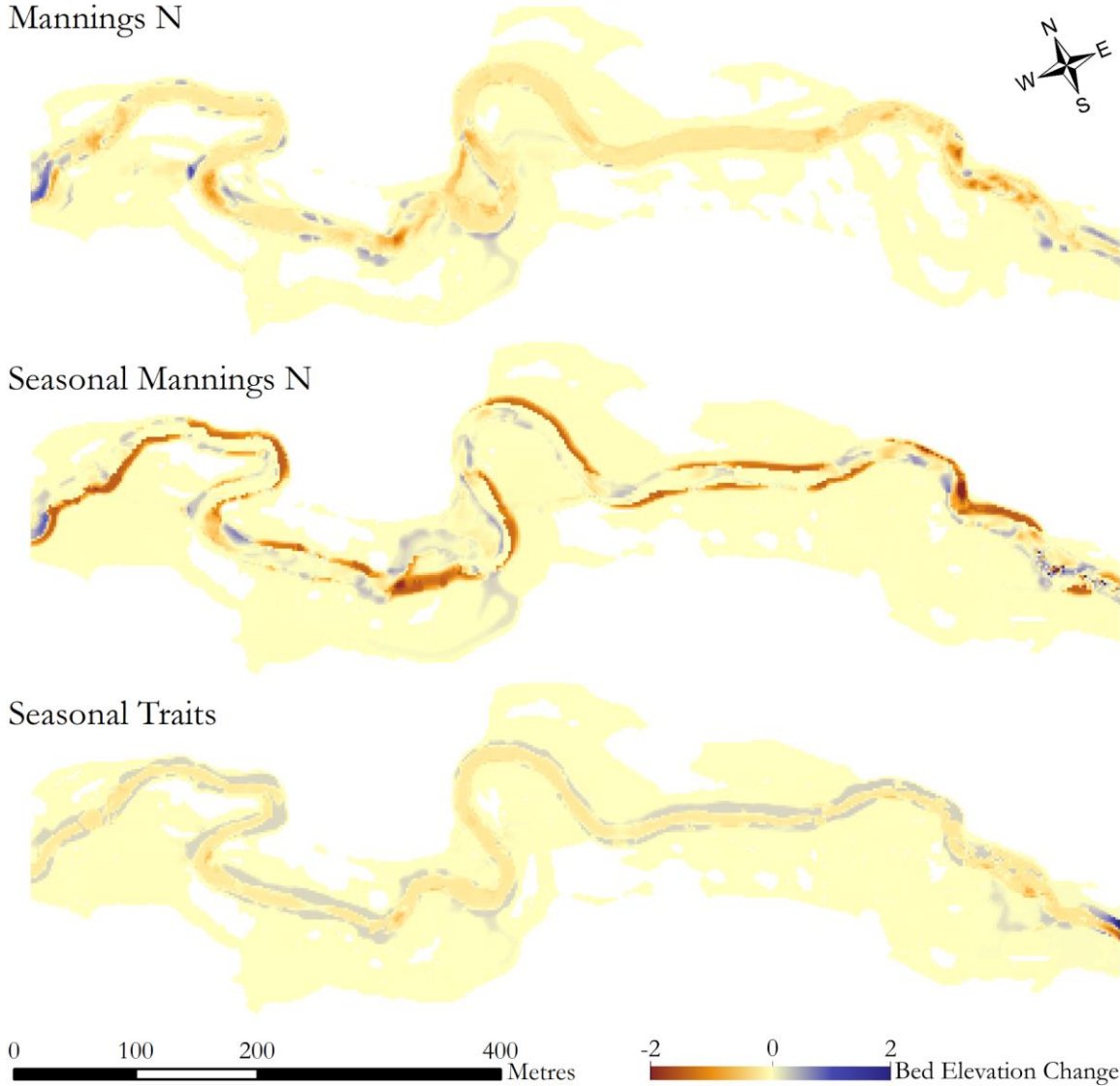


Figure 5-7 Elevation changes across the study area for the entire modelling period for the different representation of vegetation with the model. Clear channel widening can be seen in the seasonal Manning’s based approach, over inducing erosion patterns, whereas the seasonal traits-based approach appears induce deposition along the channel margins.

mobility across the reach in areas expected to undergo lateral shift such as the outer bend of some meanders. For example, lateral erosion of around 2 m is identified within the central meander. However, the channel remains broadly stable in areas where it would be expected to be stable and follows an avulsion pattern through the central bar system. Conversely, the meander bends in the seasonal Manning’s n simulation show a much higher degree of mobility, following the meander bend development that would be expected in a typical system. Erosion of around 6 – 8 m is produced within the central bar, demonstrating the increased mobility compared to a constant roughness value. This is in line with the lateral erosion identified within

the field observations (4 – 10 m). There is also a large avulsion present entering the large central bar region, which is typical of this reach (Tomsett and Leyland, In Review) with deposition occurring in the former channel. However, there is also significant channel widening on relatively straight sections of the reach suggesting an overly active level of erosion for these regions. This sort of erosion has not been observed in the field and suggests that a lowering in seasonal roughness may be contributing to the reach becoming overactive. For example, within the first straight there is lateral shift of 8 m occurring whereas field monitoring notes this to be a stable section with no lateral migration. This particular section has also been stable for the prior 20 years (Tomsett and Leyland, In Review), and as such is unlikely to see this magnitude of change. The seasonal traits simulation appears to experience high levels of deposition at the channel edges, whereby it is likely that decreased velocities caused by vegetation roughness has led to increased deposition. In the central meander for example, 2 – 4 m of lateral deposition is occurring, opposite to what is noted in the field. There are signs of bar development in some locations, but there are no avulsions or large shifts in planform that are typical of the reach and present in the Manning's simulations. However, many of the vegetated sections are far more stable, along with the straight sections of channel as has been observed through field surveys.

When we look at the change that occurred in the peak flow event over 20-22nd January (Figure 5-8), we can see that in both of the Manning's based approaches, the majority of geomorphic work occurred during the peak flow event, especially over then initial part of the central bend sequence. However, we can see that the flood event in the seasonal traits-based approach led to little change occurring during this time with the majority of change experienced during the remaining simulation time steps. For the constant Manning's approach, the channel reworking in the central belt occurred at this time, with the flood peak high enough to induce geomorphic change. However, in the seasonal approach the channel switching in this location did not occur here, but in a section of structurally large vegetation where an avulsion would not necessarily be expected.

The process by which the avulsion is formed is also different between the two scenarios, as shown in Figure 5-9. This highlights two originally dry cells (Locations A and B, see Figure 5-8)) which become eroded and subsequently form part of the main channel. For the constant Manning's approach, the reworking was rapid as the result of a flood peak. However, for the seasonal Manning's, the avulsion occurs gradually over time when a change in roughness is prescribed at the onset of winter. This shows that when the roughness values are changed from

Mannings N

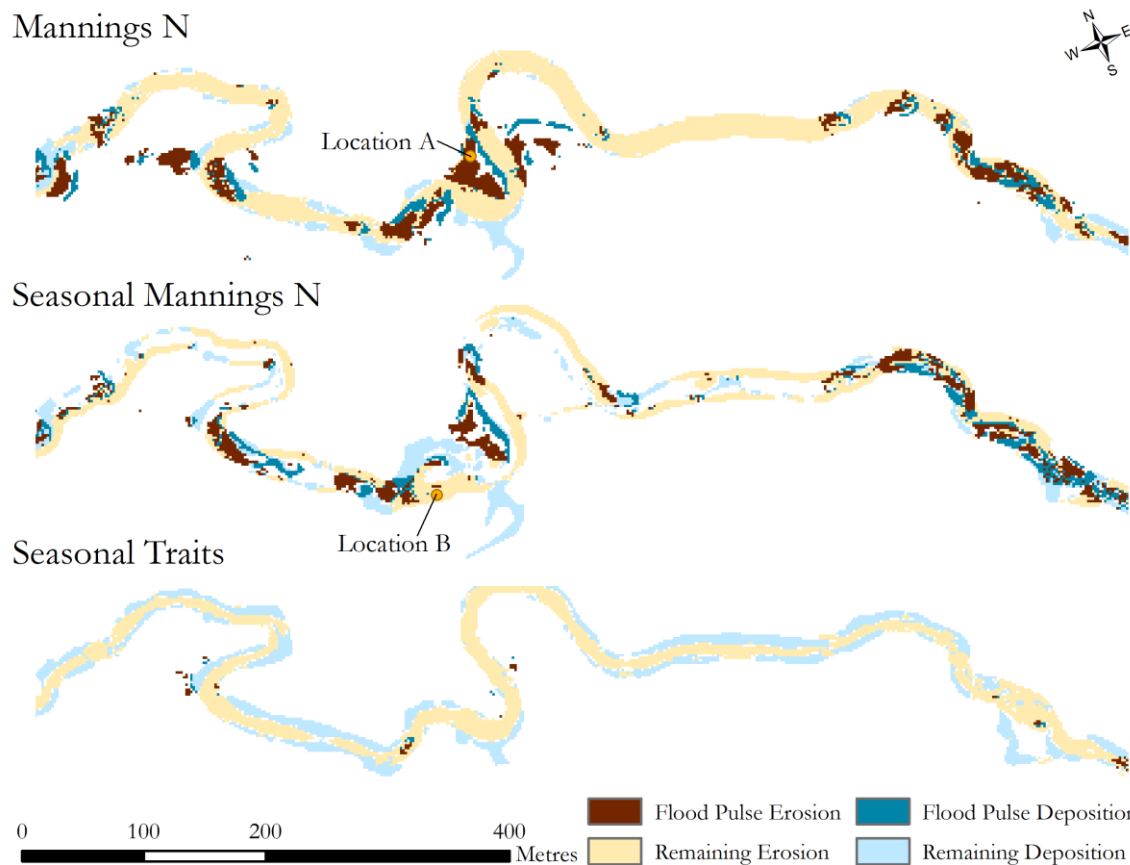


Figure 5-8 Erosion and deposition that occurred during throughout the modelling run (in lighter shades) and those that occurred during the high flow event (in darker shades). Only change over 0.05 m in magnitude are included. The influence of the flood peak clearly varies between model runs, with both Manning’s based models seeing more change during the high flow event.

summer to winter, there is a following increase in the rates of erosion which would suggest a sensitivity in the model to roughness values for certain types of erosion. The sharp change in elevation during the flood peak on the secondary bar location implies that higher roughness values help to model quick changes in morphology when peak flows are expected to undertake channel reworking, and that incorrectly parametrised roughness values in certain locations can lead to morphological evolution that is less likely to occur. It is also clear that the majority of outer bend erosion did not occur at this time either and that high flows did not represent the main cause of meander development. For the traits-based approach, geomorphic change is universally low magnitude and corresponds with areas where flow was likely constricted, increasing flow velocities and subsequent bed shear stresses. However, the geomorphic change is not dominated by peak flows, suggesting that this representation of vegetation is acting to reduce bed shear stress effectively, and reduce the signals of excessive erosion in vegetated sections found in both the Manning’s representations.

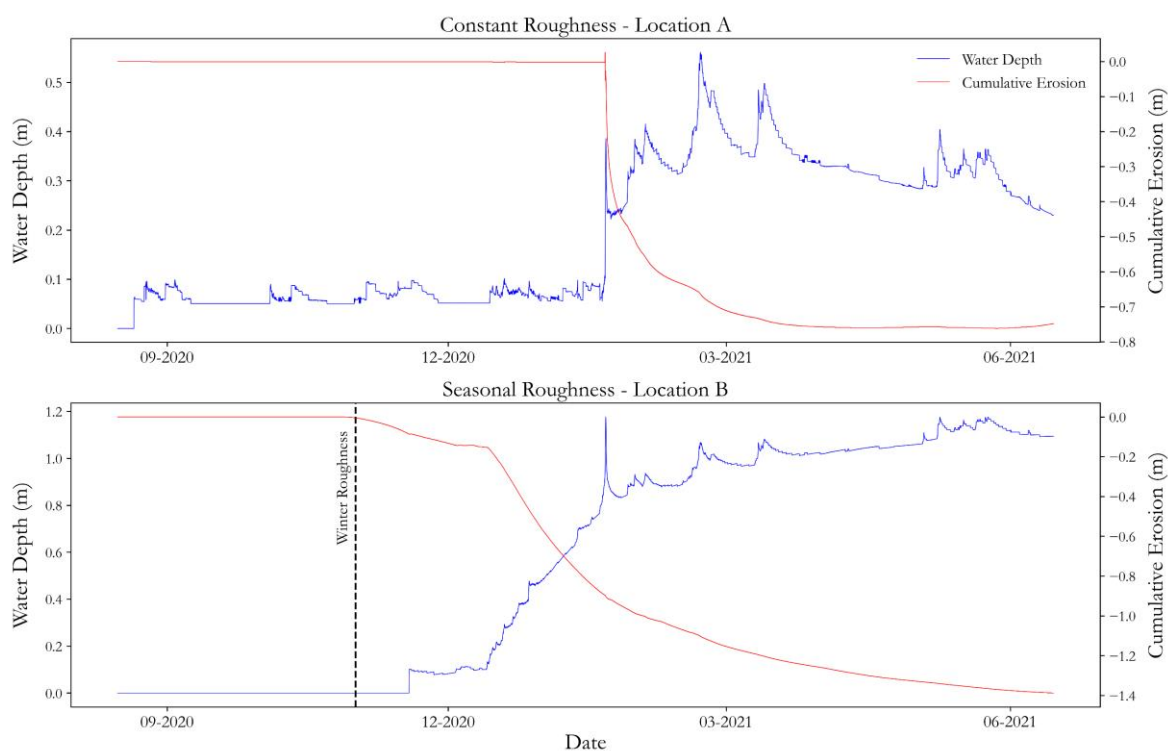


Figure 5-9 Comparison of two new channel developments at separate locations (A and B) between the different Manning's based vegetation roughness approaches. Location A shows a rapid shift from a low water depth to a predominant channel forming, with greater water depths resulting from a singular high flow event. Location B demonstrates a more gradual erosion process, initiated by a change in seasonal roughness values when values for winter are prescribed.

5.5.2 Peak Flows

Depth averaged velocities during the peak flow event on the 21st January 2021 can be seen in Figure 5-10. The velocities for both Manning's based approaches are similar for this event, with both models showing peak flows of just under 3 ms^{-1} and the majority of flows under 2.5 ms^{-1} . Peak velocities measured in the field were 1.5 ms^{-1} during lower flow conditions, suggesting the model is simulating sensible flow velocities. The seasonal Manning's approach does appear to have higher flow velocities on the floodplain where overland flow is being routed, likely resulting from the decreased relative roughness values used for winter months. This is clear through the central bar section whereby the previous morphological change is routing flow in multiple directions.

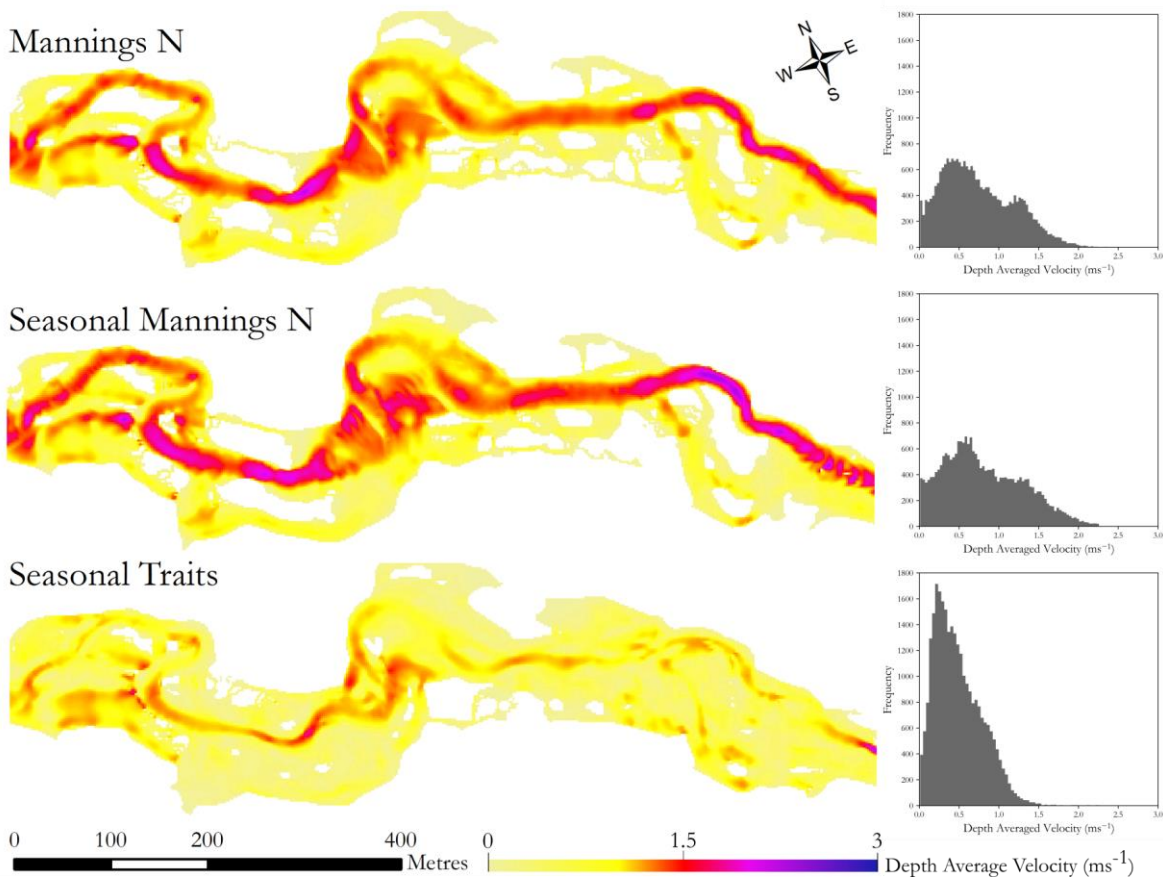


Figure 5-10 Comparisons of depth averaged flow velocities (ms^{-1}) across the study site, including channel and floodplain, for the peak flow event on the 21st January. The three histograms show the distributions of velocities across the model domain, highlighting the slower nature of flow in the traits-based approach especially in and around the channel edges.

Comparatively, the flow velocities experienced for the traits-based approaches are much lower, with fewer locations showing very high flow velocities apart from in the more constricted channel areas. Peak velocities here were just under 2 ms^{-1} , with the majority of velocities under 1.5 ms^{-1} implying that the velocities in the channels were lower than should be for such a high flow event. This extends on to the floodplain whereby the flow velocities are much slower, and although there are some higher values within the former channels on the floodplain DTM, these are less apparent than in the Manning’s based model runs. In some cases, this is likely to better represent flow velocities on the floodplain, such as through dense vegetation, but in other places it appears to be overly slowing the flow down through the reach, limiting the rates of erosion expected for such a flow event. The difference in these flow peaks can be seen in Figure 5-10 which compares the histograms of flood velocities for all occupied grid squares experiencing flow over 0.01 ms^{-1} . The flow velocities for the traits-based approach are much more closely distributed around the slower speeds with less variation, yet there is a double peak experienced

for Manning's based approaches implying an in and out of channel peak in velocities experienced.

The result of this slowing of flow results in a much larger proportion of the flood plain being inundated. The two Manning's based approaches have similar levels of overbank flow extent, predominantly favouring former channels as expected with some reasonably sized patches of dry ground across the floodplain. Both however cover a much smaller extent of the floodplain when compared to the traits-based approaches. This is to be expected as a greater level of impedance to the celerity of the flood wave leads to a greater backup of flow, resulting in increased floodplain inundation.

5.5.3 Bar vs Vegetation Bank Changes

By comparing the locations of cells A and C outlined in Figure 5-1, one with a seasonal herbaceous vegetation covering and the other a wooded section, it is possible to see some of the changes different vegetation representations have on morphological and hydrodynamic responses. Figure 5-11 shows the relationships between bed shear stresses and erosion between time steps, with depth averaged flow velocities and cumulative erosion providing some context for this change.

For the bar section, the location of the grid cell is towards the end of an avulsed channel that is formed during the constant Manning's simulation, where avulsions would be expected or some geomorphic reworking. The constant Manning's roughness sees very little change or consistent flow velocities over this bar section until the peak flows experienced in the January flood provides velocities high enough to start to rework sediment. This leads to a step change in morphology that is then maintained despite some consistently higher velocities, as this becomes the new predominant channel. Conversely the seasonal approach sees a mixture of deposition and erosion when higher shear stresses are experienced. Some of this deposition appears to lead to a blockage in flow until the flood peak where this is reworked to remove sediment and maintain flow until the summer period whereby water depths become more inconsistent again. The traits-based methods however see an absence of flow for much of the year apart from a select few peak events, and only the peak flow event sees a small amount of reworking. This can be seen by the relatively fewer points in the scatter plot, and the clustering around low bed shear stress values and lack of variation in erosion and deposition values. The vegetated section sees much the same pattern, whereby both the Manning's based discretisation experience changes during the peak flow event in January, with both seeing rapid changes in elevation. However, they both also experience reworking earlier on at a more consistent rate, likely due to

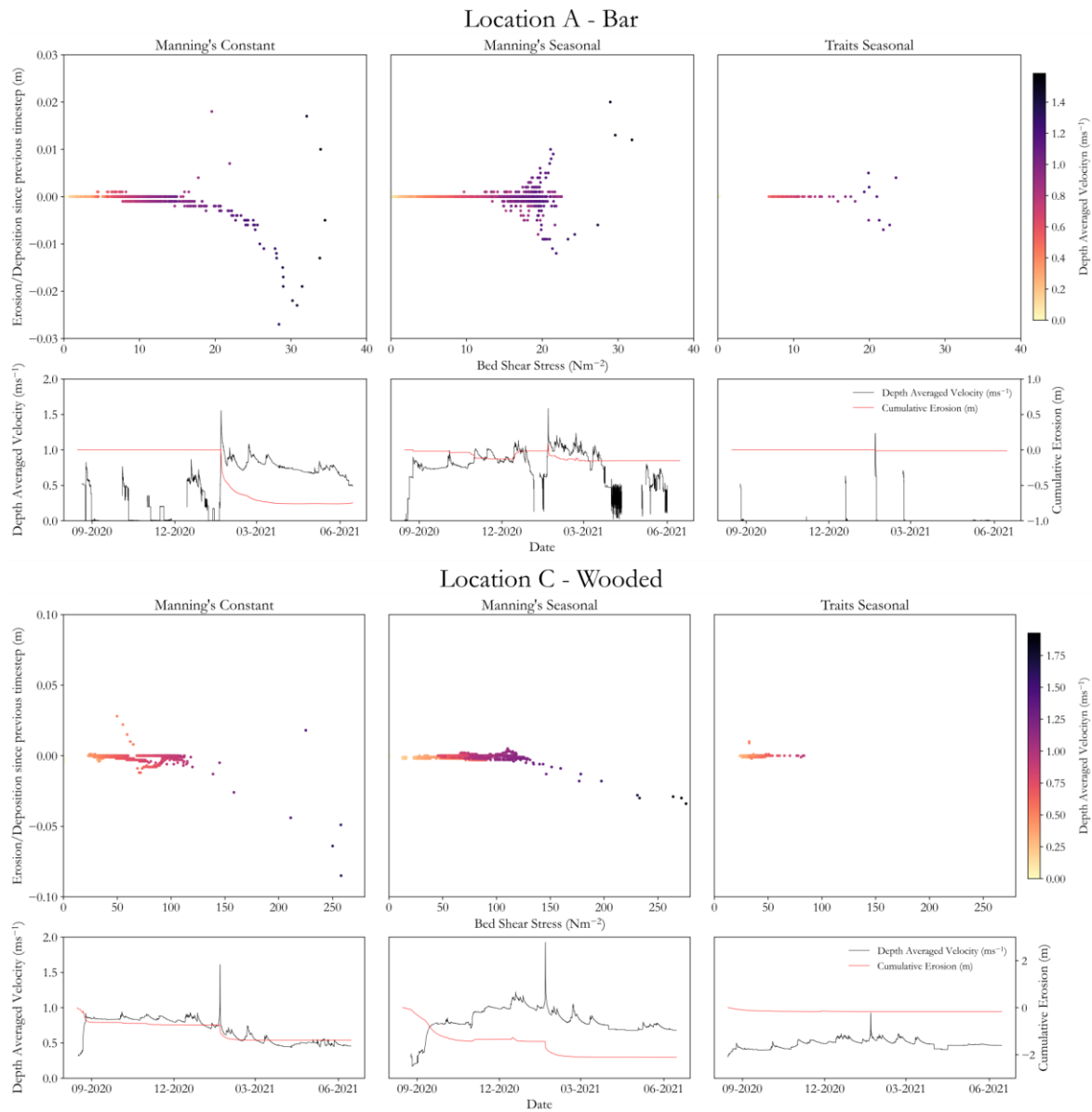


Figure 5-11 Comparison of erosion and deposition rates at two locations (A and C) based on the shear stress being exerted on a cell. The top panels refer to a cell representing bar morphology and the bottom to a cell from a wooded reach. The scatter plots show the change in elevation compared to the previous outputted time step and the bed shear stress experienced at this time, coloured by the depth averaged velocity. The context graphs below the scatter plots show cumulative change in elevation in red and the depth averaged velocities through time in black.

the higher flow velocities causing bank erosion through the application of shear stress to adjacent dry cells. The traits-based approach remains far more stable and experiences very little erosion at all as expected within this section.

From this we can see that flow peaks are important in driving geomorphic reworking, and that outside of these high flows, reworking, especially in vegetated reaches, is less prevalent as

expected. The rates of change are different between the sites, and the variability in deposition and erosion clearer on the bar location which fits in with the active nature of the channel sections with smaller vegetative influence. By including a seasonal component to vegetation there is a clear impact on flow velocities and subsequent geomorphic work as a result, possibly causing a mix of erosion and deposition signals depending on the time of year. On both sites, the inclusion of traits-based methods provides a drop in depth averaged velocities which leads to lower shear stress values being experienced, thus limiting the eroding capability of the system. The model does appear to require higher shear stresses to induce geomorphic change within vegetated sites, as would be expected with higher soil cohesion due to underlying root structure.

5.6 Discussion

Figure 5-12 shows the morphological change identified on this reach relevant to the time period being modelled. The main identified patterns from the field are general vegetation stability for preventing erosion and that channel mobility was far greater in locations absent of tree and shrub guilds. Some of this change is evident in different vegetation discretisation methods used within this study, but no single method really captures the expected morphological evolution completely.

Using a traits-based approach led to highly stabilised channels, whereby there was little morphological evolution across the simulation run. Most of this change occurred in and around the channel with deposition at the channel edge, suggesting that during the modelling, interactions between discretised vegetation and flow led to slower velocities, increased deposition, and channel narrowing which focussed the flows into a central channel for erosion. This slowing at the channel edges would explain the reduction in lateral erosion, as this is triggered based on bed shear stresses within the adjacent wet cells. Therefore, a reduction in flow velocities alongside increased τ_{crit} would reduce the lateral erosion potential. This large reduction in flow velocity could be down to the parameterisation of the drag coefficients, uncertainty in the cylinder based discretisation of the vegetation, or the vegetation density, all of which contribute to the modelled drag within Delft and have been observed to be important in determining measured drag forces (Nepf and Vivoni, 2000; Sand-Jensen, 2008; Kim and Stoesser, 2011). However, this does result in increased channel stabilisation in areas where the Manning's based discretisation's increase erosion beyond what is expected or observed in the field. This is especially so for areas in Figure 5-12 where erosion was not observed but predicted by the Manning's models, particularly for the initial vegetation interactions and the large wooded section at the end of the study reach. This implies that the traits-based methodology has the potential to stabilise channels and better represent some aspects of morphological evolution.

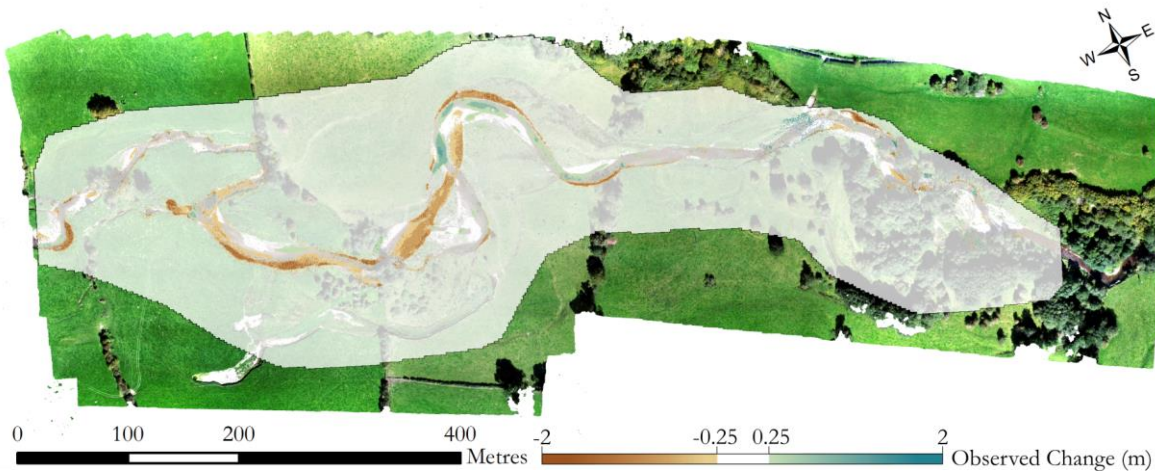


Figure 5-12 Observed morphological change at the field site between September 2020 and June 2021, a time period comparable to the model run time. Similarities to the vegetation representation techniques are the stabilisation around vegetation in the traits-based approach, and the formation of a new channel and the extensive outer bend erosion within the constant and seasonal Manning's based approaches respectively.

This flow velocity reduction effect is not present when using Manning's based roughness parameters, with flow velocities in the channel akin to those measured during field campaigns. Velocities of between $0.5 - 1.5 \text{ ms}^{-1}$ were measured across low to medium flow levels in the field, but outside of peak flows. As the traits-based model only hits these values during peak flows, this suggests a general underestimation of flow velocity as a result of this discretisation method. This is in contrast to the Manning's based models which had flow velocities above those measured in the field during this peak flow which is more likely to have occurred. These higher velocities led to a higher proportion of morphological change happening during the peak flows, and the overall patterns of erosion more closely matching those observed within the field site for some sections. Such change included the formation of new channels and the erosion of banks on the outer edge of meanders, which was not seen in the traits-based approaches. However, the timings of these changes were not always as expected, with the seasonal Manning's seeing an avulsion forming through a vegetated section in a progressive manner, as opposed to the more rapid switching seen at this site. The consistent Manning's based approach resulted in avulsions occurring at times and locations expected and seen in real life yet saw a distinct drop in lateral erosion. Yet this approach also led to areas of excessive erosion in locations identified as stable in Figure 5-12, especially those with heavily vegetated banks, raising doubts over the applicability of a purely Manning's based approach to vegetation discretisation. This may imply that a mixed approach, whereby larger vegetation should be structurally discretised, may be the optimal solution.

However, the flow velocities experienced overbank suggests that these Manning's based models account for overbank flow extent less well when compared to real world conditions. Figure 5-13 is a photo of the study site around 6 hours prior to the flood peak recorded in 2020, which was slightly higher than the water depths prescribed for these model runs. The image shows a large inundation extent even before maximum flows which more closely resembled the floodplain extent of the traits-based modelling. This implies that although the traits-based approach was affecting flow velocities in and near to the channel too much, in terms of effective floodplain parameterisation it may have been performing better.

This work clearly demonstrates that the way in which vegetation is represented within hydrodynamic models is important, not only in terms of whether a basic roughness or more complex structural approach is used, but also how temporal changes such as those induced by seasonality are incorporated. We know that metrics can be used to relate complex vegetation parameters to a simple Manning's n representation of roughness (De Doncker *et al.*, 2009; De Doncker *et al.*, 2011) and that these properties vary seasonally. The seasonal element of roughness was compared to consistent values, and the timing of the onset of changing roughness appeared to alter the morphological response of the reach, inducing change in a previously higher roughness 'vegetated area' where change would be less likely. Values of τ_{crit} were constant across these periods, and as such this change is due to alterations in roughness as opposed to alteration in erodibility of the soil layers of adjacent cells. Although the location of the avulsion through winter roughness was unlikely based on the reaches true vegetation location, the increased subsequent bank erosion is a better representation of reality than the consistent Manning's approach. Consequently, not only are the correct roughness parameters required, but they also need to be adequately altered for seasonal changes. Although this has been successfully employed by Song, Schmalz and Fohrer (2014) and Song *et al.* (2017) to reduce uncertainties in water surface elevations, these were not assessed against the likely morphological results of these changes in roughness. This research demonstrates that the roughness not only affects the in-channel processes, but also the morphological response of a system throughout the year and interactions across the floodplain during peak flows. This is where the traits-based methods start to show a potential strength in relation to inducing slower flood velocities and a greater flood extent providing some promise for the method as an approach for better representing floodplains and vegetated banks.



Figure 5-13 Image of the study site (model domain boundary approximated in red) during a flood event in February 2020. It was captured approximately 6 hours prior to the observed peak in flood inundation. Image provided by the landowners.

Some issues that appear to exist in the outputs reported here may be caused by the model set up. One issue is with the fact that meander development is initiated by the bed shear stress of adjacent wet cells being applied to adjacent dry cells (Lesser *et al.*, 2004). This allows the lateral migration of channels adjacent to the channel. This method requires accurate representation of shear stresses at the banks, with the traits-based approach clearly affecting shear stresses at these margins through inducing an increased drag. Yet, by comparison the lateral erosion experienced during both Manning's simulations suggests an overactive implementation of lateral erosion, with channel widening in sections that are far less active (see Figure 5-12) occurring. The methodology itself has also been subject to questions over whether it accurately represents real world change (Williams *et al.*, 2016; Banda and Meon, 2018), with alternate erosion schemes based on gradients introduced by Williams *et al.* (2016) proving to be a more realistic method.

The vegetation model uses a structural approach to infer drag, using the same methods applied in numerous investigations. Whilst it is common for drag to be directly measured to identify suitable coefficients of drag, here they are specified from the literature based on likely foliage

conditions, as these play a key role in determining drag coefficients for woody and herbaceous plants (Jalonen, Järvelä and Aberle, 2012; Västilä, Järvelä and Aberle, 2013). However, the effect of increased foliage area also leads to plant reconfiguration during higher flows (Järvelä, 2002b; Whittaker *et al.*, 2013), and although the coefficients of drag are lowered at higher water depths, this is not fully representative of typical foliage conditions. Being able to introduce the flexibility of plants would enable better representations of vegetation under different flow conditions, especially under flood levels. This may explain the lower flow speeds over the bars in the traits model due to non-flexible vegetation slowing the flow too much. However, this variation across different flow depths is not always captured in Manning's based representations of roughness either, and although depth varying values can be used (e.g. Anderson, Rutherford and Western, 2006), they are not always implemented despite the requirement for them. This issue is less important for larger woody vegetation, as although branching structure in certain species may interact with flow, across the banks and floodplains the predominant interaction is with the trunks near the ground. This may also help to explain the better flooding extent in forested sections of the traits model, as water can flow through these reaches but with lower velocities, moving between trunks, as opposed to a continually rough and non-passable surface.

The biggest limitation in this study is likely the feedback changes between morphology and any parametrisation and discretisation of vegetation. Eco-geomorphic feedbacks are vitally important in the stabilisation of bars, cohesion of riverbanks, and alteration of flood waves. When the morphology changes, the spatial variation in each vegetation class also alters, but this is not always fed back into hydrodynamic roughness which have spatially stationary levels of roughness. The incorporation of these feedbacks was undertaken by Oorschot *et al.* (2016) who used a vegetation feedback to adjust vegetation discretisation from simple spatial variations to more complex removal and regrowth patterns based on a coupled vegetation model with Delft3D. This study also used a structural based method to representing vegetation for two vegetation types at different life stages, founding that static representations of vegetation over constricted the channel and stopped planform evolution. This is similar to the issues presented with the traits-based approaches in this research, whereby the presence of vegetation constricted channel movement across the entire reach, not just those experiencing the 'pinning' effect of vegetation. Such thresholds for vegetation removal were also applied in hydrodynamic modelling by Caponi, Vetsch and Siviglia (2020) with some success, revealing how bar mobility influenced vegetation colonisation success. Just as seasonality is vitally important for representing vegetation, effectively incorporating vegetation models adjacent to their hydrodynamic counterparts may offer the best solution to fully modelling the interactions between vegetation and hydrology.

5.7 Conclusion and Future Work

A traits-based discretisation of vegetation across a nearly 1 km river reach was incorporated into a 2D morphodynamic model for the first time. Even with relatively simple approaches that use cylinders to represent vegetation structure, this novel method to represent vegetation can be used in the modelling domain. More work is needed to refine the parameterisation of the traits-based approach, but the results herein show that it induces more stability in the reach as one would expect. Furthermore, this modelling study demonstrates that simply changing the manner in which we discretise and represent vegetation within a model, and the incorporation of seasonally varying vegetation data, has a distinct impact on the results. Adjustments in seasonal roughness values through typical Manning's n approaches led to alterations in morphological response, and that using a traits-based structural approach led to increased stabilisation of the river corridor on the whole. The timing of these seasonal shifts, along with the adjacent peaks in flow levels, may have a significant influence on the response of a model and consequently any form of planning that is based off of it.

Vegetation itself is increasingly becoming a central theme in the restoration of rivers and in their flood management schemes (Harvey and Gooseff, 2015; Lane, 2017; Wilkinson *et al.*, 2019), with many studies modelling the effects that these interventions can have (Gao, Holden and Kirkby, 2017; Ferguson and Fenner, 2020). The changes presented here, purely based on the broad vegetation discretisation methods and seasonality inclusion, are similar to the scales of change expected with the introduction of different vegetation schemes such as natural flood management. As a result of this, it may be argued that the models are as sensitive to the changes in vegetation as they are to successful parameterisation, with this being exemplified by differences in suggested Manning's n values for forests of 50% between Chow (1959) and Medeiros, Hagen and Weishampel (2012). This implies that a more vegetation dependent structural technique may prove more effective within modelling, at least for determining suitable roughness parameters if vegetation structure cannot be incorporated into the model itself. Likewise, these variations in roughness are clearly time dependent, and the incorporation of seasonally varying models may produce more accurate representations of real world conditions (e.g. Song *et al.*, 2017). Consequently, not only is it important to represent vegetation in the most accurate way possible, but also to appropriately vary this through time as vegetation condition and subsequent properties change.

This leaves a space for research seeking to establish the best way in which to represent vegetation in models, both in relation to the local influence on drag, and seasonality, in order to improve the accuracy of modelling to fully represent a dynamic vegetated reach. Herein, the

first improvements in the discretisation of vegetation in a morphodynamic model have been undertaken, including adjustments to current hydrological and flow conditions, accounting for seasonality, and using a more holistic approach for vegetation characterisation. However, these initial outputs reveal that the model is highly sensitive to the methods of roughness discretisation, causing significant divergence in output metrics. Further research is needed to undertake a full sensitivity analysis around the choice of parameters used to represent traits-based vegetation in the model. This is important as the traits-based approach to mapping and analysing vegetation is scalable and applicable to different fluvial domains, making it highly attractive for future work. Consequently, accurately and reliably incorporating a traits-based method into the modelling framework would allow for a simpler and more reproducible method to vegetation discretisation and should be pursued within future research.

Chapter 6 Synthesis and conclusion

The purpose of this chapter is to bring together the key themes that emerge from the body of work presented in this thesis, broadly covering the current state of the art in river corridor remote sensing (Chapter 2), the development of novel eco-geomorphic survey methods (Chapter 3), the survey and extraction of vegetation functional traits using remote sensing (Chapter 4) and a preliminary modelling study (Chapter 5). A broad synthesis of the contributions made by this collective research in relation to the research questions outlined in the introduction is undertaken. Finally, limitations and opportunities for further research are discussed.

6.1 Research Synthesis

The role that vegetation plays as a first order control in fluvial geomorphology is well established, yet the methods by which we capture, analyse, and model vegetation to establish impacts across scales is still very much emerging. Key drivers of this methodological development are the improving remote sensing techniques, such as Uncrewed Aerial Vehicles (UAVs) and their sensor payloads, which are increasing the spatial and temporal resolution and scales at which we can capture vegetation data.

Research Question 1 set out to understand *“What is the current state-of-the-art in river corridor remote sensing and how can it potentially be used to measure eco-geomorphic feedbacks?”*

Chapter 2 (**Paper 1; Tomsett and Leyland, 2019**) shows that the number and variety of remote sensing methods for monitoring and analysing river corridors is vast, and that this is only set to grow with the advent of new sensors and more advanced collection techniques and platforms. These methods range from high resolution sensing methods such as Terrestrial Laser Scanning (TLS) through to satellite remote sensing and Internet of Things based monitoring. However, current research tends to focus on the monitoring of morphological evolution, or the development of methods designed to improve our monitoring capabilities from remote sensing. Conversely, there are relatively few studies investigating process-form interactions in the field, which forces research to infer processes from observed change. Current trends in platform innovation, the introduction of new sensors, and a wider variety of commercially available options at reducing costs, are all likely to help shift this balance to increasing collection of process-form data to help improve our understanding of fluvial processes.

Recent years have seen several advances in the use of Particle Image Velocimetry (PIV) techniques, tracking ‘seed’ particles, mainly on the surfaces of rivers, to estimate water velocities and subsequent discharge measurements. Field PIV techniques such as these have been used during flooding and under regular flow scenarios (Piton *et al.*, 2018; Kinzel and Legleiter, 2019), alongside developing methods of best practice to ensure output data and results are accurate (Pearce *et al.*, 2020; Pizarro, Dal Sasso and Manfreda, 2020). The development of this technique has led to a number of toolkits being published which can be used with various imagery sources to rapidly produce 2-dimensional velocity layers across the surface of a river (e.g. Patalano, García and Rodríguez, 2017). Such methods are a good example of the type of process-form interaction monitoring advances that are advocated at the end of Chapter 2, helping to provide river flow process context to the ‘snapshot’ survey methods of pre- and post-event morphology.

Alongside the highlighted need for platform and sensor development to allow continued insight into geomorphic systems, methodological advances in data processing are needed to i) keep pace with technology and the production of ‘big data’ sets and ii) continue innovation, for example in the image processing domain. Recent advances have focussed on the increasing ease with which Structure from Motion (SfM) analysis can now be performed, with accessible software and high-powered PCs allowing high quality output from UAV captured imagery. The more recent advent of active sensing methods such as UAV Laser Scanning (UAV-LS) requires a continued drive to develop tools capable of processing this type of data. New and novel methods of classification, segregation and processing of point cloud data are beginning to be developed and outputs from such methods are becoming more advanced in their complexity (Burt, Disney and Calders, 2019; Krisanski *et al.*, 2021). Advances in data processing methods and tools represents one of the key challenges highlighted in Chapter 2 which will enable significant advances in science conducted within the river corridor.

Chapter 3 (**Paper 2; Tomsett and Leyland, 2021**) embraced the challenges outlined in Chapter 2, through the development of a novel UAV based remote sensing package and accompanying data processing tools. A UAV based Laser Scanning (UAV-LS) and MultiSpectral (UAV-MS) system was developed, demonstrating some of the advances in technology that can lead to clear and tangible benefits over existing (e.g. SfM) methods. The methodology delivers an advance in our ability to collect data for vegetated river reaches, improving capture of the below canopy topography, as well as being able to identify vegetation elements in far more detail than is possible through SfM methods alone (Figure 6-1). Integration of a multispectral camera within the sensor package enables the extraction of information on plant phenology through band indices and improves classification results for a given reach. Chapter 3 demonstrates an advance on previous work, by using a multi sensor system to improve the potential to monitor vegetated

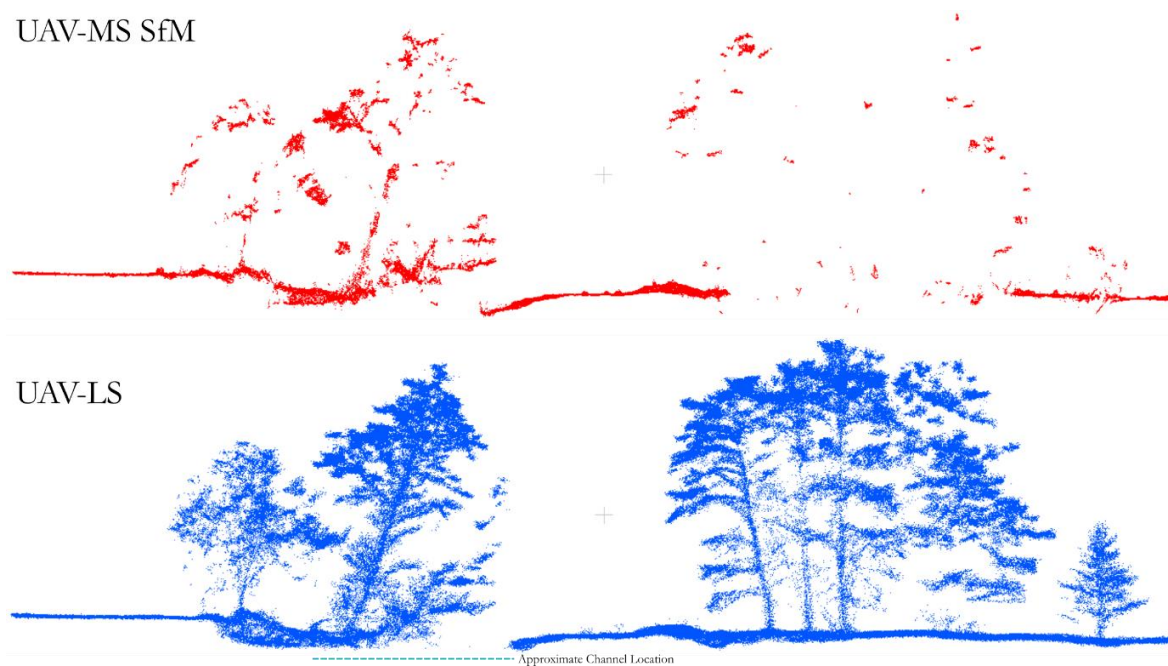


Figure 6-1 Comparison of vegetated cross sections for UAV-MS SfM derived point clouds (red) and from UAV-LS point clouds (blue). The difference between visible vegetation structure and ground point returns is clearly shown between the two datasets, highlighting the benefit of UAV-LS for eco-geomorphic research.

river reaches at scales and resolutions which were hitherto not possible. As a result, the current limitations that were outlined in Chapter 2 with regards to difficulties of measuring and monitoring vegetated reaches are beginning to be overcome. The new survey method developed offers a pathway to measure eco-geomorphic feedbacks at scales not yet achieved, through the collection of high resolution ecological and geomorphic data, beyond existing individual plant scales (e.g. Manners, Schmidt and Wheaton, 2013) and catchment scales (e.g. Henshaw *et al.*, 2013) already undertaken.

With any survey methodology, there are limits of applicable scale and resolution. Just as ground based features below the pixel resolution of a satellite image may not be detectable, the small-scale complexity that is captured in high resolution methods such as TLS, UAV-SfM, and UAV-LS, cannot be directly collected and applied to larger systems that are beyond the range of these spatially limited techniques. The methods presented within Chapter 3 are also limited by the point densities of the sensors themselves; for example with many current data analysis methods being developed for very high resolution TLS surveys (possible sub cm point densities), the use of these methods on UAV-LS data (with lower point densities) is potentially limited. As such, the need for co-dependent developments in both sensor packages and the computing power and algorithms to handle the vast and varied point cloud data this is collected are essential, with improvements in this area beginning to appear (Krisanski *et al.*, 2021).

The final element of RQ1 seeks to explore how advances in remote sensing could be used for investigating eco-geomorphic feedbacks. In a practical sense, the success of a given remote sensing technique or method comes down to its ability to collect suitable information on both the ecological and geomorphological processes. As has been shown by Diehl *et al.* (2018) and Butterfield *et al.* (2020), to fully understand eco-geomorphic interactions and feedbacks a more holistic approach in relation to the system of interest is required. For example, the aggregation of many data sets across morpho-climatically varying river catchments could lead to a greater understanding of eco-geomorphic processes. However, in relation to this point, our mechanisms and platforms for sharing ad-hoc big data within the science community are currently lagging far behind our ability to create it. Chapter 2 outlined the need for a shared data protocol, whereby the data made freely available to all could be used to further scientific endeavours, but also on which new analysis methods could be tested, creating an overall benefit to the community. Such a platform and mechanism of standardised sharing of river corridor monitoring data is currently a considerable way from being implemented.

Research Question 2 asked “*What properties of vegetation are important in relation to modulation of fluvial geomorphic change? Can these be readily measured and quantified using remote sensing, so that variations in vegetation and morphology can be readily assessed through space and time?*”

Whilst there are numerous vegetation properties which are capable of directly influencing flow and geomorphic change, herein those identified as important in the wider literature, which had the potential to be extracted from remote sensing methods, and which were relevant as inputs into a hydrodynamic model were selected as candidates for exploration. The ability to extract specific vegetation properties as outlined in Chapter 4 (**Paper 3; Tomsett and Leyland, In Review**), and shown in Figure 6-2, demonstrates the benefits of UAV-LS data. The results from Chapter 4 (Paper 3; **Tomsett and Leyland, In Review**) emphasised this further by using both UAV-LS and TLS data to create cylindrical models and frontal area calculations of riparian vegetation. The advantage of this method is that it allows the discretisation of vegetation into distinct guilds which can be used to classify the reach in order to investigate links to eco-geomorphic processes and feedbacks. This represents the first application of remote sensing datasets to create guilds defined within a functional traits framework, advancing existing methods beyond the field measurements used by Diehl *et al.* (2017) and the species classification approach of Butterfield *et al.* (2020). The new approach allows the collection of many relevant traits such as tree diameter (DBH), number of stems, plant vertical distribution, height, and frontal area; all of which have been shown to influence drag and affect flow velocities and sediment transport (Nepf and Vivoni, 2000; Lightbody and Nepf, 2006; Follett and Nepf, 2012; Vasilopoulos, 2017).

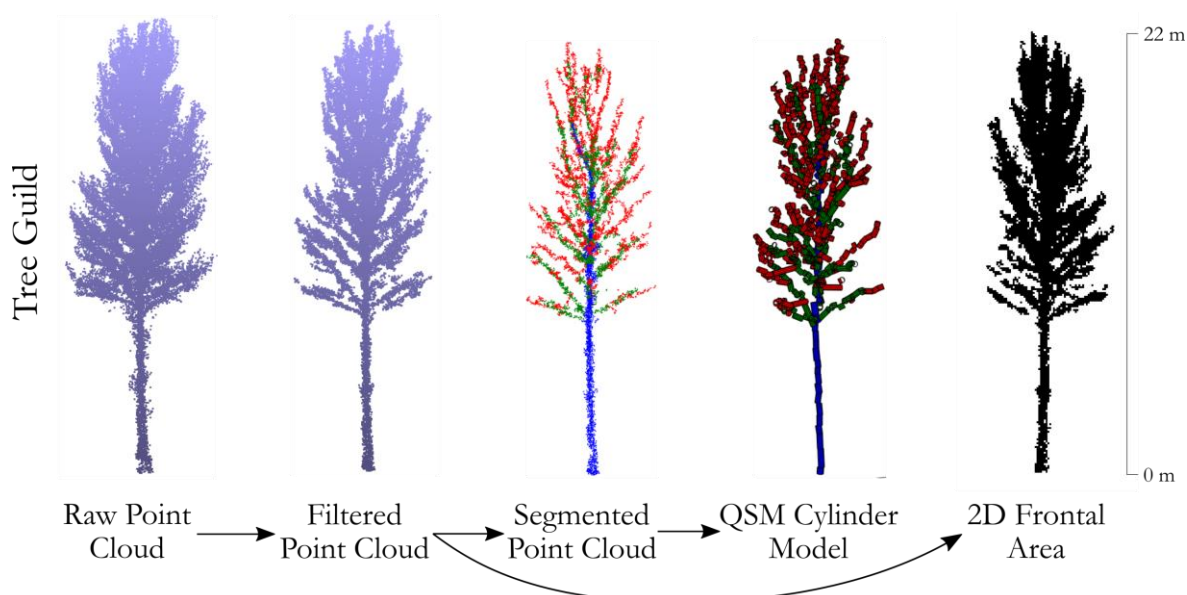


Figure 6-2 Vegetation metric extraction technique introduced in Chapter 4, showing the processing routine taking a raw vegetation point cloud and producing cylindrical models and 2D frontal areas.

The challenge herein was to transfer this fine scale analysis of individual plants up to reach scale analysis. Such methods have been touched upon in previous research, for example, the upscaling from TLS to ALS (Airborne Laser Scanning) datasets by Manners, Schmidt and Wheaton (2013) and Bywater-Reyes, Wilcox and Diehl (2017). Analysing individual plants to gain a classification on a plant-by-plant basis would require total coverage of each individual plant, thereby eliminating those which were not fully resolved in the survey data from being classified. To overcome this, the use of global scale metrics, such as canopy height and vertical distribution, combined with multispectral data, are used to group areas of similar structural properties relating to their individual guilds. This is line with other studies that have found a combination of spectral and structural characteristics can all help to improve classification results (Arroyo *et al.*, 2010b; Forzieri *et al.*, 2010). The inclusion of seasonally varying data which captures vegetation at different phenological states further helps to advance this classification, with seasons that provide a better distinction between guilds being preferentially used. For example, the use of winter vertical skewness helps to differentiate between wooded species, whilst spectral indices can help to separate out different species of herbaceous vegetation. The accuracy of classification was similar to that reported by Butterfield *et al.* (2020), with the majority of errors coming from misclassifications to similar guilds. This suggests that hydraulically relevant vegetation trait data can be extracted from remote sensing data to good effect, and that expanding this methodology to test other locations would be essential to underpinning the possibility of making this a more widely adopted technique. It also builds upon work by

Manners, Schmidt and Wheaton (2013) who started to bridge the gap between patch scale and larger mapping of vegetation extents.

One of the benefits of the system developed in Chapter 3, was that it was capable of collecting high quality and high-resolution morphological data underneath dense canopy cover. This was used effectively in the methods developed in Chapter 4, where the combination of UAV-MS SfM and UAV-LS point clouds give unparalleled point density and coverage of a vegetated river corridor from a UAV platform. The resultant data enables the assessment of geomorphic change through time, with repeat surveys across all seasons allowing the morphological regime of the system to be elucidated. It is clear from the historical analysis and high-resolution monitoring undertaken in Chapter 4 that the study site on the river Teme is a highly active reach. However, the benefits of the through-canopy coverage allows the monitoring of erosion in locations where satellite imagery and SfM could not, and this ability provides the science community with an opportunity to better monitor, model and understand eco-geomorphic interactions. In Chapter 4, preliminary links were established between the magnitude of geomorphic change and the vegetation present, with a larger proportion of change over 2 m taking place within guilds that have a smaller stabilising effect according to the literature. The conclusions drawn within Chapter 4, that these feedbacks are complex but there is evidence that guild assemblages interact with flow differently, support and provide further context to the traits-based feedbacks researched by (Diehl *et al.*, 2018; Hortobágyi *et al.*, 2018).

Chapter 4 raised some important questions in relation to the use of remote sensing for eco-geomorphic research. Part of RQ2 referred to the ease at which these methods could be deployed and data quantified for assessment. Throughout Chapters 3 and 4, the considerable volume of bespoke processing required to deliver useful data limits the widespread application of these traits-based methods until routines are included in open-source distributions, for example bundled within CloudCompare (<https://www.danielgm.net/cc/>). This was also the case for SfM techniques in their infancy, which have since become a pervasive technique in high resolution surveying. Together, this positions the UAV-LS methods developed in Chapter 4 at a compromise between good spatial coverage and the ability to access remote locations, offset against high initial costs and challenging and time-consuming processing. It would appear that these latter points are beginning to be addressed with cheaper commercial setups and more advanced processing techniques now becoming available.

The spatial coverage of the UAV-LS and UAV-MS methods does come at some cost of resolution, with ground-based TLS methods being required to characterise smaller herbaceous species, and some trees that are smaller or in dense canopies unlikely to have good

reconstructions using cylinder models. Although increasing point densities and accuracy is likely to come with newer sensors, such advances come with the drawback of increasing data volumes and processing times, alongside the requirement for ever more complex filtering techniques. Therefore, despite the spatial resolution of the UAV-LS outlined in Chapter 4 being a potentially limiting factor, it may also serve to help differentiate the method at being effective across large spatial extents for vegetation modelling. Chapter 4, has shown these methods to be effective for reach scale classifications, whether improvements in point density correlate to better classification results is not yet clear. The importance of using time varying datasets is clear, however. This is especially the case when attempting to improve the accuracy of classifications and monitor a range of species within a domain. A consequence of this is the requirement to obtain seasonal data, and as such only sites that are accessible and safe to fly year-round can be monitored.

Chapter 4 demonstrates that it is possible to characterise vegetation across large areas with remote sensing data, and that this could improve our understanding of eco-geomorphic feedbacks. However, these feedbacks and interactions can take place over long timescales, and to fully understand the long-term trajectories of change in river systems, a modelling approach is typically used. Chapter 5 (**Paper 4; Tomsett and Leyland, In Prep**) therefore seeks to build upon this research by applying the vegetation classifications within a simple modelling scenario, addressing questions of how vegetation is represented within model domains in relation to their spatial and structural variability and the importance of seasonality.

This was addressed in Research Question 3, *“Does how we represent vegetation in relation to complexity and temporal evolution in fluvial model domains matter? What can novel representations of vegetation tell us about the eco-geomorphic feedbacks of a river system?”*

Chapter 5 attempts to establish how the use of three different methods of representing vegetation in a 2D model comparatively impacts output flow metrics and morphology. Comparisons between traditional bulk roughness, a seasonal bulk roughness, and a traits-based 3D vegetation model, show considerable differences in their outputs and raise a number of questions about how we choose to best represent vegetation. The distinct spatial variability in erosion and deposition across the model domain suggested that small changes in parameterisation led to large changes in the model outputs. The model was sensitive to seasonal bulk roughness, with changes from the upper and lower extremes of values suggested by Chow (1959) leading to different morphological responses. As relatively small changes from continuous to seasonal values led to such clear changes, models that do not incorporate elements of seasonality on heavily vegetated reaches may be limiting their real-world

applicability. This would support current research which demonstrates the need for seasonality to be incorporated into hydrodynamic models (Song *et al.*, 2017). This is relevant considering many studies aim to alter roughness, for example to test Natural Flood Management (NFM) strategies, which might ultimately be used to inform policy making. If the roughness used to parameterise different vegetation categories is inadequate, or not seasonally adjusted, then the results that are subsequently produced may be less informative than initially expected.

The inclusion of a structurally based 3D vegetation model, applied to a 2D domain, revealed the strong influence vegetation has on adjacent flow along the modelled reach, with velocities in the channel lower than would be expected for peak flows. However, the outputs from this scenario did suggest that the representation was having the expected effect, by reinforcing banks and slowing the flow within heavily vegetated areas, more so than outputs from the bulk roughness scenarios revealed. The traits-based scenario did lead to areas of the reach that are in reality highly mobile becoming stabilised, but also prevented the channel-widening seen in the bulk roughness scenarios in areas where the channel has been consistently stable, as the long-term decadal analysis within Chapter 4 demonstrated. Correct parametrisation of this 3D model may help to better represent vegetation across the floodplain, as well as within the channel, and could be used as a template for other models to consider how structurally varying vegetation can influence flow and subsequent morphology.

6.2 Future Work

One of the principle questions that this research aimed to address was to the extent to which remote sensing could be used to enhance our understanding of eco-geomorphic feedbacks. Herein we have determined that remote sensing can be used to establish vegetation traits and have started to explore the relationships between guild presence and geomorphic activity. There are many avenues of research that can be further developed from this initial work, both in terms of monitoring and modelling, with the aim of improving our understanding of the links that exist between vegetation and morphology.

The challenge of isolating individual elements that affect channel form is likely to remain for the foreseeable future, especially in field scenarios outside of flume conditions. Many studies have determined the individual plant elements that directly impact drag and sediment (Follett and Nepf, 2012; Jalonon, Järvelä and Aberle, 2012), but the aggregated responses which are typical of field conditions remain limited. The high-resolution UAV-LS methods presented here provide the basis for scalability to multiple sites. From this, the directions and magnitudes of change in response to varying flow events through different vegetation guilds can be inferred.

Currently, such work has been focussed on a small number of rivers with similar guilds, and this is the first work to apply these methods to a new reach, despite the benefits of traits-based approaches being their transferability and applicability to a variety of scenarios (Violle *et al.*, 2007; Lytle *et al.*, 2017). The extent to which this is true within the fluvial domain is currently undetermined. Although vegetation trait response to hydrological conditions is well documented and can be applied across several scenarios (e.g. Baattrup-Pedersen *et al.*, 2018), traits-based interactions with morphology and flow are less well documented. In order to prove that traits-based methods should be widely adopted amongst the research community, evidence of applicability between domains is required, and this should be an avenue of research that is pursued in tandem with isolating the effects of different guilds, as both complement each other. Ultimately, the potential for traits-based research to better characterise vegetation could well minimise variability between similar reaches that are spatially explicit.

For traits-based methods to be broadly applied elsewhere, several conditions must be met. Firstly, the scalability to other datasets must be tested. For a method to be truly applicable to a number of sites, being able to use a combination of different sensors and datasets is required. This will include the construction of 3D point clouds and orthoimagery for successful structural and spectral analysis from different sources of data. Linking these methodological principles to wider ALS and satellite data could open up the possibility of creating guilds-based classifications for larger river corridors that are beyond the scope of UAV data collection. Work by Manners, Schmidt and Wheaton (2013) scaling from TLS to ALS has already been undertaken with good levels of success. Using the same variations in structural and spectral data for ALS and satellite imagery instead of UAV-LS and UAV-MS as used within this study may present a suitable solution to scaling such analysis to larger extents.

A potential limitation of this research avenue would be gaining enough coverage of data across the variety of guilds found within the river corridor. This represents the second condition for successful rollout of this method. A database of spatial datasets for different vegetation traits would need to be collated, not only to provide useful training data for creating guild maps of new study sites, but also to analyse the links between guild locations and their morphological response. Such data sharing would be unique, but has already begun for traits-based research with the use of the 'TRY' database (Kattge *et al.*, 2020). This currently consists of tabular records, but the potential to link this to spatial datasets could open up a raft of new research that can make use of such a rich resource.

Within the modelling domain, vegetation is mostly still poorly represented, with small changes in vegetation parameters leading to large changes in model outputs. Identification of how best

to parametrise traits within a model is required, identifying the sensitivity of model outputs to different parameters such as drag coefficients and plant structure. Moreover, currently very few models will accept more complex, functional representations of vegetation. The seasonality and depth varying influence that vegetation has is often overlooked, despite being of significant importance (O'Hare *et al.*, 2010; Song, Schmalz and Fohrer, 2014). Future research aiming to incorporate even simple vegetation models will help to improve modelling and make the results more widely applicable. Wrapped into this is the requirement for a better representation of the impact vegetation has below the surface, where linking above ground traits to below ground traits would help to better inform variations in the substrate between different guilds. Chapter 5 showed that including variations in substrate as well as above ground vegetation structure helped to maintain channel stability in regions where it was expected and where bulk roughness parameters alone failed to do so. Incorporating such variations more widely into modelling practice would help to better replicate reality and improve model outputs.

There are still some limitations with the broad methodological and processing approaches outlined in this thesis. The first major obstacle is the processing requirements for such extensive datasets. Despite the increasing computing power and storage capabilities, the ability for a wide variety of users with a range of processing power is limited by what technology is available to them. As such, those outside organisations without access to such facilities may struggle to benefit from this approach and may view the increased cost of the surveying equipment and processing time as unjustified. It is hoped that the falling cost of computing power and equipment, as well as availability of off-the-shelf surveying kit, can improve accessibility.

6.3 Conclusion

This research has sought to improve the current tools, methods, and scientific understanding in relation to eco-geomorphic interactions, transcending the spatial scales of current research by using novel UAV based remote sensing techniques and modelling studies. As a result, new methods of analysing and reconstructing riparian vegetation have been developed at a range of scales, from individual plant reconstruction, through guild identification, up to reach scale classifications. These classifications have subsequently been implemented within a hydrodynamic model, demonstrating the impact that different vegetation discretisation methods have on model outcomes and suggesting some exciting possibilities for future work.

Until now, despite the known influence that vegetation has on both flow and morphology, attempts to fully capture the structural variability beyond the patch scale have not been undertaken within the river corridor. This research has developed novel remote sensing

methods, coupled with other methods identified in the fields of ecology and forestry, to capture vegetation structure within the river corridor and apply this to a full reach scale classification of structural and spectral properties. Accounting for vegetation in this way has improved our understanding of feedbacks, with different morphological responses being linked to different guild presence. Moreover, the methods herein reveal that there is potential to transition between different scales of analysis, building on a growing body of research aiming to establish links between different scales of surveying, with the overall aim of making patch scale research applicable to large scale studies. Currently, this method has been applied to a reach roughly 1 km in length, but the same equipment could be used to cover extended areas. The benefits of this scaling approach have been demonstrated through the implementation of reach scale modelling. The importance of incorporating seasonality and adequately accounting for vegetation properties is clear, helping to replicate morphological responses identified in the field.

Vegetation is important in modulating geomorphic processes across nearly all Earth surface process domains and varies across both space and time. This research has primarily focussed on river corridors, from the broad techniques used to monitor them, through to links between vegetation and form. Yet, the implications of these methods, whereby vegetation are classified by their effects on, and responses to, their physical environment, can be applied to numerous other fields where vegetation is a component control on morphological evolution. Moreover, the importance of accounting for seasonality can be transferred beyond the river corridor, and should become an integral component of any study looking at process form interactions which are modulated by vegetation (dead or alive). The results of this research, although framed in a fluvial context, extend beyond this domain to the wider geomorphic body of research. Methods of analysing vegetation, scaling results from patch to reach scales, accounting for vegetation phenology, and incorporating them in to modelling studies, are all linked to the wider problems that geomorphological researchers face. As a result, it is hoped that the research presented here will benefit the wider geomorphic community beyond those investigating riparian vegetation, and that the methods can be used to pursue new avenues of research which better help us to understand eco-geomorphology across a range of spatial and temporal scales.

List of References

- Abad, J. and Garcia, M. (2009) 'Experiments in a high-amplitude Kinoshita meandering channel: 1. Implications of bend orientation on mean and turbulent flow structure', *Water Resources Research*, 45, p. 19.
- Abalharth, M. *et al.* (2015) 'Using LiDAR to characterize logjams in lowland rivers', *Geomorphology*, 246, pp. 531-541.
- Abelleira Martínez, O.J. *et al.* (2016) 'Scaling up functional traits for ecosystem services with remote sensing: concepts and methods', *Ecology and Evolution*, 6(13), pp. 4359-4371.
- Abernethy, B. and Rutherford, I.D. (2001) 'The distribution and strength of riparian tree roots in relation to riverbank reinforcement', *Hydrological Processes*, 15(1), pp. 63-79.
- Adam, E. and Mutanga, O. (2009) 'Spectral discrimination of papyrus vegetation (*Cyperus papyrus* L.) in swamp wetlands using field spectrometry', *ISPRS Journal of Photogrammetry and Remote Sensing*, 64(6), pp. 612-620.
- Adelabu, S. and Dube, T. (2015) 'Employing ground and satellite-based QuickBird data and random forest to discriminate five tree species in a Southern African Woodland', *Geocarto International*, 30(4), pp. 457-471.
- Adrian, R. (1991) 'Particle-imaging techniques for experimental fluid mechanics', *Annual review of fluid mechanics*, 23(1), pp. 261-304.
- Aguiar, F.C. *et al.* (2018) 'The abundance and distribution of guilds of riparian woody plants change in response to land use and flow regulation', *Journal of Applied Ecology*, 55(5), pp. 2227-2240.
- Aguirre-Gutiérrez, J. *et al.* (2021) 'Pantropical modelling of canopy functional traits using Sentinel-2 remote sensing data', *Remote Sensing of Environment*, 252, p. 112122.
- Al-Ali, Z.M. *et al.* (2020) 'A comparative study of remote sensing classification methods for monitoring and assessing desert vegetation using a UAV-based multispectral sensor', *Environmental Monitoring and Assessment*, 192(6), p. 389.
- Alaibakhsh, M. *et al.* (2017) 'Delineation of riparian vegetation from Landsat multi-temporal imagery using PCA', *Hydrological Processes*, 31(4), pp. 800-810.
- Albani, D., Nardi, D. and Trianni, V. (2017) 'Field Coverage and Weed Mapping by UAV Swarms', in Bicchi, A. and Okamura, A. (eds.) *2017 Ieee/Rsj International Conference on Intelligent Robots and Systems*. New York: Ieee, pp. 4319-4325.

List of References

- Alho, P. *et al.* (2009) 'Application of boat-based laser scanning for river survey', *Earth Surface Processes and Landforms*, 34(13), pp. 1831-1838.
- Almeida, M., Hildmann, H. and Solmaz, G. (2017) 'DISTRIBUTED UAV-SWARM-BASED REAL-TIME GEOMATIC DATA COLLECTION UNDER DYNAMICALLY CHANGING RESOLUTION REQUIREMENTS', in Stachniss, C., Forstner, W. and Schneider, J. (eds.) *International Conference on Unmanned Aerial Vehicles in Geomatics*. Gottingen: Copernicus Gesellschaft Mbh, pp. 5-12.
- Alvarez, L. *et al.* (2018) 'Merging Unmanned Aerial Systems (UAS) Imagery and Echo Soundings with an Adaptive Sampling Technique for Bathymetric Surveys', *Remote Sensing*, 10(9), p. 1362.
- Amarnath, G. (2014) 'An algorithm for rapid flood inundation mapping from optical data using a reflectance differencing technique', *Journal of Flood Risk Management*, 7(3), pp. 239-250.
- Anderson, B.G., Rutherford, I.D. and Western, A.W. (2006) 'An analysis of the influence of riparian vegetation on the propagation of flood waves', *Environmental Modelling & Software*, 21(9), pp. 1290-1296.
- Andrews, E.D. (1984) 'Bed-material entrainment and hydraulic geometry of gravel-bed rivers in Colorado', *GSA Bulletin*, 95(3), pp. 371-378.
- Antonarakis, A., Richards, K. and Brasington, J. (2008a) 'Object-based land cover classification using airborne LiDAR', *Remote Sensing of Environment*, 112(6), pp. 2988-2998.
- Antonarakis, A. *et al.* (2009) 'Leafless roughness of complex tree morphology using terrestrial lidar', *Water Resources Research*, 45, p. 14.
- Antonarakis, A.S., Richards, K.S. and Brasington, J. (2008b) 'Object-based land cover classification using airborne LiDAR', *Remote Sensing of Environment*, 112(6), pp. 2988-2998.
- Apan, A., Raine, S. and Paterson, M. (2002) 'Mapping and analysis of changes in the riparian landscape structure of the Lockyer Valley catchment, Queensland, Australia', *Landscape and Urban Planning*, 59(1), pp. 43-57.
- Applanix (2016) *APX-15 UAV Datasheet*. Available at: https://www.applanix.com/downloads/products/specs/APX15_DS_NEW_0408_YW.pdf (Accessed: 25/01/2018).
- Applanix (2017) *POS AV Datasheet*. Available at: https://www.applanix.com/downloads/products/specs/posav_datasheet.pdf (Accessed: 25/01/2018).
- Aranuvachapun, S. and Walling, D.E. (1988) 'Landsat-MSS radiance as a measure of suspended sediment in the Lower Yellow River (Hwang Ho)', *Remote Sensing of Environment*, 25(2), pp. 145-165.
- Armanini, A., Righetti, M. and Grisenti, P. (2005) 'Direct measurement of vegetation resistance in prototype scale', *Journal of Hydraulic Research*, 43(5), pp. 481-487.

- Armstrong, R. and Singh, H. (2012) *Mesophotic Coral Reefs of the Puerto Rico Shelf*. Amsterdam: Elsevier Science Bv. Seafloor Geomorphology as Benthic Habitat: Geohab Atlas of Seafloor Geomorphic Features and Benthic Habitats.
- Arroyo, L. *et al.* (2010a) 'Integration of LiDAR and QuickBird imagery for mapping riparian biophysical parameters and land cover types in Australian tropical savannas', *Forest Ecology and Management*, 259(3), pp. 598-606.
- Arroyo, L.A. *et al.* (2010b) 'Integration of LiDAR and QuickBird imagery for mapping riparian biophysical parameters and land cover types in Australian tropical savannas', *Forest Ecology and Management*, 259(3), pp. 598-606.
- Assmann, J.J. *et al.* (2019) 'Vegetation monitoring using multispectral sensors – best practices and lessons learned from high latitudes', *Journal of Unmanned Vehicle Systems*, pp. 54 - 75.
- Baatrup-Pedersen, A. *et al.* (2018) 'Structural and functional responses of plant communities to climate change-mediated alterations in the hydrology of riparian areas in temperate Europe', *Ecology and Evolution*, 8(8), pp. 4120-4135.
- Baatrup-Pedersen, A. *et al.* (2015) 'Plant trait characteristics vary with size and eutrophication in European lowland streams', *Journal of Applied Ecology*, 52(6), pp. 1617-1628.
- Baatrup-Pedersen, A. *et al.* (2016) 'Functional trait composition of aquatic plants can serve to disentangle multiple interacting stressors in lowland streams', *Science of The Total Environment*, 543, pp. 230-238.
- Baatrup-Pedersen, A., Larsen, S.E. and Riis, T. (2002) 'Long-term effects of stream management on plant communities in two Danish lowland streams', *Hydrobiologia*, 481(1-3), pp. 33-45.
- Baewert, H. *et al.* (2014) 'Roughness determination of coarse grained alpine river bed surfaces using Terrestrial Laser Scanning data', *Zeitschrift Fur Geomorphologie*, 58, pp. 81-95.
- Bagheri, O., Ghodsian, M. and Saadatseresht, M. (2015) 'Reach scale application of UAV plus SfM method in shallow rivers hyperspatial bathymetry', in Arefi, H. and Motagh, M. (eds.) *International Conference on Sensors & Models in Remote Sensing & Photogrammetry*. Gottingen: Copernicus Gesellschaft Mbh, pp. 77-81.
- Baki, A. and Gan, T. (2012) 'Riverbank migration and island dynamics of the braided Jamuna River of the Ganges–Brahmaputra basin using multi-temporal Landsat images', *Quaternary International*, 263, pp. 148-161.
- Banda, M.S. and Meon, I.G. (2018) *Morphological development of meandering rivers due to changing discharge regimes*. Dissertation, Technische Universität Braunschweig.
- Bande, S. and Shete, V. (2017) *Smart flood disaster prediction system using IoT & Neural Networks*. New York: Ieee. Proceedings of the 2017 International Conference on Smart Technologies for Smart Nation.

List of References

- Bandini, F. *et al.* (2018) 'Technical note: Bathymetry observations of inland water bodies using a tethered single-beam sonar controlled by an unmanned aerial vehicle', *Hydrology and Earth System Sciences*, 22(8), pp. 4165-4181.
- Bennett, A. and Leonard, J. (2000) 'A behavior-based approach to adaptive feature detection and following with autonomous underwater vehicles', *Ieee Journal of Oceanic Engineering*, 25(2), pp. 213-226.
- Berezowski, T. *et al.* (2015) 'Towards rainfall interception capacity estimation using ALS LiDAR data', in *2015 Ieee International Geoscience and Remote Sensing Symposium*. New York: Ieee, pp. 735-738.
- Bernhardt, E. *et al.* (2007) 'Restoring rivers one reach at a time: Results from a survey of US river restoration practitioners', *Restoration Ecology*, 15(3), pp. 482-493.
- Bertoldi, W., Drake, N.A. and Gurnell, A.M. (2011) 'Interactions between river flows and colonizing vegetation on a braided river: exploring spatial and temporal dynamics in riparian vegetation cover using satellite data', *Earth Surface Processes and Landforms*, 36(11), pp. 1474-1486.
- Bertoldi, W., Gurnell, A. and Drake, N. (2011a) 'The topographic signature of vegetation development along a braided river: Results of a combined analysis of airborne lidar, color air photographs, and ground measurements', *Water Resources Research*, 47, p. 13.
- Bertoldi, W., Gurnell, A. and Welber, M. (2013a) 'Wood recruitment and retention: The fate of eroded trees on a braided river explored using a combination of field and remotely-sensed data sources', *Geomorphology*, 180, pp. 146-155.
- Bertoldi, W., Gurnell, A.M. and Drake, N.A. (2011b) 'The topographic signature of vegetation development along a braided river: Results of a combined analysis of airborne lidar, color air photographs, and ground measurements', *Water Resources Research*, 47, p. 13.
- Bertoldi, W., Gurnell, A.M. and Welber, M. (2013b) 'Wood recruitment and retention: The fate of eroded trees on a braided river explored using a combination of field and remotely-sensed data sources', *Geomorphology*, 180, pp. 146-155.
- Best, J. *et al.* (2010) 'A new methodology for the quantitative visualization of coherent flow structures in alluvial channels using multibeam echo-sounding (MBES)', *Geophysical Research Letters*, 37, p. 6.
- Bhuiyan, F., Hey, R. and Wormleaton, P. (2007) 'Hydraulic evaluation of W-weir for river restoration', *Journal of Hydraulic Engineering-Asce*, 133(6), pp. 596-609.
- Bian, C. *et al.* (2016) 'Pedestrian Tracking from an Unmanned Aerial Vehicle', in Baozong, Y. *et al.* (eds.) *Proceedings of 2016 Ieee 13th International Conference on Signal Processing*. New York: Ieee, pp. 1067-1071.
- Bjerklie, D. *et al.* (2005) 'Estimating discharge in rivers using remotely sensed hydraulic information', *Journal of Hydrology*, 309(1), pp. 191-209.

- Blöschl, G. *et al.* (2007) 'At what scales do climate variability and land cover change impact on flooding and low flows?', *Hydrological Processes*, 21(9), pp. 1241-1247.
- Blott, S.J. and Pye, K. (2001) 'GRADISTAT: a grain size distribution and statistics package for the analysis of unconsolidated sediments', *Earth Surface Processes and Landforms*, 26(11), pp. 1237-1248.
- Bolognesi, M. *et al.* (2017) 'Measurement of surface velocity in open channels using a lightweight remotely piloted aircraft system', *Geomatics Natural Hazards & Risk*, 8(1), pp. 73-86.
- Boothroyd, R. *et al.* (2017) 'Modeling complex flow structures and drag around a submerged plant of varied posture', *Water Resources Research*, 53(4), pp. 2877-2901.
- Bowen, Z. and Waltermire, R. (2002) 'Evaluation of light detection and ranging (LIDAR) for measuring river corridor topography', *Journal of the American Water Resources Association*, 38(1), pp. 33-41.
- Box, E. (1981) *Macroclimate and Plant Forms: An Introduction to Predictive Modeling in Phytogeography*. 1 edn.: Springer Netherlands.
- Box, E.O. (1996) 'Plant functional types and climate at the global scale', *Journal of Vegetation Science*, 7(3), pp. 309-320.
- Brando, V. and Dekker, A. (2003) 'Satellite hyperspectral remote sensing for estimating estuarine and coastal water quality', *IEEE Transactions on Geoscience and Remote Sensing*, 41(6), pp. 1378-1387.
- Brasington, J., Vericat, D. and Rychkov, I. (2012) 'Modeling river bed morphology, roughness, and surface sedimentology using high resolution terrestrial laser scanning', *Water Resources Research*, 48, p. 18.
- Brede, B. *et al.* (2019) 'Non-destructive tree volume estimation through quantitative structure modelling: Comparing UAV laser scanning with terrestrial LIDAR', *Remote Sensing of Environment*, 233, p. 111355.
- Brodu, N. and Lague, D. (2012) '3D terrestrial lidar data classification of complex natural scenes using a multi-scale dimensionality criterion: Applications in geomorphology', *ISPRS Journal of Photogrammetry and Remote Sensing*, 68, pp. 121-134.
- Brothers, D. *et al.* (2015) 'The Palos Verdes Fault offshore Southern California: Late Pleistocene to present tectonic geomorphology, seascape evolution, and slip rate estimate based on AUV and ROV surveys', *Journal of Geophysical Research-Solid Earth*, 120(7), pp. 4734-4758.
- Brunier, G. *et al.* (2016) 'Structure-from-Motion photogrammetry for high-resolution coastal and fluvial geomorphic surveys', *Geomorphologie-Relief Processus Environnement*, 22(2), pp. 147-161.
- Brunke, M. and Gonser, T. (1997) 'The ecological significance of exchange processes between rivers and groundwater', *Freshwater Biology*, 37(1), pp. 1-33.
- Buffin-Belanger, T. *et al.* (2006) 'Spatial heterogeneity of near-bed hydraulics above a patch of river gravel', *Water Resources Research*, 42(4), p. 12.

List of References

- Buffin-Belanger, T. and Roy, A.G. (2005) '1 min in the life of a river: selecting the optimal record length for the measurement of turbulence in fluvial boundary layers', *Geomorphology*, 68(1-2), pp. 77-94.
- Burt, A., Disney, M. and Calders, K. (2019) 'Extracting individual trees from lidar point clouds using treeseg', *Methods in Ecology and Evolution*, 10(3), pp. 438-445.
- Butterfield, B.J. *et al.* (2020) 'Associations between riparian plant morphological guilds and fluvial sediment dynamics along the regulated Colorado River in Grand Canyon', *River Research and Applications*, 36(3), pp. 410-421.
- Bywater-Reyes, S., Wilcox, A. and Diehl, R. (2017) 'Multiscale influence of woody riparian vegetation on fluvial topography quantified with ground-based and airborne lidar', *Journal of Geophysical Research-Earth Surface*, 122(6), pp. 1218-1235.
- Camporeale, C. *et al.* (2013) 'Modeling the interactions between river morphodynamics and riparian vegetation', *Reviews of Geophysics*, 51(3), pp. 379-414.
- Caponi, F., Vetsch, D.F. and Siviglia, A. (2020) 'A model study of the combined effect of above and below ground plant traits on the ecomorphodynamics of gravel bars', *Scientific Reports*, 10(1), p. 17062.
- Carbonneau, P., Bergeron, N. and Lane, S. (2005) 'Automated grain size measurements from airborne remote sensing for long profile measurements of fluvial grain sizes', *Water Resources Research*, 41(11).
- Carbonneau, P., Bizzi, S. and Marchetti, G. (2018) 'Robotic photosieving from low-cost multicopter sUAS: a proof-of-concept', *Earth Surface Processes and Landforms*, 43(5), pp. 1160-1166.
- Carling, P. *et al.* (2000) 'The morphodynamics of fluvial sand dunes in the River Rhine, near Mainz, Germany. I. Sedimentology and morphology', *Sedimentology*, 47(1), pp. 227-252.
- Carrivick, J.L. and Smith, M.W. (2019) 'Fluvial and aquatic applications of Structure from Motion photogrammetry and unmanned aerial vehicle/drone technology', *WIREs Water*, 6(1), p. e1328.
- Cartisano, R. *et al.* (2013) 'Assessing and mapping biomass potential productivity from poplar-dominated riparian forests: A case study', *Biomass & Bioenergy*, 54, pp. 293-302.
- Casado, M. *et al.* (2016) 'Quantifying the Effect of Aerial Imagery Resolution in Automated Hydromorphological River Characterisation', *Remote Sensing*, 8(8), p. 19.
- Casas, A. *et al.* (2010) 'A method for parameterising roughness and topographic sub-grid scale effects in hydraulic modelling from LiDAR data', *Hydrol. Earth Syst. Sci.*, 14(8), pp. 1567-1579.
- Casbeer, D. *et al.* (2006) 'Cooperative forest fire surveillance using a team of small unmanned air vehicles', *International Journal of Systems Science*, 37(6), pp. 351-360.
- Casper, A. *et al.* (2009) 'Combined GIS and ROV technologies improve characterization of water quality in Coastal Rivers of the Gulf of Mexico', in *Oceans 2009, Vols 1-3*. New York: Ieee, pp. 2555-+.

- Castellarin, A., Di Baldassarre, G. and Brath, A. (2011) 'FLOODPLAIN MANAGEMENT STRATEGIES FOR FLOOD ATTENUATION IN THE RIVER PO', *River Research and Applications*, 27(8), pp. 1037-1047.
- Cavalli, M. *et al.* (2008) 'The effectiveness of airborne LiDAR data in the recognition of channel-bed morphology', *Catena*, 73(3), pp. 249-260.
- Caviedes-Voullième, D. *et al.* (2013) '2D river flood simulation using interpolated river bed geometry'.
- Ceulemans, R., McDonald, A.J.S. and Pereira, J.S. (1996) 'A comparison among eucalypt, poplar and willow characteristics with particular reference to a coppice, growth-modelling approach', *Biomass and Bioenergy*, 11(2), pp. 215-231.
- Champion, P.D. and Tanner, C.C. (2000) 'Seasonality of macrophytes and interaction with flow in a New Zealand lowland stream', *Hydrobiologia*, 441(1), pp. 1-12.
- Chan, J.C.-W. and Paelinckx, D. (2008) 'Evaluation of Random Forest and Adaboost tree-based ensemble classification and spectral band selection for ecotope mapping using airborne hyperspectral imagery', *Remote Sensing of Environment*, 112(6), pp. 2999-3011.
- Chanson, H. *et al.* (2011) 'High-frequency turbulence and suspended sediment concentration measurements in the Garonne River tidal bore', *Estuarine Coastal and Shelf Science*, 95(2-3), pp. 298-306.
- Charogiannis, A., Zadrazil, I. and Markides, C. (2016) 'Thermographic particle velocimetry (TPV) for simultaneous interfacial temperature and velocity measurements', *International Journal of Heat and Mass Transfer*, 97, pp. 589-595.
- Chen, J., Ye, F. and Li, Y.B. (2017) 'Travelling Salesman Problem for UAV Path Planning with Two Parallel Optimization Algorithms', in *2017 Progress in Electromagnetics Research Symposium - Fall*. New York: Ieee, pp. 832-837.
- Chen, Z., Hu, C. and Muller-Karger, F. (2007) 'Monitoring turbidity in Tampa Bay using MODIS/Aqua 250-m imagery', *Remote Sensing of Environment*, 109(2), pp. 207-220.
- Chow, V.T. (1959) 'Open-channel hydraulics. Caldwell'. New Jersey, USA: The Blackburn Press.
- Chu, Z. *et al.* (2006) 'Changing pattern of accretion/erosion of the modern Yellow River (Huanghe) subaerial delta, China: Based on remote sensing images', *Marine Geology*, 227(1), pp. 13-30.
- Clapuyt, F., Vanacker, V. and Van Oost, K. (2016) 'Reproducibility of UAV-based earth topography reconstructions based on Structure-from-Motion algorithms', *Geomorphology*, 260, pp. 4-15.
- Cobby, D. *et al.* (2003a) 'Two-dimensional hydraulic flood modelling using a finite-element mesh decomposed according to vegetation and topographic features derived from airborne scanning laser altimetry', *Hydrological processes*, 17(10), pp. 1979-2000.

List of References

- Cobby, D.M., Mason, D.C. and Davenport, I.J. (2001) 'Image processing of airborne scanning laser altimetry data for improved river flood modelling', *ISPRS Journal of Photogrammetry and Remote Sensing*, 56(2), pp. 121-138.
- Cobby, D.M. *et al.* (2003b) 'Two-dimensional hydraulic flood modelling using a finite-element mesh decomposed according to vegetation and topographic features derived from airborne scanning laser altimetry', *Hydrological processes*, 17(10), pp. 1979-2000.
- Coleman, J.M. (1969) 'Brahmaputra river: Channel processes and sedimentation', *Sedimentary Geology*, 3(2), pp. 129-239.
- Colomina, I. and Molina, P. (2014) 'Unmanned aerial systems for photogrammetry and remote sensing: A review', *Isprs Journal of Photogrammetry and Remote Sensing*, 92, pp. 79-97.
- Cook, K. (2017) 'An evaluation of the effectiveness of low-cost UAVs and structure from motion for geomorphic change detection', *Geomorphology*, 278, pp. 195-208.
- Corenblit, D. *et al.* (2015) 'Engineer pioneer plants respond to and affect geomorphic constraints similarly along water–terrestrial interfaces world-wide', *Global Ecology and Biogeography*, 24(12), pp. 1363-1376.
- Corenblit, D. *et al.* (2011) 'Feedbacks between geomorphology and biota controlling Earth surface processes and landforms: A review of foundation concepts and current understandings', *Earth-Science Reviews*, 106(3), pp. 307-331.
- Corenblit, D. and Steiger, J. (2009) 'Vegetation as a major conductor of geomorphic changes on the Earth surface: toward evolutionary geomorphology', *Earth Surface Processes and Landforms*, 34(6), pp. 891-896.
- Costanza, R. *et al.* (1997) 'The value of the world's ecosystem services and natural capital', *Nature*, 387(6630), pp. 253-260.
- Cotton, J.A. *et al.* (2006) 'The effects of seasonal changes to in-stream vegetation cover on patterns of flow and accumulation of sediment', *Geomorphology*, 77(3), pp. 320-334.
- Covault, J. *et al.* (2014) 'Submarine channel initiation, filling and maintenance from sea-floor geomorphology and morphodynamic modelling of cyclic steps', *Sedimentology*, 61(4), pp. 1031-1054.
- Coveney, S. and Roberts, K. (2017) 'Lightweight UAV digital elevation models and orthoimagery for environmental applications: data accuracy evaluation and potential for river flood risk modelling', *International journal of remote sensing*, 38(8-10), pp. 3159-3180.
- Cranfield Univeristy (2018) *Using drones to map rivers for ecological monitoring and assessment*. Available at: <https://www.cranfield.ac.uk/case-studies/research-case-studies/mapping-rivers> (Accessed: 21/11/2018).

- Creutin, J. *et al.* (2003) 'River gauging using PIV techniques: a proof of concept experiment on the Iowa River', *Journal of Hydrology*, 277(3-4), pp. 182-194.
- Croke, J. *et al.* (2013) 'The use of multi temporal LiDAR to assess basin-scale erosion and deposition following the catastrophic January 2011 Lockyer flood, SE Queensland, Australia', *Geomorphology*, 184, pp. 111-126.
- Crosato, A. and Saleh, M.S. (2011) 'Numerical study on the effects of floodplain vegetation on river planform style', *Earth Surface Processes and Landforms*, 36(6), pp. 711-720.
- Dandois, J. *et al.* (2017) 'What is the point? Evaluating the structure, color, and semantic traits of computer vision point clouds of vegetation', *Remote Sensing*, 9(4), p. 355.
- Darby, S.E., Rinaldi, M. and Dapporto, S. (2007) 'Coupled simulations of fluvial erosion and mass wasting for cohesive river banks', *Journal of Geophysical Research: Earth Surface*, 112(F3).
- Darby, S.E. *et al.* (2010) 'A physically based model to predict hydraulic erosion of fine-grained riverbanks: The role of form roughness in limiting erosion', *Journal of Geophysical Research: Earth Surface*, 115(F4).
- Davies, N.S. and Gibling, M.R. (2010) 'Cambrian to Devonian evolution of alluvial systems: The sedimentological impact of the earliest land plants', *Earth-Science Reviews*, 98(3), pp. 171-200.
- de Almeida, R. *et al.* (2016) 'Large barchanoid dunes in the Amazon River and the rock record: Implications for interpreting large river systems', *Earth and Planetary Science Letters*, 454, pp. 92-102.
- De Bello, F., Lepš, J. and Sebastià, M.T. (2006) 'Variations in species and functional plant diversity along climatic and grazing gradients', *Ecography*, 29(6), pp. 801-810.
- De Doncker, L. *et al.* (2009) 'Relation between resistance characteristics due to aquatic weed growth and the hydraulic capacity of the river Aa', *River Research and Applications*, 25(10), pp. 1287-1303.
- De Doncker, L. *et al.* (2011) 'Deriving the relationship among discharge, biomass and Manning's coefficient through a calibration approach', *Hydrological Processes*, 25(12), pp. 1979-1995.
- De Rose, R. and Basher, L. (2011) 'Measurement of river bank and cliff erosion from sequential LIDAR and historical aerial photography', *Geomorphology*, 126(1), pp. 132-147.
- Deltares (2021) 'Delft3D-FLOW User Manual' V 3.15. Available at: https://content.oss.deltares.nl/delft3d/manuals/Delft3D-FLOW_User_Manual.pdf.
- Deng, F. *et al.* (2017) '3D Digitisation of Large-Scale Unstructured Great Wall Heritage Sites by a Small Unmanned Helicopter', *Remote Sensing*, 9(5), p. 17.
- Deruyter, G. *et al.* (2015) 'The use of terrestrial laser scanning for measurements in shallow-water: Correction of the 3D coordinates of the point cloud', in *Informatics, Geoinformatics and Remote Sensing, Vol I*. Sofia: Stef92 Technology Ltd, pp. 1203-1209.

List of References

- Detert, M. and Weitbrecht, V. (2015) 'A low-cost airborne velocimetry system: proof of concept', *Journal of Hydraulic Research*, 53(4), pp. 532-539.
- Di Baldassarre, G., Schumann, G. and Bates, P.D. (2009) 'A technique for the calibration of hydraulic models using uncertain satellite observations of flood extent', *Journal of Hydrology*, 367(3-4), pp. 276-282.
- Diehl, R.M. *et al.* (2017) 'Applying Functional Traits to Ecogeomorphic Processes in Riparian Ecosystems', *BioScience*, 67(8), pp. 729-743.
- Diehl, R.M. *et al.* (2018) 'Development of an eco-geomorphic modeling framework to evaluate riparian ecosystem response to flow-regime changes', *Ecological Engineering*, 123, pp. 112-126.
- Dietrich, J. (2016) 'Riverscape mapping with helicopter-based Structure-from-Motion photogrammetry', *Geomorphology*, 252, pp. 144-157.
- Dietrich, J. (2017) 'Bathymetric Structure-from-Motion: extracting shallow stream bathymetry from multi-view stereo photogrammetry', *Earth Surface Processes and Landforms*, 42(2), pp. 355-364.
- Dilley, M. *et al.* (2005) *Natural Disaster Hotspots: A Global Risk Analysis*. Washington, World Bank. Available at: <https://openknowledge.worldbank.org/handle/10986/7376>.
- Dixon, S.J. *et al.* (2018) 'The planform mobility of river channel confluences: Insights from analysis of remotely sensed imagery', *Earth-Science Reviews*, 176, pp. 1-18.
- Doughty, C.L. and Cavanaugh, K.C. (2019) 'Mapping Coastal Wetland Biomass from High Resolution Unmanned Aerial Vehicle (UAV) Imagery', *Remote Sensing*, 11(5), p. 540.
- Douville, H., K. *et al.* (2021) 'Water Cycle Changes', in Masson-Delmotte, V., P. *et al.* (eds.) *Climate Change 2021: The Physical Science Basis*. Cambridge University Press.
- Durand, M. *et al.* (2016) 'An intercomparison of remote sensing river discharge estimation algorithms from measurements of river height, width, and slope', *Water Resources Research*, 52(6), pp. 4527-4549.
- Duro, D.C., Franklin, S.E. and Dube, M.G. (2012) 'A comparison of pixel-based and object-based image analysis with selected machine learning algorithms for the classification of agricultural landscapes using SPOT-5 HRG imagery', *Remote Sensing of Environment*, 118, pp. 259-272.
- Edmondson, V. *et al.* (2018) 'A smart sewer asset information model to enable an 'Internet of Things' for operational wastewater management', *Automation in Construction*, 91, pp. 193-205.
- Elci, S., Aydın, R. and Work, P.A. (2009) 'Estimation of suspended sediment concentration in rivers using acoustic methods', *Environmental Monitoring and Assessment*, 159(1-4), pp. 255-265.

- Eleftherakis, D. *et al.* (2014) 'Observations regarding coarse sediment classification based on multi-beam echo-sounder's backscatter strength and depth residuals in Dutch rivers', *Journal of the Acoustical Society of America*, 135(6), pp. 3305-3315.
- Eltner, A. *et al.* (2016) 'Image-based surface reconstruction in geomorphometry - merits, limits and developments', *Earth Surface Dynamics*, 4(2), pp. 359-389.
- Emanuel, R.E. *et al.* (2014) 'Vegetation and topographic influences on the connectivity of shallow groundwater between hillslopes and streams', *Ecohydrology*, 7(2), pp. 887-895.
- EMLID (2021) 'RTK GNSS modules for UAV mapping'. Available at: <https://emlid.com/reach/> (Accessed: 06/05/2021).
- Entwistle, N., Heritage, G. and Milan, D. (2018) 'Recent remote sensing applications for hydro and morphodynamic monitoring and modelling', *Earth Surface Processes and Landforms*, 43(10), pp. 2283-2291.
- Environment Agency (2017) 'Environment Agency uncovers landscape with laser mapping'. River maintenance, flooding and coastal erosion: GOV.UK. Available at: <https://www.gov.uk/government/news/environment-agency-uncovers-landscape-with-laser-mapping>.
- Espinoza-Villar, R. *et al.* (2018) 'Spatio-temporal monitoring of suspended sediments in the Solimoes River (2000-2014)', *Comptes Rendus Geoscience*, 350(1-2), pp. 4-12.
- Fairbairn, W.A. (1967) 'Erosion in the River Findhorn Valley', *Scottish Geographical Magazine*, 83(1), pp. 46-52.
- Fallon, M.F. *et al.* (2013) 'Relocating Underwater Features Autonomously Using Sonar-Based SLAM', *Ieee Journal of Oceanic Engineering*, 38(3), pp. 500-513.
- Fang, R. and Strimbu, B.M. (2019) 'Comparison of Mature Douglas-Firs' Crown Structures Developed with Two Quantitative Structural Models Using TLS Point Clouds for Neighboring Trees in a Natural Regime Stand', *Remote Sensing*, 11(14), p. 1661.
- Fang, X. *et al.* (2010) 'Prediction of snowmelt derived streamflow in a wetland dominated prairie basin', *Hydrology and Earth System Sciences*, 14(6), pp. 991-1006.
- Fausch, K.D. *et al.* (2002) 'Landscapes to Riverscapes: Bridging the Gap between Research and Conservation of Stream Fishes: A Continuous View of the River is Needed to Understand How Processes Interacting among Scales Set the Context for Stream Fishes and Their Habitat', *BioScience*, 52(6), pp. 483-498.
- Fawcett, D., Blanco-Sacristán, J. and Benaud, P. (2019) 'Two decades of digital photogrammetry: Revisiting Chandler's 1999 paper on "Effective application of automated digital photogrammetry for geomorphological research" – a synthesis', *Progress in Physical Geography: Earth and Environment*, 43(2), pp. 299-312.

List of References

- Felzenszwalb, P.F. and Huttenlocher, D.P. (2004) 'Efficient Graph-Based Image Segmentation', *International Journal of Computer Vision*, 59(2), pp. 167-181.
- Feng, L. *et al.* (2012). SPIE.
- Ferguson, C. and Fenner, R. (2020) 'The impact of Natural Flood Management on the performance of surface drainage systems: A case study in the Calder Valley', *Journal of Hydrology*, 590, p. 125354.
- Fiorelli, E. *et al.* (2006) 'Multi-AUV control and adaptive sampling in Monterey Bay', *Ieee Journal of Oceanic Engineering*, 31(4), pp. 935-948.
- Fleit, G. *et al.* (2016) 'Investigation of the Effects of Ship Induced Waves on the Littoral Zone with Field Measurements and CFD Modeling', *Water*, 8(7), p. 21.
- Flener, C. *et al.* (2013) 'Seamless Mapping of River Channels at High Resolution Using Mobile LiDAR and UAV-Photography', *Remote Sensing*, 5(12), pp. 6382-6407.
- Flener, C. *et al.* (2015) 'Empirical Modeling of Spatial 3D Flow Characteristics Using a Remote-Controlled ADCP System: Monitoring a Spring Flood', *Water*, 7(1), p. 217.
- Follett, E. and Nepf, H. (2012) 'Sediment patterns near a model patch of reedy emergent vegetation', *Geomorphology*, 179, pp. 141–151.
- Fonstad, M.A. *et al.* (2013) 'Topographic structure from motion: a new development in photogrammetric measurement', *Earth Surface Processes and Landforms*, 38(4), pp. 421-430.
- Forth Rivers Trust (2018) *Monitoring*. Available at: <http://www.fishforth.co.uk/rfft/monitoring/> (Accessed: 21/11/2018).
- Forzieri, G. *et al.* (2011) 'SPECTRAL-ALS DATA FUSION FOR DIFFERENT ROUGHNESS PARAMETERIZATIONS OF FORESTED FLOODPLAINS', *River Research and Applications*, 27(7), pp. 826-840.
- Forzieri, G. *et al.* (2010) 'Riparian Vegetation Mapping for Hydraulic Roughness Estimation Using Very High Resolution Remote Sensing Data Fusion', *Journal of Hydraulic Engineering*, 136(11), pp. 855-867.
- Fox, G.A. *et al.* (2007) 'Measuring streambank erosion due to ground water seepage: correlation to bank pore water pressure, precipitation and stream stage', *Earth Surface Processes and Landforms*, 32(10), pp. 1558-1573.
- Frappart, F. *et al.* (2005) 'Floodplain water storage in the Negro River basin estimated from microwave remote sensing of inundation area and water levels', *Remote Sensing of Environment*, 99(4), pp. 387-399.
- Frasson, R.P.d.M. *et al.* (2019) 'Global Relationships Between River Width, Slope, Catchment Area, Meander Wavelength, Sinuosity, and Discharge', *Geophysical Research Letters*, 46(6), pp. 3252-3262.

- Frölke, G. (2017) 'Validate results of river bends modelled by Delft3D 4 Suite and D-Flow FM'.
- Fu, B.H. and Burgher, I. (2015) 'Riparian vegetation NDVI dynamics and its relationship with climate, surface water and groundwater', *Journal of Arid Environments*, 113, pp. 59-68.
- Fujita, I. and Hino, T. (2003) 'Unseeded and seeded PIV measurements of river flows videotaped from a helicopter', *Journal of Visualization*, 6(3), pp. 245-252.
- Fujita, I. and Kunita, Y. (2011) 'Application of aerial LSPIV to the 2002 flood of the Yodo River using a helicopter mounted high density video camera', *Journal of Hydro-environment Research*, 5(4), pp. 323-331.
- Furquim, G. *et al.* (2018) 'How to Improve Fault Tolerance in Disaster Predictions: A Case Study about Flash Floods Using IoT, ML and Real Data', *Sensors*, 18(3), p. 20.
- Furukawa, Y. and Ponce, J. (2010) 'Accurate, dense, and robust multiview stereopsis', *IEEE transactions on pattern analysis and machine intelligence*, 32(8), pp. 1362-1376.
- Gabrlik, P. (2015) 'The use of direct georeferencing in aerial photogrammetry with micro UAV', *IFAC-PapersOnLine*, 48(4), pp. 380-385.
- Gallay, M. *et al.* (2016) 'HIGH RESOLUTION AIRBORNE LASER SCANNING AND HYPERSPECTRAL IMAGING WITH A SMALL UAV PLATFORM', in Halounova, L. *et al.* (eds.) *XXIII ISPRS Congress, Commission I*. Gottingen: Copernicus Gesellschaft Mbh, pp. 823-827.
- Gao, J.H., Holden, J. and Kirkby, M. (2017) 'Modelling impacts of agricultural practice on flood peaks in upland catchments: An application of the distributed TOPMODEL', *Hydrological Processes*, 31(23), pp. 4206-4216.
- Garnier, E. *et al.* (2006) 'Assessing the Effects of Land-use Change on Plant Traits, Communities and Ecosystem Functioning in Grasslands: A Standardized Methodology and Lessons from an Application to 11 European Sites', *Annals of Botany*, 99(5), pp. 967-985.
- Gaskin, S. *et al.* (2003) 'Erosion of undisturbed clay samples from the banks of the St-Lawrence River', *Canadian Journal of Civil Engineering*, 30, pp. 585-595.
- Geoscience Australia (2018) *Digital Elevation Data*. Available at: <http://www.ga.gov.au/scientific-topics/national-location-information/digital-elevation-data> (Accessed: 21/11/2018).
- Gerritsen, H. *et al.* (2008) *Validation Document Delft3D-FLOW; a software system for 3D flow simulations*.
- Ghose, B., Kar, A. and Husain, Z. (1979) 'The Lost Courses of the Saraswati River in the Great Indian Desert: New Evidence from Landsat Imagery', *The Geographical Journal*, 145(3), pp. 446-451.
- Gilvear, D., Tyler, A. and Davids, C. (2004) 'Detection of estuarine and tidal river hydromorphology using hyper-spectral and LiDAR data: Forth estuary, Scotland', *Estuarine Coastal and Shelf Science*, 61(3), pp. 379-392.

List of References

- Gleason, C., Garambois, P. and Durand, M. (2017) *Tracking River Flows from Space*. Available at: <https://eos.org/project-updates/tracking-river-flows-from-space> (Accessed: 17/05/2019).
- Glennie, C., Kusari, A. and Facchin, A. (2016) 'Calibration and stability analysis of the vlp-16 laser scanner', *The International Archives of Photogrammetry, Remote Sensing and Spatial Information Sciences*, 40, p. 55.
- Gomez Selvaraj, M. *et al.* (2020) 'Detection of banana plants and their major diseases through aerial images and machine learning methods: A case study in DR Congo and Republic of Benin', *ISPRS Journal of Photogrammetry and Remote Sensing*, 169, pp. 110-124.
- Good, J.E.G., Bryant, R. and Carlill, P. (1990) 'Distribution, Longevity and Survival of Upland Hawthorn (*Crataegus monogyna*) Scrub in North Wales in Relation to Sheep Grazing', *Journal of Applied Ecology*, 27(1), pp. 272-283.
- Göthe, E. *et al.* (2017) 'Environmental and spatial controls of taxonomic versus trait composition of stream biota', *Freshwater Biology*, 62(2), pp. 397-413.
- Göthe, E. *et al.* (2016) 'Structural and functional responses of floodplain vegetation to stream ecosystem restoration', *Hydrobiologia*, 769(1), pp. 79-92.
- Graham, D.J., Rice, S.P. and Reid, I. (2005) 'A transferable method for the automated grain sizing of river gravels', *Water Resources Research*, 41(7).
- Gran, K. and Paola, C. (2001) 'Riparian vegetation controls on braided stream dynamics', *Water Resources Research*, 37(12), pp. 3275-3283.
- Greenberg, J.A. *et al.* (2012) 'USING LIDAR DATA ANALYSIS TO ESTIMATE CHANGES IN INSOLATION UNDER LARGE-SCALE RIPARIAN DEFORESTATION', *Journal of the American Water Resources Association*, 48(5), pp. 939-948.
- Gregory, K.J. (2006) 'The human role in changing river channels', *Geomorphology*, 79(3-4), pp. 172-191.
- Gualtieri, C. *et al.* (2018) 'A field study of the confluence between Negro and Solimões Rivers. Part 1: Hydrodynamics and sediment transport', *Comptes Rendus Geoscience*, 350(1), pp. 31-42.
- Gubbi, J. *et al.* (2013) 'Internet of Things (IoT): A vision, architectural elements, and future directions', *Future Generation Computer Systems-the International Journal of Escience*, 29(7), pp. 1645-1660.
- Guerrero, M. and Lamberti, A. (2011) 'Flow Field and Morphology Mapping Using ADCP and Multibeam Techniques: Survey in the Po River', *Journal of Hydraulic Engineering-Asce*, 137(12), pp. 1576-1587.
- Gunawan, B. *et al.* (2012) 'The application of LS-PIV to a small irregular river for inbank and overbank flows', *Flow Measurement and Instrumentation*, 24, pp. 1-12.

- Gupta, N., Atkinson, P.M. and Carling, P.A. (2013) 'Decadal length changes in the fluvial planform of the River Ganga: bringing a mega-river to life with Landsat archives', *Remote Sensing Letters*, 4(1), pp. 1-9.
- Gurnell, A. (2014) 'Plants as river system engineers', *Earth Surface Processes and Landforms*, 39(1), pp. 4-25.
- Gurnell, A.M. and Midgley, P. (1994) 'Aquatic weed growth and flow resistance: Influence on the relationship between discharge and stage over a 25 year river gauging station record', *Hydrological Processes*, 8(1), pp. 63-73.
- Ha, H.K. *et al.* (2009) 'Using ADV backscatter strength for measuring suspended cohesive sediment concentration', *Continental Shelf Research*, 29(10), pp. 1310-1316.
- Haala, N. *et al.* (2011) 'Performance test on UAV-based photogrammetric data collection', *Proceedings of the International Archives of the Photogrammetry, Remote Sensing and Spatial Information Sciences*, 38(1/C22), pp. 7-12.
- Hackenberg, J. *et al.* (2015) 'SimpleTree —An Efficient Open Source Tool to Build Tree Models from TLS Clouds', *Forests*, 6(11), pp. 4245-4294.
- Hackney, C. *et al.* (2015) 'Modulation of outer bank erosion by slump blocks: Disentangling the protective and destructive role of failed material on the three-dimensional flow structure', *Geophysical Research Letters*, 42(24), pp. 10663-10670.
- Harvey, J. and Gooseff, M. (2015) 'River corridor science: Hydrologic exchange and ecological consequences from bedforms to basins', *Water Resources Research*, 51(9), pp. 6893-6922.
- Hauser, D., Glennie, C. and Brooks, B. (2016) 'Calibration and Accuracy Analysis of a Low-Cost Mapping-Grade Mobile Laser Scanning System', *Journal of Surveying Engineering*, 142(4), p. 9.
- Hellweger, F.L. *et al.* (2004) 'Use of satellite imagery for water quality studies in New York Harbor', *Estuarine Coastal and Shelf Science*, 61(3), pp. 437-448.
- Henshaw, A.J. *et al.* (2013) 'An assessment of the degree to which Landsat TM data can support the assessment of fluvial dynamics, as revealed by changes in vegetation extent and channel position, along a large river', *Geomorphology*, 202, pp. 74-85.
- Herbst, M. *et al.* (2007) 'Seasonal and interannual variability of canopy transpiration of a hedgerow in southern England', *Tree Physiology*, 27(3), pp. 321-333.
- Heritage, G. *et al.* (2019) 'Quantifying and contextualising cyclone-driven, extreme flood magnitudes in bedrock-influenced dryland rivers', *Advances in Water Resources*, 123, pp. 145-159.
- Heritage, G. and Hetherington, D. (2007) 'Towards a protocol for laser scanning in fluvial geomorphology', *Earth Surface Processes and Landforms*, 32(1), pp. 66-74.

List of References

- Heritage, G.L. and Milan, D.J. (2009) 'Terrestrial Laser Scanning of grain roughness in a gravel-bed river', *Geomorphology*, 113(1), pp. 4-11.
- Hilldale, R.C. and Raff, D. (2008) 'Assessing the ability of airborne LiDAR to map river bathymetry', *Earth Surface Processes and Landforms*, 33(5), pp. 773-783.
- Himmelstoss, E.A. *et al.* (2018) 'Digital Shoreline Analysis System (version 5.0)' U.S. Geological Survey.
- Hirabayashi, Y. *et al.* (2013) 'Global flood risk under climate change', *Nature Climate Change*, 3(9), pp. 816-821.
- Hodge, R., Brasington, J. and Richards, K. (2009) 'Analysing laser-scanned digital terrain models of gravel bed surfaces: linking morphology to sediment transport processes and hydraulics', *Sedimentology*, 56(7), pp. 2024-2043.
- Hodgkin, S.E. (1984) 'Scrub encroachment and its effects on soil fertility on Newborough Warren, Anglesey, Wales', *Biological Conservation*, 29(2), pp. 99-119.
- Hofle, B. and Rutzinger, M. (2011) 'Topographic airborne LiDAR in geomorphology: A technological perspective', *Zeitschrift Fur Geomorphologie*, 55, pp. 1-29.
- Horritt, M.S., Mason, D.C. and Luckman, A.J. (2001) 'Flood boundary delineation from Synthetic Aperture Radar imagery using a statistical active contour model', *International Journal of Remote Sensing*, 22(13), pp. 2489-2507.
- Hortobágyi, B. *et al.* (2017) 'Above-and belowground responses of *Populus nigra* L. to mechanical stress observed on the Allier River, France', *Géomorphologie: relief, processus, environnement*, 23(3), pp. 219-231.
- Hortobágyi, B. *et al.* (2018) 'Niche construction within riparian corridors. Part I: Exploring biogeomorphic feedback windows of three pioneer riparian species (Allier River, France)', *Geomorphology*, 305, pp. 94-111.
- Hossain, M.A., Gan, T.Y. and Baki, A.B.M. (2013) 'Assessing morphological changes of the Ganges River using satellite images', *Quaternary International*, 304, pp. 142-155.
- Houborg, R., Fisher, J.B. and Skidmore, A.K. (2015) 'Advances in remote sensing of vegetation function and traits', *International Journal of Applied Earth Observation and Geoinformation*, 43, pp. 1-6.
- Howden, D. (2009) 'Continuous Swarm Surveillance via Distributed Priority Maps', in Korb, K., Randall, M. and Hendtlass, T. (eds.) *Artificial Life: Borrowing from Biology, Proceedings*. Berlin: Springer-Verlag Berlin, pp. 221-231.
- HR Wallingford (2014) *ARC-Boat delivers benefits for the Environment Agency*. Available at: <http://www.hrwallingford.com/news/arc-boats-delivers-benefits-for-environment-agency> (Accessed: 12/12/2018).

- Huang, H.Q. and Nanson, G.C. (1998) 'The influence of bank strength on channel geometry: an integrated analysis of some observations', *Earth Surface Processes and Landforms*, 23(10), pp. 865-876.
- Hughes, A.O. (2016) 'Riparian management and stream bank erosion in New Zealand', *New Zealand Journal of Marine and Freshwater Research*, 50(2), pp. 277-290.
- Hupp, C.R. and Osterkamp, W. (1996) 'Riparian vegetation and fluvial geomorphic processes', *Geomorphology*, 14(4), pp. 277-295.
- Hyde, K.D. *et al.* (2016) 'Influences of vegetation disturbance on hydrogeomorphic response following wildfire', *Hydrological Processes*, 30(7), pp. 1131-1148.
- Iglhaut, J. *et al.* (2019) 'Structure from Motion Photogrammetry in Forestry: a Review', *Current Forestry Reports*, 5(3), pp. 155-168.
- Isikdogan, F., Bovik, A. and Passalacqua, P. (2015) 'Automatic Channel Network Extraction From Remotely Sensed Images by Singularity Analysis', *Ieee Geoscience and Remote Sensing Letters*, 12(11), pp. 2218-2221.
- Islam, A. and Guchhait, S.K. (2017) 'Search for social justice for the victims of erosion hazard along the banks of river Bhagirathi by hydraulic control: a case study of West Bengal, India', *Environment Development and Sustainability*, 19(2), pp. 433-459.
- Istanbulluoglu, E. and Bras, R.L. (2005) 'Vegetation-modulated landscape evolution: Effects of vegetation on landscape processes, drainage density, and topography', *Journal of Geophysical Research: Earth Surface*, 110(F2).
- Jaakkola, A. *et al.* (2010) 'A low-cost multi-sensoral mobile mapping system and its feasibility for tree measurements', *Isprs Journal of Photogrammetry and Remote Sensing*, 65(6), pp. 514-522.
- Jaakkola, A. *et al.* (2017) 'Autonomous Collection of Forest Field Reference-The Outlook and a First Step with UAV Laser Scanning', *Remote Sensing*, 9(8), p. 12.
- Jackson, B.M. *et al.* (2008) 'The impact of upland land management on flooding: insights from a multiscale experimental and modelling programme', *Journal of Flood Risk Management*, 1(2), pp. 71-80.
- Jacobs, J.M. *et al.* (2021) 'Snow depth mapping with unpiloted aerial system lidar observations: a case study in Durham, New Hampshire, United States', *The Cryosphere*, 15(3), pp. 1485-1500.
- Jalonen, J., Järvelä, J. and Aberle, J. (2012) 'Leaf area index as vegetation density measure for hydraulic analyses', *Journal of Hydraulic Engineering*, 139(5), pp. 461-469.
- Jalonen, J. *et al.* (2014) 'Deriving Floodplain Topography and Vegetation Characteristics for Hydraulic Engineering Applications by Means of Terrestrial Laser Scanning', *Journal of Hydraulic Engineering*, 140(11), p. 12.

List of References

- Jalonen, J. *et al.* (2015) 'Determining Characteristic Vegetation Areas by Terrestrial Laser Scanning for Floodplain Flow Modeling', *Water*, 7(2), pp. 420-437.
- James, C.S. *et al.* (2008) 'Influence of foliage on flow resistance of emergent vegetation', *Journal of Hydraulic Research*, 46(4), pp. 536-542.
- James, L.A. *et al.* (2012) 'Geomorphic change detection using historic maps and DEM differencing: The temporal dimension of geospatial analysis', *Geomorphology*, 137(1), pp. 181-198.
- James, M.R. and Robson, S. (2012) 'Straightforward reconstruction of 3D surfaces and topography with a camera: Accuracy and geoscience application', *Journal of Geophysical Research-Earth Surface*, 117, p. 17.
- James, M.R. and Robson, S. (2014) 'Mitigating systematic error in topographic models derived from UAV and ground-based image networks', *Earth Surface Processes and Landforms*, 39(10), pp. 1413-1420.
- Järvelä, J. (2002a) 'Determination of flow resistance of vegetated channel banks and floodplains', *River Flow 2002*, pp. 311-318.
- Järvelä, J. (2002b) 'Flow resistance of flexible and stiff vegetation: a flume study with natural plants', *Journal of Hydrology*, 269(1), pp. 44-54.
- Järvelä, J. (2004) 'Determination of flow resistance caused by non-submerged woody vegetation', *International Journal of River Basin Management*, 2(1), pp. 61-70.
- Javernick, L., Brasington, J. and Caruso, B. (2014) 'Modeling the topography of shallow braided rivers using Structure-from-Motion photogrammetry', *Geomorphology*, 213, pp. 166-182.
- Javernick, L.A. (2013) 'Modeling flood-induced processes causing Russell lupin mortality in the braided Ahuriri River, New Zealand'.
- Jeffries, R., Darby, S.E. and Sear, D.A. (2003) 'The influence of vegetation and organic debris on floodplain sediment dynamics: case study of a low-order stream in the New Forest, England', *Geomorphology*, 51(1), pp. 61-80.
- Jha, S.K., Mariethoz, G. and Kelly, B.F.J. (2013) 'Bathymetry fusion using multiple-point geostatistics: Novelty and challenges in representing non-stationary bedforms', *Environmental Modelling & Software*, 50, pp. 66-76.
- Jodeau, M. *et al.* (2008) 'Application and evaluation of LS-PIV technique for the monitoring of river surface velocities in high flow conditions', *Flow Measurement and Instrumentation*, 19(2), pp. 117-127.
- Johansen, K., Phinn, S. and Witte, C. (2010) 'Mapping of riparian zone attributes using discrete return LiDAR, QuickBird and SPOT-5 imagery: Assessing accuracy and costs', *Remote Sensing of Environment*, 114(11), pp. 2679-2691.

- Jones, A.F. *et al.* (2007) 'High-resolution interpretative geomorphological mapping of river valley environments using airborne LiDAR data', *Earth Surface Processes and Landforms*, 32(10), pp. 1574-1592.
- Julian, J.P. and Torres, R. (2006) 'Hydraulic erosion of cohesive riverbanks', *Geomorphology*, 76(1), pp. 193-206.
- Jung, H.C. *et al.* (2010) 'Characterization of complex fluvial systems using remote sensing of spatial and temporal water level variations in the Amazon, Congo, and Brahmaputra Rivers', *Earth Surface Processes and Landforms*, 35(3), pp. 294-304.
- Jupiter, S.D. and Marion, G.S. (2008) 'Changes in forest area along stream networks in an agricultural catchment of the Great Barrier Reef Lagoon', *Environmental Management*, 42(1), pp. 66-79.
- Kail, J. *et al.* (2007) 'The use of large wood in stream restoration: experiences from 50 projects in Germany and Austria', *Journal of Applied Ecology*, 44(6), pp. 1145-1155.
- Kang, R.S. (2012) 'GEOMORPHIC EFFECTS OF MOSSES IN A LOW-ORDER STREAM IN FAIRFAX COUNTY, VIRGINIA', *Physical Geography*, 33(4), pp. 360-382.
- Karaim, M., Elsheikh, M. and Noureldin, A. (2018) *GNSS Error Sources* (Accessed: 17/11/2021).
- Karim, F. *et al.* (2012) 'Modelling wetland connectivity during overbank flooding in a tropical floodplain in north Queensland, Australia', *Hydrological Processes*, 26(18), pp. 2710-2723.
- Kasprak, A. *et al.* (2012) 'A LIDAR-DERIVED EVALUATION OF WATERSHED-SCALE LARGE WOODY DEBRIS SOURCES AND RECRUITMENT MECHANISMS: COASTAL MAINE, USA', *River Research and Applications*, 28(9), pp. 1462-1476.
- Kasvi, E. *et al.* (2019) 'Comparison of remote sensing based approaches for mapping bathymetry of shallow, clear water rivers', *Geomorphology*, 333, pp. 180-197.
- Kattge, J. *et al.* (2020) 'TRY plant trait database – enhanced coverage and open access', *Global Change Biology*, 26(1), pp. 119-188.
- Kattge, J. *et al.* (2011) 'TRY—a global database of plant traits', *Global change biology*, 17(9), pp. 2905-2935.
- Kessler, A.C. *et al.* (2012) 'Lidar Quantification of Bank Erosion in Blue Earth County, Minnesota', *Journal of Environmental Quality*, 41(1), pp. 197-207.
- Khorram, S. *et al.* (2016) 'Future Trends in Remote Sensing', in *Principles of Applied Remote Sensing*. Cham: Springer International Publishing, pp. 277-285.
- Kim, S.J. and Stoesser, T. (2011) 'Closure modeling and direct simulation of vegetation drag in flow through emergent vegetation', *Water Resources Research*, 47(10).

List of References

- Kim, Y. and Bang, H. (2018) 'Introduction to Kalman Filter and Its Applications', in *Introduction and Implementations of the Kalman Filter*. Intech Open.
- Kinoshita, R. (1967) 'An Analysis of the Movement of Flood Waters by Aerial Photography Concerning Characteristics of Turbulence and Surface Flow', *Journal of the Japan society of photogrammetry*, 6(1), pp. 1-17.
- Kinzel, P.J. and Legleiter, C.J. (2019) 'sUAS-based remote sensing of river discharge using thermal particle image velocimetry and bathymetric lidar', *Remote Sensing*, 11(19), p. 2317.
- Kinzel, P.J., Legleiter, C.J. and Nelson, J.M. (2013) 'Mapping river bathymetry with a small footprint green LiDAR: Applications and challenges', *JAWRA Journal of the American Water Resources Association*, 49(1), pp. 183-204.
- Kinzel, P.J. *et al.* (2007) 'Evaluation of an experimental LiDAR for surveying a shallow, braided, sand-bedded river', *Journal of Hydraulic Engineering*, 133(7), pp. 838-842.
- Kongsberg (2013) *Application Note: Complete portable integrated solution for Laser Scanner (LiDAR 3D) and Multibeam Bathymetric Survey System (TOPO-BATHY)*. Available at: [https://www.km.kongsberg.com/ks/web/nokbg0397.nsf/AllWeb/0C80D888A970C502C1257C75004B91F6/\\$file/Application_Note_Integrating-multibeam-bathymetry-and-LiDAR-3D-data.pdf?OpenElement](https://www.km.kongsberg.com/ks/web/nokbg0397.nsf/AllWeb/0C80D888A970C502C1257C75004B91F6/$file/Application_Note_Integrating-multibeam-bathymetry-and-LiDAR-3D-data.pdf?OpenElement) (Accessed: 01/11/2018).
- Konsoer, K. *et al.* (2017) 'Length scales and statistical characteristics of outer bank roughness for large elongate meander bends: The influence of bank material properties, floodplain vegetation and flow inundation', *Earth Surface Processes and Landforms*, 42(13), pp. 2024-2037.
- Kourgialas, N.N. and Karatzas, G.P. (2013) 'A hydro-economic modelling framework for flood damage estimation and the role of riparian vegetation', *Hydrological Processes*, 27(4), pp. 515-531.
- Kraus, K. (2007) *Photogrammetry: geometry from images and laser scans*. Berlin: Walter de Gruyter.
- Krieger, G. *et al.* (2007) 'TanDEM-X: A satellite formation for high-resolution SAR interferometry', *IEEE Transactions on Geoscience and Remote Sensing*, 45(11), pp. 3317-3341.
- Krisanski, S. *et al.* (2021) 'Forest Structural Complexity Tool—An Open Source, Fully-Automated Tool for Measuring Forest Point Clouds', *Remote Sensing*, 13(22), p. 4677.
- Kruger, D. *et al.* (2007) 'Optimal AUV path planning for extended missions in complex, fast-flowing estuarine environments', in *Proceedings of the 2007 Ieee International Conference on Robotics and Automation, Vols 1-10*. New York: Ieee, pp. 4265-+.
- Kuenzer, C. *et al.* (2013) 'Flood Mapping and Flood Dynamics of the Mekong Delta: ENVISAT-ASAR-WSM Based Time Series Analyses', *Remote Sensing*, 5(2), p. 687.

- Kuenzer, C. *et al.* (2015) 'Remote Sensing of River Delta Inundation: Exploiting the Potential of Coarse Spatial Resolution, Temporally-Dense MODIS Time Series', *Remote Sensing*, 7(7), pp. 8516-8542.
- Kummu, M. *et al.* (2011) 'How close do we live to water? A global analysis of population distance to freshwater bodies', *PloS one*, 6(6), pp. e20578-e20578.
- Kummu, M. *et al.* (2008) 'Riverbank changes along the Mekong River: Remote sensing detection in the Vientiane–Nong Khai area', *Quaternary International*, 186(1), pp. 100-112.
- Kyle, G. and Leishman, M.R. (2009) 'Plant functional trait variation in relation to riparian geomorphology: The importance of disturbance', *Austral Ecology*, 34(7), pp. 793-804.
- Lague, D. (2020) 'Chapter 8 - Terrestrial laser scanner applied to fluvial geomorphology', in Tarolli, P. and Mudd, S.M. (eds.) *Developments in Earth Surface Processes*. Amsterdam, The Netherlands: Elsevier, pp. 231-254.
- Lague, D., Brodu, N. and Leroux, J. (2013) 'Accurate 3D comparison of complex topography with terrestrial laser scanner: Application to the Rangitikei canyon (NZ)', *ISPRS journal of photogrammetry and remote sensing*, 82, pp. 10-26.
- Lallias-Tacon, S., Liebault, F. and Piegay, H. (2014) 'Step by step error assessment in braided river sediment budget using airborne LiDAR data', *Geomorphology*, 214, pp. 307-323.
- Lane, S.N. (2017) 'Natural flood management', *Wiley Interdisciplinary Reviews-Water*, 4(3), p. 14.
- Lane, S.N. *et al.* (1998) 'Three-dimensional measurement of river channel flow processes using acoustic Doppler velocimetry', *Earth Surface Processes and Landforms*, 23(13), pp. 1247-1267.
- Langhammer, J. *et al.* (2017) 'UAV-Based Optical Granulometry as Tool for Detecting Changes in Structure of Flood Depositions', *Remote Sensing*, 9(3), p. 240.
- Langhammer, J. and Vackova, T. (2018) 'Detection and Mapping of the Geomorphic Effects of Flooding Using UAV Photogrammetry', *Pure and Applied Geophysics*, 175(9), pp. 3223-3245.
- Larson, M.D. *et al.* (2018) 'Multi-depth suspended sediment estimation using high-resolution remote-sensing UAV in Maumee River, Ohio', *International Journal of Remote Sensing*, 39(15-16), pp. 5472-5489.
- Lawless, M. and Robert, A. (2001) 'Three-dimensional flow structure around small-scale bedforms in a simulated gravel-bed environment', *Earth Surface Processes and Landforms*, 26(5), pp. 507-522.
- Lawson, J.R. *et al.* (2015) 'Heterogeneous flows foster heterogeneous assemblages: relationships between functional diversity and hydrological heterogeneity in riparian plant communities', *Freshwater Biology*, 60(11), pp. 2208-2225.
- Lee, C.S. and Hsiao, F.B. (2012) 'Implementation of vision-based automatic guidance system on a fixed-wing unmanned aerial vehicle', *Aeronautical Journal*, 116(1183), pp. 895-914.

List of References

- Lega, M. *et al.* (2012) 'Using Advanced Aerial Platforms and Infrared Thermography to Track Environmental Contamination', *Environmental Forensics*, 13(4), pp. 332-338.
- Lega, M. and Napoli, R.M.A. (2010) 'Aerial infrared thermography in the surface waters contamination monitoring', *Desalination and Water Treatment*, 23(1-3), pp. 141-151.
- Legleiter, C.J. (2012) 'Remote measurement of river morphology via fusion of LiDAR topography and spectrally based bathymetry', *Earth Surface Processes and Landforms*, 37(5), pp. 499-518.
- Legleiter, C.J. and Fosness, R.L. (2019) 'Defining the Limits of Spectrally Based Bathymetric Mapping on a Large River', *Remote Sensing*, 11(6), p. 665.
- Legleiter, C.J., Kinzel, P.J. and Nelson, J.M. (2017) 'Remote measurement of river discharge using thermal particle image velocimetry (PIV) and various sources of bathymetric information', *Journal of Hydrology*, 554, pp. 490-506.
- Legleiter, C.J. *et al.* (2016) 'Evaluating the capabilities of the CASI hyperspectral imaging system and Aquarius bathymetric LiDAR for measuring channel morphology in two distinct river environments', *Earth Surface Processes and Landforms*, 41(3), pp. 344-363.
- Lejot, J. *et al.* (2007) 'Very high spatial resolution imagery for channel bathymetry and topography from an unmanned mapping controlled platform', *Earth Surface Processes and Landforms*, 32(11), pp. 1705-1725.
- Leopold, L.B. and Langbein, W.B. (1966) 'River meanders', *Scientific American*, 214(6), pp. 60-73.
- Lesser, G.R. *et al.* (2004) 'Development and validation of a three-dimensional morphological model', *Coastal Engineering*, 51(8), pp. 883-915.
- Leyland, J. *et al.* (2015) 'A self-limiting bank erosion mechanism? inferring temporal variations in bank form and skin drag from high resolution topographic data', *Earth Surface Processes and Landforms*, 40(12), pp. 1600-1615.
- Leyland, J. *et al.* (2017) 'Extreme flood-driven fluvial bank erosion and sediment loads: direct process measurements using integrated Mobile Laser Scanning (MLS) and hydro-acoustic techniques', *Earth Surface Processes and Landforms*, 42(2), pp. 334-346.
- Li, Q. *et al.* (2012) 'AUV Rolling Motion Control in Inland Rivers Based on Sliding Mode Control Improved by Artificial Immunity Algorithm', in Tan, R.H., Sun, J. and Liu, Q.S. (eds.) *Automatic Manufacturing Systems Ii, Pts 1 and 2*. Stafa-Zurich: Trans Tech Publications Ltd, pp. 1150-1154.
- Lightbody, A.F. and Nepf, H.M. (2006) 'Prediction of near-field shear dispersion in an emergent canopy with heterogeneous morphology', *Environmental Fluid Mechanics*, 6(5), pp. 477-488.
- Lin, Y.-C. *et al.* (2019) 'Evaluation of UAV LiDAR for Mapping Coastal Environments', *Remote Sensing*, 11(24), p. 2893.

- Lin, Y., Hyyppa, J. and Jaakkola, A. (2011) 'Mini-UAV-Borne LIDAR for Fine-Scale Mapping', *Ieee Geoscience and Remote Sensing Letters*, 8(3), pp. 426-430.
- Lin, Y.C. and Saripalli, S. (2012) 'Road Detection and Tracking from Aerial Desert Imagery', *Journal of Intelligent & Robotic Systems*, 65(1-4), pp. 345-359.
- Lindberg, E. *et al.* (2012) 'Estimation of stem attributes using a combination of terrestrial and airborne laser scanning', *European Journal of Forest Research*, 131(6), pp. 1917-1931.
- Loicq, P. *et al.* (2018) 'Improving representation of riparian vegetation shading in a regional stream temperature model using LiDAR data', *Science of the Total Environment*, 624, pp. 480-490.
- Longbotham, N. *et al.* (2014) *2014 6th Workshop on Hyperspectral Image and Signal Processing: Evolution in Remote Sensing (WHISPERS)*. 24-27 June 2014.
- Lotsari, E. *et al.* (2015) 'Gravel transport by ice in a subarctic river from accurate laser scanning', *Geomorphology*, 246, pp. 113-122.
- Lowe, D.G. (1999) *Computer vision, 1999. The proceedings of the seventh IEEE international conference on Computer Vision, Kerkyra, Greece, 20-27 September 1999*. Ieee.
- Lu, C.D. *et al.* (2006) 'QUANTITATIVE MODELING OF SUSPENDED SEDIMENT IN MIDDLE CHANGJIANG RIVER FROM MODIS', *Chinese Geographical Science*, 16(1), pp. 79-82.
- Lucieer, V. *et al.* (2013) 'Do marine substrates 'look' and 'sound' the same? Supervised classification of multibeam acoustic data using autonomous underwater vehicle images', *Estuarine Coastal and Shelf Science*, 117, pp. 94-106.
- Lukacs, B.A. *et al.* (2019) 'Carbon forms, nutrients and water velocity filter hydrophyte and riverbank species differently: A trait-based study', *Journal of Vegetation Science*, 30(3), pp. 471-484.
- Lytle, D.A. *et al.* (2017) 'Linking river flow regimes to riparian plant guilds: a community-wide modeling approach', *Ecological applications*, 27(4), pp. 1338-1350.
- Ma, L., Wang, X. and Li, S. (2019) 'Accuracy analysis of GPS broadcast ephemeris in the 2036th GPS week', *IOP Conference Series: Materials Science and Engineering*, 631, p. 042013.
- Macedo, M.N. *et al.* (2013) 'Land-use-driven stream warming in southeastern Amazonia', *Philosophical Transactions of the Royal Society B-Biological Sciences*, 368(1619), p. 9.
- Mader, D. *et al.* (2015) 'UAV-BASED ACQUISITION OF 3D POINT CLOUD - A COMPARISON OF A LOW-COST LASER SCANNER AND SFM-TOOLS', in Mallet, C. *et al.* (eds.) *Isprs Geospatial Week 2015*. Gottingen: Copernicus Gesellschaft Mbh, pp. 335-341.

List of References

- Magdaleno, F. and Fernandez-Yuste, J.A. (2011) 'Meander dynamics in a changing river corridor', *Geomorphology*, 130(3-4), pp. 197-207.
- Maier, K.L. *et al.* (2013) 'Deep-sea channel evolution and stratigraphic architecture from inception to abandonment from high-resolution Autonomous Underwater Vehicle surveys offshore central California', *Sedimentology*, 60(4), pp. 935-960.
- Makkeasorn, A., Chang, N.B. and Li, J.H. (2009) 'Seasonal change detection of riparian zones with remote sensing images and genetic programming in a semi-arid watershed', *Journal of Environmental Management*, 90(2), pp. 1069-1080.
- Malard, F. *et al.* (2002) 'A landscape perspective of surface-subsurface hydrological exchanges in river corridors', *Freshwater Biology*, 47(4), pp. 621-640.
- Malek, S.A. *et al.* (2017) 'Real-Time Alpine Measurement System Using Wireless Sensor Networks', *Sensors*, 17(11), p. 30.
- Mancini, A. *et al.* (2015) 'High-resolution mapping of river and estuary areas by using unmanned aerial and surface platforms', *Unmanned Aircraft Systems (ICUAS), 2015 International Conference on*. IEEE, pp. 534-542.
- Mandlburger, G. *et al.* (2015) 'Complementing airborne laser bathymetry with UAV-based lidar for capturing alluvial landscapes', *Remote Sensing for Agriculture, Ecosystems, and Hydrology XVII*, 9637, p. 96370A.
- Mangiarotti, S. *et al.* (2013) 'Discharge and suspended sediment flux estimated along the mainstream of the Amazon and the Madeira Rivers (from in situ and MODIS Satellite Data)', *International Journal of Applied Earth Observation and Geoinformation*, 21, pp. 341-355.
- Manners, R., Schmidt, J. and Wheaton, J.M. (2013) 'Multiscalar model for the determination of spatially explicit riparian vegetation roughness', *Journal of Geophysical Research-Earth Surface*, 118(1), pp. 65-83.
- Manners, R.B. *et al.* (2015) 'When do plants modify fluvial processes? Plant-hydraulic interactions under variable flow and sediment supply rates', *Journal of Geophysical Research: Earth Surface*, 120(2), pp. 325-345.
- Marchamalo, M. *et al.* (2007) 'Fish habitat characterization and quantification using LIDAR and conventional topographic information in river survey', in Neale, C.M.U., Owe, M. and Durso, G. (eds.) *Remote Sensing for Agriculture, Ecosystems, and Hydrology Ix*. Bellingham: Spie-Int Soc Optical Engineering.
- Marchetti, Z.Y. *et al.* (2020) 'Vegetation and hydrogeomorphic features of a large lowland river: NDVI patterns summarizing fluvial dynamics and supporting interpretations of ecological patterns', *Earth Surface Processes and Landforms*, 45(3), pp. 694-706.
- Marcus, W.A. and Fonstad, M.A. (2010) 'Remote sensing of rivers: the emergence of a subdiscipline in the river sciences', *Earth Surface Processes and Landforms*, 35(15), pp. 1867-1872.

- Marteau, B. *et al.* (2017) 'Application of Structure-from-Motion photogrammetry to river restoration', *Earth Surface Processes and Landforms*, 42(3), pp. 503-515.
- Martinez, J.M. and Le Toan, T. (2007) 'Mapping of flood dynamics and spatial distribution of vegetation in the Amazon floodplain using multitemporal SAR data', *Remote Sensing of Environment*, 108(3), pp. 209-223.
- Martinez, K. *et al.* (2017) 'A geophone wireless sensor network for investigating glacier stick-slip motion', *Computers & Geosciences*, 105, pp. 103-112.
- Martinis, S., Kersten, J. and Twele, A. (2015) 'A fully automated TerraSAR-X based flood service', *ISPRS Journal of Photogrammetry and Remote Sensing*, 104, pp. 203-212.
- McCabe, M.F. *et al.* (2017) 'The Future of Earth Observation in Hydrology', *Hydrology and earth system sciences*, 21(7), pp. 3879-3914.
- McClinton, J.T. and White, S.M. (2015) 'Emplacement of submarine lava flow fields: A geomorphological model from the Ninós eruption at the Galapagos Spreading Center', *Geochemistry Geophysics Geosystems*, 16(3), pp. 899-911.
- McCoy-Sulentic, M.E. *et al.* (2017) 'Changes in Community-Level Riparian Plant Traits over Inundation Gradients, Colorado River, Grand Canyon', *Wetlands*, 37(4), pp. 635-646.
- McGill, B.J. *et al.* (2006) 'Rebuilding community ecology from functional traits', *Trends in ecology & evolution*, 21(4), pp. 178-185.
- McMahon, J.M. *et al.* (2017) 'An investigation of controlling variables of riverbank erosion in sub-tropical Australia', *Environmental Modelling & Software*, 97, pp. 1-15.
- Medeiros, S.C., Hagen, S.C. and Weishampel, J.F. (2012) 'Comparison of floodplain surface roughness parameters derived from land cover data and field measurements', *Journal of Hydrology*, 452-453, pp. 139-149.
- Meer, C. *et al.* (2011) 'Numerical simulations of upstream and downstream overdeepening', *Oikos*.
- Mertes, L.A.K. (2002) 'Remote sensing of riverine landscapes', *Freshwater Biology*, 47(4), pp. 799-816.
- Mian, O. *et al.* (2015) 'Direct georeferencing on small unmanned aerial platforms for improved reliability and accuracy of mapping without the need for ground control points', *The International Archives of Photogrammetry, Remote Sensing and Spatial Information Sciences*, 40(1), p. 397.
- MicaSense (2018) *RedEdge MX Integration Guide*. Available at: <https://support.micasense.com/hc/en-us/articles/215924497-RedEdge-Integration-Guide> (Accessed: 17/11/2021).
- MicaSense (2021) *RedEdge-MX*. Available at: <https://micasense.com/rededge-mx/> (Accessed: 17/11/2021).

List of References

- Micheletti, N., Chandler, J, Lane, S (2015) 'Structure from Motion (SfM) Photogrammetry', in Cook, S., Clarke, I, Nield, J (ed.) *Geomorphological Techniques*. London: British Society for Geomorphology.
- Michez, A. *et al.* (2017) 'Multi-temporal monitoring of a regional riparian buffer network (>12,000 km) with LiDAR and photogrammetric point clouds', *Journal of Environmental Management*, 202, pp. 424-436.
- Michez, A. *et al.* (2013) 'LiDAR derived ecological integrity indicators for riparian zones: Application to the Houille river in Southern Belgium/Northern France', *Ecological Indicators*, 34, pp. 627-640.
- Michta, E. *et al.* (2017) 'IoT based flood embankments monitoring system', in Romaniuk, R.S. and Linczuk, M. (eds.) *Photonics Applications in Astronomy, Communications, Industry, and High Energy Physics Experiments 2017*. Bellingham: Spie-Int Soc Optical Engineering.
- Milan, D., Heritage, G. and Hetherington, D. (2007) 'Application of a 3D laser scanner in the assessment of erosion and deposition volumes and channel change in a proglacial river', *Earth Surface Processes and Landforms*, 32(11), pp. 1657-1674.
- Millar, R.G. and Quick, M.C. (1998) 'Stable Width and Depth of Gravel-Bed Rivers with Cohesive Banks', *Journal of Hydraulic Engineering*, 124(10), pp. 1005-1013.
- Miorandi, D. *et al.* (2012) 'Internet of things: Vision, applications and research challenges', *Ad Hoc Networks*, 10(7), pp. 1497-1516.
- Mirijovský, J. and Langhammer, J. (2015) 'Multitemporal monitoring of the morphodynamics of a mid-mountain stream using UAS photogrammetry', *Remote Sensing*, 7(7), pp. 8586-8609.
- Mirijovsky, J. and Vavra, A. (2012) 'UAV photogrammetry in fluvial geomorphology', in *12th International Multidisciplinary Scientific Geoconference, Sgem 2012, Vol. Ii*. Sofia: Stef92 Technology Ltd, pp. 909-916.
- Mitra, P. *et al.* (2016) *Flood forecasting using Internet of things and Artificial Neural Networks*. New York: Ieee. 7th Ieee Annual Information Technology, Electronics & Mobile Communication Conference Ieee Iemcon-2016.
- Moerman, E. (2010) *Delft 3D Bed Composition*. Available at: https://oss.deltares.nl/documents/portlet_file_entry/183920/Delft3D_Bed_Composition.doc/ba6d997a-d741-455f-a911-9a293464db92?download=true (Accessed: 05/05/2021).
- Moretto, J. *et al.* (2014) 'Short-term geomorphic analysis in a disturbed fluvial environment by fusion of LiDAR, colour bathymetry and dGPS surveys', *Catena*, 122, pp. 180-195.
- Morgan, J.A., Brogan, D.J. and Nelson, P.A. (2017) 'Application of Structure-from-Motion photogrammetry in laboratory flumes', *Geomorphology*, 276, pp. 125-143.
- Mostafa, M. (2002) *Proceedings, ASPRS Annual Meeting, Washington, DC, 22 April*.

- Mostafa, M. and Hutton, J. (2001) *Proceedings, The American Society of photogrammetry and remote sensing annual meeting, St. Louis, MO, USA, April.*
- Muller, E. (1997) 'Mapping riparian vegetation along rivers: old concepts and new methods', *Aquatic Botany*, 58(3), pp. 411-437.
- Muste, M., Yu, K. and Spasojevic, M. (2004) 'Practical aspects of ADCP data use for quantification of mean river flow characteristics; Part I: moving-vessel measurements', *Flow Measurement and Instrumentation*, 15(1), pp. 1-16.
- Myint, S.W. *et al.* (2011) 'Per-pixel vs. object-based classification of urban land cover extraction using high spatial resolution imagery', *Remote Sensing of Environment*, 115(5), pp. 1145-1161.
- Nagai, M. *et al.* (2009) 'UAV-Borne 3-D Mapping System by Multisensor Integration', *Ieee Transactions on Geoscience and Remote Sensing*, 47(3), pp. 701-708.
- Nagai, M. *et al.* (2004) *Proceedings of the ISPRS Congress, Geo-Imagery Bridging Continents, Istanbul, Turkey, 12–23 July 2004.*
- Nagler, P.L. *et al.* (2005) 'Predicting riparian evapotranspiration from MODIS vegetation indices and meteorological data', *Remote Sensing of Environment*, 94(1), pp. 17-30.
- Naiman, R.J. *et al.* (2005) 'Origins, patterns, and importance of heterogeneity in riparian systems', in *Ecosystem function in heterogeneous landscapes*. Springer, pp. 279-309.
- Naiman, R.J., Decamps, H. and Pollock, M. (1993) 'THE ROLE OF RIPARIAN CORRIDORS IN MAINTAINING REGIONAL BIODIVERSITY', *Ecological Applications*, 3(2), pp. 209-212.
- Nakano, K. *et al.* (2018) 'On A Fundamental Evaluation Of A Uav Equipped With A Multichannel Laser Scanner', *ISPRS - International Archives of the Photogrammetry, Remote Sensing and Spatial Information Sciences*, 42(2), pp. 753-758.
- Nallaperuma, B. and Asaeda, T. (2020) 'The long-term legacy of riparian vegetation in a hydrogeomorphologically remodelled fluvial setting', *River Research and Applications*, 36(8), pp. 1690-1700.
- NASA (2019a) *Hydrology*. Available at: <https://swot.jpl.nasa.gov/hydrology.htm> (Accessed: 17/05/2019).
- NASA (2019b) *Water: Sustaining Life*. Available at: <https://nisar.jpl.nasa.gov/missionthemes/water/> (Accessed: 17/05/2019).
- National Trust (2018) *River Ouse at Sheffield Park*. Available at: <https://www.nationaltrust.org.uk/sheffield-park-and-garden/features/river-ouse-at-sheffield-park> (Accessed: 21/11/2018).

List of References

- Nepf, H.M. and Vivoni, E.R. (2000) 'Flow structure in depth-limited, vegetated flow', *Journal of Geophysical Research: Oceans*, 105(C12), pp. 28547-28557.
- Nigam, N. *et al.* (2012) 'Control of Multiple UAVs for Persistent Surveillance: Algorithm and Flight Test Results', *Ieee Transactions on Control Systems Technology*, 20(5), pp. 1236-1251.
- Noarayanan, L., Murali, K. and Sundar, V. (2012) 'Manning's 'n' co-efficient for flexible emergent vegetation in tandem configuration', *Journal of Hydro-environment Research*, 6(1), pp. 51-62.
- O'hare, J. *et al.* (2011) 'Physical constraints on the distribution of macrophytes linked with flow and sediment dynamics in British rivers', *River Research and Applications*, 27(6), pp. 671-683.
- O'Hare, M. *et al.* (2016) 'Plant traits relevant to fluvial geomorphology and hydrological interactions', *River Research and Applications*, 32(2), pp. 179-189.
- O'Neal, M.A. and Pizzuto, J.E. (2011) 'The rates and spatial patterns of annual riverbank erosion revealed through terrestrial laser-scanner surveys of the South River, Virginia', *Earth Surface Processes and Landforms*, 36(5), pp. 695-701.
- O'Briain, R., Shephard, S. and Coghlan, B. (2017) 'Pioneer macrophyte species engineer fine-scale physical heterogeneity in a shallow lowland river', *Ecological Engineering*, 102, pp. 451-458.
- O'Hare, M.T. *et al.* (2010) 'Variability in roughness measurements for vegetated rivers near base flow, in England and Scotland', *Journal of Hydrology*, 385(1), pp. 361-370.
- Odonkor, P. *et al.* (2017) 'A DISTRIBUTED INTELLIGENCE APPROACH TO USING COLLABORATING UNMANNED AERIAL VEHICLES FOR OIL SPILL MAPPING', in *Proceedings of the Asme International Design Engineering Technical Conferences and Computers and Information in Engineering Conference, 2017, Vol 2a*. New York: Amer Soc Mechanical Engineers.
- Ollero, A. (2010) 'Channel changes and floodplain management in the meandering middle Ebro River, Spain', *Geomorphology*, 117(3-4), pp. 247-260.
- Oorschot, M.v. *et al.* (2016) 'Distinct patterns of interaction between vegetation and morphodynamics', *Earth Surface Processes and Landforms*, 41(6), pp. 791-808.
- Ortiz, A., Simo, M. and Oliver, G. (2002) 'A vision system for an underwater cable tracker', *Machine Vision and Applications*, 13(3), pp. 129-140.
- Oyen, A. *et al.* (2012) 'Application of synthetic aperture radar methods for morphological analysis of the Salar de Uyuni distal fluvial system', in *2012 Ieee International Geoscience and Remote Sensing Symposium*. New York: Ieee, pp. 3875-3878.
- Palmer, M.A. *et al.* (2009) 'Climate change and river ecosystems: protection and adaptation options', *Environmental management*, 44(6), pp. 1053-1068.

- Palmquist, E.C., Sterner, S.A. and Ralston, B.E. (2019) 'A comparison of riparian vegetation sampling methods along a large, regulated river', *River Research and Applications*, 35(6), pp. 759-767.
- Parsapour-Moghaddam, P. and Rennie, C.D. (2018) 'Calibration of a 3D Hydrodynamic Meandering River Model Using Fully Spatially Distributed 3D ADCP Velocity Data', *Journal of Hydraulic Engineering*, 144(4), p. 04018010.
- Parsapour, P., Rennie, C. and Slaney, J. (2018) 'Hydrodynamic Simulation of an Irregularly Meandering Gravel-Bed River: Comparison of MIKE 21 FM and Delft3D Flow models', *E3S Web of Conferences*, 40, p. 02004.
- Parsons, D.R. *et al.* (2005) 'Morphology and flow fields of three-dimensional dunes, Rio Parana, Argentina: Results from simultaneous multibeam echo sounding and acoustic Doppler current profiling', *Journal of Geophysical Research-Earth Surface*, 110(F4), p. 9.
- Passalacqua, P. *et al.* (2010) 'A geometric framework for channel network extraction from lidar: Nonlinear diffusion and geodesic paths', *Journal of Geophysical Research: Earth Surface*, 115(F1).
- Patalano, A., García, C.M. and Rodríguez, A. (2017) 'Rectification of Image Velocity Results (RIVeR): A simple and user-friendly toolbox for large scale water surface Particle Image Velocimetry (PIV) and Particle Tracking Velocimetry (PTV)', *Computers & Geosciences*, 109, pp. 323-330.
- Pavelsky, T.M. and Smith, L.C. (2008) 'RivWidth: A Software Tool for the Calculation of River Widths From Remotely Sensed Imagery', *IEEE Geoscience and Remote Sensing Letters*, 5(1), pp. 70-73.
- Pearce, S. *et al.* (2020) 'An evaluation of image velocimetry techniques under low flow conditions and high seeding densities using unmanned aerial systems', *Remote Sensing*, 12(2), p. 232.
- Pears, B. *et al.* (2020) 'Early Medieval Place-Names and Riverine Flood Histories: A New Approach and New Chronostratigraphic Records for Three English Rivers', *European Journal of Archaeology*, 23(3), pp. 381-405.
- Pearson, E. *et al.* (2017) 'Can high resolution 3D topographic surveys provide reliable grain size estimates in gravel bed rivers?', *Geomorphology*, 293, pp. 143-155.
- Pereira, E. *et al.* (2009) 'Unmanned Air Vehicles for Coastal and Environmental Research', *Journal of Coastal Research*, pp. 1557-1561.
- Perroy, R.L. *et al.* (2010) 'Comparison of gully erosion estimates using airborne and ground-based LiDAR on Santa Cruz Island, California', *Geomorphology*, 118(3-4), pp. 288-300.
- Petryk, S. and Bosmajian, G. (1975) 'Analysis of Flow through Vegetation', *Journal of the Hydraulics Division*, 101(7), pp. 871-884.

List of References

- Phillips, C.J., Marden, M. and Suzanne, L.M. (2014) 'Observations of root growth of young poplar and willow planting types', *New Zealand Journal of Forestry Science*, 44(1), p. 15.
- Picco, L. *et al.* (2017) 'Medium and short term riparian vegetation, island and channel evolution in response to human pressure in a regulated gravel bed river (Piave River, Italy)', *Catena*, 149, pp. 760-769.
- Picco, L. *et al.* (2013) 'Evaluating short-term morphological changes in a gravel-bed braided river using terrestrial laser scanner', *Geomorphology*, 201, pp. 323-334.
- Pickett, S.T. *et al.* (1995) 'Ecological Understanding The Nature of Theory and the Theory of Nature', *Biological Journal of the Linnean Society*, 54(1), p. 107.
- Piton, G. *et al.* (2018) 'Reconstructing Depth-Averaged Open-Channel Flows Using Image Velocimetry and Photogrammetry', *Water Resources Research*, 54(6), pp. 4164-4179.
- Pitre, R.R., Li, X.R. and Delbalzo, R. (2012) 'UAV Route Planning for Joint Search and Track Missions- An Information-Value Approach', *Ieee Transactions on Aerospace and Electronic Systems*, 48(3), pp. 2551-2565.
- Pizarro, A., Dal Sasso, S.F. and Manfreda, S. (2020) 'Refining image-velocimetry performances for streamflow monitoring: Seeding metrics to errors minimization', *Hydrological Processes*, 34(25), pp. 5167-5175.
- Poole, G.C. (2002) 'Fluvial landscape ecology: addressing uniqueness within the river discontinuum', *Freshwater Biology*, 47(4), pp. 641-660.
- Postel, S. and Richter, B. (2012) *Rivers for life: managing water for people and nature*. Island Press.
- Powers, C., Hanlon, R. and Schmale, D.G. (2018) 'Tracking of a Fluorescent Dye in a Freshwater Lake with an Unmanned Surface Vehicle and an Unmanned Aircraft System', *Remote Sensing*, 10(1), p. 10.
- Proud, S.R. *et al.* (2011) 'Rapid response flood detection using the MSG geostationary satellite', *International Journal of Applied Earth Observation and Geoinformation*, 13(4), pp. 536-544.
- Quétier, F. *et al.* (2007) 'Plant-trait-based modeling assessment of ecosystem-service sensitivity to land-use change', *Ecological Applications*, 17(8), pp. 2377-2386.
- Rango, A. and Anderson, A.T. (1974) 'Flood hazard studies in the Mississippi river basin using remote sensing', *JAWRA Journal of the American Water Resources Association*, 10(5), pp. 1060-1081.
- Rapple, B. *et al.* (2017) 'What drives riparian vegetation encroachment in braided river channels at patch to reach scales? Insights from annual airborne surveys (Drome River, SE France, 2005-2011)', *Ecohydrology*, 10(8), p. 16.
- Raspini, F. *et al.* (2018) 'Continuous, semi-automatic monitoring of ground deformation using Sentinel-1 satellites', *Scientific Reports*, 8(1), p. 7253.

- Rathinam, S. *et al.* (2007) 'Autonomous searching and tracking of a river using an UAV', in *2007 American Control Conference, Vols 1-13*. New York: Ieee, pp. 2035-2040.
- Rathinam, S., Kim, Z.W. and Sengupta, R. (2008) 'Vision-Based Monitoring of Locally Linear Structures Using an Unmanned Aerial Vehicle', *Journal of Infrastructure Systems*, 14(1), pp. 52-63.
- Rathore, M.M.U. *et al.* (2015) 'Real-Time Big Data Analytical Architecture for Remote Sensing Application', *IEEE Journal of Selected Topics in Applied Earth Observations and Remote Sensing*, 8(10), pp. 4610-4621.
- Rau, J.Y. *et al.* (2011) 'Static error budget analysis for a land-based dual-camera mobile mapping system', *Journal of the Chinese Institute of Engineers*, 34(7), pp. 849-862.
- Raunonen, P. *et al.* (2013) 'Fast Automatic Precision Tree Models from Terrestrial Laser Scanner Data', *Remote Sensing*, 5(2), pp. 491-520.
- Reich, P.B., Wright, I.J. and Lusk, C.H. (2007) 'Predicting leaf physiology from simple plant and climate attributes: a global GLOPNET analysis', *Ecological Applications*, 17(7), pp. 1982-1988.
- Remondi, F., Burlando, P. and Vollmer, D. (2016) 'Exploring the hydrological impact of increasing urbanisation on a tropical river catchment of the metropolitan Jakarta, Indonesia', *Sustainable Cities and Society*, 20, pp. 210-221.
- Ren, L. *et al.* (2021) 'Vegetation Properties in Human-Impacted Riparian Zones Based on Unmanned Aerial Vehicle (UAV) Imagery: An Analysis of River Reaches in the Yongding River Basin', *Forests*, 12(1), p. 22.
- Resop, J. and Hession, W. (2010) 'Terrestrial Laser Scanning for Monitoring Streambank Retreat: Comparison with Traditional Surveying Techniques', *Journal of Hydraulic Engineering*, 136(10), pp. 794-798.
- Resop, J.P., Lehmann, L. and Hession, W.C. (2019) 'Drone Laser Scanning for Modeling Riverscape Topography and Vegetation: Comparison with Traditional Aerial Lidar', *Drones*, 3(2), p. 35.
- Richards, K., Brasington, J. and Hughes, F. (2002) 'Geomorphic dynamics of floodplains: ecological implications and a potential modelling strategy', *Freshwater Biology*, 47(4), pp. 559-579.
- Richman, A. and Hambidge, C. (2017) *Monitoring Llangarron water quality from space*. Available at: <https://defradigital.blog.gov.uk/2017/01/27/monitoring-llangarron-water-quality-from-space/> (Accessed: 12/12/2018).
- Rinaldi, M. *et al.* (2008) 'Numerical simulation of hydrodynamics and bank erosion in a river bend', *Water Resources Research*, 44(9).
- Rivaes, R.P. *et al.* (2014) 'Modeling the Evolution of Riparian Woodlands Facing Climate Change in Three European Rivers with Contrasting Flow Regimes', *Plos One*, 9(10), p. 14.

List of References

- Roca, D. *et al.* (2016) 'Novel Aerial 3D Mapping System Based on UAV Platforms and 2D Laser Scanners', *Journal of Sensors*, p. 8.
- Rodriguez-Canosa, G.R. *et al.* (2012) 'A Real-Time Method to Detect and Track Moving Objects (DATMO) from Unmanned Aerial Vehicles (UAVs) Using a Single Camera', *Remote Sensing*, 4(4), pp. 1090-1111.
- Rogowski, P., Terrill, E. and Chen, J.L. (2014) 'Observations of the frontal region of a buoyant river plume using an autonomous underwater vehicle', *Journal of Geophysical Research-Oceans*, 119(11), pp. 7549-7567.
- Rossi, L., Mammi, I. and Pelliccia, F. (2020) 'UAV-Derived Multispectral Bathymetry', *Remote Sensing*, 12(23), p. 3897.
- Roussel, J.-R. *et al.* (2020) 'lidR: An R package for analysis of Airborne Laser Scanning (ALS) data', *Remote Sensing of Environment*, 251, p. 112061.
- Rowland, J.C. *et al.* (2016) 'A morphology independent methodology for quantifying planview river change and characteristics from remotely sensed imagery', *Remote Sensing of Environment*, 184, pp. 212-228.
- Ruiz, A. *et al.* (2002) *FLOOD RISK MAPPING BASED ON AIRBORNE LASER SCANNER DATA: CASE OF THE LLOBREGAT RIVER*.
- Ruiz, J.J., Caballero, F. and Merino, L. (2018) 'MGRAPH: A Multigraph Homography Method to Generate Incremental Mosaics in Real-Time From UAV Swarms', *Ieee Robotics and Automation Letters*, 3(4), pp. 2838-2845.
- Saarinen, N. *et al.* (2013) *Area-Based Approach for Mapping and Monitoring Riverine Vegetation Using Mobile Laser Scanning*.
- Salo, J. *et al.* (1986) 'River dynamics and the diversity of Amazon lowland forest', *Nature*, 322(6076), pp. 254-258.
- Samiappan, S. *et al.* (2019) 'Remote Sensing of Wildfire Using a Small Unmanned Aerial System: Post-Fire Mapping, Vegetation Recovery and Damage Analysis in Grand Bay, Mississippi/Alabama, USA', *Drones*, 3(2), p. 43.
- San Juan, V., Santos, M. and Andujar, J.M. (2018) 'Intelligent UAV Map Generation and Discrete Path Planning for Search and Rescue Operations', *Complexity*, p. 17.
- Sand-Jensen, K. (2008) 'Drag forces on common plant species in temperate streams: consequences of morphology, velocity and biomass', *Hydrobiologia*, 610(1), pp. 307-319.
- Sand-Jensen, K. and Pedersen, O. (1999) 'Velocity gradients and turbulence around macrophyte stands in streams', *Freshwater Biology*, 42(2), pp. 315-328.

- Santos, A.L.M.R.d. *et al.* (2018) 'Purus River suspended sediment variability and contributions to the Amazon River from satellite data (2000–2015)', *Comptes Rendus Geoscience*, 350(1), pp. 13-19.
- Savage, V.M., Webb, C.T. and Norberg, J. (2007) 'A general multi-trait-based framework for studying the effects of biodiversity on ecosystem functioning', *Journal of theoretical biology*, 247(2), pp. 213-229.
- Scherzinger, B. and Hutton, J. (2021) *Applanix IN-Fusion Technology Explained*. Available at: https://www.applanix.com/pdf/Applanix_IN-Fusion.pdf (Accessed: 17/11/2021).
- Schindler, R.J. and Robert, A. (2004) 'Suspended sediment concentration and the ripple-dune transition', *Hydrological Processes*, 18(17), pp. 3215-3227.
- Schindler, R.J. and Robert, A. (2005) 'Flow and turbulence structure across the ripple-dune transition: an experiment under mobile bed conditions', *Sedimentology*, 52(3), pp. 627-649.
- Schneider, P. *et al.* (2011) 'Towards improved instrumentation for assessing river-groundwater interactions in a restored river corridor', *Hydrology and Earth System Sciences*, 15(8), pp. 2531-2549.
- Sear, D.A. *et al.* (2010) 'Logjam controls on channel:floodplain interactions in wooded catchments and their role in the formation of multi-channel patterns', *Geomorphology*, 116(3), pp. 305-319.
- Șerban, G. *et al.* (2016) 'Flood-prone area delimitation using UAV technology, in the areas hard-to-reach for classic aircrafts: case study in the north-east of Apuseni Mountains, Transylvania', *Natural Hazards*, 82(3), pp. 1817-1832.
- Sfahani, Z., Vali, A. and Behnamgol, V. (2017) 'Pure Pursuit Guidance and Sliding Mode Control of an Autonomous Underwater Vehicle for Pipeline Tracking', in *2017 5th International Conference on Control, Instrumentation, and Automation*. New York: Ieee, pp. 279-283.
- Shi, J. *et al.* (2016) *2016 IEEE International Geoscience and Remote Sensing Symposium (IGARSS)*. 10-15 July 2016.
- Shi, Y., Zhang, L. and Wei, G. (2014) 'The design and application of the groundwater monitoring system based on the internet of things in the HeiHe river basin', in Choi, S.B., Yarlagadda, P. and AbdullahAlWadud, M. (eds.) *Sensors, Mechatronics and Automation*. Stafa-Zurich: Trans Tech Publications Ltd, pp. 319-325.
- Shields, F.D. *et al.* (2003) 'Use of acoustic doppler current profilers to describe velocity distributions at the reach scale', *JAWRA Journal of the American Water Resources Association*, 39(6), pp. 1397-1408.
- Shintani, C. and Fonstad, M.A. (2017) 'Comparing remote-sensing techniques collecting bathymetric data from a gravel-bed river', *International Journal of Remote Sensing*, 38(8-10), pp. 2883-2902.
- Simmons, S.M. *et al.* (2017) 'An evaluation of the use of a multibeam echo-sounder for observations crossMark of suspended sediment', *Applied Acoustics*, 126, pp. 81-90.

List of References

- Simmons, S.M. *et al.* (2010) 'Monitoring Suspended Sediment Dynamics Using MBES', *Journal of Hydraulic Engineering-Asce*, 136(1), pp. 45-49.
- Simon, A. *et al.* (2000) 'Bank and near-bank processes in an incised channel', *Geomorphology*, 35(3), pp. 193-217.
- Singh, A. *et al.* (2007) 'Autonomous robotic sensing experiments at San joaquin river', in *Proceedings of the 2007 Ieee International Conference on Robotics and Automation, Vols 1-10*. New York: Ieee, pp. 4987-+.
- Smith, J. *et al.* (2008) 'Groundwater-surface water interactions, nutrient fluxes and ecological response in river corridors: Translating science into effective environmental management', *Hydrological Processes*, 22(1), pp. 151-157.
- Smith, M., Asal, F. and Priestnall, G. (2004) 'The use of photogrammetry and LIDAR for landscape roughness estimation in hydrodynamic studies', *International Archives of Photogrammetry Remote Sensing and Spatial Information Sciences*, 35, pp. 714-719.
- Smith, M. and Vericat, D. (2015) 'From experimental plots to experimental landscapes: topography, erosion and deposition in sub-humid badlands from Structure-from-Motion photogrammetry', *Earth Surface Processes and Landforms*, 40(12), pp. 1656-1671.
- Smith, M., Vericat, D. and Gibbins, C. (2011) 'Through-water terrestrial laser scanning of gravel beds at the patch scale', *Earth Surface Processes and Landforms*, 37(4), pp. 411-421.
- Smith, M.W. and Vericat, D. (2014) 'Evaluating shallow-water bathymetry from through-water terrestrial laser scanning under a range of hydraulic and physical water quality conditions', *River Research and Applications*, 30(7), pp. 905-924.
- Snively, K.N. (2009) *Scene reconstruction and visualization from internet photo collections*. Doctor of Philosophy. University of Washington. Available at: <https://www.cs.cornell.edu/~snively/publications/thesis/thesis.pdf>.
- Snellen, M. *et al.* (2013) 'An inter-comparison of sediment classification methods based on multi-beam echo-sounder backscatter and sediment natural radioactivity data', *Journal of the Acoustical Society of America*, 134(2), pp. 959-970.
- Socuvka, V. and Veliskova, Y. (2015) 'Evaluation of reservoir degradation state by Autonomous Underwater Vehicle (AUV)', in Riha, J., Julinek, T. and Adam, K. (eds.) *14th International Symposium - Water Management and Hydraulic Engineering 2015*. Brno: Brno Univ Technology, Fac Civil Engineering, pp. 191-198.
- Solari, L. *et al.* (2016) 'Advances on Modelling Riparian VegetationHydromorphology Interactions', *River Research and Applications*, 32(2), pp. 164-178.

- Song, S., Schmalz, B. and Fohrer, N. (2014) 'Simulation and comparison of stream power in-channel and on the floodplain in a German lowland area', *Journal of Hydrology and Hydromechanics*, 62(2), pp. 133-144.
- Song, S. *et al.* (2017) 'Seasonality of Roughness - the Indicator of Annual River Flow Resistance Condition in a Lowland Catchment', *Water Resources Management*, 31(11), pp. 3299-3312.
- Southwest Regional Coastal Monitoring Programme (2009) *Swath Bathymetry*. Available at: http://www.channelcoast.org/southwest/survey_techniques/bathymetric/?link=swath_bathymetry.html (Accessed: 21/11/2018).
- Staedter, T. (2018) *100,000 IoT Sensors Monitor a 1,400-Kilometer Canal in China*. Available at: <https://spectrum.ieee.org/tech-talk/telecom/internet/a-massive-iot-sensor-network-keeps-watch-over-a-1400kilometer-canal> (Accessed: 31/10/2018).
- Stanford, J.A. and Ward, J.V. (1993) 'AN ECOSYSTEM PERSPECTIVE OF ALLUVIAL RIVERS - CONNECTIVITY AND THE HYPORHEIC CORRIDOR', *Journal of the North American Benthological Society*, 12(1), pp. 48-60.
- Starek, M.J. *et al.* (2013) 'Space-Time Cube Representation of Stream Bank Evolution Mapped by Terrestrial Laser Scanning', *IEEE Geoscience and Remote Sensing Letters*, 10(6), pp. 1369-1373.
- Stek, T.D. (2016) 'Drones over Mediterranean landscapes. The potential of small UAV's (drones) for site detection and heritage management in archaeological survey projects: A case study from Le Pianelle in the Tappino Valley, Molise (Italy)', *Journal of Cultural Heritage*, 22, pp. 1066-1071.
- Stöcker, C. *et al.* (2017) 'Quality Assessment of Combined Imu/gnss Data for Direct Georeferencing in the Context of Uav-Based Mapping', *ISPRS - International Archives of the Photogrammetry, Remote Sensing and Spatial Information Sciences*, 42W6, p. 355.
- Storz-Peretz, Y. *et al.* (2016) 'Flow recession as a driver of the morpho-texture of braided streams', *Earth Surface Processes and Landforms*, 41(6), pp. 754-770.
- Stow, D. *et al.* (2019) 'Illumination Geometry and Flying Height Influence Surface Reflectance and NDVI Derived from Multispectral UAS Imagery', *Drones*, 3(3), p. 55.
- Straatsma, M. and Huthoff, F. (2011) 'Uncertainty in 2D hydrodynamic models from errors in roughness parameterization based on aerial images', *Physics and Chemistry of the Earth, Parts A/B/C*, 36(7), pp. 324-334.
- Straatsma, M.W. and Baptist, M. (2008) 'Floodplain roughness parameterization using airborne laser scanning and spectral remote sensing', *Remote Sensing of Environment*, 112(3), pp. 1062-1080.
- Strom, K.B. and Papanicolaou, A.N. (2007) 'ADV measurements around a cluster microform in a shallow mountain stream', *Journal of Hydraulic Engineering-Asce*, 133(12), pp. 1379-1389.

List of References

- Stromberg, J.C. and Merritt, D.M. (2016) 'Riparian plant guilds of ephemeral, intermittent and perennial rivers', *Freshwater Biology*, 61(8), pp. 1259-1275.
- Su, T.C. (2017) 'A study of a matching pixel by pixel (MPP) algorithm to establish an empirical model of water quality mapping, as based on unmanned aerial vehicle (UAV) images', *International Journal of Applied Earth Observation and Geoinformation*, 58, pp. 213-224.
- Suhari, K. and Gunawan, P. (2017) *The Anyar River Depth Mapping from Surveying Boat (SHUMOO) Using ArcGIS and Surfer*. New York: Ieee. 2017 International Conference on Control, Electronics, Renewable Energy and Communications.
- Sweeney, B.W. *et al.* (2004) 'Riparian deforestation, stream narrowing, and loss of stream ecosystem services', *Proceedings of the National Academy of Sciences of the United States of America*, 101(39), pp. 14132-14137.
- Tabacchi, E. *et al.* (2019) 'Species composition and plant traits: Characterization of the biogeomorphological succession within contrasting river corridors', *River Research and Applications*, 35(8), pp. 1228-1240.
- Taddia, Y. *et al.* (2020) 'Multispectral UAV monitoring of submerged seaweed in shallow water', *Applied Geomatics*, 12(1), pp. 19-34.
- Tal, M. and Paola, C. (2007) 'Dynamic single-thread channels maintained by the interaction of flow and vegetation', *Geology*, 35(4), pp. 347-350.
- Tamminga, A. *et al.* (2015) 'Hyperspatial remote sensing of channel reach morphology and hydraulic fish habitat using an unmanned aerial vehicle (UAV): A first assessment in the context of river research and management', *River Research and Applications*, 31(3), pp. 379-391.
- Tamminga, A.D., Eaton, B.C. and Hugenholtz, C.H. (2015) 'UAS-based remote sensing of fluvial change following an extreme flood event', *Earth Surface Processes and Landforms*, 40(11), pp. 1464-1476.
- Tanentzap, A.J. *et al.* (2012) 'The more stems the merrier: advantages of multi-stemmed architecture for the demography of understorey trees in a temperate broadleaf woodland', *Journal of Ecology*, 100(1), pp. 171-183.
- Tauro, F. *et al.* (2015) 'Large-scale particle image velocimetry from an unmanned aerial vehicle', *IEEE/ASME Transactions on Mechatronics*, 20(6), pp. 3269-3275.
- Telling, J. *et al.* (2017) 'Review of Earth science research using terrestrial laser scanning', *Earth-Science Reviews*, 169, pp. 35-68.
- Tester, P.A. *et al.* (2006) 'A test of an autonomous underwater vehicle as a monitoring tool in shallow water', *African Journal of Marine Science*, 28(2), pp. 251-255.

- Thakur, P.K., Laha, C. and Aggarwal, S.P. (2012) 'River bank erosion hazard study of river Ganga, upstream of Farakka barrage using remote sensing and GIS', *Natural Hazards*, 61(3), pp. 967-987.
- Thames Water (2018) *Thames Water takes to skies to help pinpoint leaks*. Available at: <https://corporate.thameswater.co.uk/Media/News-releases/Thames-Water-takes-to-skies-to-help-pinpoint-leaks> (Accessed: 21/11/2018).
- Thoma, D.P. *et al.* (2005) 'Airborne laser scanning for riverbank erosion assessment', *Remote Sensing of Environment*, 95(4), pp. 493-501.
- Thoms, M.C. and Parsons, M. (2002) 'Eco-geomorphology: an interdisciplinary approach to river science', *International Association of Hydrological Sciences, Publication*, 276, pp. 113-119p.
- Thumser, P. *et al.* (2017) 'RAPTOR-UAV: Real-time particle tracking in rivers using an unmanned aerial vehicle', *Earth Surface Processes and Landforms*, 42(14), pp. 2439-2446.
- Tommaselli, A. and Torres, F. (2016) 'A light-weight laser scanner for UAV applications', in Halounova, L. *et al.* (eds.) *XXIII ISPRS Congress, Commission I*. Gottingen: Copernicus Gesellschaft Mbh, pp. 711-715.
- Tomsett, C. and Leyland, J. (2019) 'Remote sensing of river corridors: A review of current trends and future directions', *River Research and Applications*, 35(7), pp. 779-803.
- Tomsett, C. and Leyland, J. (2021) 'Development and Testing of a UAV Laser Scanner and Multispectral Camera System for Eco-Geomorphic Applications', *Sensors*, 21(22), p. 7719.
- Tomsett, C. and Leyland, J. (In Review) 'Exploring the 4D scales of eco-geomorphic interactions along a river corridor using repeat UAV Laser Scanning (UAV-LS), multispectral imagery, and a functional traits framework', *Earth Surface Dynamics*.
- Tonina, D. *et al.* (2019) 'Mapping river bathymetries: Evaluating topobathymetric LiDAR survey', *Earth Surface Processes and Landforms*, 44(2), pp. 507-520.
- Townsend, P.A. (2001) 'Mapping seasonal flooding in forested wetlands using multi-temporal radarsat SAR', *Photogrammetric Engineering and Remote Sensing*, 67(7), pp. 857-864.
- Trilaksono, B.R. *et al.* (2011) 'Hardware-in-the-loop simulation for visual target tracking of octorotor UAV', *Aircraft Engineering and Aerospace Technology*, 83(6), pp. 407-419.
- Tubau, X. *et al.* (2015) 'Submarine canyons of Santa Monica Bay, Southern California: Variability in morphology and sedimentary processes', *Marine Geology*, 365, pp. 61-79.
- Turner, D., Lucieer, A. and Wallace, L. (2014) 'Direct Georeferencing of Ultrahigh-Resolution UAV Imagery', *IEEE Transactions on Geoscience and Remote Sensing*, 52(5), pp. 2738-2745.
- Udden, J.A. (1914) 'Mechanical composition of clastic sediments', *Bulletin of the Geological Society of America*, 25(1), pp. 655-744.

List of References

Umar, M., Rhoads, B.L. and Greenberg, J.A. (2018) 'Use of multispectral satellite remote sensing to assess mixing of suspended sediment downstream of large river confluences', *Journal of Hydrology*, 556, pp. 325-338.

Unique Group (2018) *NORBIT iWBMS Multibeam Sonar*. Available at: <https://www.uniquegroup.com/item/1019/MultibeamEchoSounders/NORBIT-iWBMS-Multibeam-Sonar.html> (Accessed: 15/11/2018).

UNISDR and CRED (2015) *The Human Cost of Weather Related Disasters: 1995-2015*. United Nations Office for Disaster Risk Reduction. Available at: https://www.unisdr.org/files/46796_cop21weatherdisastersreport2015.pdf.

USGS (2018) *Datasets*. Available at: <https://viewer.nationalmap.gov/basic/> (Accessed: 21/11/2018).

Van Bodegom, P. *et al.* (2012) 'Going beyond limitations of plant functional types when predicting global ecosystem-atmosphere fluxes: exploring the merits of traits-based approaches', *Global Ecology and Biogeography*, 21(6), pp. 625-636.

Van Iersel, W. *et al.* (2016) *XXIII ISPRS Congress, Commission VII, 12–19 July 2016, Prague, Czech Republic*. International Society for Photogrammetry and Remote Sensing.

Van Rijn, L.C. (1993) *Principles of sediment transport in rivers, estuaries and coastal seas*. Aqua publications Amsterdam.

Vargas-Luna, A. *et al.* (2016) 'Representing plants as rigid cylinders in experiments and models', *Advances in Water Resources*, 93, pp. 205-222.

Vasilopoulos, G. (2017) *Characterising the structure and fluvial drag of emergent vegetation*. University of Southampton. Available at: <https://eprints.soton.ac.uk/415780/>.

Västilä, K. and Järvelä, J. (2014) 'Modeling the flow resistance of woody vegetation using physically based properties of the foliage and stem', *Water Resources Research*, 50(1), pp. 229-245.

Västilä, K. and Järvelä, J. (2018) 'Characterizing natural riparian vegetation for modeling of flow and suspended sediment transport', *Journal of Soils and Sediments*, 18(10), pp. 3114-3130.

Västilä, K., Järvelä, J. and Aberle, J. (2013) 'Characteristic reference areas for estimating flow resistance of natural foliated vegetation', *Journal of Hydrology*, 492, pp. 49-60.

Velodyne Lidar (2016) *VLP-16 User manual*. Available at: <https://velodynelidar.com/wp-content/uploads/2019/12/63-9243-Rev-E-VLP-16-User-Manual.pdf> (Accessed: 17/11/2021).

Velodyne Lidar (2018) *Puck Data Sheet* (Accessed: 17/11/2021).

Violle, C. *et al.* (2007) 'Let the concept of trait be functional!', *Oikos*, 116(5), pp. 882-892.

- Vörösmarty, C.J. *et al.* (2010) 'Global threats to human water security and river biodiversity', *Nature*, 467, p. 555.
- Waldron, L.J. (1977) 'The Shear Resistance of Root-Permeated Homogeneous and Stratified Soil', *Soil Science Society of America Journal*, 41(5), pp. 843-849.
- Wallace, L. *et al.* (2016) 'Assessment of Forest Structure Using Two UAV Techniques: A Comparison of Airborne Laser Scanning and Structure from Motion (SfM) Point Clouds', *Forests*, 7(3), p. 62.
- Wang, C. and Wang, P. (2007) 'Hydraulic Resistance Characteristics of Riparian Reed Zone in River', *Journal of Hydrologic Engineering*, 12(3), pp. 267-272.
- Wang, C.K. *et al.* (2011a) 'Mesoscale Terrestrial Laser Scanning of Fluvial Gravel Surfaces', *IEEE Geoscience and Remote Sensing Letters*, 8(6), pp. 1075-1079.
- Wang, D. *et al.* (2018) 'Artificial Mangrove Species Mapping Using Pléiades-1: An Evaluation of Pixel-Based and Object-Based Classifications with Selected Machine Learning Algorithms', *Remote Sensing*, 10(2), p. 294.
- Wang, J.J. and Lu, X.X. (2010) 'Estimation of suspended sediment concentrations using Terra MODIS: An example from the Lower Yangtze River, China', *Science of The Total Environment*, 408(5), pp. 1131-1138.
- Wang, J.J. *et al.* (2009) 'Retrieval of suspended sediment concentrations in large turbid rivers using Landsat ETM+: an example from the Yangtze River, China', *Earth Surface Processes and Landforms*, 34(8), pp. 1082-1092.
- Wang, S.M. *et al.* (2013) 'Application of Environmental Internet of Things on water quality management of urban scenic river', *International Journal of Sustainable Development and World Ecology*, 20(3), pp. 216-222.
- Wang, X. *et al.* (2011b) 'Evaluating nitrogen removal by vegetation uptake using satellite image time series in riparian catchments', *Science of the Total Environment*, 409(13), pp. 2567-2576.
- Ward, J.V. (1989) 'The Four-Dimensional Nature of Lotic Ecosystems', *Journal of the North American Benthological Society*, 8(1), pp. 2-8.
- Wasson, J.G. *et al.* (2010) 'Large-scale relationships between basin and riparian land cover and the ecological status of European rivers', *Freshwater Biology*, 55(7), pp. 1465-1482.
- Watanabe, Y. and Kawahara, Y. (2016) 'UAV photogrammetry for monitoring changes in river topography and vegetation', in Kim, J.H. *et al.* (eds.) *12th International Conference on Hydroinformatics*. Amsterdam: Elsevier Science Bv, pp. 317-325.

List of References

- Wawrzyniak, V. *et al.* (2017) 'Coupling LiDAR and thermal imagery to model the effects of riparian vegetation shade and groundwater inputs on summer river temperature', *Science of the Total Environment*, 592, pp. 616-626.
- Wei, Y.J. and Zhang, Y.W. (2016) 'Effective Waterline Detection of Unmanned Surface Vehicles Based on Optical Images', *Sensors*, 16(10), p. 18.
- Wen, L., Yang, X.H. and Saintilan, N. (2012) 'Local climate determines the NDVI-based primary productivity and flooding creates heterogeneity in semi-arid floodplain ecosystem', *Ecological Modelling*, 242, pp. 116-126.
- Wentworth, C.K. (1922) 'A scale of grade and class terms for clastic sediments', *The journal of geology*, 30(5), pp. 377-392.
- Westoby, M.J. *et al.* (2012) 'Structure-from-Motion' photogrammetry: A low-cost, effective tool for geoscience applications', *Geomorphology*, 179, pp. 300-314.
- Whittaker, P. *et al.* (2013) 'A drag force model to incorporate the reconfiguration of full-scale riparian trees under hydrodynamic loading', *Journal of Hydraulic Research*, 51(5), pp. 569-580.
- Wiel, M.J.V.D. and Darby, S.E. (2007) 'A new model to analyse the impact of woody riparian vegetation on the geotechnical stability of riverbanks', *Earth Surface Processes and Landforms*, 32(14), pp. 2185-2198.
- Wilcox, A.C. and Wohl, E.E. (2007) 'Field measurements of three-dimensional hydraulics in a step-pool channel', *Geomorphology*, 83(3-4), pp. 215-231.
- Wilkinson, M.E. *et al.* (2019) 'Natural flood management: small-scale progress and larger-scale challenges', *Scottish Geographical Journal*, 135(1-2), pp. 23-32.
- Williams, P.A. and Buxton, R.P. (1986) 'HAWTHORN (CRATAEGUS MONOGYNA) POPULATIONS IN MID—CANTERBURY', *New Zealand Journal of Ecology*, 9, pp. 11-17.
- Williams, R.D. *et al.* (2013) 'Hydraulic validation of two-dimensional simulations of braided river flow with spatially continuous aDcp data', *Water Resources Research*, 49(9), pp. 5183-5205.
- Williams, R.D. *et al.* (2016) 'Assessment of a numerical model to reproduce event-scale erosion and deposition distributions in a braided river', *Water Resources Research*, 52(8), pp. 6621-6642.
- Wilson, C. *et al.* (2003) 'Open Channel Flow through Different Forms of Submerged Flexible Vegetation', *Journal of Hydraulic Engineering*, 129.
- Wilson, C.A.M.E. *et al.* (2006) '3D numerical modelling of a willow vegetated river/floodplain system', *Journal of Hydrology*, 327(1), pp. 13-21.
- Wolf P, D.B., Wilkinson B (2014) *Elements of Photogrammetry with Application in GIS*. 4th edn.: McGraw-Hill Education: Maidenhead.

- Woodget, A. *et al.* (2015) 'Quantifying submerged fluvial topography using hyperspatial resolution UAS imagery and structure from motion photogrammetry', *Earth Surface Processes and Landforms*, 40(1), pp. 47-64.
- Woodget, A.S. and Austrums, R. (2017) 'Subaerial gravel size measurement using topographic data derived from a UAV-SfM approach', *Earth Surface Processes and Landforms*, 42(9), pp. 1434-1443.
- Woodget, A.S. *et al.* (2017) 'Drones and digital photogrammetry: from classifications to continuums for monitoring river habitat and hydromorphology', *Wiley Interdisciplinary Reviews-Water*, 4(4), p. 20.
- Woodget, A.S., Fyffe, C. and Carbonneau, P.E. (2018) 'From manned to unmanned aircraft: Adapting airborne particle size mapping methodologies to the characteristics of sUAS and SfM', *Earth Surface Processes and Landforms*, 43(4), pp. 857-870.
- Wright, I.J. *et al.* (2005) 'Assessing the generality of global leaf trait relationships', *New phytologist*, 166(2), pp. 485-496.
- WWF (2018) *Saving The Earth - A Sustainable Future For Soils And Water*. WWF: WWF. Available at: <https://www.wwf.org.uk/updates/saving-earth-sustainable-future-soils-and-water>.
- Xiang, X.B. *et al.* (2016) 'Subsea Cable Tracking by Autonomous Underwater Vehicle with Magnetic Sensing Guidance', *Sensors*, 16(8), p. 22.
- Yamazaki, D. *et al.* (2014) 'Development of the Global Width Database for Large Rivers', *Water Resources Research*, 50(4), pp. 3467-3480.
- Yang, F. *et al.* (2017) *Cooperative Search of UAV Swarm Based on Improved Ant Colony Algorithm in Uncertain Environment*. New York: Ieee. Proceedings of 2017 Ieee International Conference on Unmanned Systems.
- Yang, X. (2007) 'Integrated use of remote sensing and geographic information systems in riparian vegetation delineation and mapping', *International Journal of Remote Sensing*, 28(1-2), pp. 353-370.
- Yao, Z.Y. *et al.* (2013) 'Planform channel dynamics along the Ningxia-Inner Mongolia reaches of the Yellow River from 1958 to 2008: analysis using Landsat images and topographic maps', *Environmental Earth Sciences*, 70(1), pp. 97-106.
- Young, S. *et al.* (2017) 'Robot-Assisted Measurement for Hydrologic Understanding in Data Sparse Regions', *Water*, 9(7), p. 20.
- Yu, G.-A. *et al.* (2020) 'Effects of riparian plant roots on the unconsolidated bank stability of meandering channels in the Tarim River, China', *Geomorphology*, 351, p. 106958.
- Zhao, K. *et al.* (2020) 'Laboratory Experiments of Bank Collapse: The Role of Bank Height and Near-Bank Water Depth', *Journal of Geophysical Research: Earth Surface*, 125(5), p. e2019JF005281.

List of References

- Zhao, M. *et al.* (2017) 'Improved discrete mapping differential evolution for multi-unmanned aerial vehicles cooperative multi-targets assignment under unified model', *International Journal of Machine Learning and Cybernetics*, 8(3), pp. 765-780.
- Zhao, S., Lu, T. and Anvar, A. (2010) *Multiple Obstacles Detection using Fuzzy Interface System for AUV Navigation in Natural Water*. New York: Ieee. Iciea 2010: Proceedings of the 5th Ieee Conference on Industrial Electronics and Applications, Vol 1.
- Zhong, L. *et al.* (2016) 'Segmentation of Individual Trees From TLS and MLS Data', *IEEE Journal of Selected Topics in Applied Earth Observations and Remote Sensing*, 10, pp. 1-14.
- Zhou, H.L. *et al.* (2015) 'Efficient Road Detection and Tracking for Unmanned Aerial Vehicle', *Ieee Transactions on Intelligent Transportation Systems*, 16(1), pp. 297-309.
- Zhu, H. *et al.* (2018) 'The Influences of Riparian Vegetation on Bank Failures of a Small Meadow-Type Meandering River', *Water*, 10(6), p. 692.